CRANFIELD UNIVERSITY

Peter John Wilkinson

Evaluation of Novel Propellants Manufactured from Commercially Available Thermoplastic Elastomers (TPE) using Resonant Acoustic Mixing

Cranfield Defence and Security

PhD
Academic Year: 2010 - 2019

Supervisor: Dr P. P. Gill
Associate Supervisor: Dr G. Kister

June 2019

© Cranfield University 2020. All rights reserved. No part of this publication may be reproduced without the written permission of the copyright owner.

ABSTRACT

The key issues in developing a sustainable gun or rocket propellants are financial, environmental, legislative and safety. Use of commercially available off the shelf polymers, in particular, thermoplastic elastomers (TPE) as a binder for propellants could address these issues. The propellant would need to have suitable mechanical and thermal properties, as well as, adequate ballistic performance. Traditional manufacture techniques for propellant are not suitable for TPE binders and so new mixing and manufacturing techniques will be investigated.

A literature review is presented detailing conventional propellants, low vulnerability (LOVA) propellants and research into using TPEs as binders for propellants. In addition, the desirable mechanical and ballistic properties of propellants are assessed.

The TPEs *PEBAX*, a polyether-block-amide (PEBA) and *SEBS,* a Styrene-ethylene/butylene-styrene were selected for analysis. A full assessment of the mechanical and thermal properties of these TPEs was conducted. They both have broadly suitable properties, however, both TPEs were substantially stiffer (greater storage modulus) than a typical binder and the lower glass transition for SEBS was above the desired minimum operational temperature. When plasticised with Dioctyl Sebacate (DOS), both PEBAX and SEBS had a reduction in the storage modulus and lower glass transition. PEBAX did not show any noticeable effect on the upper (melt) transition, conversely SEBS showed a larger reduction in the upper (glass) transition. SEBS was down selected for further evaluation due to its better availability, purity and greater solubility in solvents.

Traditional mixing and manufacturing techniques where not suitable for processing of propellants with TPE binders. Slurry processing (used in manufacture of pressed PBXs) was selected to coat the filler, creating a moulding powder. This was replicated with a novel method using resonant acoustic mixing (RAM). The moulding powder was then consolidated by remote hot pressing to simulate an industrial extrusion or rolling process. This process was used to successfully manufacture two propellants using SEBS as the binder, *AP/SEBS* containing ammonium perchlorate (AP) as a filler and *RDX/SEBS* with RDX. Inert fillers of sugar and talc were trialled, and mechanical testing of these inerts was found to be generally in good agreement with the live fills.

Initial combustion work on RDX/SEBS by closed bomb analysis at low pressure was indicative of good burning, with a low burn rate.

Both AP/SEBS and RDX/SEBS were subject to thermal and mechanical analysis. This showed that the glass transitions (T_g) were only slightly changed from pure SEBS. In comparison to AP-composite propellants, both the storage modulus (E') from DMA and Young's modulus (E_0) from tensile testing were substantially greater. The maximum stress (σ_m) was similar, however the maximum extension (ε_b) was less. With further optimisation, such as use of bonding agents, plasticisers, optimised particle size and improve manufacturing methods, it is believed that the maximum extension could be increased. Therefore a SEBS based propellant should deform less to an applied force, but still have a similar extension and hence elasticity to hydroxyl-terminated polybutadiene (HTPB) composite propellants. These theoretical improved mechanical properties should result in a safer propellant.

This research has increased the knowledge and understanding of propellants based on commercially available TPEs. It is anticipated that this will be valuable in developing sustainable propellants of the future.

ACKNOWLEDGEMENTS

Firstly I would like to thank my supervisor Dr Philip Gill for his great encouragement and guidance over the many years it has taken me to complete this thesis. Thanks must also go to my associate supervisor Dr Guillaume Kister. I owe a debt of gratitude to Cranfield University for supporting me in this PhD, with particular thanks to Prof. Jacqueline Akhavan. A big thank you also goes to everybody who has helped me with this research. This includes Dr John Bellerby, Dr Mike Williams, Jim Clements, Dr Matt Andrews, Dr James Padfield, Sally Gaulter and Matt Weaver. I would to like to give a thank you to my work colleagues, past and present, Roger, Maggie and Niki, as well as Susan for their support. A final mention for my understanding wife and son.

TABLE OF CONTENTS

ABSTRACT i
ACKNOWLEDGEMENTS iii
TABLE OF CONTENTS v
LIST OF FIGURES ix
LIST OF TABLES xviii
LIST OF EQUATIONS xxiv
GLOSSARY xxv
1 Introduction 1
1.1 Aim 1
1.2 Objectives 1
1.3 Thesis Outline 2
2 Literature Review 4
2.1 Obsolescence of Propellants 5
2.2 Desirable Properties of the Novel Propellant 7
2.3 Solid Propellants 11
2.3.1 Gun propellants 11
2.3.2 Comparison of LOVA Propellants and Conventional Nitrocellulose Based Gun Propellants. 15
2.3.3 Rocket Propellants 20
2.4 Inert Binders 24
2.4.1 Composite Rocket Propellant Binders 24
2.4.2 Theory of Thermoplastic Elastomers 28
2.4.3 Commercially Available Thermoplastic Elastomers 32
2.4.4 Evaluation of Commercial Thermoplastic Elastomers (TPE) as a binder for Propellants 38
2.5 Energetic Fillers 46
2.5.1 Ammonium Perchlorate (AP) 47
2.5.2 Ammonium Nitrate (AN) 48
2.5.3 Ammonium Dinitramide (ADN) 50
2.5.4 Hydrazinium Nitroformate (HNF) 50
2.5.5 Nitramines 52
2.5.6 FOX-7 (1,1-diamino-2,2-dinitroethene) 54
2.5.7 CL-20 (Hexanitrohexaazaisowurtzitane) 55
2.5.8 Summary of Energetic Fillers 55
2.6 Plasticisers 56
2.6.1 Selection of a Plasticiser 57
2.6.2 Theory of Plasticisation 58
2.6.3 Inert (Non-energetic) Plasticisers 59
2.7 Research into Propellants with TPE binders. 62
2.8 Manufacturing Processes 68

2.8.1 Nitrocellulose Based Propellants 68
2.8.2 Composite Rocket Propellants 70
2.8.3 Other Energetic Composites Manufacturing Methods 71
2.8.4 Resonant Acoustic Mixing 71
3 Experimental Methods 74
3.1 Preparation of Samples 74
3.1.1 Preparation of Moulding Powder 74
3.1.2 Hot Pressing of Samples 76
3.1.3 Preparation of cured HTPB 76
3.1.4 List of Chemicals 78
3.2 Analytical Methods 78
3.2.1 Density Measurements 78
3.2.2 Thermal Analysis 79
3.2.3 Dynamic Mechanical Analysis (DMA) 79
3.2.4 Uniaxial Tensile Testing 85
3.2.5 Fourier Transform Infrared (FTIR) Spectroscopy 85
3.2.6 Nuclear Magnetic Resonance (NMR) Spectroscopy 85
3.2.7 Particle Size Analysis 85
3.2.8 Microscopy 86
3.2.9 Ballistic Performance Testing 86
4 Characterisation of Selected TPEs 87
4.1 Introduction 87
4.2 Reported properties of selected TPEs 88
4.2.1 PEBAX 88
4.2.2 SEBS 89
4.3 Nuclear Magnetic Resonance (NMR) Spectroscopy 91
4.3.1 PEBAX 91
4.3.2 SEBS 94
4.4 Fourier Transform Infrared (FTIR) Spectroscopy 97
4.4.1 PEBAX 97
4.4.2 SEBS 98
4.5 Differential scanning calorimetry (DSC) analysis 98
4.5.1 PEBAX 99
4.5.2 SEBS 103
4.5.3 HTPB/N100 105
4.6 Dynamic Mechanical Analysis (DMA) – Temperature Scan 107
4.6.1 PEBAX 107
4.6.2 SEBS 109
4.6.3 HTPB/N100 112
4.7 Dynamic Mechanical Analysis (DMA) – Frequency Scan 114
4.7.1 PEBAX 114
4.7.2 SEBS 117

4.7.3 HTPB/N100 122
4.8 Comparison of Thermal and Mechanical Properties of TPEs with HTPB/N100 127
5 Characterisation of TPEs Blended with Plasticisers 131
5.1 Introduction 131
5.2 Density Measurements 132
5.3 Differential Scanning Calorimetry (DSC) Analysis 135
5.3.1 PEBAX Plasticised with DOS 135
5.3.2 SEBS Plasticised with DOS 138
5.3.3 HTPB/N100 Plasticised with DOS 141
5.4 Dynamic Mechanical Analysis (DMA) – Temperature Scans 143
5.4.1 PEBAX Plasticised with DOS 143
5.4.2 SEBS Plasticised with DOS 146
5.4.3 HTPB/N100 Plasticised with DOS 150
5.5 Comparison of the Thermal and Mechanical Properties of TPEs and HTPB/N100 Plasticised with DOS 152
6 Characterisation of TPEs Filled with an Inert Filler (Hand Mixed) 156
6.1 Introduction 156
6.2 TPEs Filled with an Inert Filler 157
6.2.1 PEBAX Filled with Sugar 158
6.2.2 SEBS Filled with Sugar 162
6.3 Plasticised TPEs Filled Sugar (Hand Mixed) 166
6.3.1 Plasticised Sugar Filled PEBAX (Hand Mixed) 167
6.3.2 Plasticised Sugar Filled SEBS 172
6.4 Conclusion 176
7 SEBS Filled with an Inert Fillers (RAM Slurry Mix) 179
7.1 Density Measurements 181
7.1.1 Density of SEBS Filled with Sugar (RAM Slurry Mix) 181
7.1.2 Density of SEBS Filled with Talc (RAM Slurry Mix) 182
7.2 Dynamic Mechanical Analysis (DMA) 184
7.2.1 DMA of SEBS Filled with Sugar (RAM Slurry Mix) 184
7.2.2 DMA of SEBS Filled with Talc (RAM Slurry Mix) 187
7.3 Tensile Testing 191
7.3.1 Tensile Testing of SEBS Filled with Sugar (RAM Slurry Mix) 191
7.3.2 Tensile Testing of SEBS Filled with Talc (RAM Slurry Mix) 196
7.4 Conclusion 200
8 Characterisation of SEBS Propellants 203
8.1 Introduction 203
8.2 Compatibility Testing of Raw Ingredients 205
8.3 Propellant Hazard Testing 205
8.4 Theoretical Performance (ICT Code) 208
8.5 Microscopy 211

8.5.1 Introduction 211
8.5.2 AP/SEBS Microscopy 211
8.5.3 RDX/SEBS Microscopy 213
8.6 Density Measurements 213
8.6.1 Introduction 213
8.6.2 AP/SEBS Density Measurements 213
8.6.3 RDX/SEBS Density Measurements 215

Table 6-10 Density Measurements (helium pycnometry) of 60 % v/v sugar PEBAX at varying plasticiser (DOS) content. 171

Table 6-11 Thermal transitions of 57 % v/v sugar SEBS at varying plasticiser (DOS) content, found by DMA. 174

Table 6-12 Density measurements of 57 % v/v sugar SEBS at varying plasticiser (DOS) content. 175

Table 6-13 Comparison of mechanical properties of filled TPEs, unplasticised and plasticised with DOS. 177

Table 7-1 Particle size distribution for inert fillers, as determined by laser diffraction using a Cilas 1190 in dry mode. Graphs of caster and icing sugar can be seen in Figure 6-1 and Figure 6-2. 180

Table 7-2 Composition of inert (sugar) filled TPEs (RAM slurry mixed). 181

Table 7-3 Density Measurements (helium pycnometry & hand measurements) of SEBS filled with sugar at varying solid loading. Samples were in duplicate. Standard deviation (σ) x1 is reported throughout this thesis..... 182

Table 7-4 Density measurements (helium pycnometry & hand measurements) of SEBS filled talc at varying solid loadings. Samples were in duplicate. 183

Table 7-5 Thermal transitions of sugar filled SEBS, found by DMA. 185

Table 7-6 Thermal transitions of talc filed SEBS, found by DMA..... 190

Table 7-7 Tensile testing results of sugar filled SEBS. Results are an average of 5 replicates. 193

Table 7-8 Tensile testing results of talc filled SEBS. 5 replicates were tested, except for 43 & 72 % v/v at -40 °C where only 4 replicates were performed due to lack of sample. 198

Table 7-9 Comparison of sugar filled SEBS with AP/AL/HTPB (lit.) and proposed acceptable properties for solid rocket motor, talc filled SEBS with JA2 (DB) propellant (lit.) and suggested widest requirements. 202

Table 8-1 Composition of AP/SEBS and RDX/SEBS propellants..... 203

Table 8-2 Particle size distribution for fillers, as determined by laser diffraction using a Cilas 1190 in dry mode (AP samples) and wet mode (RDX)..... 204

Table 8-3 Vacuum stability compatibly testing of SEBS with AP and RDX, in accordance with STANAG 4147 part 1B[260]..... 205

Table 8-4 Propellant hazard testing of AP/SEBS and RDX/SEBS propellants. Standard deviation (σ) x1 is reported throughout this thesis..... 207

Table 8-5 Composition of propellants for performance calculations by ICT thermodynamic code. 209

Table 8-6 Density measurements (helium pycnometry & hand measurements) of AP/SEBS propellants at varying solid loadings. Samples were in duplicate. Standard deviation is abbreviated to σ throughout this thesis. 214

Table 8-7 RDX/SEBS propellant density measurements. 215

Table 8-8 DSC phase change data for AP, SEBS & AP/SEBS propellants. Samples of AP/SEBS were tested in triplicate. 219

Table 8-9 DSC thermal decomposition data for AP, SEBS & AP/SEBS Propellants. Samples of AP/SEBS were tested in triplicate. 220

Table 8-10 TGA Thermal Decomposition Data for AP, SEBS & AP/SEBS Propellants. Samples of AP/SEBS were tested in triplicate. 220

Table 8-11 DSC Phase change data for RDX, SEBS & RDX/SEBS (67/33 % v/v) propellant. Samples of RDX/SEBS were tested in triplicate. 223

Table 8-12 DSC Thermal decomposition data for RDX, SEBS & RDX/SEBS (67/33 % v/v) propellant. Samples of RDX/SEBS were tested in triplicate. 224

Table 8-13 TGA Thermal decomposition data for RDX, SEBS & RDX/SEBS (67/33 % v/v) propellant. Samples of RDX/SEBS were tested in triplicate. 224

Table 8-14 Glass transition (Tg) determined by DSC (midpoint) for SEBS, AP/SEBS and RDX/SEBS propellant. Two samples of each composition was tested. 225

Table 8-15 DSC data AP/SEBS (71/29 % v/v) propellant at differing heating rates. Samples were in triplicate. 227

Table 8-16 Comparison of E_a AP/SEBS (71/29 % v/v) propellant by DSC & literature values for E_a of AP/HTPB propellants. 228

Table 8-17 First and second transition for formulations of AP/SEBS Propellants. Results for single cantilever DMA at 1 Hz. Samples of AP/SEBS were tested in duplicate. 232

Table 8-18 First and second transition for formulations of RDX/SEBS (67/33 % v/v) and AP/SEBS (65/35 % v/v) Propellants, and SEBS. Results for single cantilever DMA at 1Hz. Samples of RDX/SEBS were tested in duplicate. 237

Table 8-19 Determination of apparent activation energies from the slope of the line (m) in Figure 8-24 240

Table 8-20 Tensile Testing results of AP/SEBS Propellant. Results are an average of 5 tests. 244

Table 8-21 Comparison of reported tensile testing of AP/HTPB Propellants, proposed properties for a solid rocket motor and sample AP/SEBS (71/29 % v/v). 247

Table 8-22 Tensile Testing results of RDX/SEBS (67/33 % v/v) Propellant at -40, 20 & 74 °C. Results are an average of 5 tests. 249

Table 8-23 Comparison of AP/SEBS (71/29 % v/v), AP/Al/HTPB and proposed acceptable properties for solid rocket motor, RDX/SEBS (67/33 % v/v) with JA2 (DB) propellant (lit.) and suggested widest requirements. 253

Table 9-1 Results from vented 'closed' bomb testing on RDX/SEBS (67/33 % v/v). 256

Table 9-2 Published data[223] from vented 'closed' bomb testing on VihtaVuori N-310 single base propellant (contains nitrocellulose (NC), diphenylamine (<2 %) & ethyl centralite (<3 %)[278]). 257

Table 9-3 Calculation of RDX/SEBS (67/33 % v/v), VihtaVuori N-310 & XM39 using the ICT thermodynamic code, version 1.00, supplied by the Fraunhofer Institute for Chemical Technology. 258

Table 10-1 Proposed desirable properties for a TPE based Rocket or Gun Propellant. 261

LIST OF EQUATIONS

2-1 29
2-2 30
2-3 30
2-4 42
2-5 42
2-6 58
2-7 59
2-8 59
3-1 77
3-2 81
3-3 81
3-4 81
3-5 82
3-6 82
3-7 82
3-8 83
3-9 83
3-10 83
8-1 226
8-2 226
9-1 254
9-2 254

GLOSSARY

LIST OF ABBREVIATIONS

A/F	Acetal/Formal
ADN	Ammonium Dinitramide
AN	Ammonium Nitrate
AP	Ammonium Perchlorate
ASTM	American Society for Testing and Materials
ATEC	Acetyl Triethyl Citrate
ATR	Attenuated Total Reflectance
BDNPA	Bis(2,2-dinitropropyl)acetal
BDNPF	Bis(2,2-dinitropropyl)formal
BTTN	1,2,4-Butanetriol Trinitrate
CA	Cellulose Acetate
CAB	Cellulose Acetate Butyrate
CDB	Composite Double-Base
CDB	Cast Double-Base
CL-20	Hexanitrohexaazaisowurtzitane
COPE	Copolyesters Elastomers
COTS	Commercially Available Off The Shelf
CTPB	Carboxyl Terminated Polybutadiene
DB	Double-Base
DCM	Dichloromethane
DDT	Deflagration to Detonation Transitions
DEGDN	Diethylene Glycol Dinitrate
DEP	Diethyl Phthalate
DMA	Dynamic Mechanical Analysis
DMAZ	Dimethylaminoethylazide
DOA	Dioctyl Adipate
DOP	Dioctyl Phthalate
DOS	Dioctyl Sebacate
DPA	Diphenylamine
DSC	Differential Scanning Calorimetry
DTA	Differential Thermal Analysis
EB	Ethylene/Butylene
EC	Ethyl Centralite
EDB	Extruded Double-Base
EMTAP	Energetic Materials Testing Assessment Policy Manual of Tests

EPDM	Ethylene Propylene Diene Methylene
ERGM	Extended Range Guide Missile
ESD	Electro Static Discharge
EVA	Ethylene-Vinyl Acetate
FOX-7	1,1-Diamino-2,2-dinitroethene
FTIR	Fourier Transform Infrared
GAP	Glycidyl Azide Polymer
GAP-A	Glycidyl Azide Prepoylmer
GPC	Gel Permeation Chromatography
HMX	Octahydro-1,3,5,7-tetranitro-1,3,5,7-tetrazocine
HNF	Hydrazinium Nitroformate
HTCE	Hydroxyl-Terminated Caprolactone Ether
HTPB	Hydroxyl-Terminated Polybutadiene
HTPE	Hydroxyl-Terminated Polyether
IM	Insensitive Munitions
IPA	Isopropyl Alcohol
IPDI	Isophorone Diisocyanate
ISO	International Organization for Standardization
ITAR	International Traffic in Arms Regulations
JANNAF	Joint Army-Navy-NASA-Air Force
KDN	Potassium Dinitramide
lit.	Literature
LOVA	Low Vulnerability Ammunition
MAPO	Tris-1-(2,methylaziridinyl)phosphine Oxide
MDI	Methylene Diphenyl Diisocyanate
MNA	N-methyl-p-nitroaniline
NASA	National Aeronautics and Space Administration
NATO	North Atlantic Treaty Organization
NC	Nitrocellulose
NDPA	2-Nitrodiphenylamine
NENA	Nitroethyl Nitramine
NEPE	Nitrate Ester Plasticised Elastomer
NG	Nitroglycerine
NMR	Nuclear Magnetic Resonance
NQ	Nitroguanidine
OB/OD	Open Burning / Open Detonation
PA	Polyamide
PBAN	Poly(butadiene-acrylic acid-acrylonitrile)
PBX	Polymer Bonded Explsoive

PCL	Polycaprolactones
PCP	Polycaprolactone Polyols
PEBA	Polyether-Block-Polyamide
PIB	Polyisobutene(polyisobutylene)
PP	Polypropylene
PSAN	Phase Stabilised Ammonium Nitrate
PTFE	Polytetrafluoroethylene
PTMG	Polytetramethylene Glycol
PU	Polyurethane
PVC	Polyvinyl Chloride
RAM	Resonant Acoustic Mixer
RDX	Cyclotrimethylenetrinitramine
RT	Room Temperature
S	Styrene
S. C.	Single Cantilever
SB	Single-Base
SBC	Styrenic Block Copolymers
SBS	Styrene-Butadiene-Styrene
SEBS	Styrene-Ethylene/Butylene-Styrene
SIS	Styrene-Isoprene-Styrene
TA	Triacetin
TB	Triple-Base
TBT	Tetrabutyl Titanate
TGA	Thermogravimetric Analysis
TMD	Theoretical Maximum Densities
TMETN	Trimethylolethane Trinitrate
TMS	Tetramethylsilane
TNT	Trinitrotoluene
TPE	Thermoplastic Elastomer
TPO	Thermoplastic Polyolefins Elastomers
TPV	Thermoplastic Vulcanisates Elastomers
TSE	Twin Screw Extruders
TTS	Time Temperature Superposition
US	United States (of America)
WLF	Williams–Landel–Ferry equation
XLDB	Cross Linked Double-Base

LIST OF ABBREVIATIONS

a_T	Shift Factor
D_{10}	Diameter at 10%
D_{50}	Diameter at 90%
D_{90}	Diameter at 50%
E'	Storage Modulus
E''	Loss Modulus
E_0	Young's Modulus
E_a	Activation Energy
F	Force Constant
I_{sp}	Specific Impulse
m/m	Mass / Mass
P	Pressure
P_{max}	Maximum Pressure
T	Temperature
T_c	Crystallisation Point
T_g	Glass Transition Point
T_m	Melting Point
v/v	Volume / Volume
α	Pressure Index
β	Heating Rate, Plasticiser Coefficient and Burn Rate Coefficient
Δ	Propellant Loading Fraction
δ	Loss Angle
ΔH	Change in Enthalpy
ΔH_{comb}	Enthalpy of Combustion
$\Delta H_{decomposition}$ or ΔH_{decomp}	Enthalpy of Decomposition
ΔH_f	Enthalpy of Fusion
ΔH_{melt}	Enthalpy of Melting
ε	Extension
ε_b	Maximum Extensions
σ	Standard Devation (x1) or Stress
σ_m	Maximum Stress

1 Introduction

Certain key factors are crucial in the success of a new propellant, these are economic, environmental, legislative and safety. Creating a new propellant with commercially available off the shelf (COTS) polymer as a binder, would be a cost-effective approach. In terms of safety, the binder would need to be a rubbery, elastomeric material. To reduce the environmental impact of disposal of unused munition, using a thermoplastic as a binder would make a propellant with the potential to be recyclable. This thesis seeks to determine whether a COTS thermoplastic elastomer (TPE) would create a propellant with suitable mechanical and thermal properties, in addition to adequate ballistic performance.

Traditional rocket composite propellants are made with curative binders, these are manufactured by mixing the liquid ‘pre-polymers’ with the filler before curing. A different method will need to be investigated in production of a new TPE propellant.

1.1 Aim

This research aims to make sustainable propellants by using commercially available off the shelf polymers while investigating new mixing/manufacturing techniques. The focus has been on using thermoplastic elastomers as the binder, these are commercially made on a large scale giving a reliable source of binder.

1.2 Objectives

1. Review the literature on elastomeric binder systems, especially ones with TPEs. Assessment of commercially available TPEs which might be suitable as a propellant binder.
2. Investigate the mechanical and thermal properties of a few suitable TPEs, comparing against the reported values (where applicable) and those applicable for a propellant.
3. Investigate whether the TPEs can be plasticised and the effect of the plasticiser on the mechanical and thermal properties.

4. Manufacture of propellant samples by developing a small scale technique for coating the filler with TPE, consolidating the coated filler and then cutting into suitable shapes for analysis.
5. Analysis the mechanical properties of inert filled TPE samples for comparison to pure TPE and live propellant.
6. Analysis the thermal and mechanical properties of the propellant samples.
7. Analyse the ballistic performance of a propellant sample.
8. Make conclusions on the suitability of propellant samples manufactured.

1.3 Thesis Outline

This thesis is divided into eleven chapters

Chapter 1 (Introduction) contains the rationale for the research project, aims, objectives and thesis outline.

Chapter 2 (Literature Review) looks at past and current gun and rocket propellants, as well as research into new propellants. There is a focus on LOVA (low vulnerability ammunition) formulations. It describes the properties of different TPEs (thermoplastic elastomers) and evaluates their use as a binder for composite propellants. Different energetic fillers and plasticiser for propellants are accessed. Commercial manufacturing methods are also described.

Chapter 3 (Experimental Methods) describes the preparation of the inert simulants and propellant samples used in this research. Details of analytical methods are provided.

Chapter 4 to 9 are results chapters.

Chapter 4 (Characterisation of Selected TPEs) determines thermal and mechanical characteristics along with the chemical composition of the selected TPEs (SEBS and PEBAX). This is compared to the data from suppliers and research on these materials. The TPEs were assessed for their usage as a binder

for propellants. HTPB (hydroxyl-terminated polybutadiene) polymer was cured and it thermal and mechanical properties were ascertained for comparison.

Chapter 5 (Characterisation of TPEs Blended with Plasticiser) determines the thermal and mechanical characteristics of the selected TPEs plasticised with a common plasticiser. The effect of the plasticiser on the TPES was assessed for its benefits in a propellant binder. This was compared to plasticised cured HTPB.

Chapter 6 (Characterisation of TPE Filled with an Inert Filler (Hand Mixed) ascertains the mechanical properties of sugar filled TPEs, both unplasticised and plasticised. The effect of the filler was described and explained.

Chapter 7 (SEBS Filled with an Inert Filler (RAM Slurry Mix) determines the mechanical properties of inert (sugar and talc) filled SEBS (TPE), produced from a novel slurry mixing technique using a resonant acoustic mixer (RAM). Comparisons were made to the hand mixed samples and between the different fillers.

Chapter 8 (Characterisation of SEBS Propellant) determines the thermal and mechanical properties of ammonium perchlorate/SEBS and RDX/SEBS propellants. These were assessed for their utility for rocket or gun propellants.

Chapter 9 (Ballistic Performance of RDX/SEBS Propellant) seeks to evaluate the ballistic performance of RDX/SEBS propellant.

Chapter 10 (Discussion) discusses the general finding in this thesis, comparing results from different chapters.

Chapter 11 (Conclusion) summarises the conclusions of this thesis and makes recommendation for future work.

2 Literature Review

This chapter will look at past and current, gun and rocket propellants, as well as research into new propellants, particularly LOVA (low vulnerability ammunition) formulations. It will evaluate different TPEs (thermoplastic elastomers) for use as propellant binders and assess plasticisers and composite propellants fillers.

This review has been divided into the following sections

2.1 Obsolescence of Propellants
2.2 Desirable Properties of the Novel Propellant
2.3 Solid Propellants
2.4 Inert Binders
2.5 Energetic Fillers
2.6 Plasticisers
2.7 Manufacturing Processes

Section 2.1 (Obsolescence of Propellants) discusses obsolescence of propellants and what the main concerns are with current propellants. This will guide my research, focusing on how propellants made with a TPE binder might address these issues.

Section 2.2 (Desirable Properties of the Novel Propellant) assesses the desired properties of the novel propellant for both a gun and rocket propellants. This will be used to both guide the composition and evaluate the properties of the novel propellant.

Section 2.3 (Solid Propellants) reviews traditional gun and rocket propellants, as well as LOVA propellants. Explaining the various types and formulations, discussing their different advantage and disadvantages. This will aid the direction of the research by understanding the properties of current propellants, identifying issues and compromises.

Section 2.3 (Inert Binders) reviews existing inert composite rocket binders and describes the theory of TPEs and co-polymers. Then looks at the commercially available TPEs, assessing their suitability for use as a propellant binder. Next, it

looks at the research into propellants with TPE binders. Finally, evaluating the use of TPEs as binders for propellants.

Section 2.5 (Energetic Fillers) examines the use of existing and possible future fillers for composite propellants. Assessing their suitability for both gun and rocket propellants.

Section 2.6 (Plasticisers) describes the theory of plasticisation and the effect of plasticisers on the mechanical properties. It then examines the different plasticisers which have been used in propellants and the research into new plasticisers. This includes both inert and energetic plasticisers, with their advantages and disadvantages being discussed.

Section 2.7 (Manufacturing Processes) describes the various different industrial manufacturing techniques for propellants. Focusing on the difference between manufacture of nitrocellulose based propellants and composite propellants. It also includes the *slurry process* for manufacture of PBXs (polymer-bonded explosives). These manufacturing processes will guide the formation of the novel propellant.

2.1 Obsolescence of Propellants

Conventional propellants; nitro-cellulose based and composite propellants have been in development for well over 5 decades. They have a range of excellent properties, however, the main issues facing the continued used of these propellants are;

- Economical – The cost of materials and manufacture.
- Environmental – The effect of; manufacture, active service or decommissioning of the propellant has on the environment.
- Legislative – Importing of materials for manufacture of propellants from outside the E.U., in particular the U.S.A., can be difficult and expensive due to regulations.
- Safety – As far as practicable, the propellant should not be vulnerable to stimuli caused accidentally or by enemy attack.

To produce a propellant as economically as possible, the materials required should be of low cost and readily available with a consistent supply. Bespoke binders specially manufactured for propellants increase this cost dramatically, especially in developing a new binder. Instead, commercially available 'off the shelf' (COTS) polymers would be an economical source of binders. This approach is not without issues. Commercial polymers are generally only available pre-blended with stabilizer, mechanical property enhancers and even bulking agents to reduce the cost. These additives might be incompatible with other ingredients in the propellant or might not be required, adding unnecessary bulk and mass. Commercial polymers can also be subject to changes in composition over time with little or no warning to the consumer. Due to stringent regulation of propellants, even a small change could require expensive and time consuming requalification of the propellant.

A 2010 NATO[1] report on the impact of munitions disposal sees a clear need for munitions being 'designed for disposal'. Open burning / open detonation (OB/OD) is the traditional method of demilitarising munitions, which is still widely used in many countries, the UK MoD see open burning as the 'better process' for large amounts of munitions[1]. However, OB/OD has been banned in several countries, including Germany, the Netherlands and a partial ban in Canada, due to environmental concerns[2]. Burning or even detonating munitions in an incinerator can reduce the environmental impact, by treatment of waste gases and smoke and careful disposal of the ash. These specialist incinerators are generally only suitable for smaller munitions, larger items require the removal of the energetic material from the casing. Removal of traditional propellants, especially polyurethane propellants (e.g. hydroxyl terminated polybutadiene (HTPB)), is difficult due to the chemical nature of the propellant[3]. Use of a thermoplastic binders (such as a TPE) would in theory allow removal of material by melting.

Supply issues are an important factor in the materials used in propellant manufacture. Sources of materials within the E.U. are becoming more prevalent as legislative issues are increasing, especially with the U.S.A. due to ITAR

(International Traffic in Arms Regulations) restricting articles with direct defence-related applications[4]. There is evidence of European firms redesigning their munitions to remove ITAR restricted components[5]. Despite the environmental advantage of using material from natural sources, such as cotton, their use generally considered undesirable. This is due to the tight specification of propellant which the natural variation of the material could adversely affect[6].

Unintentional ignition or explosion of propellants can cause catastrophic incidents, damaging equipment, and injuring or killing personnel. In response to this, LOVA gun propellants have been developed which are less vulnerable to accidental stimuli or energy attack. This has been achieved by removing the nitroglycerine (NG) and reducing the amount of nitrocellulose (NC), replacing it with an inert binder and a nitramine[7]. Similarly, composite rocket propellants are considered less vulnerable than double base rocket propellants, containing NG and NC. Primarily, the NG causes the poor sensitiveness to impact and low temperature of ignition, leaving the propellant vulnerable to impact and sources of heat. Additionally, the inert binder improves the mechanical properties of the propellant making it less likely to break apart on impact, which would otherwise leave the propellant in a dangerous state on ignition. TPEs have excellent mechanical properties due to their ability to absorb impacts without fracturing, which should produce any even more resilient propellant[8].

2.2 Desirable Properties of the Novel Propellant

The desirable properties of a propellant depends on both the application (e.g. gun ammunition or rocket motor) and the composition of the propellant. Utilising an inert TPE binder will create a composite propellant, with an oxidizer this will be similar to a traditional rubber composite rocket propellant. If an energetic (explosive) filler is used, the propellant would be similar to a LOVA gun propellants (such as XM39), these contain RDX as the filler in a CAB/NC binder. In LOVA propellants, the filler provides the vast majority of the energy for the propellant as the energetic component of the binder is generally only a small percentage (e.g. 4 % for XM39).

For rocket motors it is necessary that the propellant has good mechanical properties in the range of temperature that it is subjected to during use, storage or transport. This is necessary to reduce the likelihood of any damage caused by impact or vibrations. Propellants in missiles attached to airframe (e.g. tactical air-to-air) are going to experience the most extreme temperatures. Stacer *et al.*[9] reports these operating temperatures as between -54 to 74 °C, with a narrower temperature range for a ballistic missile (-18 to 43 °C). Not only can the temperature of the munition affect its mechanical properties, but also the force and frequencies of any shock or vibration, Bose *et al*.[10] suggest this can be between 5 to 30 G-force at 5 to 300 Hz during improper handling or road transportation, up to 2500 Hz for air transport. Stacer *et al.*[9] also suggest desirable mechanical properties for tactical air-to-air and ballistic missiles, see Table 2-1. These are mostly based on uniaxial tensile testing at the temperature extremes and room temperature, and ambient pressure. He also recommends testing the maximum extension at higher strain rate and operating pressure (6.9 MPa). Bose *et al.*[10] suggest simply a tensile strength of > 1 MPa and elongation > 10 % at room temperature for a rocket launcher.

The performance of the propellant is of course an important aspect. Davenas[11] reports that the lowest specific impulse for a rocket motor (based on a standard motor, assumed 70:1 expansion ratio) is around 1860 m s^{-1} for a CDB (composite double-base) propellant, with the lowest burn-rate being around 5 mm s^{-1} at operating pressure (7 MPa). The burn-rate for rocket propellants is often measured using a strand burner, while a rocket motor is required to measure the specific impulse, however this can be a scaled test motor. As for gun propellants, Agrawal[12] reports that the lowest force constant is around 940 J g^{-1}.

For gun propellants, the mechanical properties are not as critical as for rocket propellants with their larger grain size, but they are still important. The temperatures they are subjected to will depend on the local climatic conditions, Nguyen *et al.*[13] suggest a range as wide as -51 to 63 °C to cover all likely locations. Indeed, Nammo produce ammunition with a safety range of -54 to 71 °C [14]. The force and frequencies of shocks and vibrations would mostly

depend on the method of transport (5 to 30 G-force at 5 to 300 Hz for road, up to 2500 Hz for air[10]). Gun propellants are typically tested by uniaxial compression, often at high-rate[15–19]. Again, testing at temperature extremes and at elevated pressures is very important. The author was unable to find any published minimum standard for these test, instead Table 2-1 contains typical results for a double base propellant.

As gun propellants experience a wider range of pressure than rocket propellants, the burn rate coefficient (β) and pressure exponential (α) are a more usually indicators of its burning behaviour. Miller *et al.*[20] reported that β was found between 0.05 to 0.39 cm s^{-1} MPa^{-1} and α was between 0.48-1.41 for a range of LOVA and traditional gun propellants. It is considered advantageous that the pressure index (α) should be around or less than 1, as being much greater than 1 implies that the propellant's burn rate is overly sensitive to pressure. For gun propellants these figure are usually found by closed vessel testing[19].

Table 2-1 Proposed desirable properties for a TPE based Rocket or Gun Propellant.

	Rocket Propellant (Tactical Air-to-air Missile * or Ballistic Missile †)	**Gun Propellant**
Minimum Operating Temperature (T_{min}) / °C	-54* or -18† [(a)]	-51 [(c)]
Maximum Operating Temperature (T_{max}) / °C	74* or 43† [(a)]	63 [(c)]
Maximum Stress Capability (σ_m) at T_{max} / MPa	>0.7 [(a)]	33 [(d)]
Young's Modulus at 25°C (MPa)	2-6 [(a)]	560 [(d)]
Maximum Extension or compression (ε_b) at 25°C (%)	>30* or >45† [(a)]	52 [(d)] (failure strain)
ε_b at T_{min} (%)	>20 at 5 cm min^{-1} or >15 at 50 m min^{-1} & 6.9 MPa [(a)]	32.5 [(d)] (failure strain)
Specific Impulse / m s^{-1}	>1860[(b)] (standard motor, assumed expansion ratio 70:1)	
Force Constant / J g^{-1}		>940[(e)]
Burn Rate / mm s^{-1}	>5[(b)] (in operating conditions, 7 MPa)	
Burn Rate Coefficient (β) / cm s^{-1} MPa^{-1}		0.05 to 0.39[(f)]
Burn rate pressure index (α)		0.48-1.41 [(f)]

[(a)] Ideal properties of a composite rocket propellant from Stacer et al.**[9]**, mechanical testing is uniaxial tensile testing of JANNAF test specimens.

[(b)] Minimum performance of a rocket motor (CDB) from Davenas **[11]**

[(c)] Suggested widest requirements by Nguyen *et al.***[13]**

[(d)] Uniaxial high-rate compression testing of JA2 (DB) propellant from Howard et al.**[17]** taking T_{min}= -50 °C and T_{max} = 60 °C, at ca. 100 s^{-1} strain rate.

[(e)] Taken from Agrawal **[12]**, minimum force constant from conventional NC propellants.

[(f)] Range of burn rate coefficient and pressure index for a range of LOVA and traditional gun propellants reported by Miller *et al.***[20]**

2.3 Solid Propellants

Solid propellants broadly have three different uses; rocket motors, gun charges and gas generators. This thesis is focused on the military applications of rocket and gun propellants, the operating requirements and conditions for these two propellants are very different. Gun propellants burn for a fraction of a second and create very high pressures (ca. 450 MPa[21]). Conversely, rocket propellants may burn for many seconds, but at a lower pressure (typically less than 15 MPa[22]). To achieve the much faster burn rate with gun propellants, they are formed into a large number of small grains in a propellant charge. On the other hand, rocket propellants are often formed into one large grain.

2.3.1 Gun propellants

Gun propellants are traditionally nitrocellulose based (such as single-, double- or triple-base) or newer LOVA propellants.

Table 2-2 Compositions selected traditional gun propellants[23]**.**

	Composition of M10 SB propellant / % m/m	**Composition of M26E1 DB gun propellant / % m/m**	**Composition of M30A1 TB propellant / % m/m**
Nitrocellulose (Binder)	96.04 (13.15 % N)	67.87 (13.15 % N)	27.9 (12.60 % N)
Nitroglycerine (Plasticiser)	-	24.70	22.42
Nitroguanidne	-	-	46.84
Stabiliser	0.98 (Diphenylamine)	5.93 (Ethyl Centalite)	1.49 (Ethyl Centalite)
Other additives	2.98	1.5	1.25

2.3.1.1 Single-Base Propellants

In single-base (SB) propellants, nitrocellulose (NC) is generally the only energetic component, making up over 90 % m/m of the composition (see Table 2-2 & Figure 2-1), it acts as both the fuel and oxidizer. A stabiliser is required to absorb the oxides of nitrogen formed from the chemical decomposition of the nitrocellulose. This is important as the oxide products catalyse the decomposition

reactions (autocatalysis), causing rapid decomposition of the propellant. A plasticiser may also be used to aid gelling of the NC. SB propellants are used in a wide variety of guns.

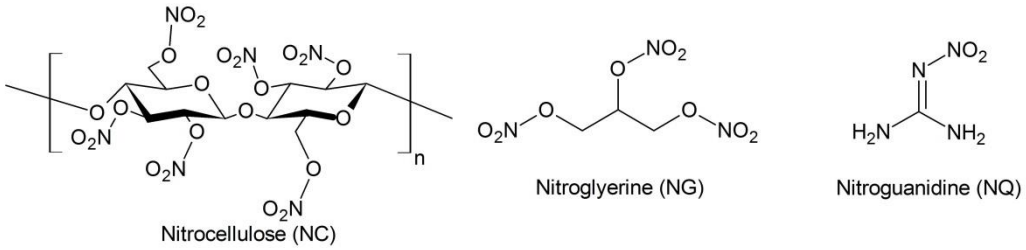

Figure 2-1 Molecular structure of nitrocellulose (NC) (depicting maximum theoretical nitration), nitroglycerine (NG) and nitroguanidine (NQ).

2.3.1.2 Double-Base Gun Propellants

These are a colloidal mixture of nitrocellulose and nitroglycerine (NG) (see Table 2-2), both of which are explosives in their own right, acting as both the fuel and oxidiser. Due to the addition of NG they have a higher energy content, giving the propellant a greater force constant than SB propellants (see Table 2-3). This comes at the disadvantage of higher erosion of the gun-barrel due to its higher flame temperature. These can be used in a wide variety of guns and rocket motors.

2.3.1.3 Triple-Base Propellants

Triple-base (TB) propellants typically have around 50 % m/m nitroguanidine (NQ) in addition to the usually DB propellant composition (see Table 2-2). This reduces the flame temperature and suppresses muzzle flash. This has the disadvantage of lowering the energy content and hence the force constant, compared to DB propellant (see Table 2-3). They are typically used for tank guns and large calibre artillery guns.

Table 2-3 Force constants and flame temperature for selected traditional gun propellants[24]**.**

	Composition of M10 SB propellant / % m/m	**Composition of M26E1 DB gun propellant / % m/m**	**Composition of M30A1 TB propellant / % m/m**
Force Constant / J g^{-1}	1013.1	1085.0	1073.4
Flame Temperature / K	3000	3132	3036

2.3.1.4 Current LOVA Gun Propellants

Since the 1980s, a different type of composite propellant has been developed for gun propellants as opposed to rocket motors. In response to the conventional gun propellants being highly prone to accidental ignition, LOVA gun propellants were developed which have reduced sensitiveness. This has been primarily achieved by removing NG and reducing the amount of NC in the formulation, replacing it with an inert binder and a nitramine (e.g. RDX). Unlike typically ammonium perchlorate (AP) containing composite rocket propellant, nitramine will burn with the required lower flame temperature for gun propellants. Nitramines generally have a lower sensitiveness than NC, in particular a higher ignition temperature. Some NC still remains in the formulation; this improves the mechanical properties and processibility, as well as increasing the impetus and burn rate. However, the burn rates are generally lower, particularly at lower pressures.[7,12]

The US led the way with developing LOVA propellants by first creating XM39[7]. This is widely regarded as *the* LOVA propellant as it was the precursor of many successful LOVA propellants. Containing RDX, CAB inert binder, an inert plasticiser and only 4 % m/m NC (see Table 2-4), it was manufactured by extrusion using solvents like a single base propellant. Two very similar propellants were then developed, M43 for the US army and EX99 for the US Navy[25]. These both contained an energetic plasticiser instead of an inert plasticiser (see Table 2-4), giving them improved performance. M43 is used in

the Cartridge 105, APFSDS-T, M900 for tank guns[7]. EX99 is used in the propelling charge EX-167[26], which is used with the extended range guide missile (ERGM) for the US Navy 5-inch gun[27]. Both M43 & EX99 has been produced by a conventional propellant batch process (mixing and extrusion); trials have conducted on both propellants with the use of twin screw extruders (TSE) for improvements to the manufacturing process[26].

Table 2-4 Composition of LOVA gun propellants XM39[28] [29] **& M43/EX99**[26]**.**

Constituent	Purpose	XM39 / % m/m	M43/EX99 / % m/m
RDX	Energetic filler	76.0	76.0
Cellulose Acetate Butyrate (CAB)	Inert Binder	12.0	12.0
Acetyl Triethyl Citrate (ATEC)	Inert Plasticiser	7.6	
Acetal/Formal (A/F)*	Energetic Plasticiser		7.6
Nitrocellulose (NC)	Improves Mechanical Properties, Impetus & Burn Rate	4.0	4.0
Ethyl Centralite (EC)	Stabiliser	0.4	0.4

*50/50 m/m mixture of bis(2,2-dinitropropyl)acetal (BDNPA) and bis(2,2-dinitropropyl)formal (BDNPF).

Eurenco Bofors have developed LOVA propellants known as NL0XX. These are a similar composition to XM39, except for using a different inert plasticiser and are manufactured using twin screw extrusion (TSE)[7]. They are being used by the US Navy for 57 mm ammunition[30]. GD-OTS Canada (Valleyfield) produce a modified version of XM39 for 105 mm tank ammunition[7], however there is no evidence of it being in service. Nitrochemie have also investigated nitramine LOVA propellant based on HTPB and inert plasticiser as well as CAB/NC. Although, Nitrochemie appear more interested in reducing the sensitiveness of their conventional NC propellant[31].

BAE Systems Land (UK) have been developing LOVA propellants (e.g. Rowanite 318) based on reducing the NC content and replacing it with a nitramine filler and an inert plasticised TPE binder[32]. TPEs should give the propellant better mechanical properties over CAB due to their better elastic properties. While BAE Systems have not publicly reported the composition of Rowanite 318, it was reported that it is based on HMX. They have also recently filed a patent for an insensitive munition (IM) propellant using the TPE - EVA (ethylene-vinyl acetate) as a binder[33]. Rowanite 318 was intended for 120 mm tank gun, recent research has seen BAE alter the composition for the lower energy applications of 105 & 155 mm artillery shells[34].

Table 2-5 Composition of LOVA TPE propellant reported in patent filled by BAE systems[33]**.**

Constituent	BAE Systems LOVA Propellant /% m/m
NC	5 to 10
Nitramine	70 to 80
Stabiliser	1
Plasticiser / binder (TPE)	Up to 16

Research in India at the High Energy Material Research Laboratory, Pune, has focused on using cellulose acetate (CA) mixed with NC as a binder for LOVA propellants. These have been formulated with both RDX[35] & HMX[36] as a filler. It is believed that these propellants have only been made on a 10 kg scale.

2.3.2 Comparison of LOVA Propellants and Conventional Nitrocellulose Based Gun Propellants.

2.3.2.1 Performance

Conventional NC-based propellants have been improved and modified over many years to suit varying applications. Force constants can vary from 940 to 1200 J g^{-1}[12] and can be tailored for individual requirement of the ammunition. For example, M30A1 (triple-base) a propellant used in artillery ammunition has a

force constant of 1073.4 J g^{-1}[24], while JA2 (double-base) used in tank ammunition is 1130.2 J g^{-1}[24]. This higher force is required to generate higher kinetic energy for better penetration of amour. The higher force is due to NC in the JA2 having a higher nitrogen content and the inclusion of the less energetic nitroguanidine (flash suppressant) in the M30A1. It is widely accepted that propellants made with nitramines, inert binders and plasticisers are capable of having the desired performance for artillery and medium calibre applications. The higher performance required for tank ammunition would necessitate the use of energetic plasticisers or binders, such as Acetal/Formal (A/F) energetic plasticiser in EX99. Some discussion has been given to some LOVA propellants not achieving as high muzzle velocities as predicted by the force constant[37], no reason is given in the report. Nevertheless, LOVA propellants have been manufactured with acceptable performance in both medium and higher energy requirement (see Table 2-6). EX99, a fielded LOVA propellant, comprising of RDX with CAB/NC binder and an energetic plasticiser has a reported force constant of 1159.0 J g^{-1}[24].

Table 2-6 Comparison of the force constant and flame temperatures for various LOVA propellants.

Propellant	Composition	Force Constant / J g^{-1}	Flame Temperature / K
XM39	RDX with CAB/NC/inert plasticiser	1096.0[38]	2725*[39]
EX99	RDX with CAB/NC binder and an energetic plasticiser	1159.0[24]	3010[24]
IBK1000 family	RDX with CAB/NC/inert binder or RDX with inert TPE binder	1040 - 1060[40]	2475 - 2530[40]
Rowanite 318	Nitramine with NC/stabiliser/plasticiser/binder (TPE)	1154[32]	
Cellulosic binder-based LOVA propellant	RDX with cellulose acetate (CA)/NC	1085.5 - 1113.0[41]	2888*[41]

*Theoretical thermochemical values

Flame temperature is often a limiting factor in producing the highest energy formulations. However, the reported flame temperatures for LOVA propellants are lower or similar to their conventional counterparts for similar force constant (see Table 2-6). For example a CAB/NC/RDX LOVA propellant (similar to XM39) has a flame temperature of 2725 K, comparable to 3010 K for M30 triple-base propellant[39]. EX99 LOVA propellant has a flame temperature of 3010 K, comparable to 3410 for JA2 propellant[24]. This should be an advantage for LOVA propellants, as lower flame temperatures should reduce barrel wear[42]. Additionally higher energy formulation may be possible, still with acceptable flame temperatures.

2.3.2.2 Burning Behaviour

Miller *et al*[20] compiled over ten years of published and unpublished data on combustion behaviour of solid propellants. The results showed in general that the burn rate coefficient (β) was generally lower for LOVA propellants and the pressure index (α) was on average higher (see Table 2-7). A propellant that burns fast raising the pressure quickly to its peak is preferred, as this maximises the efficiency of the propelling charge[12]. The undesirable lower burn rate coefficient (β), is to some degree offset by the increased pressure index (α).

Table 2-7 Comparison of the burn rate coefficient (β) & pressure index (α) for LOVA propellants XM39 & EX99 to M30[20]**.**

Propellant	Composition	Burn Rate Coefficient (β) / cm s^{-1} MPa^{-1}	Pressure Index (α)
XM39	RDX with CAB/NC/inert plasticiser	0.048-0.05	0.72-1.00
EX99	RDX with CAB/NC binder and an energetic plasticiser	0.070-0.085	0.72-1.41
M30	Triple-base propellant	0.219-0.226	0.80-0.90

Penny[32] also reported a much lower burn rate for the new LOVA propellant Rowanite 318 of 75 mm s^{-1} compared to 144 mm s^{-1} for a conventional propellant under the same conditions. Assumed that the pressure index (α) is similar, this

would indicate a reduction in the efficiency of the propellant to achieve the maximum muzzle velocity. In theory a lower burn rate should lead to a reduced risk of deflagration to detonation transitions (DDT) occurring[8]. Widely shown is the much reduced initial burn rate[32][20][38], Wildegger-Gaissmaier[43] links this low initial burn rate to the reduce vulnerability of the propellant.

Vogelsanger *et al.*[31] reported that HTPB-propellants often have pressure index (α) that are very high (α >> 1). Furthermore, Leach *et al.*[37] state that the ballistic behaviour is complex and not fully understood. Additionally Vogelsanger *et al.*[31] suggest that polymer-bonded propellants (in particular inert binders) create excessive amount of unburnt residue and increased HCN due to their poor oxygen balance.

2.3.2.3 Sensitiveness

Kirshienbaum *et al.*[39] tested various LOVA for their sensitiveness and compared them to conventional propellants, some results are summarised in Table 2-8. They concluded that in general the LOVA propellants tested were less sensitive to impact than the NC based propellants, with Kraton(TPE)/RDX having the lowest sensitiveness. Adding small amounts of NC into CAB/RDX slightly increased the sensitiveness. The auto-ignition and explosion temperature were all significantly higher for LOVA propellants than conventional. However, unglazed CAB/NC/RDX had substantially lower temperatures than the glazed version (the type of glaze was not reported)[39]. Higher ignition / explosion temperatures should increase the time in reaction to slow cook-off and under spall attack[8].

Table 2-8 Comparison of the sensitiveness of various LOVA propellants to M30.

Propellant	Composition	Auto-ignition Temperature* / °C	Explosion Temperature† / °C	Impact Sensitivity‡ / cm
Similar to XM39	CAB/NC/RDX (glazed)	193	297	36.7 ± 5.0
	CAB/NC/RDX (unglazed)	187	253	27.6 ± 3.7
HTPB propellant	HTPB/HMX	228	294	32.0 ± 3.5
TPE Propellant	Kraton (TPE) /RDX	192	306	43.0 ± 2.5
M30	Triple-base propellant	169	212	16.2 ± 3.6

* Determined by DTA, 10 °C min^{-1} in static air.

† 40 mg samples, the 5-second time-to-explosion temperatures are reported.

‡ 30 mg sample with a 2.5 kg steel weight**[39]**.

Pillai *et al.*[35] tested the friction sensitiveness of CA/NC/RDX, a LOVA propellant made from cellulose acetate (CA) which has similar properties to CAB. They showed that the friction sensitiveness (Julius Peter apparatus) of CA/NC/RDX was 55-67 cm, compared to 29 cm for a conventional triple-base propellant. The LOVA propellant Rowanite 318 was compared to conventional propellants, the FofI (impact sensitivity) was better than any of the NC/NG propellants, it had a similar or better figure of friction (friction sensitiveness) and a much higher ignition temperature[8].

2.3.2.4 Ignition

LOVA propellants are known to be difficult to ignite, this is most conspicuous with formulation not containing any nitrocellulose[31]. This is due to the higher ignition temperature and low burn rate at low pressure. Conversely, this behaviour results in the propellant being less likely to ignite unintentionally. If ignition did occur the effect should be smaller, for example a slower burn or possibly self-extinguish[8]. Current LOVA propellants can be ignited with black powder, but require increased effort. Future LOVA propellant (not containing NC) are likely to have an even

higher ignition temperature, making them so hard to ignite they would be disregarded without redesigned ignitors[44].

2.3.3 Rocket Propellants

Solid Rocket propellants are either double-base or composite propellants. Notably, double-base propellants are common to both gun and rocket propellants, but with different compositions.

2.3.3.1 Double-Base Propellants

For rocket propellants there are broadly two different types of double-base propellants, extruded (EDB) and cast (CDB), depending on the method of manufacture of the propellant grain.

EDBs have relatively low specific impulses (I_{sp}) for rocket propellants, ranging from 1512 to 2305 m s^{-1} (expansion ratio 69:1)[45]. Furthermore, the specific impulse of CDB are generally lower (typically 1560 to 2160 m s^{-1}[22]) than that of an EDB propellants, due to the additional non-energetic additives (see Table 2-9). However, the improved safety and mechanical life from case bonding make them useful when high velocities are not required, such as anti-tank guided weapons.

Table 2-9 Composition of JPN extruded double-base (ECB) rocket propellant[46] **and typical cast double-base (CDB) propellant**[22]**.**

	Composition of EDB (JPN Propellant) / % m/m	**Typical CDB propellant / % m/m**
Nitrocellulose (Binder)	51.5	45 – 55
Nitroglycerine (Plasticiser)	43.0	25 – 40
Diethyl phthalate (Plasticiser)	3.2	-
Ethyl Centalite (Stabiliser / Plasticiser)	1.0	-
Plasticisers & stabilisers (not specified)	-	12 – 22
Other additives	1.3	1 – 2

There are many advantages to DB propellants, which keeps them in use today. They are made by a well-known process, which is inexpensive (moderately

expensive for CDB) and have good mechanical strength (e.g. 11.5 MPa tensile strength at 20 °C[47]). They are generally quite stiff with a high elastic modulus (e.g. 1.3 GPa at 25 °C (DMA)[48]), with a poor low elongation capacity, especially at low temperature (e.g. 6.3 % at -40 °C (uniaxial tensile testing)[47]). Complex grain shapes can be produced by either casting or extrusion. Significantly they have a smokeless burn with a fairly non-toxic exhaust. Platonisation (or plateau burning) is also possible, this involves the introduction of small amount of copper or lead salts (e.g. lead sterate) into the propellant. The burn rate at lower pressures is increased, while remaining the same at higher pressures. This has the effect creating a very low pressure index at standard operating pressures, seem by a plateau on a plot of burn rate against pressure (see Figure 2-2). This helps to stabilise the pressure inside the chamber during the relatively long burn of rocket propellants. [46]; [49]; [50].

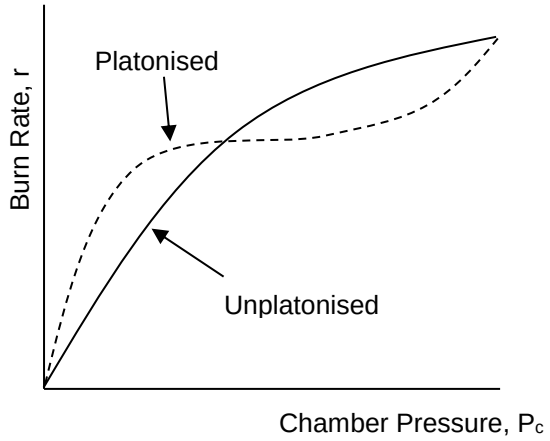

Figure 2-2 Burning rate versus pressure for a platonised and unplatonised propellants. Adapted from reference [51]**.**

Many problems exist with DB propellants; storage is a major issue for this type of propellant. In high temperature storage, chemical decomposition of the nitrate esters produces a gaseous product, which may cause ‘gas cracking’. While at low temperatures mechanical cracking can occur. Nitroglycerine (or other plasticisers) may also bleed out or migrate. Another important issue is their low performance (specific impulse), energising by simple addition of aluminium would

be ineffective due to the low oxygen balance of DB propellants. Therefore an oxidiser (usually ammonium perchlorate) is added with the aluminium. This results in the specific impulse being raised to over 2600 m s^{-1}. However, this has several consequences; firstly, the propellant can no longer be platonised. Secondly, the exhaust is now smoky, mostly due to the aluminium that forms small particles of solid aluminium oxide in the exhaust, as well as secondary smoke caused by the AP. Higher specific impulses can be achieved without these complications by addition of nitramines, such as RDX or HMX. However this makes the propellant more sensitive and expensive to manufacture. DB propellants containing RDX or HMX would usually be classed as a 1.1-type, as they can experience a transition from deflagration to detonation, due to their smaller critical diameter. These are considered more dangerous than class 1.3 (non-detontable). Nitramine can also have the effect of causing combustion instability, a suppressant (e.g. zirconium carbide) is necessary to stop the propellant burning at unstable burning rate.[52]; [50]

2.3.3.2 Composite Propellants

The major constituents of DB propellants (nitrocellulose and nitroglycerine) are both explosives with the potential to detonate, which is undesirable. A correctly functioning rocket propellant is merely burning very fast, so by using separate compounds as fuels and oxidisers this risk is mitigated. The polymer provides both the majority of fuel and acts as a binder, holding the oxidizer and other additives in a matrix. Both thermoplastics and thermosetting polymers can be used, however todays composite rocket propellants only have a rubbery binder made from cross-linking polymers by a curing reaction. Ammonium perchlorate (AP) is used as the oxidiser in vast majority of compositions, due to its good stability and excellent performance (high burn rate and density).

Rubbery composites have many advantages over other rocket propellants. Firstly, they are generally classed as nondetonable material (class 1.3), due to the large critical diameter (diameter at which detonation occurs) of the propellant being greater than the grain diameter. They have excellent mechanical properties

over a wide range of temperature (-55 to +70°C). They typically have low glass transitions, the temperature at which binder changes from soft rubber to a brittle glass state, which can be reduced further by addition of plasticiser. This hard brittle state can have serious implication for the safety of the propellant. Plasticisers also reduce the viscosity, making casting easier and enable high solid loading (the ratio of oxidisers and fuels to binder). By careful control of the curing process rubber composites maybe extruded (extrudable curables). The specific impulse is high, (typically 2550 to 2600 m s^{-1} for HTPB, expansion ratio 68:1[53]) especially if the composition is aluminised. Rubber composites will burn smoothly, adding aluminium will improve this further acting as a combustion instability suppressant, although this effect does depend on the particle size distribution[3]. Addition of nitroamines (such as RDX or HMX) can be used to increase the energy of the propellant. However propellants with nitroamines are expensive to manufacture, mostly due to the hazardous processing. They can also be detonatable, making them a hazard class 1.1.[46]

One of the major disadvantages of rubber composites is their complex processing, which involves a curing process which must be controlled or the mechanical properties of binder will be affected. Stress cracking has been known to occur during storage, for large motors cracks can also occur because of shrinkage during curing. For tactical systems, these propellants also have the shortcoming of having a smoky exhaust in moderate or high humidity environment. This is due to the ammonium perchlorate forming hydrogen chloride (HCl) and chlorine (Cl_2) gas, which then forms with droplets of water to form an aerosol, visible as a large white smoky plume[54]. If aluminium is included in the composition the smoke will be increased, due to oxidation to alumina, which are visible as small solid particles. The exhaust fumes are also toxic, again hydrogen chloride is one of the major culprits. The exhaust may also interfere with electromagnetic radiation and so remote guidance of rockets can be problematic[46].

Overall, composite propellants can be used in a wide variety of rocket motors. They have very good safety characteristics over a wide range of temperature. As

well as good burning characteristics, over a wide range of burn rates and are capable of very high performance, especially is aluminised. Their main disadvantage is the smoky, toxic exhaust, especially true of aluminised propellants. Even in non-aluminised propellants smoke is formed from the toxic hydrogen chloride forming droplets.

2.4 Inert Binders

2.4.1 Composite Rocket Propellant Binders

Plastic composite propellants are made from a thermoplastic and an oxidant, usually ammonium perchlorate. These were widely used in British rockets in the 1950's and 60's, but by the late 1970's rubbery composites were found to have much better mechanical properties, especially at very low temperature, hence they have no applications today. With the creation of TPEs, it is believed that thermoplastic propellant may be viable again.

A typical plastic composite contained Polyisobutene (polyisobutylene) (PIB) as a binder, plasticised with ethyl oleate (see Figure 2-3).

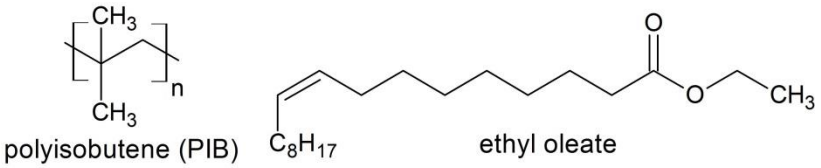

Figure 2-3 Molecular structure of polyisobutene and ethyl oleate (plasticiser).

Plastic composites are easy and relativity inexpensive to manufacture, additionally there is no potentially dangerous exothermic curing reaction. The ingredients are mixed in a heated incorporator, before being extruded into a vacuum chamber to de-aerate. The grain size is limited by the tendency for plastic propellants to deform under their own weight, known as slumping; this typically limits the size to less than 15 cm. Plastic composites are known to have a good chemical shelf life.[51]; [55]

The main disadvantage of plastic composites are their poor mechanical properties, particularly a poor stress resistance at low temperature. Typically the

composition burned at too high a temperature, this could be reduced by the addition of ammonium picrate. However, this reduced the total energy of the formulation, reducing the specific impulse.

Rubbery composite propellants are the most common type of solid rocket propellant used today[46]. These are made by forming a thermosetting polymer, by far the most common are polyurethanes. Polyurethanes are organic polymers which contain urethane (carbamate) linkages. These are created by reacting an alcohol with an isocyanate group, with no other products being formed. Early polyurethane propellants were made by reacting a diol (e.g. glycol) with a di-functional isocyanate (see Figure 2-4).

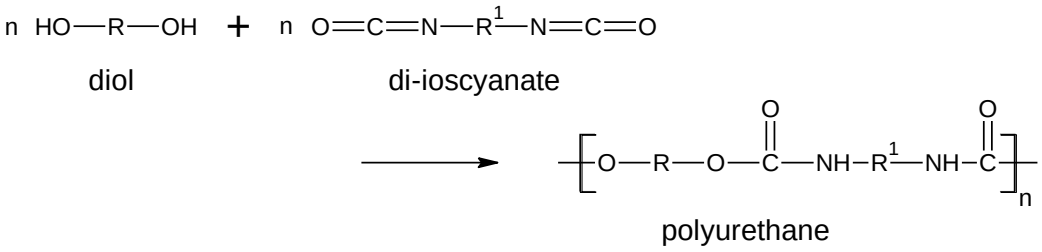

Figure 2-4 Reaction of a diol with an isocyanate to form a polyurethane.

This forms a linear polyurethane were the polymeric chains are entangled, but not cross-linked. This results in the polymer having a low mechanical strength. Improved properties can be achieved by adding multi-functional alcohols or isocyanates. This creates cross-linking between the polymer chains. [49]; [56]

Modern polyurethane binders are made by starting with a polymer and forming urethane cross-linkages. The most widely used composite propellant being cured hydroxyl-terminated polybutadiene (HTPB), which is manufactured from hydroxyl-terminated polybutadiene prepolymer cured with an isocyanate. The HTPB prepolymer is synthesised by free radical polymerisation of 1,3-butadiene, which forms some branched chains. This leads to a hydroxyl functionality (number of hydroxyl group per number of molecules) of about 2.2-2.4, hence a di- or multi-functional isocyanate may be used to obtain the desired cross-linked matrix (see Figure 2-5). The degree of cross-linking is important to maintain a

good low-temperature elasticity, but still able to withstand stresses (high temperature and pressure) during use[51]. HTPB prepolymer is mixed with the curing agent (usually a di-isocyanate), ammonium perchlorate, aluminium powder and other additive such as plasticisers and cure catalysts.

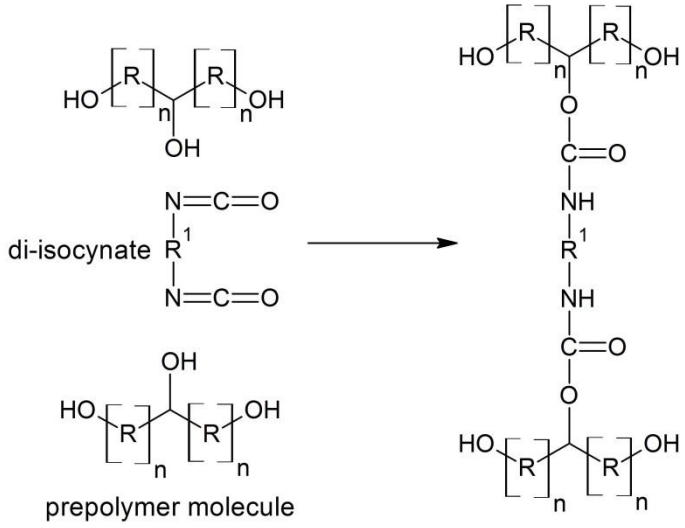

Figure 2-5 Illustration of crosslinking in isocyanate cured HTPB propellant binders, showing the extra-functionality of the HTPB prepolymer.

Other prepolymers can be used in a similar manner to form composite propellants. Carboxyl terminated polybutadiene (CTPB) have a similar structure to HTPB (see Figure 2-6), but with the hydroxyl groups replaced by carboxyl groups. Poly(butadiene-acrylic acid-acrylonitrile) (PBAN) is another carboxyl containing prepolymer. Both CTPB and PBAN are cured using with epoxides or aziridines, as opposed to isocyanates.

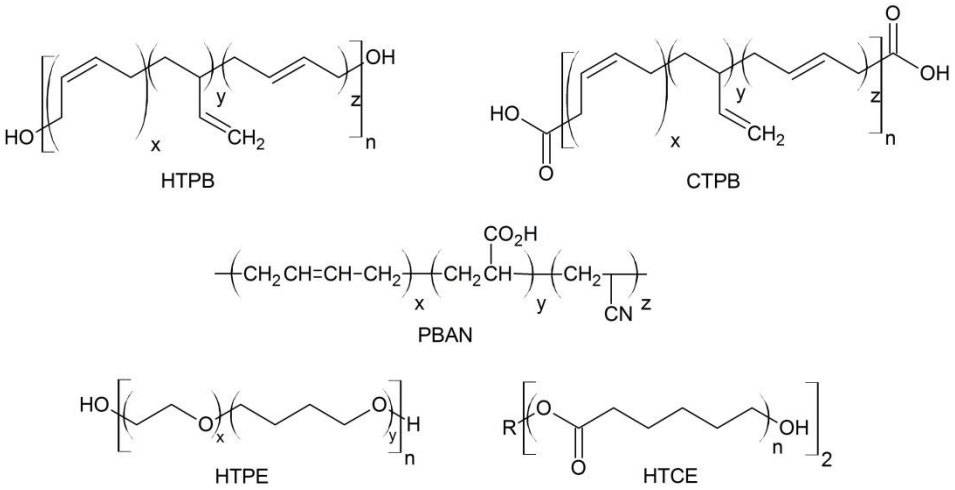

Figure 2-6 Molecular structure of composite propellant prepolymers; Hydroxy-terminated polybutadiene (HTPB), Carboxyl-terminated polybutadiene (CTPB), Poly(butadiene-acrylic acid-acrylonitrile) (PBAN), Hydroxyl-terminated polyether (HTPE), Hydroxyl-terminated caprolactone ether (HTCE).

Hydroxyl-terminated polyethers (HTPE) are becoming a more important type of composite propellant. ATK have developed a propellant based on a block copolymer of poly-1,4-butanediol (Terathane®) and polyethylene glycol, called TPEG (see Figure 2-6). TPEG is difuntional and so requires a multi-function isocyanate as a curing agent to obtain cross-linking. Some full-scale rocket motors of HTPE have passed all of the Insensitive Munitions tests including cook-off and fragment impact, unlike HTPB propellant. Even when a munition has failed, the response to the slow cook-off test has been better than similar HTPB munitions[3]. HTPE can also be used with energetic plasticisers (e.g. n-ButylNENA) which cannot be used with HTPB due to poor solubility. Energetic plasticisers primarily act to plasticise the propellant, but they also have secondary roles to modify the oxygen balance or energy content, and can act as a burn rate modifiers.[57]

Hydroxyl-terminated caprolactone ethers (HTCE), which are also known as Polycaprolactones (PCL) or polycaprolactone polyols (PCP), have been evaluated for use in composite propellants (see Figure 2-6). They are commercially available and have a wide range of mechanical properties as they

are often manufactured as a copolymer. Similarly to HTPE they can be used with energetic platicisers.[49]; [56]

2.4.2 Theory of Thermoplastic Elastomers

The general feature of all TPEs is that they contain polymer chains which are 'held together' at their working temperature. But when they are heated up this cross-linking becomes ineffective (fugitive) and the chains are able to move, enabling the polymer to flow (a thermoplastic). On cooling these cross-links reform and the polymer regains its rubbery properties (Figure 2-7).

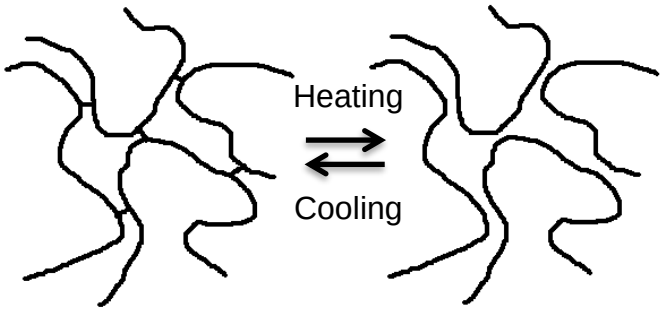

Figure 2-7 Schematic showing fugitive cross-links which break on heating and reform on cooling. Adapted from [58]

These heat fugitive cross-links can in theory be formed by a variety of ways[58]:

1. Ionic cross-linking
2. Cross-linking by hydrogen bonding
3. Cross-linking by thermally unstable covalent bonds
4. Linking molecules by small crystalline structures
5. Use of block copolymers
6. Blending thermoplastic into rubbery materials

In practice it is only 5 and 6 which are commonly used in commercial thermoplastic elastomers. As blended thermoplastics were believed to be unsuitable for use with propellants as the mixture's properties may well alter considerably when compounded, it was decided to concentrate on block copolymers only.

2.4.2.1 Variation of Melting Point and Glass Transition with Copolymer Composition

2.4.2.1.1 Random Co-polymers

A random copolymer will usually produce a polymer with a melting point and glass transition in between the two values of each homopolymer. Figure 2-8 shows the typically effect on melting point and glass transition of changing the molar fraction of two polymers in a copolymer.

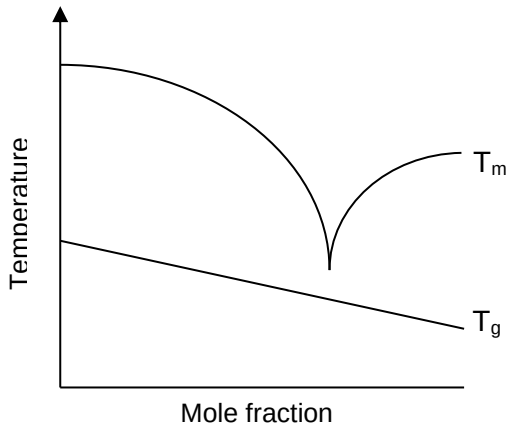

Figure 2-8 Schematic of a typical random copolymer showing how the melting point (T_m) and glass transition (T_g) vary as the molar fraction of the two polymers is changed. Adapted from reference [59]**.**

An equation for depression of the melting point(2-1) can be thermodynamically derived[60].

$$\frac{1}{T_m} - \frac{1}{T_{m\,5}} = -\frac{R}{\Delta H_u}\ln T_5 \qquad \text{2-1}$$

Where 6_a is the melting point of the copolymer, $6_{a\,5}$ is the melting point of homopolymer 1, T_5 is the mole fraction of polymer 1 in the copolymer, $¿^*_{Ù\,è\,æ}$ is the enthalpy of fusion.

2.4.2.2 Polymer Blends

An equation for the change in glass transition in polymer blends is harder to derive, as only compatible polymers give a linear dependency of the $6_Ú$ with the mole fraction (as shown in Figure 2-8). Hence the Gordon-Taylor expression(2-2)

for the composition dependency of polymer blends contains a model specific constant (K), which can be related to the specific volumes or bond flexibility.

$$€. \; L \; \frac{• Ú€. ÚEw • Û€. Û}{• ÚEw • Û} \qquad \textbf{2-2}$$

Where $6_Ú$ is the glass transition of the copolymer, $6_{Ú5}$ and $6_{Ú6}$ are the glass transition of pure polymer 1 and 2, S_5 and S_6 are the weight fraction of polymer 1 and 2. By assuming that the constant - N $6_{Ú5}$ ¤$6_{Ú6}$, the Gordon-Taylor equation (2) can be simplified into the Fox equation(2-3)[61].

$$\frac{Ú}{€.} \; L \; \frac{• Ú}{€. Ú} \; E \frac{• Û}{€. Û} \qquad \textbf{2-3}$$

Again an equation for the change in melting point can be very complex if phase separation occurs. For completely miscible blends the melting point depression can be described in equation 2-1.

2.4.2.2.1 Block Copolymers

With block copolymers a completely different effect on the melting points and glass transitions can be observed; providing the blocks are long enough to crystallise independently they can retain their individual values of T_m and T_g. The most popular grouping is combining a polymer with a high melting point (A) and one with a low melting point (B). This will result in a high melting point from A, but a low glass transition from B. The melting point of block A may be slightly lowered due to block B (and indeed melting point of B may be increased due to A), but this effect is usually small, if observed at all.

The effect on glass transitions in block copolymers is much harder to predict. Some block copolymers (e.g. styrene block copolymers such as SBS, styrene-butadiene-styrene) can have two glass transitions. In SBS the T_g of the polybutadiene block is typically around -65 °C, while the polystyrene block is around 100 °C. This means that at ambient temperatures (or any temperature between their T_g values) the butadiene block will be in a rubbery phase, while the polystyrene block is glassy. The polystyrene end blocks form discrete domains of

the polymer. This effectively anchors each end of a chain usually into different domains and results in the chains being effectively cross-linked together (see Figure 2-9). When SBS is heated up above its T_g for the polystyrene block, these domains will break up and the polymer chains are free to move and flow. Hence SBS can act as an elastomer around ambient temperatures due to the polystyrene domains creating virtual cross-links between chains. When heated up it acts as a thermoplastic, as these heat fugitive cross links are lost and the polymer softens[59]. This temperature range between the two glass transitions is known as the service temperature window. For a propellant it is important that this temperature range is over the desired storage and working temperatures. If the lower glass transition is too high, the propellant could become brittle and break apart on impact. While if the upper glass transition is too low, the propellant could become deformed.

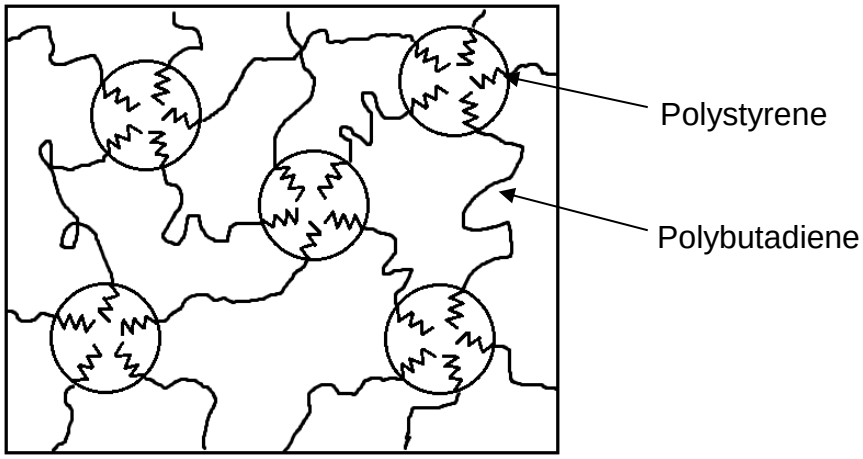

Figure 2-9 Schematic of polystyrene domains in styrene-butadiene-styrene (SBS). Adapted from reference [58]**.**

2.4.2.3 Relaxations of Polyethylene

Polyethylene is well known to exhibit 3 relaxation transitions known as α, β & γ **(**in order of decreasing temperature), these are shown in Figure 2-10 as sudden decreases in the storage modulus or peaks in the loss modulus or tan δ.

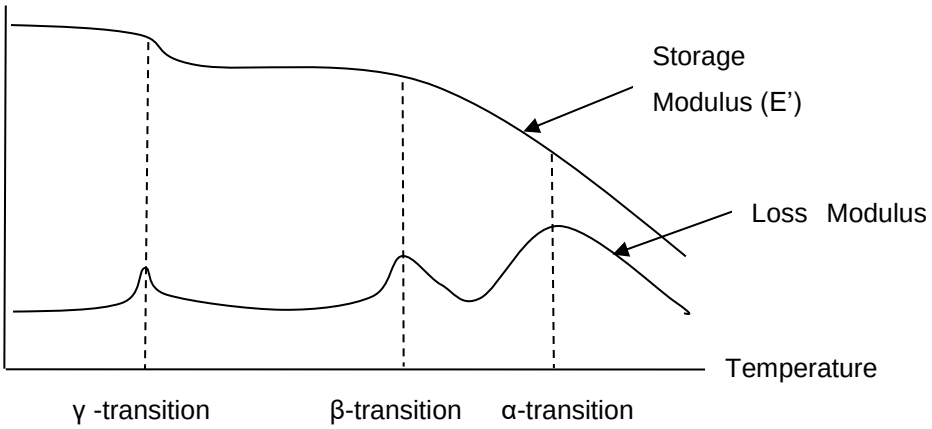

Figure 2-10 Schematic of the three relaxation transition of polyethylene. Adapted from reference [62]**.**

These relaxation transitions are known to correspond to different motions within the polyethylene chain. The γ-transition (which occurs between -150 to -120 ºC) is thought by many to be the glass transition (T_g). However, this view is very controversial with Khanna *et al*[62] believing it to be connected to only the motion of short chain segments. The β-transition (around -30 to +10 ºC) is attributed to the motion of the interfacial region by Popli *et al*[63], but both Khanna *et al*[62] and Boyd[64] believe that this is the true glass transition. There is a general agreement that the α-transition (around 30 to 120 ºC) originates from a type of motion in the crystals.

2.4.3 Commercially Available Thermoplastic Elastomers

In 2014, 3.8 million tons of TPEs were produced globally, with styrenic block copolymer being the most common, accounting for 1.9 million tons[65]. TPEs accounted for 30 % of the global share of elastomers in 2017, the remaining 70 % being the more cost-efficient thermoset. However, it is reported that TPEs are replacing some thermosets due to their superior flexibility and better moulding[66]. Many different types of commercial TPEs exist for a variety of different uses. Each of these can usually be formulated from different monomers, as well as, having different chain lengths and ratio of polymers, allowing for further alteration of the TPEs properties. Figure 2-11 shows a selection of

different TPEs, focusing on those most likely to useful. Below is a summary of different TPEs and their properties in relation to use as a propellant binder.

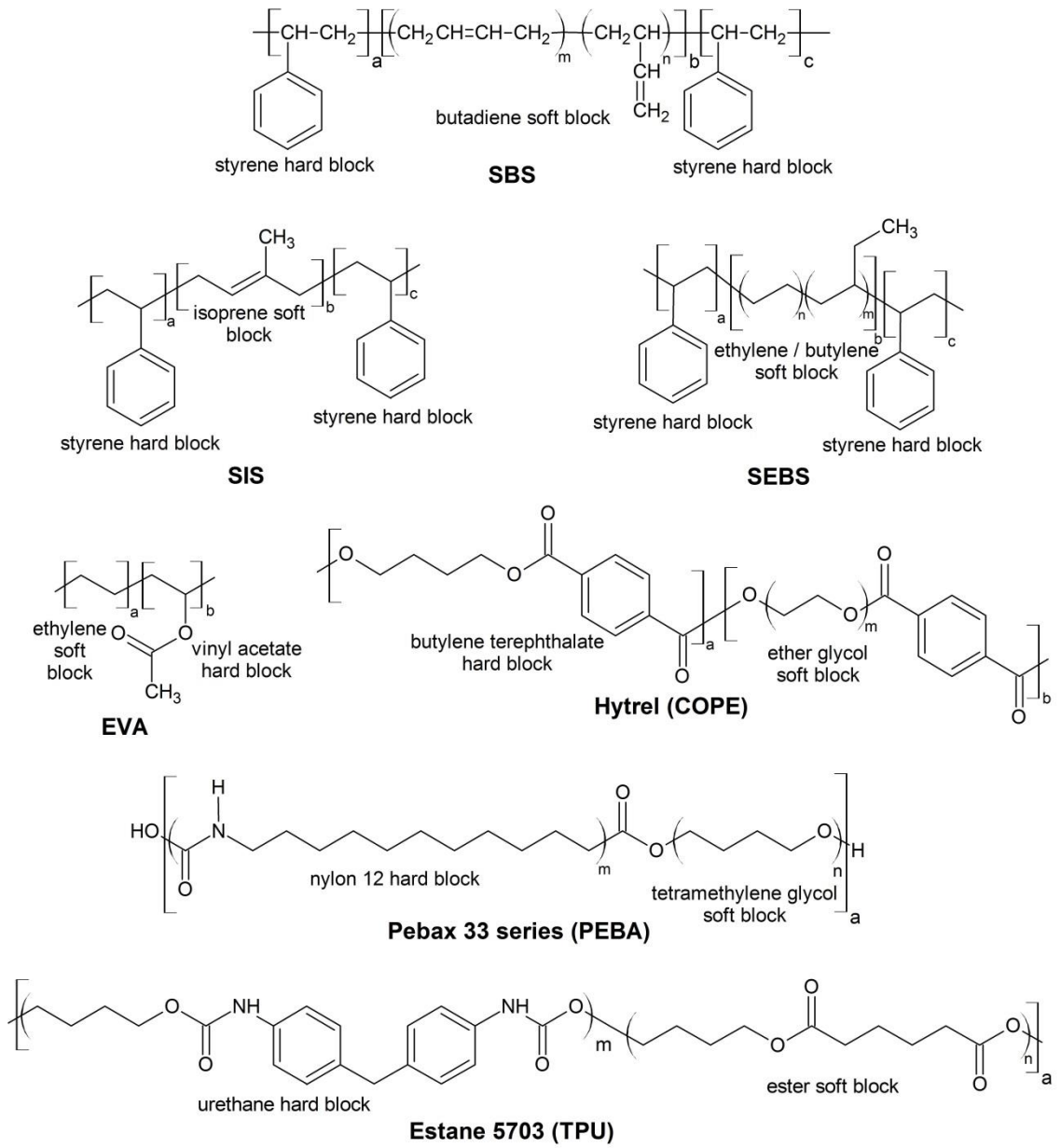

Figure 2-11 The molecular structure of selected TPEs.

2.4.3.1 Styrenic Block Copolymers (SBC)

Styrenic block copolymer TPEs have an A-B-A block structure, where A is the hard polystyrene segment and B is the soft segment. *Kraton* is a common brand name. The styrenic TPE *SBS* contains butadiene as the soft segment, *SIS* has isoprene, while *SEBS* has a random copolymer of ethylene and butylene. SBS

(styrene-butadiene-styrene) is probably the highest volume styrenic TPE. Styrenic TPEs are typically used in footwear, adhesives, bitumen modifications and some seals[67]. SEBS (styrene-ethylene/butylene-styrene) is manufactured by selective hydrogenation of the butadiene C=C bond. Not only does this improve the chemical resistance by eliminating the reactive double bond, it also improves the mechanical properties (increased tensile strength from up to 33 MPa for SBS[68] to 38 MPa for SEBS[69]). SIS (styrene-isoprene-styrene) is the softest (lowest modulus) of the styrenic TPEs, it also has the lowest viscosity during processing with a melt flow as low as 2 g per 10 minutes (5 kg load, 200 °C). It still maintains a tensile high strength (up to 28 MPa) and excellent elasticity (up to 1300 % elongation)[70]. Styrenic TPEs are always used commercially compounded with oil, polymers and/or fillers. This has a great economical advantage as the relatively expensive TPEs can be bulked out with inexpensive fillers and oils (up to 75 %). Additionally they can be formulated to meet the processing requirements (e.g. melt flow) and tailor physical and mechanical properties[71].

2.4.3.2 Ethylene Vinyl Acetate (EVA)

EVA is a copolymer of ethylene (soft block) and vinyl acetate (hard block). It is generally used as expanded foam for sport equipment and heel shock absorbers in shoes, in the non-expanded form it is used as a hot melt adhesive and in football boot cleats. The ratio of the two blocks can be altered to tailor its properties. It has good environmental stress cracking resistance and some grades can retain their elasticity down to -70 °C. EVA tends to have a low softening point, resulting in a low upper useable temperature. This is often improved by crosslinking with peroxides, creating a permeant crosslink (thermoset)[72]; [73].

2.4.3.3 Copolyesters Elastomers (COPE)

COPE TPEs have an A-B block structure, containing an ester as the hard block. Typically the ester block is polybutylene terephthalate, while the soft block will be an aliphatic polyether or polyester glycol. *Hytrel* is a common brand, this is a

copolymer of polybutylene terephthalate (hard block) with polyether glycol (soft block). COPE TPEs have a high tensile strength (up to 50 MPa), good flexibility over a wide range of temperature (T_g as low as -60 °C) and a wide range of hardness (24 to 70, shore D hardness)[74]. This makes them useful as engineering TPEs. They are tougher over a wide range of temperatures and easier to process than polyurethane TPEs (TPUs) [75,76].

2.4.3.4 Polyamide Elastomers

Polyamide elastomers contain a polyamide (nylon) block as the hard segment and either polyesters, polyethers, or polycarbonates for the soft. Polyether-*block*-polyamides (PEBAs) are the most common polyamide elastomer, in particular the Pebax brand. These are segmented block copolymers of the type $(A\text{-}B)_n$. The Pebax 33 series contains the polyamide nylon-12 as the hard block and polytetramethylene glycol (PTMG) as the soft block. PEBAs have great flexibility (up to 640 % elongation at break), good dynamic properties, outstanding impact resistance at low temperature ($T_g \approx$ -60 °C, unbreakable by ISO 180 at -40 °C), high tensile strength (up to 63.5 MPa) and easy processing[77]. They are used in noiseless gear, sport shoes and high performance extrusion products, e.g. paint spray hoses[76]; [78].

2.4.3.5 Polyurethane TPEs (TPUs)

TPUs are manufactured by reacting a diisocyanate with either a polyether, polyester or caprolactone glycol. Polyester TPUs have the best mechanical properties, for example Estane 5703 has tensile strength of 31 MPa and 630 % elongation at break[79]. These are used for thin walled flexible tubing and dental parts. The Estane brand is a common example of the polyester type, Estane 5703 has a urethane (hard) block made from MDI (Methylene diphenyl diisocyanate) and tetramethylene glycol with a poly(butylene adipate) soft block[80]. TPUs bridge the gap between typical rubbers and rigid plastics, they tend to be relatively hard with a Shore A hardness typically 70 to 80[67]; [81].

2.4.3.6 Thermoplastic Polyolefins Elastomers (TPO)

These are a blend of PP (polypropylene) with uncrosslinked EPDM (ethylene propylene diene methylene) rubber. These are typically relatively very hard elastomers (>80 Shore A), with limited range of elastomeric properties (tensile strength 13 to 22 MPa[82])[67]; [76].

2.4.3.7 Thermoplastic Vulcanisates Elastomers (TPV)

Again these are a blend of PP with EPDM, this time it is heated with a crosslinking agent, usually sulphur. They have a wide range of hardness (60A to 50D Shore) and reasonable elastomeric properties (Tensile strength 5 to 21 MPa, up to 620 % elongation at break.[67,83]

Table 2-10 Typical properties of different type of thermoplastic elastomers (TPEs).

TPE type	Hardness / Shore	Tensile Strength / MPa	Elongation at Break / %	Glass Transition / °C	Vicat Soften Point, Maximum Service Temperature / Glass Transition (T_g) / °C
SBS**[68]**; **[84]**	70A to 75A	up to 33	up to 880	-90	95 (T_g)
SEBS)**[69]**; **[84]**	60A to 75A	up to 38	up to 880	-55	95 (T_g)
SIS**[70]**; **[84]**	32A to 65A	up to 28	up to 1300	-60	95 (T_g)
EVA**[73]**; **[85]**	28D to 40A	up to 0.2		down to -70	55-65 (maximum service temperature)
COPE**[74]**	24D to 70D	up to 50	up to 480	down to -60	up to 150 (Vicat softening point)
PEBA**[77]**	25D to 72D	up to 63.5	up to 640	down to -60	130 to 174 (Vicat softening point)
TPU**[79]**	70A to 80A	typically 31	typically 630	-40 to -60	85 (Vicat softening point)
TPO**[82]**; **[76]**	>80A	13 to 22	up to 500	-	-
TPV**[82]**; **[67]**	60A to 50A	5 to 21	up to 620	-	-

2.4.3.8 Suitable Commercial TPEs for Propellants

The key properties of a TPE for use as a propellant binder are; suitable elastomeric properties (not too hard) over a wide range of temperatures, good compatibility and aging, as well as, low processing temperature (see section 2.4.4). Of the different types of commercially available TPEs; SEBS, COPE and PEBA are the most likely to be suitable (see Table 2-10). EVA would also be a

good candidate provided the formulation has a suitably wide temperature range where it is elastomeric. TPU and TPO will probably be too hard for propellants. TPV containing sulphur are also undesirable due to the health implication of SO_2 in the exhaust[86]. TPO and TPV are also less than ideal as they obtain their elastomeric properties by being blends.

2.4.4 Evaluation of Commercial Thermoplastic Elastomers (TPE) as a binder for Propellants

The binder is a fundamental part of a propellant and is highly influential in many of the properties of the final propellant. Two major types of binders are used in propellants; inert binders (e.g. HTPB) or energetic binders (e.g. NC). The key properties of a binder are:

1. Processing – Being able to manufacture the propellant in a safe and cost-efficient manner.
2. Mechanical Properties – Produce a propellant with good mechanical properties over the range of operating & storage temperatures.
3. Burning Characteristics – The propellant must have the chosen performance, burn well and cleanly (if required).
4. Cost & Availability – Ideally low cost and easy to obtain
5. Ageing – Long shelf life
6. End of Life Consideration – Easy disposal, preferably recycled.

2.4.4.1 Processing

The ability to safely and cost-efficiently manufacture a propellant is obviously crucial to a viable propellant; moreover the binder is one of the major factors in determining this. A number of factors are key to achieving this:

1. Ease of mixing – It should be easy to mix the components of the propellant together, hence this requires the binder (or pre-binder) to have a low viscosity[87]. For example Poly bd® R-45M HTPB pre-binder has a viscosity of 4000 mPa.s at 30 °C[88]. The mixture may be heated to reduce the viscosity and aid mixing. The viscosity could also be reduced by addition of a plasticiser or solvent. A typical HTPB based premix (with

plasticiser, curatives & other additives) can have a viscosity as low as 255 mPa.s at 60 °C[89]. If a solvent is added to the mixture, this will have to be removed later and can give rise to shrinking and cracking[90]. Use of solvents has an adverse environmental impact and reduction or elimination of their use in propellant processing has been investigated[91].

2. Low temperature processing – Excessive heating during manufacture can increase the chances of an accidental initiation of the propellant and an increase in degradation of the binder[92]. The typically maximum processing temperature for gun propellant is c.a. 120 °C[93].

3. Good Flow / Extrudable – The propellant mixture needs to be poured into a cast or extruded to form propellant grains. Rocket motors are either cast or extruded, while all grains of gun propellant are typically extruded[94]. Casting a rocket motor requires the mixture to have a lower viscosity than if it was extruded. The viscosity of 532 Pa s at 60 °C was reported as the average end mix viscosity of typical AP/HTPB cast propellant after addition of the curative[87]. In comparison a double base propellant (JA2 equivalent) was found to have a viscosity of 117 kPa s at 80 °C (shear rate of 1 s^{-1})[95].

4. Good Pot Life – For a cured binder system there will be a period of time after the curing agent has been added that the viscosity remains low enough for the propellant to be worked on, this is known as the ‘pot life’. After this period the propellant would be too viscous to mix, transport or cast into motors. Thermoplastics (such as PVC and TPEs) do not generally have a pot life as they typically use temperature to reduce the viscosity to a workable range.[46]

5. Short Cure Times – While a long pot life is useful for the first part of propellant manufacture a short cure time is clearly helpful once casted, allowing for faster manufacture of the propellant[96].

In industry, TPE are typically processed by extrusion or injection moulding. The extrusion process would be very suitable for the manufacture of propellant and is

used for the manufacture of extruded double based propellant and PVC composite propellants[97]. However, typical processing temperatures of TPE are around 200 °C[98], this is required to reduce the viscosity sufficiently. This would be too high for processing energetic material (ca. 120 °C for processing gun propellant[93]). This issue is compounded as composite propellant would be a highly filled TPEs. Despite the filler particle not generally altering the viscosity of the polymer, they interfere with the flow lines of the liquid phase, giving rise to a larger apparent viscosity[99]. The processing temperature could be reduced in a number of ways. Firstly, by selecting a TPE which can be processed at a lower temperature, but with commercially available TPEs this would still be too high. The TPE could be plasticised to reduce it viscosity[100] or addition of a suitable solvent into the mix should give a large reduction in its viscosity[101].

Instead of extrusion processing, a propellant may be shaped by hot pressing. This involves placing a moulding powder (filler coated with polymer) into a hot mould and subjecting it to a compression force to consolidate the powder. This can operate with a polymer that has a much higher viscosity[102], as the process involves sintering which takes place using surface flow mechanisms and plastic deformation. The moulding powder is usually manufactured by a solvent evaporation process. Here the polymer is dissolved in a suitable solvent, then mixed with the filler before evaporating the solvent.

2.4.4.2 Mechanical Properties

A propellant binder needs to be sufficiently elastic so that stress cracks do not occur in storage, in service or during combustion[103]. The propellant must also be sufficiently strong and stiff so that it does not break apart, deform[104] or slump[51] over time. Conventionally, the binder used in composite propellants is in it ‘rubber’ state for the entirety of its storage and operational temperature range. This requires it glass transition point (T_g) to be below the minimum storage or operated temperatures. Plasticisers maybe incorporated in to reduce the glass transition and increase the plasticity.

The mechanical properties are also greatly affected by the addition of a large percentage of filler. The hard filler will impart a large effect on the overall mechanical properties of the composite. This is mainly due to the steric hindrance of the filler particles, but also related to the interaction between the filler and binder[103]. This interaction can be modified by use of a 'bonding agent', these additives increase the strength of the interaction between the filler and the binder, hence increasing the mechanical properties in the vicinity of the solids[105]. Bonding agents will increase the viscosity of the uncured mix, one study finding an increase of up to 70 % in the apparent viscosity of a HTPB propellant when it contained the bonding agent[106].

TPEs should have very good mechanical properties for propellants[8]. Being elastomers they are in a rubbery state in their working temperature range. They are well known for their ability to dissipate or absorb energy on impact, this stops craze (a network of fine defects) or crack propagation[107]. TPEs are regarded as having a wide working range of temperature, known as the service temperature window (typical -30 to +140 °C[67]). The service temperature range is dictated by a lower glass transition point (T_g) and the softening point. A very wide service temperature range would be preferable, even for TPEs it will be difficult to find a TPE that is suitable. Additionally, to achieve processing at relatively low temperatures the softening point will have to be low, reducing the upper service temperature. TPEs are available which have very low working temperatures (e.g. -68 °C[108]), however these may not have other desirable properties, for example too lower an upper service temperature. Even TPEs which do not have low enough service temperatures could potentially be improved by use of a plasticiser, reducing their T_g. Alternatively, there may need to a compromise over the service temperature range in order to obtain the improved mechanical properties of TPEs.

2.4.4.3 Burning Characteristics

The performance of a propellant is typically reported differently depending on whether it is a gun or rocket propellant. For gun propellants, the impetus or force

constant is generally reported. This is the amount of energy in a propellant that can be used to propel a projectile.

For rocket propellants, the specific impulse ( ) is commonly reported. This informs us of the total impulse (thrust x time) of a propellant in a specified rocket motor. The specific impulse can be split into two terms characteristic velocity ( ) which depend on the propellant and the trust coefficient ( ), dependant on the motor hardware, were:

2-4

The characteristics velocity ( ) is a more useful measure for comparing rocket propellant but generally specific impulses are reported with standard rocket motors.

In addition to knowing the performance of the propellant it is important to know how fast the propellant is burning, known as the burning rate. The burning rate depends on the propellant burning surface area, the propellant density and the rate of regression . The rate of regression can then be related to two useful coefficients of a propellant by Vieille's Law(2-5):

2-5

Where the is the propellant burning rate coefficient and is the propellant pressure exponent.

The burning characteristic depends greatly on the choice of filler, either an oxidiser (possibly with aluminium) or nitramine, and the solid loading. The performance (the impetus or specific impulse) is an obvious key property of a propellant; also the energy density is important, too low an energy density would result in an unfeasibly large volume of propellant needed in the munition[8].

Ignition issues have been noted with nitramine propellants with inert binders (see section 2.3.2.4).

Other burning characteristics are important as well, for gun propellant an important factor is barrel wear. This is typically governed by the flame temperature and any corrosive or reducing products formed[109]. Propellant containing oxidisers tend to have flame temperatures too high for gun propellants. Additionally, chlorine containing compounds (e.g. AP) produce corrosive HCl when burning in a propellant, this corrosive gas would create too much barrel wear for a gun. Hence AP is not used in gun propellants. Excessive amount of soot can also lead to carbonaceous deposit creating additional problems. For rocket propellant the amount of smoke formed is also an important property for tactical reasons. The amount of smoke is principally due to either poor combustion of the propellant creating excessive amount of soot, aluminised compositions creating aluminium oxide or HCl from chlorine contain compounds[110].

Commercial TPEs would be inert binders (non-energetic), in a propellant containing an oxidiser they would act as the fuel, while in a nitramine filled propellant they would not be adding to the energy of the propellant. Compared to an energetic binder this would result in a lower energy density and lowered performance. This could potentially be offset by reducing the binder content, providing the mechanical properties are acceptable. A propellant made from a nitramine and inert HTPB binder ('YH01012') has been reported to have a force constant of 1170 J g^{-1} with a flame temperature of only 2900 K[37], which compares favourably with a double-base propellant (940 to 1180 J g^{-1} & 2600 to 3600 K[12]). The exact composition is not known and energy may have been increased using an energetic plasticiser. More typically, a force constant of 1082 J g^{-1} with flame temperature of just 2802 K was reported for a RDX / inert binder (cellulose acetate) based propellant[35]. As a TPE propellant may have other desirable characteristics, ballistic performance broadly similar to that of traditional propellant would probably be acceptable.

2.4.4.4 Sensitiveness

Reduced vulnerability characteristics of a munition have many benefits, including increased safety, more flexibility and reduced safety measures on handling, transport and storage[111]. The propellant is an important component in influencing the vulnerability[112]. It would therefore be logical that any new propellant being developed would show a tendency for improving the safety characteristics when inserted into a munition. TPEs have an excellent ability to absorb impacts, hence they should greatly reduce the force of impact or friction onto the energetic component, reducing the sensitiveness.

Small scale hazard testing of Rowanite 318 (TPE/NC/nitramine based propellant) by BAE Systems, has shown a lower overall sensitiveness (sensitivity to impact (FofI), friction and ignition temperature) of the propellant compared to double-base propellants. Further, IM testing on same propellant has given an equal to better response to testing for all criteria compared to a high energy conventional propellant[32]. TNO have also tested IBK1037 (TPE/RDX composition) and found an improvement in the shaped charge test when compared to a similar commercial available propellant[40].

2.4.4.5 Cost and Availability

Ideally the binder would be made from a low cost material and have suitable properties. Elastomers manufactured for the mass market could fulfil these requirements. The elastomer needs be in good supply (constantly available), never altering or changing composition. Supply from the USA can also be an issue due to International Traffic in Arms Regulations (ITAR) which restricts and controls the export of defence and military related technologies[4].

Commercial TPEs are one of the more expensive polymers ranging from €2 to €13 per kg as reported in 2007[113]. However, they are considerably lower in cost than manufacturing a specialist polymer. While availability may be very good, they are usually only available pre-blended with stabilizers, bulking agents or mechanical property enhancers. These can be changed over time at the will of the manufacturer to ‘improve’ their product or maximise profits. Even small

changes to a propellants composition could potentially have a dramatic effect. For instance, a new component could be incompatible with the other ingredients or migrate over time. The mechanical properties could be altered, particular at extreme temperatures, making it more susceptible to cracking or deforming. Requalification of the propellant due to small changes would be prohibitively expensive.

2.4.4.6 Ageing

A good binder would ideally be chemically stable and not require a chemical stabiliser in its formulation. The binder should also be chemically inert and not react with any of the other ingredients in the propellant. Its mechanical properties should not change over time, notably, it is undesirable for a binder to harden and become brittle with age. For example, HTPB propellants will become more stiff and brittle over time due to oxidative cross-linking of the binder[114]. TPEs are commercial polymers and as such they have excellent ageing properties, if stabilisers are required these are well known, often TPEs do not even require any[115]. Despite generally being fairly chemically inert, some TPEs may interact with the chosen filler and additives over time. This would typically cause a degradation of the polymer which would impact on the mechanical properties of the polymer. For instance, HNF is known to be incompatible with cured HTPB causing oxidation of the C=C bond, leading to the polymer becoming rigid and hard[116].

2.4.4.7 End of Life Considerations

Decommissioning of munitions by removal of current propellants can be extremely difficult, consequently munitions are often destroyed by open burning / open detonation. Being able to recycle would clearly have a significant environmental advantage.[117] Due to the lack of permanent crosslinking, propellant with a TPE binder should be more easily recycled. This could be achieved either by heating to melt the binder, use of solvents or a combination of heat and solvent.

2.5 Energetic Fillers

Energetic filler can either be an oxidiser, which releases oxygen to burn the binder as a fuel, or an explosive, which will burn, generating heat which decomposes the binder. Oxidisers tend to be more favourable for use in rocket motors, mostly due to their high flame temperatures. Explosive fillers tend to have small critical diameters, this is not an issue for gun propellants were the grain size is even smaller. Hence explosive fillers can generally be used without the concern of the propellant becoming detonatable. However for larger grains found in rocket motors would be detonable (type 1.1). Explosives (usually nitramines) are added to some rocket propellants, however they are never the main energetic component (< 40 % m/m [46]) to reduce this risk of detonation.

Table 2-11 and Figure 2-12 lists the energetic fillers that are evaluated in this section for incorporating into a TPE propellants.

Table 2-11 Current and potential energetic fillers for propellants.

Energetic filler	Oxidiser or explosive	Suitable for rocket or gun propellants
Ammonium Perchlorate (AP)	Oxidiser	Rocket
Ammonium Nitrate (AN)	Oxidiser	Rocket
Ammonium Dinitramide (ADN)	Oxidiser	Rocket
Hydrazinium Nitroformate (HNF)	Oxidiser	Rocket
Nitramines (RDX & HMX)	Explosive	Rocket and gun
FOX-7	Explosive	Rocket and gun
CL-20	Explosive	Rocket and gun

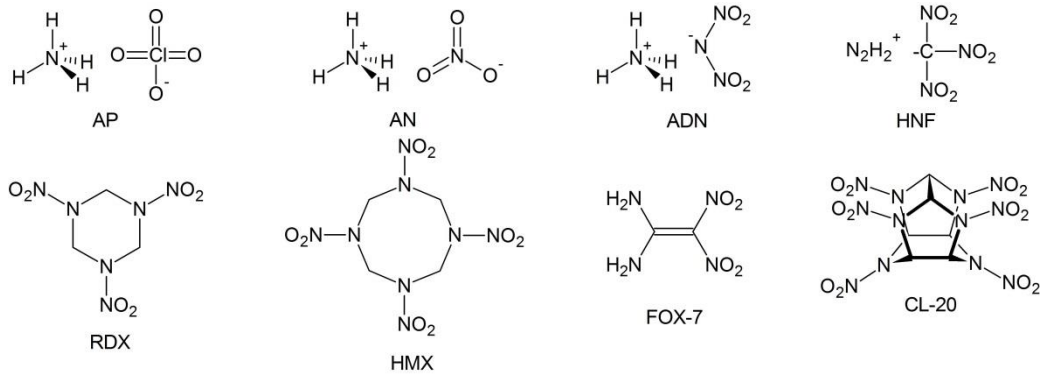

Figure 2-12 Molecular structure of Ammonium Perchlorate (AP), Ammonium Nitrate (AN), Ammonium Dinitramide (ADN), Hydrazinium Nitroformate (HNF), Nitramines (RDX & HMX), FOX-7 and CL-20

2.5.1 Ammonium Perchlorate (AP)

AP is by far the most widely used oxidiser in solid rocket propellants, this is due to its good stability and excellent performance (high burn rate and density). Use of AP does have its problems, combustion of AP containing propellant typically contains 14.5 g of hydrogen chloride (HCl) and up to 1.4 g of chlorine gas per 100 g of propellant burnt[118]. These are highly corrosive and toxic, as well as contributing to acid rain. There have been instances of this having a measurable impact of the environment around launch sites, most notable the NASA Space Shuttle launch pad. Here acid deposition due to HCl in the exhaust from solid fuelled rockets has caused an increase in fish and plant mortality and a reduction in plant diversity. However this has been described as ‘a small manageable impact’ by NASA[119]. Recently there has been growing concern about the toxicity of perchlorate compounds, which are known to interfere with thyroid ability to produce hormones[120]. The US environmental protection agency has proposed to regulate the amount of perchlorate ions in drinking water, somewhere between 4 and 23 µg L^{-1}[121]. This would have an immense impact on the manufacture, demilitarisation and possibly even use of AP containing propellants[122].

The production of HCl in the exhaust has a further issue of creating considerable smoke, by forming an aerosol with water in the atmosphere or exhaust giving it a

white plume. This problem is further increased when aluminium is used as a fuel, due to formation of aluminium oxide[51]. Reduced smoke propellants have been developed by removing the aluminium, lowering the energy density. Later high-energy minimum smoke propellants were developed by removing most of the AP and replacing it with a mixture of nitrate ester plasticisers (nitrate ester plasticised elastomers, NEPE) and RDX or HMX. These tend to be vulnerable to impact and detonable (class 1.1), as well as having a limited range of burning rates (approx. 2 to 15 mm s^{-1} at 7 MPa) [49].

2.5.2 Ammonium Nitrate (AN)

There has been a large amount of research into using AN as an oxidising filler in composite propellants [123];[124];[118];[125]. Despite this, the references to AN being employed in munitions are; a pyrotechnic igniter composition of the VULCAIN liquid rocket engine for the ARIANE 5 – made from PSAN (phase stabilised ammonium nitrate) and HTPB binder[126], and ESSM rocket motor (assuming it was not changed from development) – containing AP and some AN with a HTPE binder and energetic plasticiser[127]. Ammonium nitrate has been a promising alternative to AP for many years. Unlike the chlorine containing AP, AN burns cleanly not emitting HCl. HCl is not only bad for the environment but also help to creates secondary smoke. Many issues have hampered the development of AN containing propellants, the main issues are:

- A phase transition around room temperature, which results in cracking due to volume changes.
- Ignition issues due to poor ability to burn under atmospheric pressure.
- Hydroscopicity.
- Poor mechanical properties.
- Low performance of AN composite propellants, including low burn rate and impulse / c*.

A lot of research and development has gone into reducing the effect of the phase transitions in ammonium nitrate, in particular the IV to III transition at 32 °C. This transition can be suppressed with the addition of other certain metal salts,

creating so-called phased stabilised ammonium nitrate (PSAN). Notably adding potassium salts, often potassium dinitramide (KDN) which has an stabilising effect without an energy penalty. Many metal salt and metal nitrates can also have a similar effect, some transition metal compound can also increase the burning rate, reduce the ignition problems. Another advantage of PSAN is that the hydroscopicity is often reduced compared to AN[124].

The issue of poor mechanical properties could well be improved by using bonding agents more suited to ammonium nitrate[128].

Ammonium nitrate not only has a lower enthalpy of formation (-4.514 kJ g^{-1}) than AP, but it density is lower as well (1.725 g cm^{-3})[129]. Therefore, AN has a lower energy density than AP. To improve the energy in the propellant an energetic binder and / or plasticiser could be used[118]. Energetic plasticisers have been used in many other propellant formulations and have been well tested over time, energetic binders are still under investigation, often due to poor mechanical properties. Lower burn rates are typical of AN propellant, which is thought to be due the slower rate of reaction of nitrogen oxides from AN in comparison to chlorine oxides from AP reacting with typical binders. The flame temperature is also reduced (typically 2000 °C), which can cause problems with efficient ignition of aluminium in aluminised propellants, catalysts may correct this. The burn rate may be altered by changing the particles size of the AN, however, this change is only small, especially in comparison to AP[124]. It has been calculated that addition of high energy fuels (such as Al, Be or hydrides) should significantly increase the impulse and overall energy, make an AN propellant more viable.[129]

Instead of using PSAN as the only oxidiser, using a mixture of PSAN and AP has many advantages. There would be a potential reduction in costs from using PSAN and the amount of HCl emitted in the exhaust would be reduced. Burn rates of the PSAN/AP propellants where comparable to AP propellants, with the specific impulse and densities only slight affected[130].

2.5.3 Ammonium Dinitramide (ADN)

ADN has been suggested as a good alternative to AP, primarily as it does not contain chlorine and has a good predicted performance (particularly specific impulse / c*)[124], increasing when aluminised[3]. ADN looks most promising for use in liquid propellants system, primarily to replace hydrazine[131,132]. For example Eurenco's LMP103S dissolves ADN in a mixture of methanol, ammonia and water[133]. More challenging is the use of ADN for solid propellants. ADN has a higher sensitiveness to both impact and friction than AP and a low auto-ignition temperature (160 °C[134]), in addition the current costs are high. ADN has needle shaped crystals which hinder solid loading[135]. To solve this, ADN is made into prills, however, it is thought this increases the sensitiveness[136]. The burn rate and pressure exponential are both very high, this is thought to be due to the ADN melting at low temperatures[137]. Possibly a burn rate modifier or improved binders could be used to reduce this[138]. ADN is also incompatible with isocyanates, spontaneously reacting and decomposing, hence traditionally cured HTPB cannot be used as a binder[139].

Using a mixture of ADN and AN has been considered, particularly for space rocket application [140,141]. It was thought that by adding the insensitive AN, the sensitiveness of the ADN propellant would be reduced, without too much effect on the overall performance. The performance was found to be reasonable for the ADN/AN mixture, although the sensitiveness did not reduce by much.

2.5.4 Hydrazinium Nitroformate (HNF)

HNF is a promising oxidiser filler, a pilot plant for its production was built at Aerospace Propulsion Products (APP) back in 1992[142]. Despite its relative poor oxygen balance in comparison to AP, its much less negative heat of formation results in a high theoretical specific impulse (2500 m s^{-1} for HNF/HTPB 86 % m/m fill, expansion ratio 60:1[142]and given it high density (1.86 – 1.93 g cm^{-3}[143]) has good specific impulse density. Unlike nitramines, the highly exothermic combustion reaction between HNF and its binder occurs on the surface of the propellant. This is more efficient at heating of the surface of the

propellant, resulting in high burn rates[144]. Unlike AP it doesn't contain chlorine and so should have a cleaner exhaust with minimum smoke. It's melting point of 115 – 124 °C should be high enough for current processing of propellants. Additionally it is not hydroscopic[145].

HNF main issues is its sensitiveness, this is highly dependent on the purity, particle size and shape. Reports of impure HNF having an extremely poor impact sensitiveness (< 1N m BAM impact), while purified HNF is much better (≥ 15 N m), in general it was found still more sensitive than AP, RDX or HMX[143]. Recently several attempts to alter he crystal shape and / or size of HNF crystals have reduced the sensitiveness. In particular, reducing the length to diameter ratio seems very important[146]; [147]. HNF composition also suffer from poor thermal stability, this has been studied with HTPB binders, which is believed to be particularly bad due to oxidation of the double bond caused by reaction of HNF with isocyanates[143]. Stability has been improved with higher purity HNF and use of stabilisers, although stabilities improved, they were still too poor for real life applications[142]. HNF compositions were found to have to very high burn rates and pressure exponentials. Similarly to AP compositions, the pressure exponential was reduced in HNF/HTPB formulations by reducing the particle size. Theoretically, burn rate modifiers should also help improve this. Reducing particle size also caused impact and friction sensitiveness to be reduced, but was still relatively poor, additionally there was a decrease in the thermal stability[148]. Theoretically, use of an energetic binder, such as GAP, should be compatible with HNF[145]. However, a study by FFI, found the stability of HNF/GAP to be poor[149]. Additional, HNF decomposes after melting (ca. 123 °C[143]), this relatively low decomposition temperature could indicate an poor reaction to thermal stimuli (eg. IM cook-off tests). A successful manufacture method has been difficult to achieve for HNF, the best method with mild reaction condition and acceptable yields is considered expensive. There is currently only limited production of HNF in China and India[145].

2.5.5 Nitramines

Unlike fillers that are oxidisers, nitramines are explosives which decompose, turning to gas at the burning surface. Nitramines being oxygen deficient do not generate a significant amount of oxidiser species. Hence, an inert binder in a nitramine composite propellant is mainly acting as a binder, holding the filler in place. The heat generated by the decomposing nitramine will decompose the binder, due to this being an endothermic process it will reduce the flame temperature and hence reduce the burn rate.

2.5.5.1 RDX

RDX is employed as an energetic filler in current LOVA gun propellants, for example XM39 or EX99. As discussed in section 2.3.1.4, replacing nitroglycerine and most of the nitrocellulose in a typical gun propellant has the effect of reducing its sensitiveness to impact, friction and heat. The RDX used in these propellants is much finer than the typical grade used as an explosive (e.g. a main charge), typically D_{50} = 4-6 µm. Bofors' requirement for EX99 in 2002 where for the RDX to have a D_{50} < 4 µm with >99% less than 16 µm, however these where not finalised[150]. The report went on to compare pastes and propellant made from this finer RDX and the coarser standard class A RDX (exact size not reported). It was found that the impact and friction sensitiveness was less for the finer RDX pastes and propellants, with the ESD (electro static discharge) tests being better or the same. Song *et al.*[151] showed that particles size of RDX affects the mechanical and thermal sensitiveness of the pure explosive. The mechanical (friction) and thermal (cook-off) sensitiveness decreased with smaller particle sizes. They also show that a broader distribution of sizes lead to increased sensitiveness. Spear *et al.*[152] research into the effect of particle size of RDX in binderless fuse trains, showed a more complicated picture. Finer particles were found to make the RDX harder to ignite, but the RDX could grow to detonation more rapidly. Decreasing the particle size of RDX also generally decreases the critical diameter [153], although this can be affected by the porosity of the RDX[154]. Increasing the critical diameter reduces the likelihood of detonation, as does reducing the propellant grain size. Hence, gun propellants with smaller

grain sizes can be considered non-detonatable (type 1.3), while larger size rocket motors with nitramine fillers are detonatable (type 1.1)[49].

The particle size of RDX has been shown to have an effect on the burning rate (β) and pressure exponential (α) of the propellant. Work at the High Energy Materials Research Laboratory, Pune on RDX/NC[155] and RDX/CA/NC[156] propellants showed that as the particle size was reduced, so did the burning rate and pressure exponential. They were also able to obtain higher bulk densities of RDX/CA/NC with smaller particle sizes. This is generally attributed to the molten layer which is formed as RDX burns[157]. It is believed that finer particles form a thicker layer which in turn reduces the burning rate. It is noted that the burning rate for RDX (& HMX) is much less dependent on the particle size than AP. The burning rate is also generally much lower for RDX propellant than AP, 1.1 mm s^{-1} compared to 5.3 mm s^{-1} for 80 % m/m filled PU (polyurethane) propellant at a pressure of 2 MPa[158].

2.5.5.2 HMX

HMX and RDX are chemical very similar, both being cyclic nitramines. Only RDX is used in current 'in service' LOVA propellants, although some high energy rocket propellants do contain HMX[49]. HMX does have a higher explosion temperature (327 °C (5-seconds)) and cook-off (210 °C) compared to RDX (260 °C & 180 °C, respectively). However, the addition cost of HMX (double or more, that of RDX) is probably the driving factor to the use of RDX[159]. Additionally, the burning rate of RDX propellant is greater than HMX for the same percentage fill, due to the larger heat released at the burning surface, increasing the flame temperature[158]; [160].

As with RDX, the burn rate (β) and pressure coefficient (α) of HMX decrease with decreasing particle sizes. Again as with RDX, the burning rate is much lower than for a comparative composite AP propellant. There is also a similar issue to RDX propellant burning at low pressures, causing ignition problems. This is believed to involve HMX melting, which then forms a layer over the burning surface[161].

HMX composite propellants also have a low flame temperature (2000 K[162]), again similar to RDX.

2.5.6 FOX-7 (1,1-diamino-2,2-dinitroethene)

First synthesised in 1998 by Latypov[163], FOX-7 is an explosive which could be used as an energetic filler in propellants. FOX-7 has many positive attributes, firstly, it should have good environmental signature, primarily due to it not contain chlorine. FOX-7 has a low friction and impact sensitiveness, better than RDX or HMX and a high decomposition temperature (238 °C, by DSC). It has a high density (1.878 g cm^{-3}) with a reasonable oxygen balance (-21.6 %), the same as RDX and HMX[164].

The properties of FOX-7/HTPB propellants were investigated by Chen *et al.*[165]. These were compared against RDX/HTPB, finding that the mechanical (friction and impact) and electrostatic sensitiveness was significantly reduced. Florczak *et al*.[166] compared AP/PBAN/Al/FOX-7 with AP/PBAN/Al/HMX compositions, containing 22 % FOX-7 or HMX. The burn rate was found to be 17 % less (at 0.1 MPa) for the FOX-7 composition compared to HMX. However, the FOX-7 composition could not be detonated when initiated by a RDX/TNT booster (HT-14), unlike the HMX composition. Lempert *et al.*[167] calculated the theoretical effect of replacing AP with FOX-7 in an inert hydrocarbon binder, they reported a slight decrease in the specific impulse up to 30 % FOX-7. Replacing more AP caused the specific impulse to dramatically decrease. Although, using an energetic binder ($C_{18.96}H_{34.64}N_{19.16}O_{29.32}$) gave them a much better specific impulse even above 30 %. Tests on compositions with energetic binders (FOX-7/GAP) gave good mechanical properties, but poor theoretical specific impulses (2230 to 2320 m s^{-1} at 70:1 expansion), they also gave poor burn rates, particularly at low pressures. A mixture of AP and FOX-7 in a nitrate ester plasticised GAP binder, did burn smoothly and produced thrust (213 to 296 N, 60 mm web, 49 to 141 bar) suitable for shoulder launch weapon[168,169].

2.5.7 CL-20 (Hexanitrohexaazaisowurtzitane)

CL-20 or HNIW is an explosive with a strained cage structure, giving it a high positive heat of formation (ca. +400 kJ mol^{-1}) [170]. Again CL-20 has the advantages of not containing chlorine, additionally it should have superior performance to RDX or HMX, thanks to its high heat of formation, high density (2.04 g cm^{-3}) and reasonable oxygen balance (-10.9 %) [127,145]. Propellant compositions made with GAP binder and 60 % m/m CL-20, had a better burn rate (27.2 mm s^{-1} at 15 MPa) than HMX, the high pressure exponential was improved with a burn rate modifier (0.94 reduced to 0.48). The sensitiveness in 30 kg fall hammer test was 3.5 to 4 m, similar to the highly vulnerable XLDB (cross linked double-base) propellant with NEPE (energetic plasticiser) [171]. Weiser *et al.*[172] tested a 70 % m/m filled composition of CL-20/GAP, finding a burning rate of 15 mm s^{-1}, twice that of a comparable HMX based composition.

CL-20 greatest disadvantage is its very complicated manufacture, this results in an extremely high price, reported as being €1000 / kg in 2005[139].

2.5.8 Summary of Energetic Fillers

For rocket propellants, none of the alternatives to AP can match all of it desirable properties, see Table 2-9. Ammonium nitrate is already used to replace part of the AP in some rocket compositions. With the poor mechanical properties of AN containing propellant appearing to have been resolved by using phased stabilised ammonium nitrate, AN propellants biggest issues is their lower performance. However, this could be offset by using energetic plasticiser, binders or both to compensate for this loss. Both ADN and HNF have a relatively poor sensitiveness compared to AP, this could possibly be improved further or deemed within acceptable limits. The higher cost in particular of HNF is a major issuse. Nitramines are already used in rocket propellants, their small critical diameter, resulting in detonatable propellants is their greatest disadvantage.

Table 2-12 Summary of properties of various energetic filler for propellants.

	AP	AN	ADN	HNF	RDX/HMX	FOX-7	CL-20
Performance (I_{sp})	High	Low	High	High	Low	Low	High
Burn Rate	Good	Low	High	High	Low	Low	High
Sensitiveness	Good*	Very Good	Poor	Poor	Good	Good	Poor†
Cost	Low	Very Low	High‡	High	Low	High‡	Very High
Environmental Impact	High	Low	Low	Low	Low	Low	Low

*Some poor IM tests results.

† Some evidence of good in formulations.

‡ Would be likely to fall with larger production.

Gun propellants already use nitramines as an energetic filler in LOVA propellants, the smaller grains size ensuring that they are non-detonatable. FOX-7 could potentially be a good alternative to nitramines, the price would have to reduce greatly as cost is a major factor for gun propellants. The extremely high cost of CL-20 would make it unstable for gun propellants.

2.6 Plasticisers

Plasticisers are used with gun and rocket propellants, in both nitrocellulose based and composite propellants. They are generally non-volatile, low molecular weight liquids, which must be compatible with the other ingredients in the propellant. Plasticisers are added to the composition for a variety of reasons depending on the type of propellant. In nitrocellulose based propellants, plasticisers improve the mechanical properties of the propellant making it less brittle (reducing the modulus and increasing the elongation), as well as decreasing the hardness. The tensile strength will also be reduced, which is undesirable. Additionally the glass transition (T_g) will be reduced. This should reduce the likelihood of the propellant cracking or breaking apart on impact, especially at lower temperatures, due to its increased flexibility. This would result in a far larger area of the propellant surface exposed on ignition, leading to unstable high rate of burning[173]. The plasticiser

also aids extrusion, reducing the viscosity of the paste or 'dough'[174]. If nitroglycerine is present, plasticiser can reduce the sensitiveness of the NG in the mix and propellant[50]. For composite propellants, addition of plasticiser is useful to reduce the viscosity when mixing the pre-cured polymer with the solid fillers to ease mixing, especially with for finer particles[175]. The mechanical properties of the propellant can also be improved, especially by the lowering of the glass transition (T_g), composite propellant are more likely to crack or facture on impact in their glass-state[46,55]. Again the polymer will become less brittle, reducing the likelihood of the binder breaking on an impact.

Plasticisers should have a good miscibility with the polymer, ideally having the ability to penetrate both the amorphous and crystalline regions. The effectiveness of the plasticisers should also be considered, however this depends on what effect on the polymers properties are desired. The plasticiser should also be long-lasting in the polymer, having a low tendency to migrate. Often there is a balance between using a smaller molecule for a plasticiser which has a higher diffusion in the polymer and therefore a greater effectiveness, and a larger molecule which has a lower vapour pressure and therefore should migrate out the polymer less.[176]

2.6.1 Selection of a Plasticiser

The propellant and explosive industry use many different plasticisers depending on the composition of the propellant and the desired effect of the plasticiser. Firstly the plasticiser must be stable over time with all the components of the propellant. Next, it must have good compatibility as a plasticiser with the binder, good miscibility and low migration. Selection also depend on required effect on the mechanical properties, does the T_g need to be lowered or do the elastic properties need to be generally improved to reduce the sensitiveness. Finally, does the propellant need the extra performance from an energetic component over an inert plasticiser.

2.6.2 Theory of Plasticisation

Several theories exist on how plasticisers affect polymers, the most simple is the *lubricity theory*. This theory states that plasticiser molecules are inserted between the polymer chains, shielding the chains from each other and so preventing a rigid network from reforming. This simple theory is unable to explain the differing efficiency of different plasticisers with polymers. The *gel theory* extends the lubricity theory, here the plasticiser breaks the attraction between polymer chains by masking the centres of attractions from each other. Further plasticiser then swells the polymers like a gel, allowing an easier movement of polymer chains. The strength of the interaction between the plasticiser and the polymer chains can be measured by the Flory–Huggins interaction parameter ( ). This must be similar to that of the interaction between the polymer chains, otherwise there will not be a good compatibility.[177]

The *free volume theory* can also be used to explain plasticisation of polymers. A rigid unplasticised polymer contains little free volume, allowing only modest motion of the polymer chains. The addition of plasticisers increase the amount of free volume, as the packing of the polymer mixture is no longer as efficient. A plasticiser that does not interact well with the polymer chains will simply fill the free volume and reduce the molecular motions. Hence, potentially having the reverse effect usually desired by addition of a plasticiser. By combining the free volume theory with that of lubricity and gel theories, it can be seen that an efficient plasticiser should also screen the attraction between polymer chains and swell the polymers allowing increased molecular motion, hence a greater effective free volume.[177]

The effect that plasticisers have on the of a polymer can be modelled using the Fox equation (2-6) [61]. This equation is based on the free volume theory and was first derived to describe the of random copolymers.

$$\frac{1}{T_g} = \frac{w_1}{T_{g1}} + \frac{w_2}{T_{g2}} \qquad \textbf{2-6}$$

Where T_g is the glass transition of the polymer blend, T_{g5} is the glass transition of the pure polymer, T_{g6} is the glass transition of the plasticiser and S_5 & S_6 are the weight fractions of the polymer and the plasticiser respectively.The effect the plasticiser has on the T_g of the polymer can be assumed to be linear (2-7).

$$T_g = T_{g5} + G \cdot S_6 \qquad \textbf{2-7}$$

Where G is the plasticiser coefficient (usually between 200 - 500 K). However, this equation (2-7) will only give a good estimate of the T_g of a plasticised polymer for low concentrations plasticiser. For larger concentrations the empirically derived Jenckel and Heusch equation (2-8) is often used.[178,179]

$$T_g = (T_{g5} + (T_{g6} - T_{g5}) \cdot k \cdot S_6) \cdot S_5 \qquad \textbf{2-8}$$

Where b is a constant that depends on the plasticiser-polymer system.

Plasticisers for propellants can be divided into inert (non-energetic) and energetic plasticisers.

2.6.3 Inert (Non-energetic) Plasticisers

Inert plasticisers will reduce the ballistic performance as they lower the oxygen balance, this affects both the force constant / specific impulse and burn rate of the propellant. The flame temperature will also be reduced, for gun propellants this is often a desirable effect of using an inert plasticiser. Typically inert plasticisers are esters or simply hydrocarbons. The ester type are by far the most common, being more polar, they have a greater effect on the polar nitrocellulose based propellant and the polar pre-cured polymers used in composite propellants[180]. See Figure 2-13 for selected common inert plasticisers. Examples of plasticisers for nitrocellulose based propellants are triacetin, diethyl phthalate (DEP) and diethyl phthalate (DOP), examples for composite propellants are dioctyl adipate (DOA) and dioctyl sebacate (DOS), while the LOVA propellant XM39 contains acetyl triethyl citrate (ATEC)[28,29].

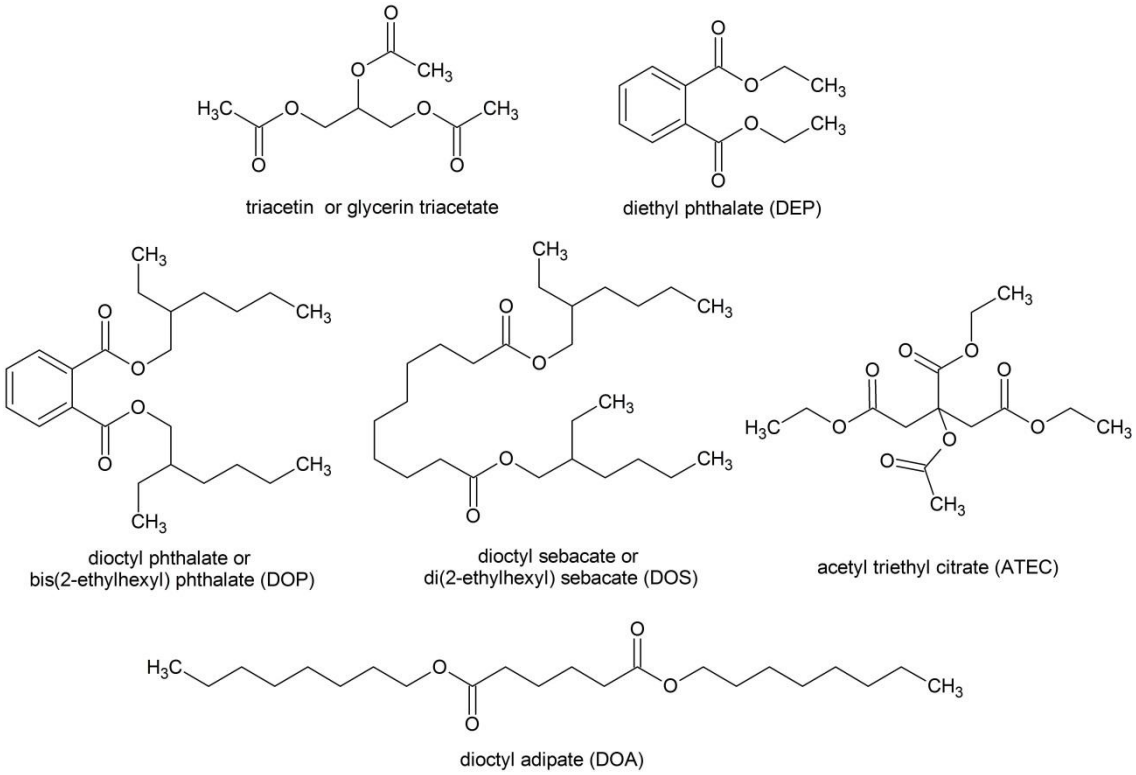

Figure 2-13 Molecular structures of typical inert (non-energetic) plasticisers.

Energetic Plasticisers

Energetic plasticisers are defined as having a positive heat of explosion (Q value) [181], they usually contribute to the oxygen balance (or are better than inert) and therefore increase the force constant / specific impulse. See Figure 2-14 for examples of energetic plasticisers.

Nitroglycerin was the first energetic plasticiser and has a high heat of explosion, producing propellant with a high force constant / specific impulse. Unfortunately, it has a high sensitiveness to friction and impact and becomes unstable at relatively low temperatures (poor thermal stability) [182]. Additionally, it has a tendency to migrate during processing and storage. This can not only leave the propellant dangerously brittle, but the migrated NG can sensitise other areas of the munition [47,183]. Many other nitrate esters have been synthesised and evaluated with improved properties. DEGDN (Diethylene glycol dinitrate) is probably the most successful of these and is used in JA2 double-base propellant. In JA2 the amount of NG is reduced to 14.9 % m/m by the addition of 24.8 % m/m

DEGDN. This reduces the sensitiveness of the propellant, but also reduces its performance compared to a pure NC/NG propellant[183]. DEGDN still has a relatively high vapour pressure, hence there can be issues with it migrating[184]. The nitrate ester BTTN (1,2,4-Butanetriol trinitrate) or mixtures of NG/BTTN or TMETN (Trimethylolethane trinitrate)/BTTN have also been used in propellants, for example chaparral, hellfire and javelin missiles[49].

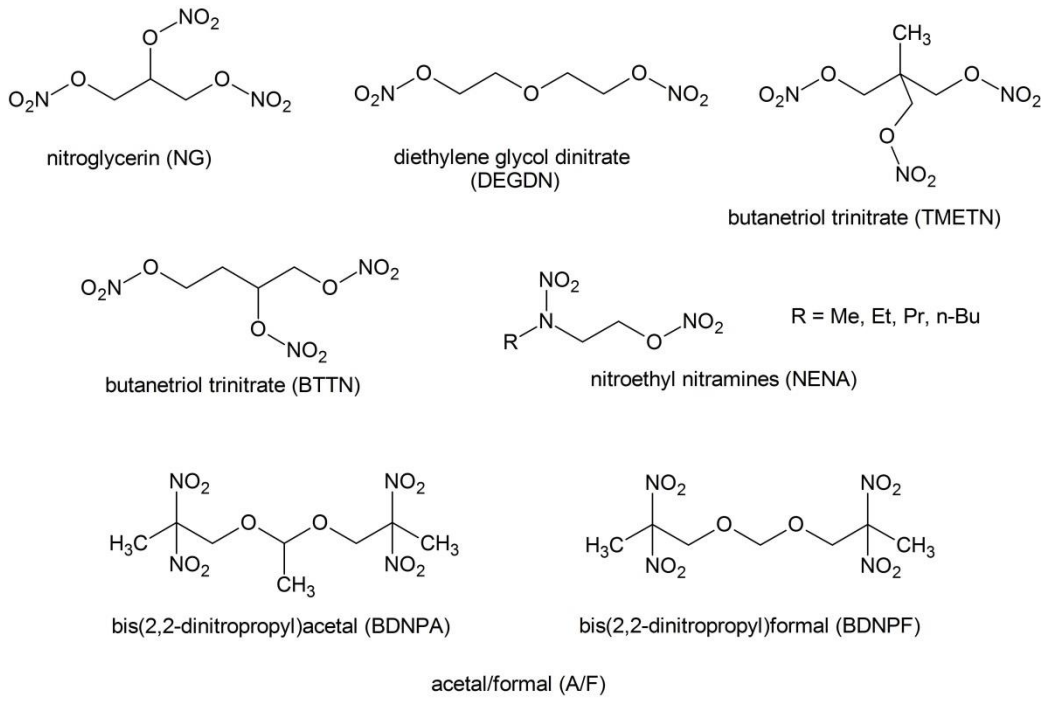

Figure 2-14 Molecular structure of typical energetic plasticisers.

Nitroethyl nitramines (NENAs) are another major group of energetic plasticiser, containing both nitrate ester and nitramine functional groups. These should aid both the force constant / specific impulse and burn rate, while reducing the burn rate exponential. They are have a good thermally stability and impact sensitiveness [57]. nBu-NENA is used in the Evolved Sea Sparrow Missile (ESSM) rocket motor, allowing a reduction in the solid loading, reducing the sensitiveness of the propellant. It is reported that HTPE being more polar than HTPB reduces the plasticiser migration [185,186]. NENAs, like all nitrate ester, degrade over time and require stabilisers. Additionally, they can have compatibility issues with AP, nevertheless a mixture of MNA (N-methyl-p-

nitroaniline) and NDPA (2-Nitrodiphenylamine) stabilisers are reported to work well stabilising a Bu-NENA (Butyl-NENA) plasticised AP/PSAN/HTPE propellant.[186].

Acetal/formal (A/F) plasticiser is a 50/50 m/m mixture of bis(2,2-dinitropropyl)acetal (BDNPA) and bis(2,2-dinitropropyl)formal (BDNPF). As both have fairly high melting points, the two are mixed together to create a lower melting point. A/F is poor at lowering the glass transition temperature and the viscosity of uncured composite mixes. A/F does have a low sensitiveness to physical hazards and good thermal and chemical stability [12]. In the past concerns have been raised about the stability of A/F on storage, particularly at elevated temperature causing increased shock sensitiveness[57]. This is believe to be due to impurities from an older manufacturing process, A/F produced by the more modern process has been shown to have no storage stability issues[187]. A/F is utilised in PBX9501, an insensitive PBX, made from HMX with 2.5 % (m/m) A/F and 2.5 % (m/m) Estane (polyester TPU) binder[188]; and EX99, an energetic plasticised LOVA propellant[26].

2.7 Research into Propellants with TPE binders.

The use of TPEs to replace a cured binder, such as HTPB, has many advantages. TPEs should be much easier to demilitarise, as removal of propellant should be achievable by heating beyond the soften point of the binder and allowing the mixture to flow out. This may require some physical force or use of a suitable solvent to achieve recovery of the propellant in a sensible time-frame. The filler could then be extracted from the binder using a suitable solvent. This removal / recovery is not possible with traditional cured propellants due to the chemistry of the binder. During mixing, a traditional composite propellant will start to cure once the curative has been added, this results in a limited time which the propellant can be mixed, referred to as the ‘pot life’. TPEs have no such time restraints, as long as the temperature is kept above the softening point it should be possible to process them. Additionally, any manufacturing waste, for example the excess material from a batch or machining waste when the propellant is reshaped, could

potentially be reincorporated into another batch, minimising any waste. It is even anticipated that TPE propellants could be extruded on a commercial scale. TPEs have the potential to have better mechanical properties and hence improved IM (insensitive munitions) properties. They also have improved chemical stability (thermal and oxidative) and therefore should have less polymer degradation giving rise to a longer serviceable life.

Although there is no in service munition that use TPEs as a propellant binder, there have been sizable research efforts into the use of these binders. Notably, the US military has been conducting research since the early 1980s and TNO in the Netherlands from the late 1990s. Various different block copolymers have been investigated as binders, the large majority are styrenic block copolymers commonly referred to by the Kraton trade name. Both the US government and TNO have formulated many propellants based on these TPEs.

A patent[189] in 1982 from the US Army details a propellant made with Kraton 1107 (SIS) coating AP using a solvent process and pressing into moulds at 150 °C. Later, a following patent[190] by the same author reports improved mechanical properties due to the use of a tetra-alkyl titanate as a bonding agent. Table 2-13 shows that on addition of tetrabutyl titanate (TBT) the Modulus appears to decrease, while the maximum stress and strain at maximum stress increased. It was claimed that these bonding agents are superior to using a conventional bonding agent for thermoplastic propellants.

Table 2-13 Tensile test results from Allen *et al.*[190] for thermoplastic AP propellant[(a)].

Bonding Agent	Test Temperature / °C	Tensile Testing		
		Average Modulus / MPa	Average Maximum Stress / KPa	Average Strain at Maximum Stress / %
TBT[(b)]	-40	13.27	1647	61.4
None	-40	*	987	4.6
TBT	23	5.85	737	27.5
None	23	10.46	317	2.8
TBT	60	3.62	316	25.0
None	60	10.11	261	5.1

[(a)] Composition (m/m): 0.5 % dioctylphthalate, 90.75 % naphthenic oil, 11.5 - 12.0 % SIS, 28.0 % 17 µm AP, 52.0 % 200 µm AP, 0-0.5 % TBT[(b)]

[(b)] Tetrabutyl titanate

* No reliable result obtained.

A report[39] from the US Lawrence Livermore National Laboratory reports that SBS formulations were attempted, but that at solid loading greater than 60 % they were too viscous for pour or cast, it goes on to recommend twin screw extrusion. Later another patent[191] from the US Air Force describes the use of highly plasticised SBS (1:1 to 1:3, polymer:plasticiser ratio) to make an AP and AP/Al composite propellant which can be cast. In 1982 a report from the fraunhofer institute[192] (Germany) details making propellants from SBS and SIS polymers with AP and NQ . Again a solvent process was used to coat the filler and it was pressed into moulds at 120 °C. Work done by TNO (Netherlands), first reported[193] in 1999, began by coating an inert (sugar) by a solvent process with various styrenic block copolymers before being extruded. They then produced a live propellant with SIS and RDX[194]. Later Driel *et al.* [40,195] report making live propellant using a non-energetic TPE with RDX, this was extruded using a double screw extruder up to a 2 kg scale. A small amount of solvent was necessary for safe processing. They found good burning rates by closed vessel testing and looked at IM properties by LSP testing (fragment impact).

Far less research has been conducted on propellants containing PEBA as a binder, Bozic & Krakovsky[196] (Serbia & Czech Republic) have the only published report of making this type of propellant. They produced one AP propellant and one aluminised AP propellant, this was then subjected to tensile testing, burning rates, DSC and TGA analysis. The energy performance was considered better (presumably more exothermic) than that of HTPB/AP propellants.

In 1999 the US Naval Air Warfare Centre in China Lake produced a Hytrel (COPE) TPE gun propellant with RDX, NQ and Acetal/Formal (A/F) energetic plasticiser. The propellant was extruded using a twin screw extruder, but this was very difficult without the use of solvents. Further work was subsequently stopped, in favour of an energetic binder. The burn rate was measured using a closed bomb and found to be reasonable (burn rate coefficient 0.0039 to 0.057 cm s^{-1} MPa^{-1}, burn rate exponent 1.04 to 1.22). Also doubt was raised about the mechanical strength, believing that the propellant was breaking up during ballistic measurements[197].

At Pune, High Energy Materials Research Laboratory in 2001 a whole range of TPEs were studied for their use as a binder in an RDX based propellant. These included EVA, Kraton (SBS and SIS), Estane (TPU), Hytrel (COPE) TPEs. These were plasticised with dioctyl phthalate (DOP), triacetin (TA) or glycidyl azide prepoylmer (GAP-A) to create an 80 % w/w RDX, 16 % w/w TPE and 4 % w/w plasticiser composition. They were manufactured by a solvent technique before being rolled through hot rollers (60 to 80 °C). The impact and friction sensitivity, ignition temperature and ballistics (closed vessel) were measured, see Table 2-14 or a summary of results. In general the sensitiveness was, as expected, was superior to conventional double-base (DB) and triple-base (TB) propellants (ref. F of I = 12 to 15, friction sensitivity = 16.8 to 19.2 kg). As predicted, the performance of inert plasticised sample was fairly low (force constants of 880 to 955 J g^{-1}), use of an energetic plasticiser (GAP-A) did increase the performance to a more reasonable level (912 to 1017 J g^{-1}). Hytrel (COPE) had the highest force constant and burn rate. Possible issues were raised with thermal

decomposition found by DSC, thought to be due to the C=C bond. All the polymers tested had a fairly high T_g (-21 to -14 °C) and fairly low softening points (55 to 89 °C). [198]

Table 2-14 Selected results from Sanghavi et al.[198] **for sensitiveness and ballistic tests on 80 % RDX / 16 % TPE / 4 % plasticiser composition (m/m).**

TPE	**EVA**		**SIS**		**SBS**		**Estane**		**Hytrel**	
Plasticiser	**DOP**	**GAP-A**	**DOP**	**GAP-A**	**DOP**	**GAP-A**	**DOP**	**GAP-A**	**DOP**	**GAP-A**
F of I[(a)]	78	62	67	55	59	43	61	53	55	51
Friction sensitiveness[(b)] / kg	36	36	36	36	36	32.4	36	36	36	32.4
Ignition temperature[(c)] / °C	228	227	202	200	205	200	237	226	233	230
Force constant[(d)] / J g^{-1}	951	1016	880	925	904	912	951	1011	955	1017
Burn rate coefficient[(d)], β / cm s^{-1} MPa^{-1}	0.026	0.073	0.027	0.096	0.034	0.062	0.037	0.077	0.181	0.215
Burn rate exponential[(d)], α	1.08	1.0	0.94	0.87	1.10	0.97	1.13	1.05	1.06	1.01

[(a)] 20 mg sample using a 2 kg free-fall weight, then normalised to tetryl (F of I = 70).

[(b)] 5 mg sample in Julius Peter's Apparatus.

[(c)] Julius Peter's Apparatus with a heating rate of 5 °C / min.

[(d)] 100 cm^{-3} closed vessel at 0.2 g cm^{-3} loading density.

Later (2007), work at Pune moved on to TPE rocket propellants, made from *Irostic,* a urethane TPE (TPU). The composition being 10 to 15 % m/m TPU binder with 3 % m/m DOA plasticiser and the remaining being AP and Al. Again, a solvent technique was employed, the propellant was then processed through hot rollers (70 to 75 °C), before being extruded in a heated (65-70 °C) vertical extrusion press. Mechanical analysis, hazard and performance testing was conducted (see Table 2-15). The article focuses on the good tensile strength of the propellant, even though the extension seem fairly poor, but given the high modulus this strain would equate to a large applied pressure. The impact and

friction sensitiveness was shown to be better than a comparable HTPB propellant. A good characteristic velocity, c* (1576 m s^{-1}) was found using a ballistic evaluation motor, tests at hot and cold temperatures (+50 & -20 °C) found only small changes in the burn rate.[199]

Table 2-15 Selected results from Mulage *et al.* [199] **for tensile testing sensitiveness and ballistic tests on TPU (Irostic) / DOA / AP / Al propellant compositions.**

	TPU (Irostic) / DOA / AP / Al propellant compositions			**HTPB propellant anaolgue†**
Percentage of TPU binder / % m/m	10	12	15	-
Maximum stress[(a)] (tensile strength) / MPa	4.1	5.0	5.9	-
Maximum extension[(a)] / %	10 - 12	12 - 14	15 - 16	-
Young's modulus[(a)] / MPa‡	245	245	228	-
Impact sensitiveness[(b)] / cm	30	32	24	46
Friction sensitiveness[(c)] / kg	12.8	14.4	16.0	36
Ignition temperature[(d)] / °C	275	274	270	-
Burn rate[(e)] at 6.9 Mpa / mm s^{-1}	12.6	11.5	9.8	-
Spectic impulse[(f)] (Isp) / m s^{-1}	-	2340	-	-
Characteristic velocity- (c*) / m s^{-1}	-	1576	-	-

[(a)] ASTM-D-638 using a Hounsfield tensile testing machine.

[(b)] 20 mg sample using a 2 kg free-fall weight.

[(c)] 5 mg sample in Julius Peter's Apparatus.

[(d)] Julius Peter's Apparatus with a heating rate of 5 °C / min.

[(e)] Acoustic strand burner with a nitrogen atmosphere.

[(f)] Determined by a ballistic evaluation motor on seven propellants strands with diameter 40 mm (ID 20 mm) and length 65 mm.

† No details of the composition of the HTPB analogue are given.

‡ Assumed units; no units given in article.

The most advanced propellant incorporating TPE in the binder is Rowanite 318. This LOVA gun propellant does contain a small amount of NC (5 to 10 %), in

addition to a TPE in the binder[32,34]. Rowanite 318 was discussed more fully in sections 2.3.1.4 and 2.3.2.

2.8 Manufacturing Processes

Different manufacturing methods are employed to produce a variety of grain sizes and shapes from different propellants. Gun propellants are typically nitrocellulose based and typically made by either the solvent, solventless or ball powder method. Rocket propellant may be either extruded (typically solventless) or cast (typically a part solvent process). A different manufacturing technique known as slurry mixing is used for some PBX formulations.

2.8.1 Nitrocellulose Based Propellants

2.8.1.1 Single-base Gun Propellants

The ‘solvent process’ for manufacture of single-base propellants produces sticks or tubular grains shapes. Firstly, the wet NC (containing at least 10 % water) is washed with ethanol to remove the water. Excess ethanol is then removed, either by centrifuge of pressed out using a hydraulic press. Then ether is added to make a 2:1 ratio with the remaining ethanol in the NC to create a paste, the total amount of solvent required is usually equal to the mass of NC. Stabilisers and plasticisers are also added at this point. Next, the paste is mixed on a kneader mixer, before being extruded and cut into the desired shape and size. Then dried and washed to remove residual solvent, before a final drying and coating (eg. with graphite) if required. [174]; [200]

In order to produce cheaper gun propellants, a faster and safer manufacturing method producing ‘ball powder’ was developed. NC in water is placed into a ‘shaping still’, followed by the addition of ethyl acetate with stabiliser (eg. DPA) and calcium carbonate to neutralise any acid. After mixing for about 30 minutes the suspension is stabilised with a protective colloid (eg. gum arabic or starch). This is followed by vigorous stirring, allowing balls of NC to form, they are then coated with a gelatinising agent (eg. a plasticiser) and often carbamate. Next,

solvent is distilled off, then the material is filtered and centrifuged. Finally it is dried and polished, before coating in graphite if required. Double-base propellants can be made by addition of NG into the slurry with the ethyl acetate or by solvent coating the propellant balls (lower NG propellants). Ball powder generally has poorer ballistic properties than extruded propellants, primarily due it shape, larger balls are often flattened (before drying) in an attempt to improve this.[174]; [196]

2.8.1.2 Extruded Double-base Gun & Rocket Propellants (EDB)

The common processes for the production of EDB propellants is known as the solventless processes. The wet NC is mixed with NG, stabiliser and any plasticisers and heated to form a paste, next any excess water is removed before being mixed on a kneader mixer. The paste is passed through hot roller (up to 100 °C) to gelatinise the NC. It can then be extruded, however, a high temperature is required (typically 70 – 80 °C). The propellant is then cut to length and dried, it then may require machining into shape and the surface inhibited by a coating.[50,174]

2.8.1.3 Cast Double-base Rocket Propellants (CDB)

EDB propellants are limited to a grain size of around 13 cm, larger DB motors are produced by casting. CDB propellant manufacture has two main processes, first; making a casting powder, second; casting and curing. To make the casting powder, dried NC, other solid ingredients, some of the inert plasticiser and possibly some of the NG are mixed with the solvent (eg. ether / alcohol). This is then kneaded on a sigma mixer with Z blades, to obtain a homogenous mixture. The ‘dough’ is then extruded into fine stick (ca. 1 mm), then cut into 1 mm lengths, before being dried and coated. Either a mould or the rocket motor itself is prepare by coating with an inhibitor, before being filled with the casting powder. Next the ‘casting liquid’ is added, this is mainly NG desensitised with an inert plasticiser (eg. Triacetin) and stabilisers. The mixture is gently warmed (up to 50 to 65 °C) for 1 to 7 days to allow gelling and coalescence of the NC to occur, producing the finished propellant. [46,50]; [174]

2.8.2 Composite Rocket Propellants

Most composite propellants are made using a pre-binder which is cured during manufacture to the final binder. Firstly a premix is prepared by mixing the pre-polymer, plasticiser, bonding agents and anti-oxidants in a planetary mixer heated to 60 °C. Then aluminium and burn rate modifiers are added to the mix. The pre-mix is then degassed before a portion of the oxidiser (eg. AP) is added, it is then degassed again while mixing before addition of another portion of the oxidiser, this is repeated until all the oxidiser is in the mix. The order of different particles sizes of the oxidant, amount and time is important to keep the viscosity low enough for efficient mixing. Once the mixture is homogenous, the cross-linker (curative) and cure catalyst is added, followed by more mixing.

The curing mixture now needs to be cast, this is typically either ‘vacuum casting’ or ‘die casting’. The mixture can be cast into either a mould or more often the body of the rocket motor. This needs to coated with a liner for thermal protection of the motor case. Vacuum casting involves placing the mould (or rocket motor body) inside an enclosure under vacuum, this is necessary to eliminate dangerous voids in the rocket motor. The casting bowl is placed above and connected by a vertical pipe. The pressure difference and gravity pulls the propellant into the mould. Slit plates in the pipe ensure that the mixture is efficiently degassed. This simple process is well suited to the low production rates that are typical of the propellant industry.

Die casting is required for propellants with very high solid loadings or for more complex shapes of rocket motors. Being faster it is also desirable for high production rates, such as when manufacturing many small motors. Die casting is similar to vacuum casting, except that the mixture is injected under pressure to aid filling. This can be achieved by a pneumatic or hydraulic piston. Alternative a screw extruder can be used, in this case the mould is filled from the bottom.

The motor must then be left to cure, this is typically done at a moderate temperature (50 - 80 °C), usually under vacuum. Finally, trimming off excess propellant may be required[46,174]; [55].

2.8.3 Other Energetic Composites Manufacturing Methods

Polymer (or plastic)-bonded explosives (PBXs) are explosives held in a polymer binder. Mostly the production of these is similar to composite propellants, the binder being a pre-polymer which is cured with isocyanates (eg. cured HTPB)[56,201]. However, non-cured polymers can also be used as a binder, these tend to be specialist explosives for nuclear weapons or booster explosives. These require a high velocity of detonation, which can be facilitated by a very high solid loading (>90 % m/m) and high overall density. Additionally, more complex shapes are required, which would be difficult to produce by casting[202]. PBXs are produced in two parts; manufacture of a moulding powder, then compacting to make a dense solid explosive[203].

Typically the slurry process is used to make the moulding powder, this has been used since the 1950's. The explosive is added to water and mixed to form a slurry. The polymer binder is dissolved into a solvent and introduced to the slurry. The mixture is then heated and a vacuum or air sweep applied to remove the solvent, leaving the polymer to coat the explosive. The slurry is then filtered, washed and dried. The moulding powder can then be compacted by several methods. The simplest is for the moulding powder to be pressed in a steel-die using a hydraulic piston, often done at a raised temperature and very high load, often with vacuum applied.[203]; [204,205]; [206]

2.8.4 Resonant Acoustic Mixing

The resonant acoustic mixer (RAM), manufactured by Resodyn, is a new type of mixer incorporating a mixing vessel attached to a vibrating plate. The RAM mixer generates a uniform shear field throughout the mixing vessel by oscillating the vibrating plate at moderate frequency (ca. 60 Hz) and relatively large displacement (14 mm). The mixer can apply a high level of G-force, up to 100 G, without the use of impellers. The frequency is continually adjusted to stay at the resonant frequency of the mechanical system, maintaining the highest efficiency[207]. According to Resodyn[208,209], the RAM mixer is well suited for propellant mixing. Citing faster mixing times (10 to 100 times faster), the ability to

mix in the end-use container and mixing solids in very viscous liquids (up to 350 000 cP end mix viscosity). Additionally, it is claimed that the process is directly scalable.

The RAM mixer can be mathematically described as a spring-mass-damper system, where energy is transfer between the spring and the moving fluid masses. At the resonance frequency, the inertia and stored forces cancel each other resulting in all the input forces becoming mixing forces. Hence all the power used by the system is transferred into the mix, making the mixer very efficient (see Figure 2-15).

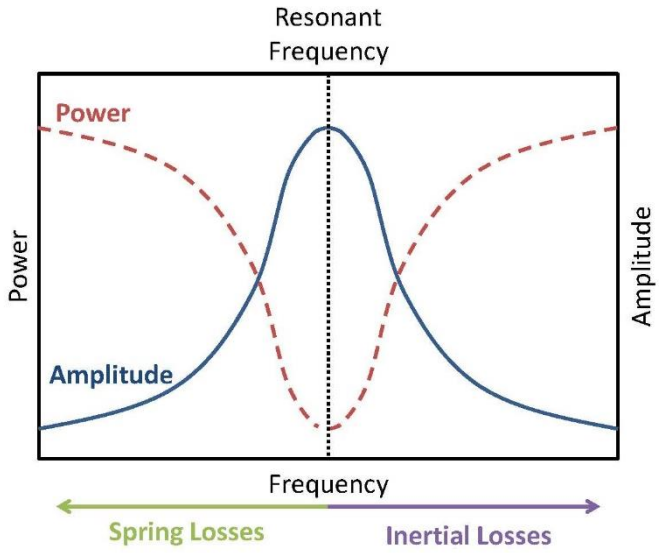

Figure 2-15 Graph showing the amplitude and power against frequency for a spring-mass-damper system. Adapted from [210]**.**

For fluid mixes, Resodyn[211] claim that the RAM mixer produces non-linear waves on the surface of the liquid known as Faraday instabilities. RAM technology is stated as being particular effective at introducing these instabilities under the proper conditions. Research supporting this theory for two miscible liquids has been conducted[212,213].

There is only a small amount of published work of research in to mixing of propellants using RAM. Most notable is research by the US Naval Air System Command[214], where Hydroxyl-terminated caprolactone ether (HTCE)/AP/Al

propellant was prepared by RAM and a conventional mixer (Baker Perkins). Despite the propellant being mixed by the RAM for only 30 minutes as compare to 100 minutes with the conventional mixer, it had similar burn rate and tensile properties. In addition, the RAM mixed propellant had a better maximum stress at higher strain rates (50 cm min^{-1}). The RAM was then tested mixing a highly filled ‘well known’ explosive formulation with a polybutadiene binder. Both the solid loading and the particle surface area (inverse of diameter) where increased, creating an extremely viscous paste. These were reported to be effectively mixed with no evidence of particle agglomeration. Resodyn[207], with support from U.S. Army Space and Missile Defence Command, used the RAM to successfully manufacture gel propellants from DMAZ (dimethylaminoethylazide) and fused silica. This is difficult by conventional processes due to low bulk density and poor wetting. Furthermore, they were able to incorporate nano aluminium and carbon components into the mix.

3 Experimental Methods

3.1 Preparation of Samples

To create consolidated sheets of TPEs filled with a solid filler and / or plasticised, a moulding powder was first manufactured. The TPE was first dissolved in a suitable solvent, then plasticiser and filler were added (if in formulation), before precipitation of TPE by evaporation of solvent or use of an anti-solvent. This moulding powder was then hot pressed into sheets, which could then be cut up for analysis.

3.1.1 Preparation of Moulding Powder

3.1.1.1 Hand Mixed Method

First a 10 % m/w solution of the TPE (PEBAX or SEBS) in either chloroform (for PEBAX) or dichloromethane (for SEBS) was made by soaking the pellets or coarse powder overnight. The correct proportion of filler and / or dioctyl sebacate (DOS) plasticiser was then added to the solution and mixed. Most of the solvent was then evaporated off by heating in a boiling water bath while being hand mixed. The samples were then left for at least 16 hours for the residual solvent to evaporate. Up to 10 g of composition was made by this process.

3.1.1.2 RAM Slurry Method

A remote mixing method utilising Resodyn's resonance acoustic mixer (RAM) LabRAM was developed. The method replicates the slurry coating method commonly associated with manufacture of pressed polymer bonded explosives (PBXs)[204]; [201]; [202]. The LabRAM had a modified controller supplied by the Falcon Project. Metal mixing pots (steel or titanium) and a PTFE lid, manufactured in-house following designs from the Falcon Project, the lid was fitted with a latex balloon (to reduced pressure build-up) and connected to a solvent pump by thin vinyl tubing (I.D. 1 mm). Mixing pots were 72 mm diameter by 72 mm height with a 300 cm^3 internal volume. A clamshell clamp attached the lid to the mixing pot.

First, SEBS was fully dissolved in toluene (20 % m/v) in a metal mixing pot. The filler was then added to the pot and gentle stirred, ensuring that polymer solution covered the solid. The mixture was then shaken at 70 G for 1 minute. The mixture was visually checked to ensure a good mix. Then the mixture was further shaken at 70 G for another minute, followed by 30 seconds at 30 G. After which the anti-solvent isopropyl alcohol (IPA) was pumped into the mixing pot while it was being shaken at 30 G. Double the volume of IPA to the volume toluene was pumped in over at least 5 minutes up to a maximum rate of 10 mL min^{-1}. Once the correct amount of IPA had been pumped into the mixing pot, the mixture was shaken for a final 30 seconds. The mixture was then filtered under vacuum and washed with IPA (ca. 100 cm^{-3}) before being dried in a vacuum desiccator for at least 5 hours. Up to 30 g of composition was made by this process.

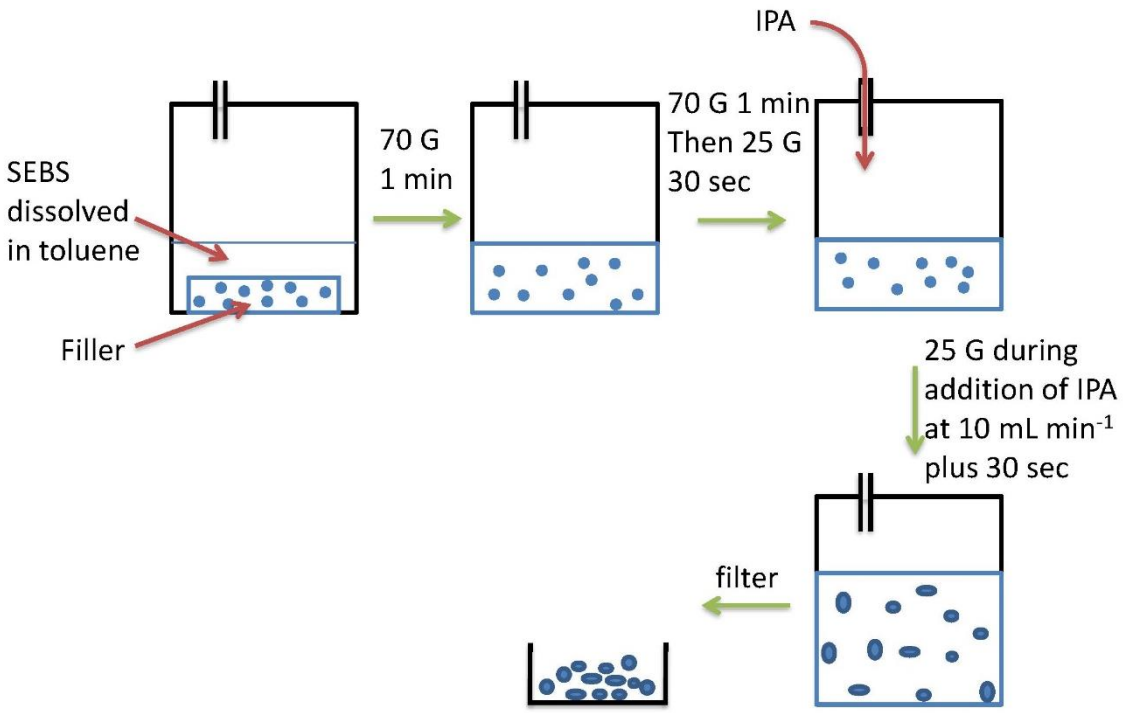

Figure 3-1 Schematic summarising the RAM slurry method.

Figure 3-2 Photographs of steel RAM mixing pot fitted with PTFE lid, rubber balloon, solvent tube and clamshell clamp (left), solvent pump (centre), RAM with mixing pot attached (right).

3.1.2 Hot Pressing of Samples

Pure samples of TPEs (SEBS and PEBAX) and moulding powder from the hand mixed method were pressed on a Moore of Birmingham temperature controlled 10 ton press. SEBS samples were pressed at 110 °C, while PEBAX was pressed at 130 °C both with 5 tons of load for a dwell time of 5 minutes. Samples were pressed in a mould 25 x 60 mm, with enough moulding powder to press to thickness of around 2 mm (unfilled) or 4 mm (filled). All moulding powder produced by the RAM slurry method was pressed using a hydraulic ram with the sample positioned in a mould on an oil heater plate (made in-house). The heater plate was heated to 125 °C and 2 tons of load was applied. Samples were pressed in a mould 55 x 100 mm, again with enough moulding powder to obtain a thickness of around 4 mm. In both cases the load was applied for 5 minutes, it was then cooled under load to 70 °C before removing the sample.

3.1.3 Preparation of cured HTPB

Cured HTPB polymer sheets were prepared from HTPB R45M prepolymer cured with Desmodur N-100. The quantity of prepolymer to curing agent was based on the ratio of alcohol to isocyanate groups being 1:1.1. The proportion by weight of

prepolymer to curing agent (I È Á¤I Ç ¼È) was then calculated using the equivalent weights for the prepolymer (' 9 È Á) and curing agent (' 9 Ç ¼È) with the ratio of alcohol to isocyanate groups :1 * ¤0 % 1å Ô ç Ùà using equation 3-1.

$$\frac{\text{“ \{t}}{\text{“ z o\{}} \; L \; \frac{q\, f\, \{t}{q\, f\, z\, o\{} \; H \; @ \; \frac{\{t}{z\, o\{} \; A \qquad \textbf{3-1}$$

The equivalent weight being the molecular mass divided by its functionality, hence the mass required to have one equivalent of reactive groups. This is the reciprocal to the OH or NCO value[56]. The proportion of antioxidant was calculated as 1 % m/m of the prepolymer.

Table 3-1 Reagents used in the formulation of HTPB/N100.

Reagent	Chemical Name	Equivalent Weight / g eq^{-1}	Formulation	
			Mass /g	Ratio /% m/m
HTPB R45M (HTPB Prepolymer)	Hydroxyl terminated polybutadiene	1389	13.031	86.13
Desmodur N-100 (Curing Agent)	Aliphatic Polyisocyanate	190.8	1.969	13.01
AO-2246 (Antioxidant)	2,2'-Methylenebis(4-methyl-6-tert-butylphenol)	-	0.130	0.86

The HTPB prepolymer was first mixed with the anti-oxidant in a centrifugal laboratory mixer (speedmixer^{TM}) at 3000 rpm for 5 min. This was followed by addition of the curing agent and mixed for a further 2 min at 3000 rpm. The sample was then degassed by placing under vacuum (*ca.* 100 mBar) for 15 min. It was then injected into warmed (70 °C) PTFE moulds using a syringe with a wide bore needle. The mould was then double bagged and placed vertically in an oven set at 70 °C. The mixture was cured for 7 days in the oven; the progress was checked by FTIR. A thin film of the sample was placed between NaCl plates and simultaneously placed in the oven. The NCO stretch band at 2200 cm^{-1} was monitored and seen to rapidly reduce after one day and was not visible from day two onwards.

A sample of HTPB/N100 plasticised with DOS was prepared to the same method, except for the addition of DOS plasticiser in the ratio of 2:1 m/m to all other constituents. This was added after the antioxidant, and mixed in a centrifugal laboratory mixer (speedmixer^{TM}) at 3000 rpm for 1 minute.

3.1.4 List of Chemicals

PEBAX, manufactured and supplied by Arkema. **SEBS**, Polystyrene-block-poly(ethylene-ran-butylene)-block-polystyrene obtained from Sigma-Aldrich, product number: 200565, CAS number: 66070-58-4, >99 % m/m purity. **DOS,** dioctyl Sebacate or bis(2-ethylhexyl) sebacate obtained from Sigma-Aldrich, product number: 290831, CAS number: 122-62-3, 90 % purity. **Caster and Icing Sugar**, manufactured by Tate and Lyle. **AP200 and AP90**, ammonium perchlorate or nominal particle size 200 and 90 µm respectively, from university stock. **RDX**, class 5 (97+ % pass through a 45 µm sieve) from university stock. **Toluene**, obtained from Fisher Scientific, product number: 10346390, CAS number: 108-88-3, 99+ % purity. **IPA**, isopropanol, obtained from Fisher Scientific, product number: 10070320, CAS number: 67-63-0, 99.5+ % purity. **DCM**, dichloromethane obtained from Fisher Scientific, product number: 10458210, CAS number: 75-09-2, 99+ % purity. **Chloroform**, obtained from Fisher Scientific, product number: 10102190, CAS number: 67-66-3, 99+ % purity.

3.2 Analytical Methods

3.2.1 Density Measurements

Measurement by helium pycnometer used an AccuPyc 1330 Pycnometer (1 cm^3). Samples of about 0.5 g were cut using a razor blade and weighed to 0.0001 of a gram. An average of five measurements was taken per sample, with the average and standard deviation (σ) recorded.

Hand measurements were used to determine the bulk density of the filled TPEs. Length and width of the whole pressed sheet was measured at least three times to a hundredth of a millimetre using digital callipers and the thickness was

measured eight times to one micrometre using a digital micrometer. Samples were weighed to one milligram.

3.2.2 Thermal Analysis

Differential scanning calorimetry (DSC) was conducted on a Mettler Toledo DSC1 or DSC3+ instrument with liquid nitrogen cooling. Samples (20-40 mg) where placed in Mettler Toledo 40 µL aluminium DSC crucibles with a hole pieced in the lid, allowing the sample to be exposed to the nitrogen atmosphere. The samples were heated from -130 °C to 200 °C, then cooled back to -130 °C, this cycle was then repeated before a final heating to 200 °C. All heating and cooling scans were at a rate of 20 °C min^{-1}.

Thermogravimetric analysis - differential scanning calorimetry (TGA/DSC) was performed on a Mettler Toledo TGA/DSC3+ instrument fitted with DSC sensors. Samples (ca. 5 mg) where placed in Mettler Toledo 100 µL aluminium crucibles with no lid. Samples were heated from 30 °C to beyond their decomposition point at 10 °C min^{-1} in a nitrogen atmosphere, unless otherwise stated.

3.2.3 Dynamic Mechanical Analysis (DMA)

3.2.3.1 Background

DMA enables us to measure the mechanical properties of a small sample (typically < 1 g) in a relatively quick, easy and non-destructive manner. Typical DMA experiments involve measuring mechanical properties as a function of temperature, referred to as a temperature scan. This is often measured at two or three different frequencies to gain some understand of how frequency dependant the response is. Alternatively a frequency scan can be performed, this measures the change in mechanical properties with frequency at a set temperature. However, it is not generally possible to measure across a wide range of frequencies at a set temperature. At higher frequencies, one is limited by the physical limitations of the instrument, while at lower frequencies the time required to make measurements becomes impracticably large. High strain rates are particular important as the mechanical response may change from rubbery to

ductile to brittle. Additionally with rubbers, high strain can lead to strain hardening with the loss of recoverable deformation[215]. TTS DMA provides an alternative to the much more difficult process of measuring directly at high strain rates by drop impact, split Hopkinson bar or Taylor impact.

3.2.3.2 Time-Temperature Superposition (TTS)

There is often a correlation between the mechanical response with frequency at a set temperature and that obtained by varying temperature at a set frequency. This means that frequency (time) and temperature can be interrelated. TTS DMA involves conducting a series of frequency scans at a series of set temperatures. Each individual isotherm curve can be shifted horizontally so that there is an overlap with the other isotherms, creating one continuous curve known as a *master curve* (see Figure 3-3). The master curve shows the predict response of the sample at frequencies beyond the limits of the instrument. Usually a reference temperature is selected and all other isotherms are shifted to fit the isotherm at that temperature.[216]

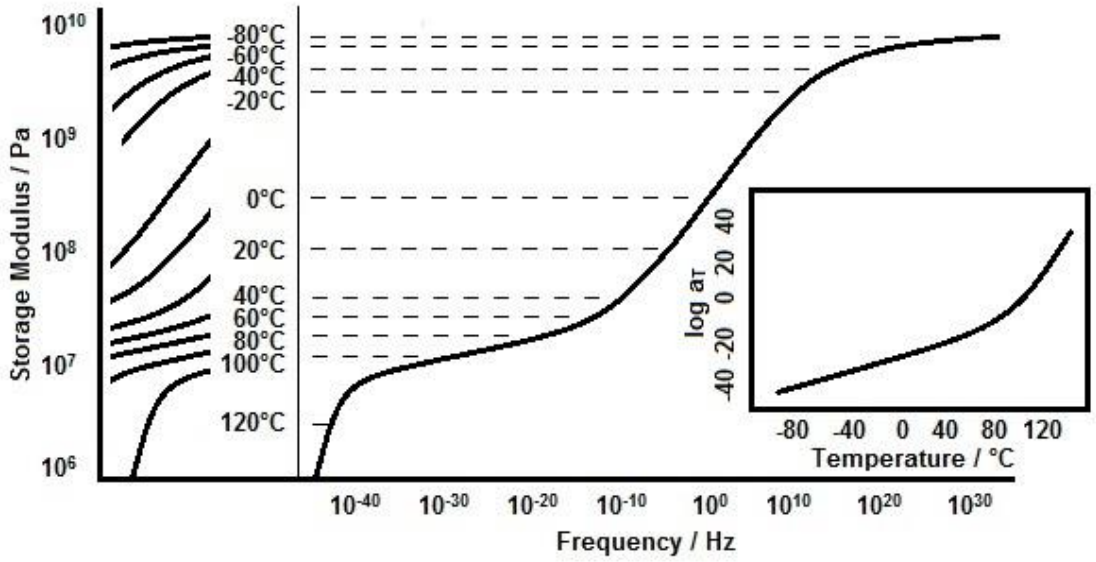

Figure 3-3 Diagram showing the construction of a master curve using time temperature superpositioning, reference temperature is 0 °C. Adapted from reference [217]**.**

The isotherms are usually described as being shifted by a shift factor (=í ;.

q:€ÙáŠ; L q:€áŠWŁ€ ; **3-2**

Where ' is the distribution of the mechanical property shifted from T to T_0. This implies that changing the temperature is the same as multiplying the time by the shift factor (=í).

For most relaxations, the Ž ‘ ‰ can be described either by the Arrhenius equation,

’ • • ‡€ L $\frac{F¤ q‡ ‰ Ú}{Ùä U Ù' €}$ F $\frac{Ú}{€Ù}$ p **3-3**

or by the William, Landel and Ferry[218] (WLF) equation.

‡€ L F $\frac{oÚk€F€Ùo}{oÛEk€F€Ùo}$ **3-4**

Where Â 'Ô Ö is the activation energy (kJ mol^{-1}), 4 is the universal gas constant and ‰ and ‰ are constants. The Arrhenius is usually applicable to transition below the glass transitions (β, γ, etc) and relaxations in crystalline polymers, while the WLF equation is nearly always applicable to glass-rubber relaxations in amorphous polymers[219]. The WLF equation is only valid at temperature at or above the T_g, usually up to about 100°C above T_g[216].

If a material obeys the Arrhenius equation, a plot of $\ln a_T$ against $1/T$ (known as an Arrhenius plot) should yield a straight line with the act as the slope. Furthermore, if the relaxation mechanism changes, the slope of the line should change with the new act. For example, high-density polyethylene has two different relaxation mechanisms between 10 and 120 °C, see Figure 3-4. Therefore an Arrhenius plot would have two straight line with different slopes indicating the two different relaxation mechanism with different act (Figure 3-4).[220]

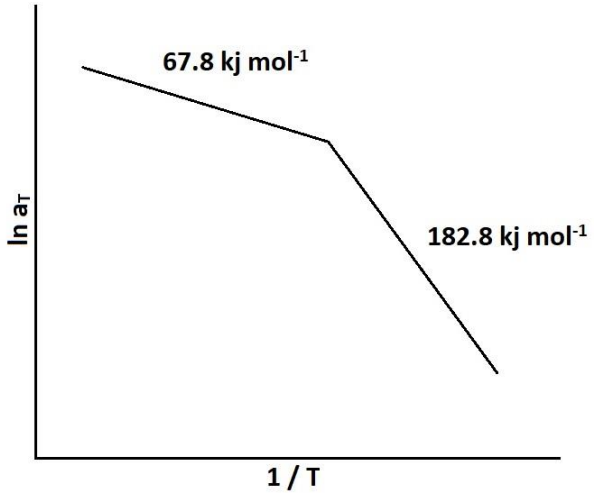

Figure 3-4 Arrhenius plot of high-density polyethylene between 10 and 120 °C, labels are the ΔE_{act}. Adapted from [220]**.**

Similarly for the WLF equation, a plot of $-(T-T_0)/\log a_T$ against $(T-T_0)$ should yield a straight line with the slope being $1/C_1$ and the intercept equalling C_2/C_1.

The Doolittle equation[221] describes the variation of free volume with viscosity.

$$\eta = A e^{B\frac{V}{V_f}} \qquad \textbf{3-5}$$

Where η is the tensile viscosity, V the total volume, V_f the free volume, A and B are constants and f is the fractional free volume. The Doolittle equation can then be linked to the WLF equation, if the fractional free volume is assumed to increase linearly with temperature. Hence:

$$f = f_g + \alpha(T - T_g) \qquad \textbf{3-6}$$

Where f is the fractional free volume at T and f_g is the fractional free volume at T_g, while α is the thermal coefficient of expansion. Hence at temperature T the Doolittle equation can be rewritten as:

$$\eta = A e^{\frac{B}{f_g + \alpha(T - T_g)}} \qquad \textbf{3-7}$$

While at Temperature T_g

$$\text{Á}k€.\ o\ L\quad mE\ n\ @\acute{U}l W_{\text{Œ}E}F\ \acute{U}A \qquad \textbf{3-8}$$

Combining these two equations gives:

$$\frac{\text{Á}k€o}{\text{Á}k€.\ o}\ L\ F\frac{n_{X\hat{U}\ddot{a}\ddot{U}}\ \grave{U}\text{Œ}\ddot{E}^{k€F€.\ o}}{\text{Œ}_{.X_{»\text{Œ}}}Ek€F€.\ o} \qquad \textbf{3-9}$$

As Ž ‘ ‰o6; Ž ‘ ‰dk6Ú o can be shown to be equal to Ž ‘ ‰p, it is possible to compare this equation with the WLF equation (2-6), resulting in the constants ‰ and ‰ being assigned as:

$$o_{\acute{U}}\ L\ {}^{n_{X\hat{U}\ddot{a}\ddot{U}}\ \grave{U}\text{Œ}\ddot{E}}\quad o_{\hat{U}}\ L\ {}^{\text{Œ}_{.X_{»\text{Œ}}}} \qquad \textbf{3-10}$$

The Doolittle constant $ is usually considered to equal unity, allowing for the fractional free volume of the glass transition (B) and the thermal coefficient of expansion of free volume (Ù) to be calculated from the WLF constants.

Not all materials can undergo time temperature superpositioning, they must be rheologically simple. The main assumption being that all the relaxation times are equally affected by temperature. Additionally, the way the sample changes (degradation, cross-linking, etc) are the same at all temperatures. Furthermore, it is assumed that different mechanisms or even the rate of these mechanisms are fairly unaffected by temperature.

To check a polymer is likely to meet the requirements of the WLF equation, a Cole-Cole or Wicket plot is usually drawn. This is a plot of the storage modulus (G') against the tan δ, which should generate a smooth arc (Figure 3-5).[216]

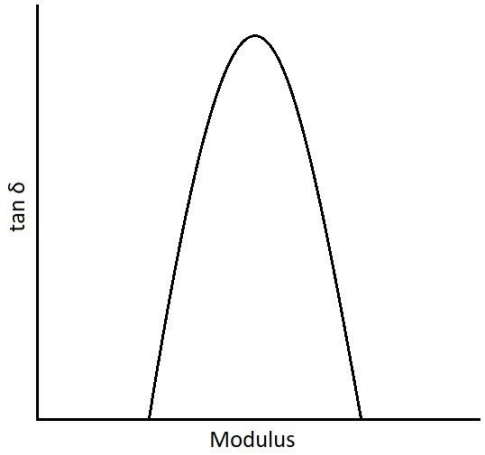

Figure 3-5 Diagrams showing a Cole-Cole or wicket plot illustrating a single relaxation time meeting the requirement for the WLF equation.

3.2.3.3 Method

A Perkin Elmer DMA 8000 with liquid nitrogen cooling was used for DMA measurements. The experiments were performed in single cantilever geometry, under a dry nitrogen atmosphere. The samples were placed in the instrument, then cooled to -100 ºC (below any expect glass transition) before being securely clamped into place with a torque wrench set at 25 cNm. The samples were prepared by cutting using a guillotine fitted with a razor blade to ca. 25 mm long by 6 mm width by 4 mm thick. The distance between clamps on the DMA was 10 mm, making the effective length of the samples ca. 10 mm

For temperature scans, the samples were then cooled to the starting temperature (-120 ºC), then heated to 120 ºC at a rate of 2 ºC min^{-1}. The storage modulus (E'), loss modulus (E'') and tan δ were obtained at frequencies of 1 and 10 Hz with a displacement of 0.050 mm (1.25 %).

For frequency scans, the samples were then cooled to about -130 ºC before being heated at 2º C min^{-1} to the first isotherm at -120 ºC. The instrument then 'soaked' at this temperature for 3 minutes before conducting a frequency scan from 0.1 Hz to 100 Hz at six different frequencies per decade (taking three averages) with a displacement of 0.100 mm (2.5 mm). Then heated to the next isotherm set at 10 ºC higher, at 2 ºC min^{-1}. This was repeated until the final

temperature of 120 ºC was reached or the response was too small to be accurately measure by the DMA.

3.2.4 Uniaxial Tensile Testing

Uniaxial tensile testing was performed on a Zwick 1445 Universal Testing System fitted with wedge grips. Room temperature was 20 °C, measurement at -40 and 74 °C were conducted inside a Zwick liquid nitrogen temperature controlled chamber. About 10 mm width samples were cut from the pressed sheet using a guillotine fitted with a razor blade, making rectangular test sample ca. 10 x 50 x 4 mm. The samples were then conditioned in the chamber for 30 minutes (for -40 and 74 °C samples), before being clamped ca. 20 mm apart. The samples were tested at a strain rate of 42.9 s^{-1} (14.3 mm min^{-1}), stress and extension are uncorrected.

3.2.5 Fourier Transform Infrared (FTIR) Spectroscopy

A Bruker Alpha FTIR spectrophotometer fitted with a platinum (diamond) ATR was used to record spectra of the polymer samples. The instrument scanned between 4000 and 400 cm^{-1} at 1 cm^{-1} resolution.

3.2.6 Nuclear Magnetic Resonance (NMR) Spectroscopy

Proton NMR spectroscopy was performed on a Bruker DPX250 spectrometer. About 10 mg of sample was dissolved in ca. 1 cm^3 of deuterated chloroform ($CDCl_3$, 99.8 % D, Cambridge Isotope Laboratory Inc) with tetramethylsilane (TMS, 99.9+ %, GOSS Scientific Instruments Ltd) as the reference. Selected NMR shifts were integrated and the values used calculate the percentage composition.

3.2.7 Particle Size Analysis

Particle size was acquired by laser defection using a CILAS 1190 particle size analyser. The particle size of RDX was determined in wet mode, by dispersing about 50 mg in water using teepol as a wetting agent. All other samples were determined in dry mode (ca. 10 to 50 g sample size).

3.2.8 Microscopy

Optical microscopy was performed using a Keyence VHX-1000 microscope with VH-Z20R (20 to 200 zoom) and VH-Z250R (250 to 2500 zoom) attachments. Analysis was conducted using the VHX software, version 1.3.0.7. Samples were illuminated from above on a contrasting blue background.

3.2.9 Ballistic Performance Testing

This was performed using a vented ‘closed’ bomb vessel, in a manner similar to that described in STANAG 4115[222]. Samples of differing mass were cut up into small pieces of about 1 x 2 x 4 mm in dimension (Figure 9-1 top left). This was placed in a paper bag with an electrical ignitor (M-TEK) and 60 mm plastic ignitor cord (Petro-Explo Z18) (Figure 9-1 bottom). The assembled charge was then placed into a 130 cm^3 bomb equipped with a Kistler gauge (Figure 9-1 top right). An oscilloscope with a 70 MHz bandwidth recorded the pressure with a sampling rate > 250 kS s^{-1}. A pressure relief port was included in the ignitor plug, this allows the pressure produced inside the bomb to decrease relatively slowly. Further details of this method are available in technical report XS160309[223], including testing with VihtaVuori N-310 propellant.

4 Characterisation of Selected TPEs

4.1 Introduction

Two potentially suitable commercially available thermoplastic elastomers (TPEs) had been selected for this thesis. They were:

1 PEBAX – Type 3533, a commercially available polyether-block-amide (PEBA) manufactured by Arkema.

2 SEBS – Styrene-ethylene/butylene-styrene, obtained from Sigma-Aldrich (>99 % m/m purity), Product No. 200565.

Primarily these were chosen for their low service temperature (indicated by the glass transition), relatively low processing temperature (indicated by melting point and extrusion temperature), excellent elongation (strain to break) and moderate hardness.

In this chapter the chemical composition and, the thermal and mechanical characteristics have been ascertained from the samples obtained. This has been compared to known data from suppliers and other research that has been undertaken. The TPEs have also been assessed for their possible utility as a binder for propellants. To make a valid comparison, HTPB polymer was cured (see section 3.1.3) and its thermal and mechanical properties were also characterised.

Nuclear magnetic resonance (NMR) and Fourier transform infrared (FTIR) spectroscopy was utilised to ascertain and confirm the composition of the TPE samples. Differential scanning calorimetry (DSC) was employed to determine glass transitions (T_g) and melting points. Dynamic mechanical analysis (DMA) was used to ascertain the mechanical properties of hot pressed samples, determining the storage modulus (E’), loss modulus (E’’) and tan δ, as well as, glass transitions. By means of time temperature superpositioning (TTS), master curves could be obtained, showing the effect of frequency on the sample over a very wide range.

4.2 Reported properties of selected TPEs

4.2.1 PEBAX

PEBAX 3533 is part of the xx33 series (manufactured by Arkema) is known to comprise of Nylon-12 (PA12) and polytetramethyleneoxide (PTMO) segments (Figure 4-1)[224]; [225]. The xx refers to the shore D hardness of the material.

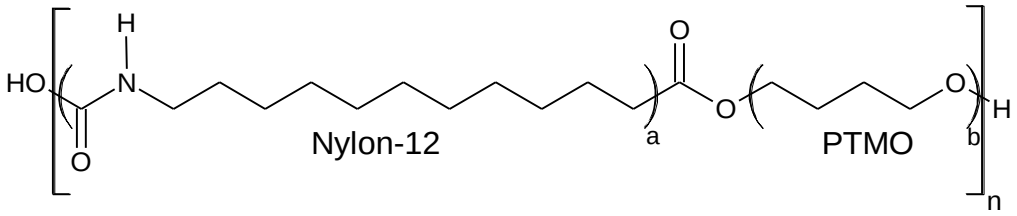

Figure 4-1 Structural formula of PEBAX

PEBAX 3533 was selected for investigation due to its low glass transition and suitable processing temperature (Table 4-1).

Table 4-1 Known properties of PEBAX 3533. Information is from PEBAX 3533 SP01 technical datasheet[226]**, unless otherwise stated.**

Composition*	PTMO / Nylon-12 / Adipic acid 74.9 / 21.2 / 3.9 83.6 / 13.0 / 3.4	 *Personal communication from Atofina*[224] *Found from NMR by Sheth*[225]
Molecular Weight	ca. 61 000 g mol^{-1}	*Personal communication from Arkema*[227]
Glass Transition	ca. -55 °C ca. -70 °C	*Personal communication from Arkema*[227] *Found from DMA by Sheth*[225]
Density	1.00 g cm^{-3}	
Melting Point	144 °C	*DSC (ISO 1183)*
Extrusion Temperature: Min / Recommended/ Max	190 °C / 205 °C / 220 °C	
Hardness (Shore D) **Instantaneous** **After 15s**	 33 25	*ISO 868*
Tensile Test **Stress at Break** **Strain at Break**	 39 MPa >600 %	*ASTM D 638*
Flexural Modulus	21 MPa	*ISO 178*

* PEBAX 3533 SP01 is also known to contain UV stabilisers.

4.2.2 SEBS

A sample of SEBS (Table 4-2 & Figure 4-2) was obtained from Sigma-Aldrich. This, unlike other commercially available samples of SEBS (Table 4-3), did not contain any fillers (>99 % m/m purity). Product number 200565 was selected because of its lower viscosity (measured dissolved in toluene).

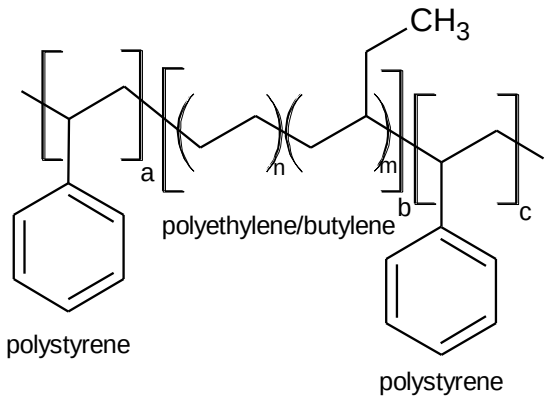

Figure 4-2 Structural formula of SEBS

Table 4-2 Known properties of SEBS, Sigma-Aldrich product No. 200565. Information taken from Sigma-Aldrich website[228] **unless otherwise stated.**

Composition	30 % Styrene 70 % Ethylene/butylene <1 % antioxidant as inhibitor	
Molecular Weight	~89,000 g mol^{-1}	*GPC*
Glass Transitions	Lower glass transition: -51°C (DSC) -44°C (DMA) Upper glass transition: 75°C (DSC) 98°C (DMA)	*For a typical composition of 30% styrene, 35% ethylene and 35% butylene, reported by Sierra et al*[229]
Density	0.91 g mL^{-1}	*25°C (lit.)*
Viscosity	550 mPa s	*20% in Toluene, Brookfield (lit.)*

Table 4-3 Properties of a typical commercial compounded sample of SEBS (MT940 from Wittenburg BV). Data is taken from Crawiton MT Series Datasheet[230] **unless otherwise stated.**

Composition	SEBS, paraffinic oil & polypropylene		*Personal communication from Wittenburg B.V.*[231]
Glass Transition	ca. -60 °C for rubber phase ca. 90 °C for styrene phase		*Personal communication from Wittenburg B.V.*[231]
Density	0.89 g cm^{-3}		*ISO 2781*
Melting Point	151 °C		*DSC*
Extrusion Temperature: Min / Max	140 °C / 200 °C		
Hardness (Shore A)	40		*ISO 868*
Tensile Test **Stress at Break** **Strain at Break**	Flow direction 2.0 MPa 268 %	Perpendicular 7.5 MPa 618 %	*ISO 37*

4.3 Nuclear Magnetic Resonance (NMR) Spectroscopy

NMR spectroscopy was used to confirm the chemical composition and determine the relative percentage of each block in the selected TPEs.

4.3.1 PEBAX

Analysis of the NMR of PEBAX (Figure 4-3) was consistent with its known constituents; either the polyether-block-amide (PEBA) or the additive adipic acid. The PEBA polymer can then be divide into its two segmented blocks; polytetramethyleneoxide (PTMO) and Nylon-12 (PA12). The peak at 4.08 ppm does not appear to correspond to either of these compounds. However, this shift is typical of a CH_2 group in the alpha position of an ester (ie –COO-C**H**$_2$-), which only occurs very infrequently when a polyether block joins a polyamide.

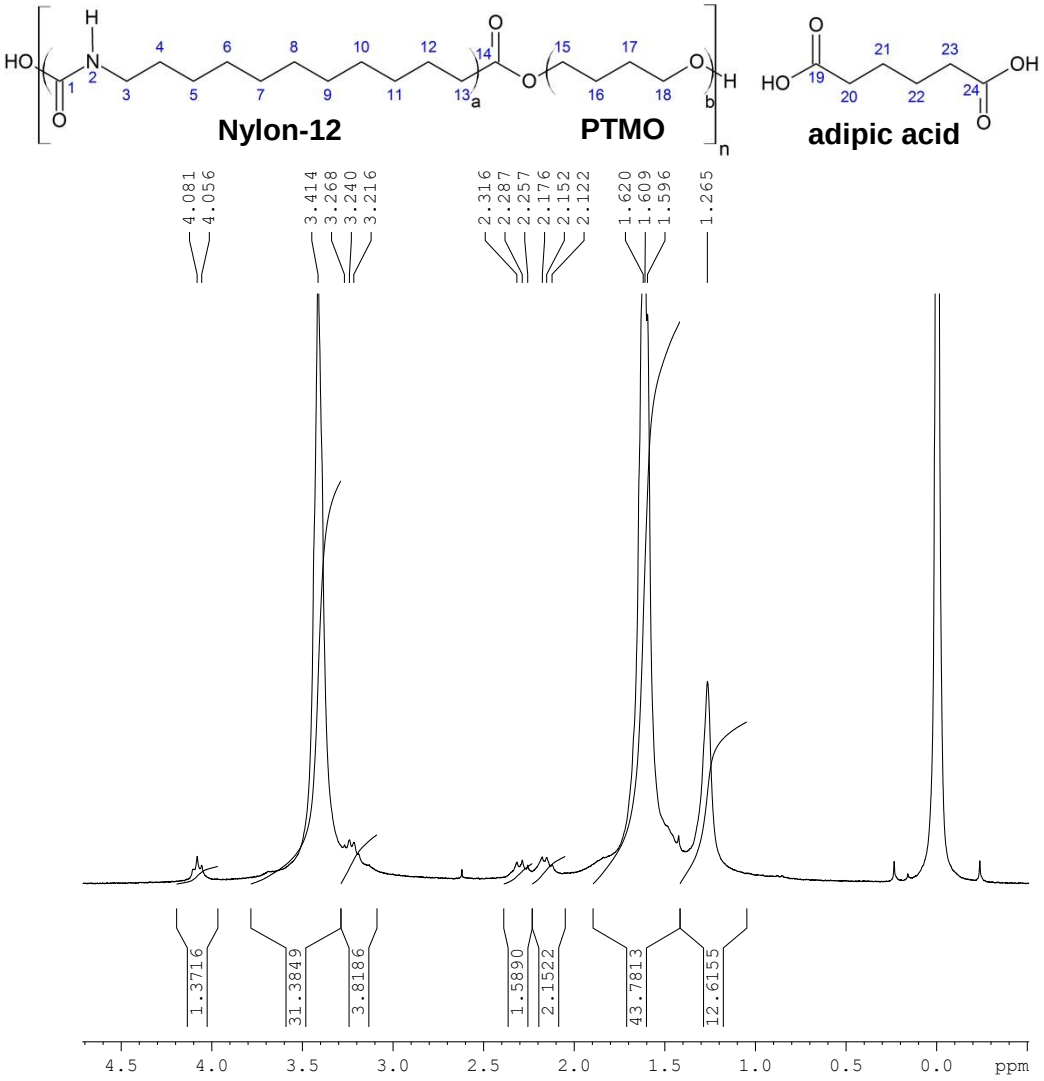

Shift (ppm)	Integration	Multiplicity	Assignment
1.27	12.62H	s	C(5)H_2 to C(11)H_2
1.61	43.78H	s	C(4)H_2, C(12)H_2, C(16)H_2, C(17)H_2, C(21)H_2, C(22)H_2
2.15	2.15H	t, J=6Hz	C(13)H_2
2.29	1.59H	t, J=7.5Hz	C(20)H_2 & C(23)H_2
3.24	3.82H	t, J=6.5Hz	C(3)H_2
3.41	31.39+3.82 -2.15=33.06H	s	C(15)H_2 & C(18)H_2
4.08	1.37H	t, J=6.25Hz	C(15')H_2 & C(18')H_2

Figure 4-3 ^{1}H NMR spectra of PEBAX dissolved in deuterated chloroform ($CDCl_3$) with assignments.

Quantitative analysis of ^{1}H spectra was able to yield the ratio of nylon-12 to PTMO as well as the amount of adipic acid. Three reference peaks were selected to use as representative of each constituent. These were the protons in the alpha position of the amide group (-NH-CO-C**H**$_2$-) for the Nylon-12, the protons in the alpha position to the ether group (-CH_2-O-C**H**$_2$-) and alpha to the ester group (-COO-C**H**$_2$-) for PTMO and the protons in the alpha position of the carboxyl group (-C**H**$_2$-COOH) for adipic acid. The peak selected for PTMO (at 3.41 ppm) was slightly convoluted with that of the protons alpha to the nitrogen atom (-CO-NH-C**H**$_2$-). To increase accuracy, the integration of both peaks were combined before subtracting the integration of the peak for the Nylon-12 (at 2.15 ppm), to yield a better estimate of the selected peak for PTMO. The integral was then multiplied by the relative mass that it represented to give the total relative mass of each constituent. This was then converted into a percentage (Table 4-4).

Table 4-4 Composition of PEBAX calculated by ^{1}H NMR

	Shift (ppm)	**Assignment**	**Position**	**Integral**	**Factor**	**Total Relative Mass (Integral x Factor)**	**Percentage / % m/m**
PTMO	3.41 & 4.08	C(15)H_2, C(18)H_2, C(15')H_2 & C(18')H_2,	-CH_2-O-C**H**$_2$- & -COO-C**H**$_2$- (PTMO)	33.06 +1.37 =34.41	18	619.9	69.7
Nylon-12	2.15	C(13)H_2	-NH-CO-C**H**$_2$- (Nylon-12)	2.15	98.5	212.0	23.8
Adipic acid	2.29	C(20)H_2 & C(23)H_2	-C**H**$_2$-COOH	1.59	36.5	58.0	6.5

These values compare fairly well with those released by Atofina[224] (see Table 4-5) apart from a notable increase in adipic acid. They are closer to the manufactures values than that calculated by Sheth[225] in his research.

Table 4-5 Comparison of determined by ^{1}H NMR, with reported values.

	Composition determined by NMR / % m/m	**Reported composition by Atofina**[224] **/ % m/m**	**Reported composition by Sheth**[225] **(NMR) / % m/m**
PTMO	69.7	74.9	83.6
Nylon-12	23.8	21.2	13.0
Adipic acid	6.5	3.9	3.4

An estimate of the PTMO segment length is possible by comparing the integration of protons in the alpha position to an ester group (which only occurs at the start and end of a PTMO segment) to that in the alpha position of an ether group. An estimate of the Nylon-12 segment can be calculated using the percentage compositions obtained earlier (Table 4-6).

Table 4-6 Estimate of Segment Length of PEBAX by ^{1}H NMR

Segment	**Integration of C(15')H_2 & C(18')H_2 (-COO-CH_2-) [a]**	**Integration of C(15)H_2 & C(18)H_2 (-CH_2-O-CH_2-) [b]**	**Average segment length (in repeating units) [(a+b)/a]**	**Segment length (g/mol) [(a+b)/2a x 72.1]**	**Segment length (g/mol) [calculated using percentages in Table 4-4]**
PTMO	1.37	31.39+3.82-2.15 =33.06	25.13	1812	
Nylon-12					461

4.3.2 SEBS

The ^{1}H NMR spectrum for SEBS dissolved in deuterated chloroform ($CDCl_3$) is shown in Figure 4-4. The spectrum shows peaks consistent with that of the known structure for SEBS, aromatic protons appearing at 6.58 & 7.07 ppm, while aliphatic protons appear at 1.26 & 1.92 ppm with terminal protons at 0.83 ppm.

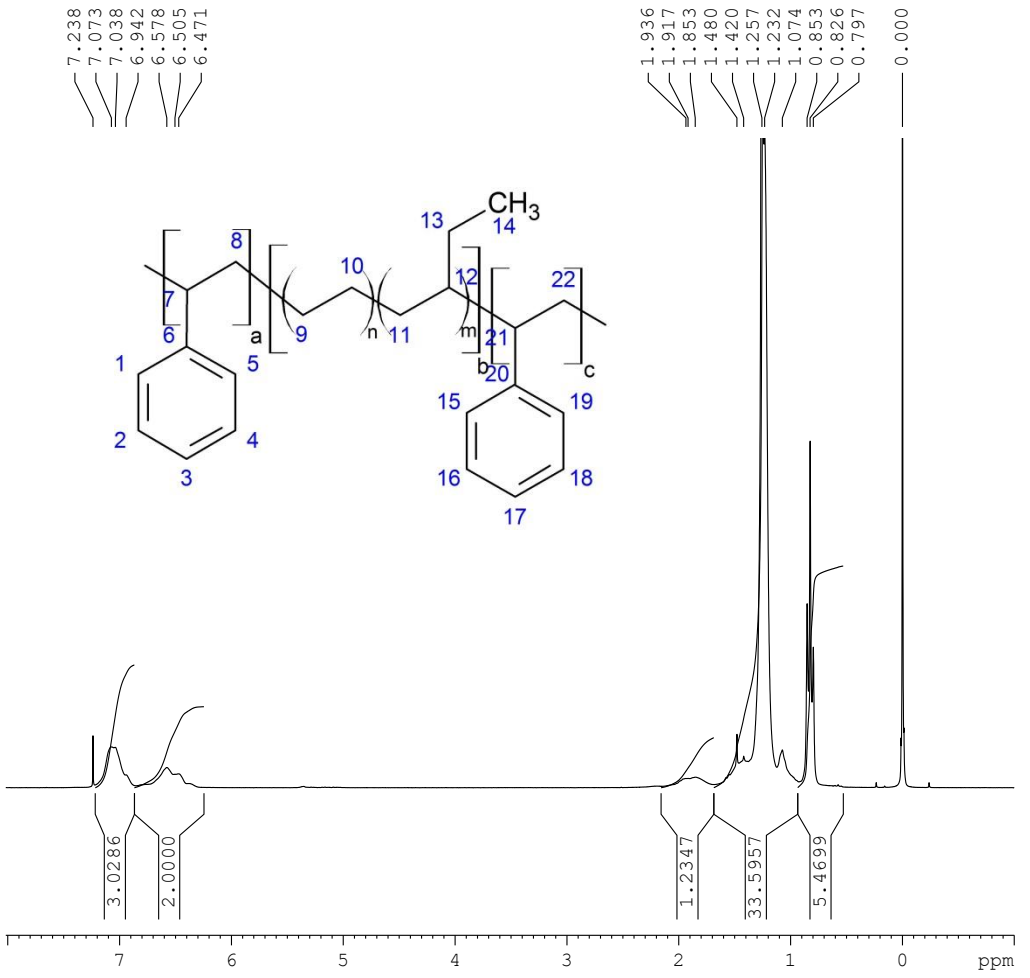

Shift (ppm)	Integration	Multiplicity	Assignment
0.83	5.47H	t J=7Hz	C(14)H_3
1.26	33.60H	m	C(8)H_2 to C(13)H_2 & C(22)H_2
1.92	1.23H	s	C(7)H, C(21)H
6.58	2.00H	m	C(2)H, C(4)H, C(16)H & C(18)H
7.07	3.03H	m	C(1)H, C(3)H, C(5)H, C(15)H, C(17)H & C(19)H

Figure 4-4 ^{1}H NMR spectra of SEBS dissolved in deuterated chloroform ($CDCl_3$) with assignments.

Calculation of the ratio of styrene (S) to ethylene/butylene (EB) was based on the comparing the integration for all aromatic protons with aliphatic protons (Table 4-7).

Table 4-7 Calculation of the Ratio of Styrene (S) to Ethylene/Butylene (EB) in SEBS by ^{1}H NMR.

Block	Integration of aromatic/aliphatic protons	Ratio of mass of segment (relative number of units x formula mass)	Percentage / % m/m
Styrene (S)	5.029 (aromatic)	$\frac{5.029}{5}$ x 104 = 104.60	28.6
Ethylene/butylene (EB)	40.300 (aliphatic)	$\frac{40.300 - (3/5 \times 5.029)}{8}$ x 56 = 260.98	71.4

Similarly the ratio of ethylene to butylene segments was calculated from the number of terminal protons (peaks at 0.83 ppm) to the number of non-terminal protons (1.26 & 1.92 ppm) (Table 4-8). It was first necessary to subtract the non-terminal protons due to the polystyrene segments leaving only those due to the EB block.

Table 4-8 Calculation of the integration of terminal protons (T) and non-terminal protons due to EB block (N) in SEBS by ^{1}H NMR.

	Integration
Terminal Protons (T)	5.47H
Non-terminal protons due to EB block. (N)	33.60+1.23 - (1.006 x 3) = 38.81H

Table 4-9 Calculation of the Ratio of Butylene (B) to Ethylene (E) in SEBS by ^{1}H NMR.

Segment	Relative number of units	Relative mass of segment (relative number of units x formula mass)	Percentage / % m/m
Butylene (B)	T/3 = 1.8233	1.8233 x 56 = 102.1	39.1
Ethylene (E) (C_4H_8)	$\frac{N - B \times 5}{8}$ = 2.8372	2.8372 x 56 = 158.9	60.9

This analysis (Table 4-7) is in reasonable agreement with the styrene content quoted by Aldrich (30 %). The butylene/ethylene ratio (Table 4-9) is also fairly close to a random 50/50 mixture as expected.

4.4 Fourier Transform Infrared (FTIR) Spectroscopy

The chemical composition of the selected TPEs was confirmed by FTIR spectroscopy.

4.4.1 PEBAX

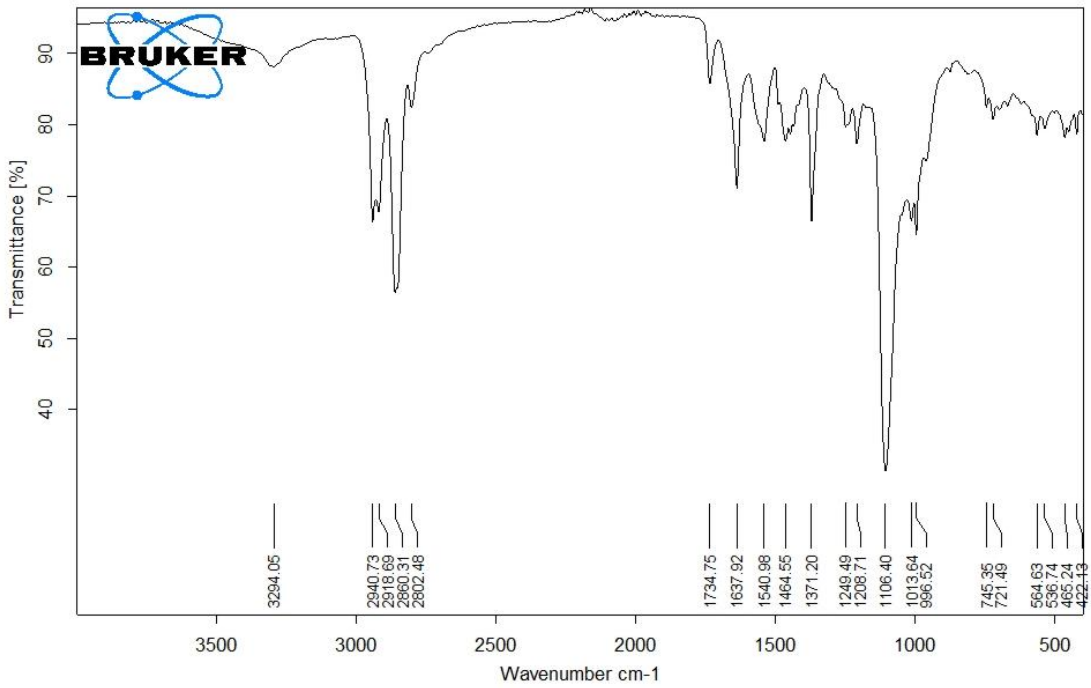

Figure 4-5 FTIR (ATR) Spectrum of PEBAX.

FTIR (ATR) 3294.1 w,b (N-H stretch); 2940.7 s, 2618.7 s, 2860.3 s, 2802.48 w (alkane C-H stretch); 1734.8 w (carboxylic acid C=O stretch); 1637.9 m (amide C=O stretch); 1541.0 m (carboxylic acid dimer O-H); 1464.6 m, 1371.2 m (alkane C-H); 1249.5 w, 1208.7 w (ether C-O stretch); 1106.4 s,b (ether C-O stretch); 1013.6 w; 996.5 w; 721.5 w (NCO bend)

FTIR analysis of hot press PEBAX yielded absorbance peaks that could be assigned to the known compounds in composition.

4.4.2 SEBS

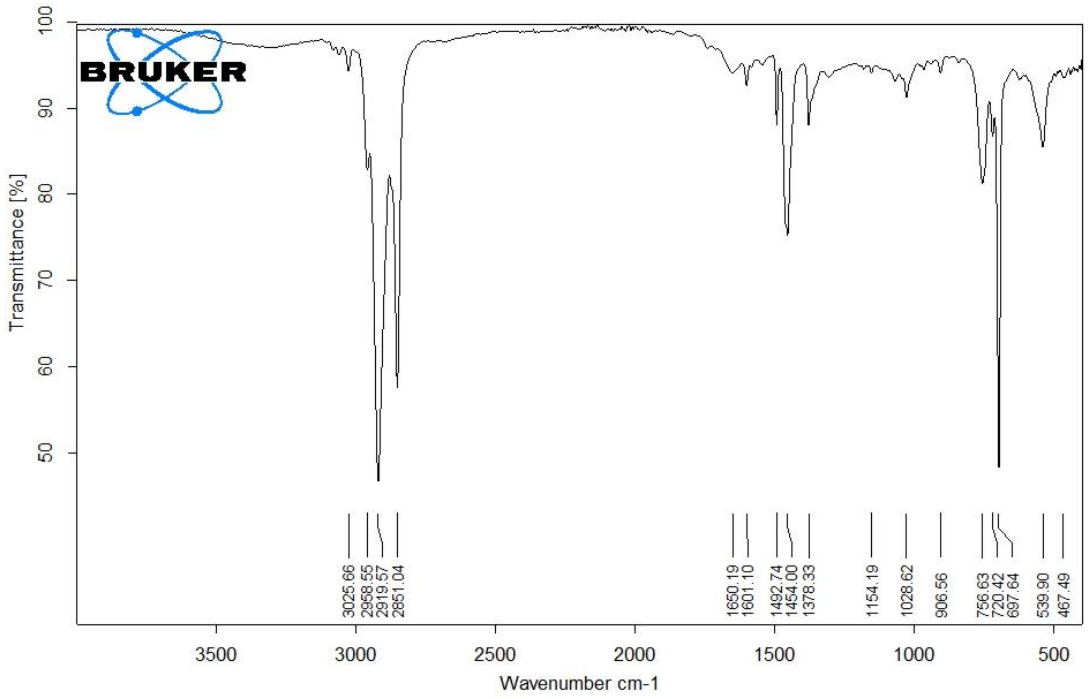

Figure 4-6 FTIR (ATR) Spectrum of SEBS.

FTIR (ATR) 3025.7 w (aromatic C-H stretch); 2958.6 w, 2919.6 s, 2851.0 s (alkane C-H stretch); 1650.2 w, 1601 w (aromatic C-H bend); 1492.7m (aromatic C-H bend); 1492.7 m, 1454.0 s, 1378.3 m (alkane C-H bend); 1028.6 w, 756.6 m, 720.4 w, 697.6 s (aromatic C-H bend), 539.9 w, b.

FTIR analysis of a thin hot press film yielded absorbance peaks that could be assigned to the known structure of SEBS. They are in good agreement with those reported by Zhou *et al*[232].

4.5 Differential scanning calorimetry (DSC) analysis

DSC analysis of the selected TPEs was employed to determine the glass transition temperature and melting points. These were compared with a cured HTPB sample (HTPB/N100).

4.5.1 PEBAX

From the DSC heating scans (Figure 4-7 & Table 4-10) the first transition (T_g) is a glass transition around -75 °C. Konyukhova et al[233] report the T_g by DSC of PTMO with an average molecular weight of 2000 g mol^{-1} as being -87 °C, while Boulares et al[234] reported the T_g to be -82 °C (inflection point) of an hydroxyl terminated polymer of PTMO-2000. This T_g can therefore be confidently assigned to the soft PTMO block in PEBAX as the T_g is close to that of pure PTMO and as expected by both Konyukhova et al[233] and Sheth[225] to be shifted slightly lower, due to the mixing of hard and soft domains. However Sheth[225] was unable to observe the T_g for PEBAX by DSC, but did find a T_g around -70 °C by DMA which was reported as being due to the PTMO block. This closeness of glass transition point for PTMO homopolymer with that found for the PTMO block in PEBAX, indicates a low level of incorporation of the other block due to incompatibility. This is consistent with its biphase structure of the block copolymer like PEBAX[235].

The first endotherm (T_{m1}) with an onset at -20 °C correlates well with Sheth's[225] report on PEBAX, where a peak around -15 °C was found. This is attributed to the melting of the PTMO block, however this is much lower temperature than the melting point for pure PTMO observed from DSC by Konyukhova et al[233] (peak at 36 °C, 10 °C min^{-1}) and Boulares et al[234] (peak at 21 °C, 20 °C min^{-1}). Sheth[225] suggests that this lowering of the melting point is due to their inability to develop thicker more perfect lamellae crystals that are found in the homopolymer.

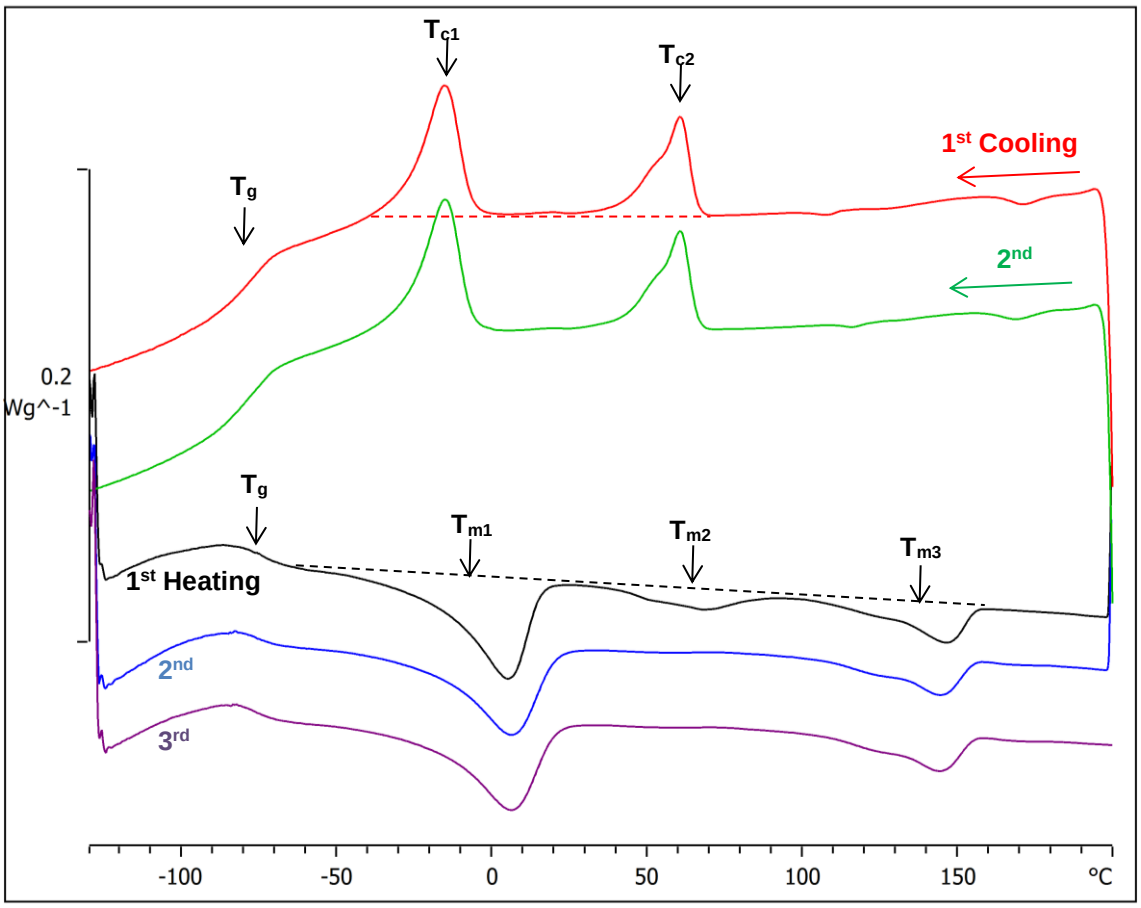

Figure 4-7 DSC thermogram of PEBAX heated between three times between -130 and 200 °C at a rate of 20 °C min^{-1}, 32.3 mg sample size.

Table 4-10 Transitions occurring on the DSC heating scans of PEBAX.

Heating Cycle	Glass Transition [T_g] (Midpoint) / °C	1st Endotherm [T_{m1}]		2nd Endotherm [T_{m2}]		3rd Endotherm [T_{m3}]	
		Onset / °C	Normalized heat of fusion / J g^{-1}	Onset / °C	Normalized heat of fusion / J g^{-1}	Onset / °C	Normalized heat of fusion / J g^{-1}
First	-75.0	-19.3	-3.12	40.5	-0.60	123.8	-1.08
Second	-76.2	-21.1	-3.30			122.0	-1.22
Third	-76.3	-21.1	-3.37			121.1	-1.21

The second endotherm (T_{m2}) with an onset of 40.5 °C which only appears on the first heating cycle does not correspond to the melting peaks of either homopolymer PTMO or polyamide (PA). Van Bogart et al[236] observed a similar endotherm in different segmented elastomers. The transition appeared when the samples were annealed but were absent from quenched samples. They suggested that this is due to annealing-induced ordering within the domain microstructure, rather than as previously thought a mixing between hard and soft segment. They stated that the endotherm caused by the annealing process could be due to either the soft or hard segment. Konyukhova et al[233] cautiously suggest that it is due to the melting of PA. Typically the process is linked with the hard block and there is not enough reason to attribute it to the melting of PTMO. Possibly thermal correlation infrared spectroscopy could be used to prove this.

The third endotherm (T_{m3}), with an onset around 122 °C, can be associated with melting of the PA block; again the melting temperature is lower than that associated with the homopolymer PA-12 (peak at 179 °C[233] and 165 °C[234]). Similarly to the first endotherm, this is due to the less perfect crystalline structures in the PA block as compared to the homopolymer.

There is no evidence by DSC of a glass transition due to the polyamide block, which occurs at 37 °C for the homopolymer PA-12. Due to the small effect of the glass transition on the heat capacity for some substances this can be sometimes very difficult to observe by DSC, however due to the large effect on the storage modulus, DMA should confirm presence of a glass transition if it exists.

The cooling scans (Table 4-11) show the glass transition (T_g) due to the PTMO block is in close agreement with the heating scans (Table 4-10).

Table 4-11 Transitions occurring on the DSC cooling scans of PEBAX.

Cooling Cycle	Glass Transtion [T_g] (Midpoint) / °C	1st Exotherm [T_{c1}]		2nd Exotherm [T_{c2}]	
		Onset / °C	Normalized heat of fusion / J g^{-1}	Onset / °C	Normalizd heat of fusion / J g^{-1}
First	-75.7*	66.4	1.63	-6.48	2.59
Second	-77.7*	66.4	1.67	-6.52	2.49

* Estimated value due to instrument unable to maintain cooling rate.

The first exotherm (T_{c1}) attributed to the crystallisation of the PA block has an onset that is much lower than the melting peak for the PA block found in the heating scans. This is also much lower than that expected by the melting point of the homopolymer PA-12 (peak at 179 °C[233] and 165 °C[234]). This effect was also seen by Sheth[225] with a steady decrease in the crystallisation temperature as the PA content was decreased. No explanation is offered as to why there is such a dramatic lowering of the crystallisation point of the PA block. However, the phenomenon *fractional or delayed supercooling* is known in blends of incompatible polymers[237]. Here the minor component is finely dispersed in the major, leading to a crystallisation point which is much lower than observed in the homopolymer. This is believed to be due to the lack of heterogeneous nucleating points, such as impurities. Hence a much larger supercooling is necessary in order to generate small crystals, created by the thermodynamic fluctuations, which act as homogenous nuclei.

The second exotherm (T_{c2}) should be assigned to the PTMO block. This is confirmed by its crystallisation point being similar to that found for the melting point of the PTMO block.

4.5.2 SEBS

From the DSC heating scans (Figure 4-8 & Table 4-12), the first transition (T_g) at -55 ºC is widely believed to correspond to the glass transition for the ethylene-butylene midblock[238]. The glass transition for the ethylene-butylene copolymer can be estimated from the glass transition for polyethylene (-111 ºC for HDPE[239]) and polybutylene (-24 ºC[240]) by applying the Fox equation[61]*. This sample of SEBS was found to be 61/39 ratio (m/m) for ethylene/butylene by NMR (see section 4.3.2), estimating the glass transition at -45 ºC. This estimated value does seem to agree fairly well with the glass transition (T_g) found by DSC, however work done by Sierra *et al.*[229] casts doubt on this being a glass transition at all. By measuring the midblock transition for SEBS polymers with varying butylene/ethylene composition they showed that the transition is most likely to be due to a β-transition from the polyethylene which known around -30 ºC in the homopolymer[62,64] (see section 2.4.2.3.

* $1/T_g = w_1/T_{g1} + w_2/T_{g2}$
Where w_1 & w_2 are the weight fractions of the two polymers

Figure 4-8 DSC thermogram of SEBS heated between three times between -130 and 200 °C at a rate of 20 °C min^{-1}, 35.3 mg sample size.

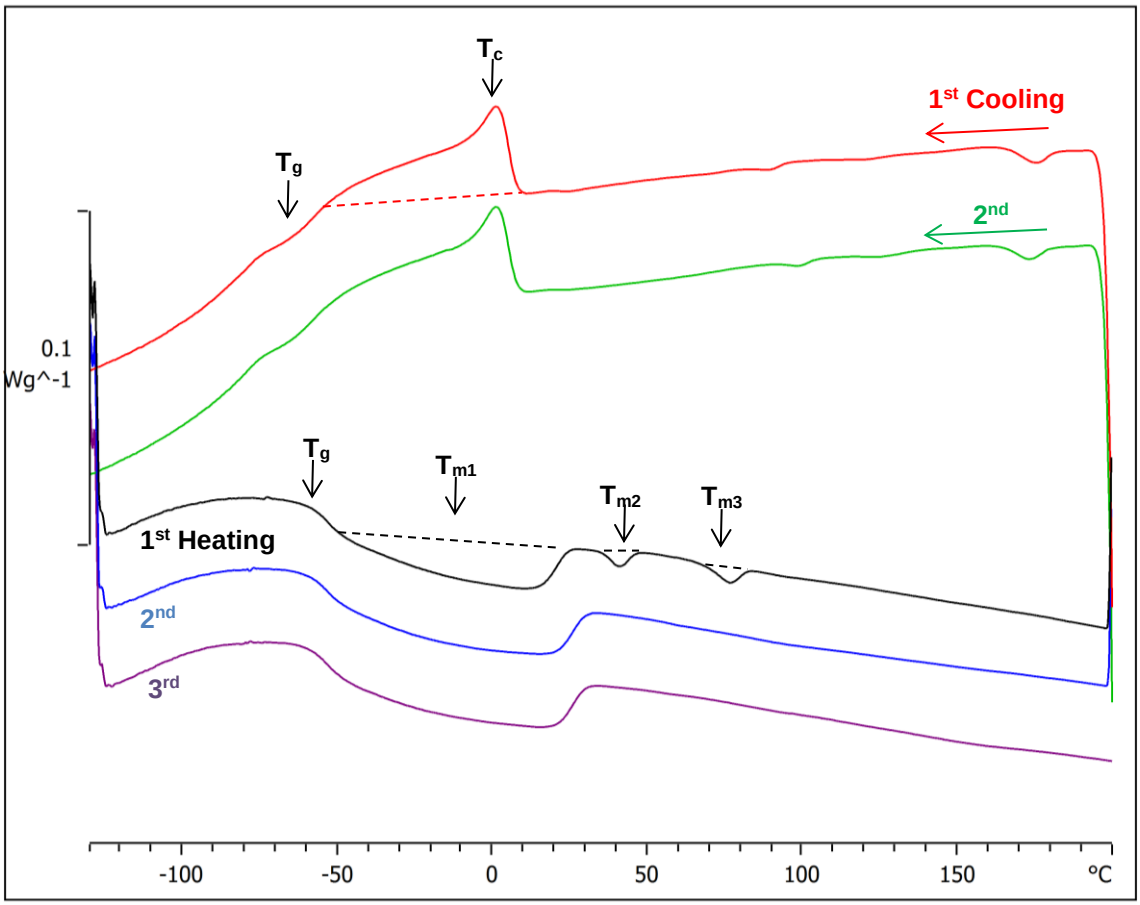

Table 4-12 Transitions on the DSC heating scans of SEBS.

Heating Cycle	First Transition [T_g] (Midpoint) / °C	1st Endotherm [T_{m1}]		2nd Endotherm [T_{m2}]		3rd Endotherm [T_{m3}]	
		Onset / °C	Normalized heat of fusion / Jg^{-1}	Onset / °C	Normalized heat of fusion / J g^{-1}	Onset /°C	Normalized heat of fusion / J g^{-1}
First	-55.7	-47.7	-1.82	35.0	-0.09	67.8	-0.13
Second	-54.8	-49.3	-2.16				
Third	-55.0	-49.4	-2.16				

The first endotherm (T_{m1}) is due to the melting of the ethylene-butylene midblock. Sierra *et al.*[229] found that the heat of fusions for T_m reduced with increasing butylene chains until the region becomes completely amorphous at around 70/30 ratio of butylene/ethylene.

From DSC there is no obvious glass transition at higher temperature due to the polystyrene block. This has been found by DSC with a mid-point temperature of 93.4 ºC for pure polystyrene with Mw of 12600 g mol^{-1} [241]. However due to the small effect the T_g has on the specific heat capacity, it may well not be possible to observe this by DSC, when polystyrene content is relativity low. However, DMA is a more sensitive technique for detecting glass transitions.

The 2nd and 3rd endotherms (T_{m2} & T_{m3}) only appear in the first thermal cycle. Zhou *et al.*[232] observed similar endotherms for SEBS and used thermal correlation infrared spectroscopy to interpret the transitions. They found an endotherm with a peak of 47 ºC (similar to the second endotherm) which they assign to the "melting of extraordinary weak crystals of ethylene in the phase interface melting, allowing the benzene ring of the polystyrene to move". A second endotherm with a peak of 69 ºC (similar to the third endotherm) was thought to be due to the heat of relaxation of polystyrene block induced by the movement of the benzene rings and melting of very weak crystals of polystyrene.

From looking at the cooling scan (Figure 4-8 & Table 4-13) there is in good correlation with the 2nd & 3rd heating scans (Table 4-12). As expected, there are no matching exotherms for the endotherms T_{m2} & T_{m3} that were seen on the first heating cycle. These are a physical ageing effects, caused by regions that slowly crystallise over a long period of time.

Table 4-13 Transitions on the DSC Cooling scans of SEBS.

Cooling Cycle	Exotherm [T_c]		Glass Transtion [T_g] (Midpoint) /°C
	Onset /°C	Normalized heat of fusion / J g^{-1}	
First	8.0	2.70	-54.4
Second	8.0	2.51	-55.1

4.5.3 HTPB/N100

Looking at the DSC heating scans (Figure 4-9 & Table 4-14), the first transition (T_g) which has a mid-point around -75 °C is widely assigned as a glass transition

associated with the polybutadiene segment (soft segment)[242,243]. This corresponds well with the glass transition of pure HTPB found to be -76 °C[244] by DSC. On the first heating scan a broad transition (T_2) from around 30 to 180 °C is also visible. This is attributed by Fluente[243] to the urethane segment (hard segment), but gives no suggestion as to the type of transition. These appears to look like a melting endotherm, probably due to small crystalline regions, which do not recrystallise for the second and third scans. In addition, no evidence could be found to assign this transition solely due to the urethane segment. There is also an absence of a glass transition due to the urethane segment, this is not unexpected due to the small percentage of the polymer. Hence the effect of the glass transitions on the heat capacity would be too small to be observed on subsequent scans, especially if it was spread over a wide temperature range.

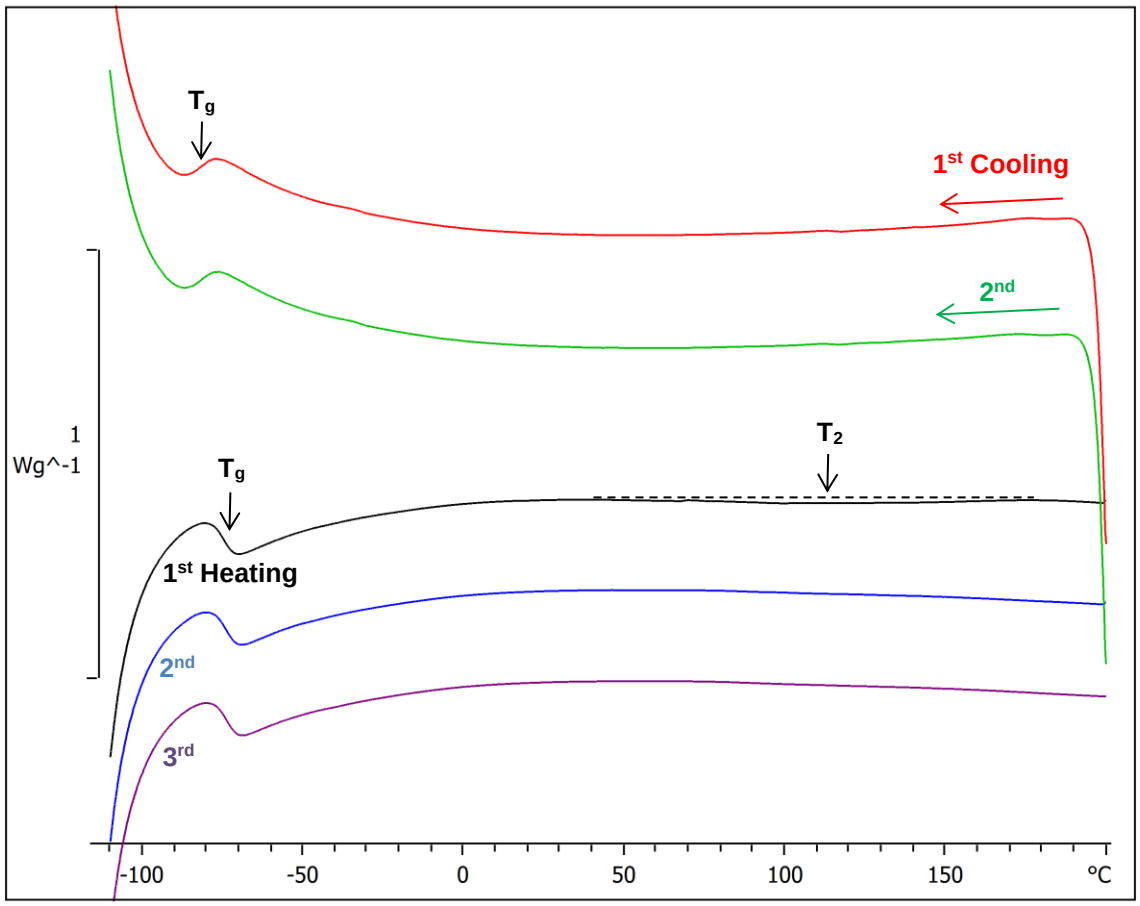

Figure 4-9 DSC thermogram of HTPB/N100 heated between three times between -130 and 200 °C at a rate of 20 °C min^{-1}, 22,6 mg sample size.

Table 4-14 Transitions on the DSC heating scans of HTPB/N100

Heating Cycle	Glass Transition [T_g] (Midpoint) /°C	Second Transition [T_2]		
		Onset /°C	Peak /°C	Normalized heat of fusion / J g^{-1}
First	-75.0	50.4	99.1	-3.0
Second	-74.5			
Third	-74.3			

The DSC cooling scans (Figure 4-9 & Table 4-15) only show the glass transition (Tg) associated with the HTPB segment. They have a midpoint of -81 °C, which is in good agreement with the heating scans (Table 4-14).

Table 4-15 Transitions on the DSC Cooling scans of HTPB/N100

Heating Cycle	Glass Transition [T_g] (Midpoint) /°C
First	-81.4
Second	-81.3

4.6 Dynamic Mechanical Analysis (DMA) – Temperature Scan

DMA was used to obtain the mechanical properties of the selected TPEs and compare them against a sample of cured HTPB (HTPB/N100). By conducting temperature scans, the storage modulus (E'), loss modulus (E'') and tan δ were obtained, these was then used to determine the glass transition (T_g) temperatures of the selected TPEs.

4.6.1 PEBAX

From the beginning of the DMA heating scan (Figure 4-10) at -120 ºC, the sample (PEBAX) is glassy, around -75 ºC (1) the sample begins to soften, shown by a dropping of the storage modulus (E') and undergoes a glass transition with the

peak of tan δ beginning around -58 ºC (T_g). This glass transition has already been assigned to the PTMO block, from the DSC scan and agrees well with the reported value for the T_g of PTMO homopolymer (*ca.* -50 ºC tan δ maxima, *f*=100 Hz [219]).

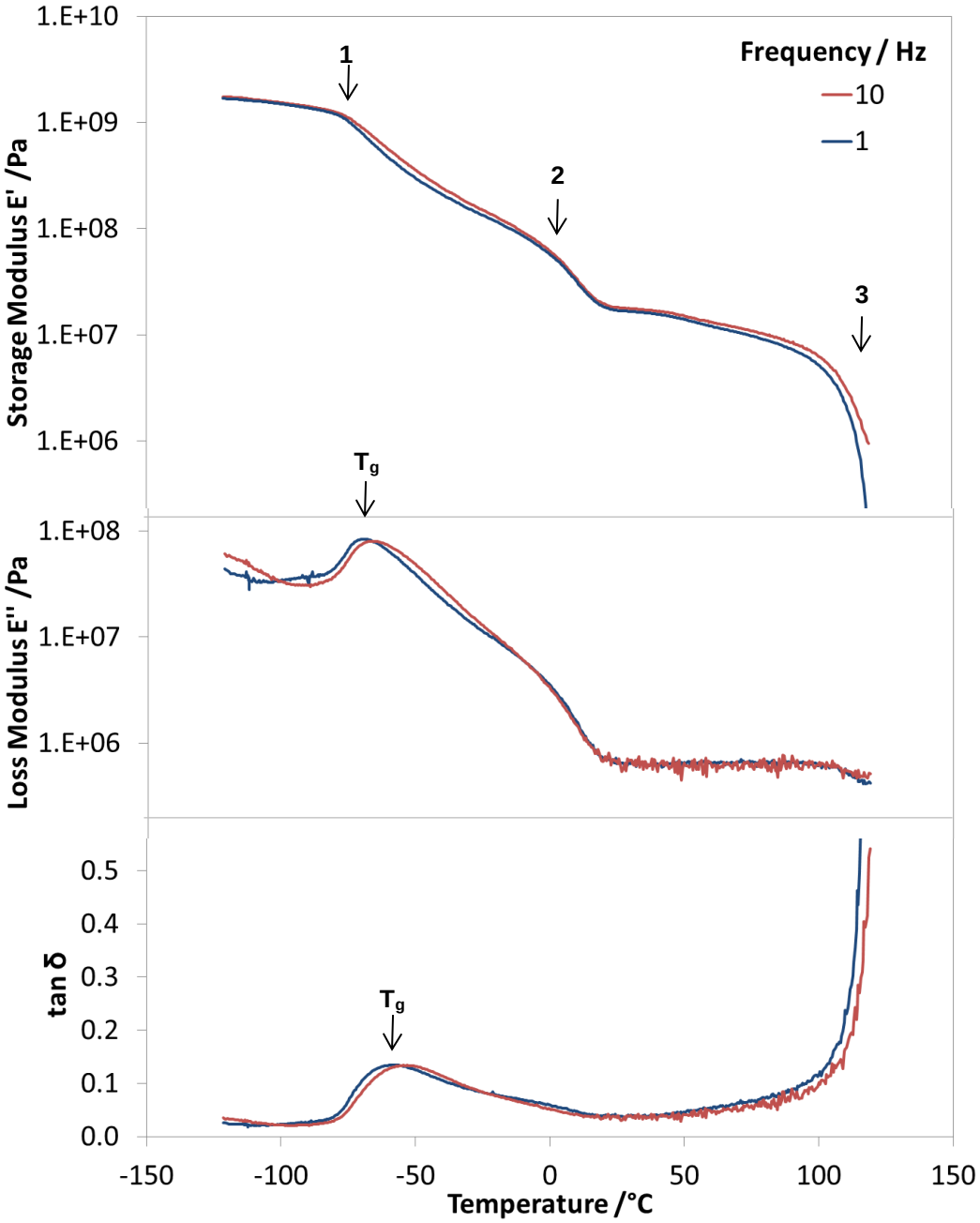

Figure 4-10 DMA thermogram of PEBAX. Single cantilever DMA at 10 & 1 Hz, 50 µm (1.25 %) displacement.

Table 4-16 Transitions occurring on the DMA scan of PEBAX.

Frequency /Hz	Glass Transition [T_g]	
	tan δ Maximum /°C	Loss Modulus Maximum /°C
1	-58.9	-69.0
10	-56.9	-66.7

At around -20 ºC (2), a slight transition is noticeable as a shoulder in the tan δ curve, which is more prevalent at 1Hz. This transition occurs between the T_g for the homopolymers and so would appear as a mixing of the hard and soft domains. Boulares *et al*[234] suggested that there is simple incorporation of the soft block into the amorphous region of the hard domain, resulting in a broad relaxation between the glass transitions. However Sheth[225] points out that that the DSC scan showed melting and partial cold crystallisation of the PTMO in this region. He suspects that the broad transition caused by the glass transition becomes combined with melting transition.

The absence of a peak in the tan δ around the glass transition for the homopolymer PA-12 (37 °C by DSC[233]) is further evidence that the hard domains are not purely PA.

Around 20 °C the storage modulus (E') starts to drop at a much slower rate, until around 100 °C (3) when a dramatic drop occurs, combined with a rapid increase in tan δ. This is due to the melting of the PA crystalline phase, which was also seen by DSC (section 4.5.1).

4.6.2 SEBS

Looking at the DMA scan of SEBS (Figure 4-11 & Table 4-17) the sample also starts in a glassy state and begins to soften at about -55 ºC (1), seen by a lowering of the Storage Modulus. There is a peak in the tan δ at around -40 ºC (T_{g1}) which varies by 5 ºC between 1 & 10 Hz frequency. This first transition correlates well with the first transition (T_g) found by DSC (mid-point *ca.* -55 ºC), which has already been discussed (section 4.5.2). A small shoulder is evident on

the tan δ curve which is believed to be due to the melting of the ethylene-butylene block[229]. Because of the small amount of crystallisation, this gives rise to only a slight effect seen by DMA. The rate of drop in the Storage modulus starts to slow down and is virtual flat at 40 ºC, before it start to drop off again. This second transition (T_{g2}) with a tan δ maximum of *ca.* 117 ºC (2) at 10 Hz (tan δ maximum at 1 Hz was not observed) is widely attributed to the glass transition of the polystyrene block[238]. This compares well with a reported temperature of 93.4 ºC for pure polystyrene of M_w=12600 g mol^{-1} found by DSC[241], suggesting a high degree of separation between the polystyrene and the ethylene-butylene domains.

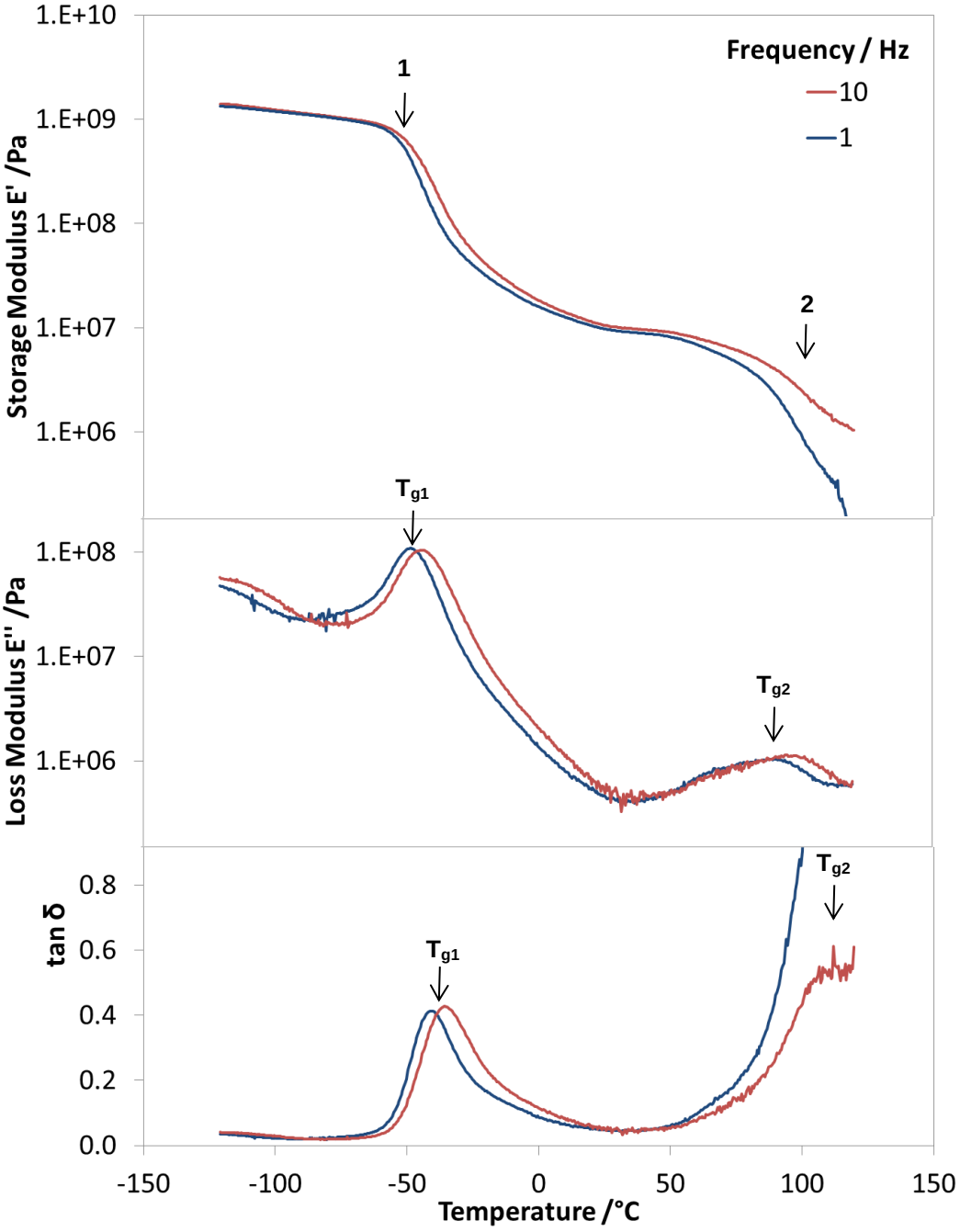

Figure 4-11 DMA thermogram of SEBS. Single cantilever DMA at 10 & 1 Hz, 50 µm (1.25 %) displacement.

Table 4-17 Transitions on the DMA scan of SEBS.

Frequency /Hz	First Transition (T_{g1})		Second Transition (T_{g2})	
	tan δ Maximum /°C	Loss Modulus Maximum /°C	tan δ Maximum /°C	Loss Modulus Maximum /°C
1	-41.0	-48.3	114.6	86.8
10	-35.9	-44.1		93.8

4.6.3 HTPB/N100

The DMA scan (Figure 4-12 & Table 4-18) shows the initial glassy state of HTPB/N100 starting to soften at around -75 ºC (1) (lowering of the storage modulus) as the sample undergoes its glass transition associated with the HTPB segment. The peak of the tan δ being around -62 ºC (T_g) and varying by 5 ºC between 1 and 10 Hz. This corresponds very well with the data reported by Plesse *et al*[245] (-61 ºC at 1 Hz) and the results of a DMA scan conducted by Siviour *et al*[246] (-63 ºC at 1 Hz & -61 ºC at 10 Hz).

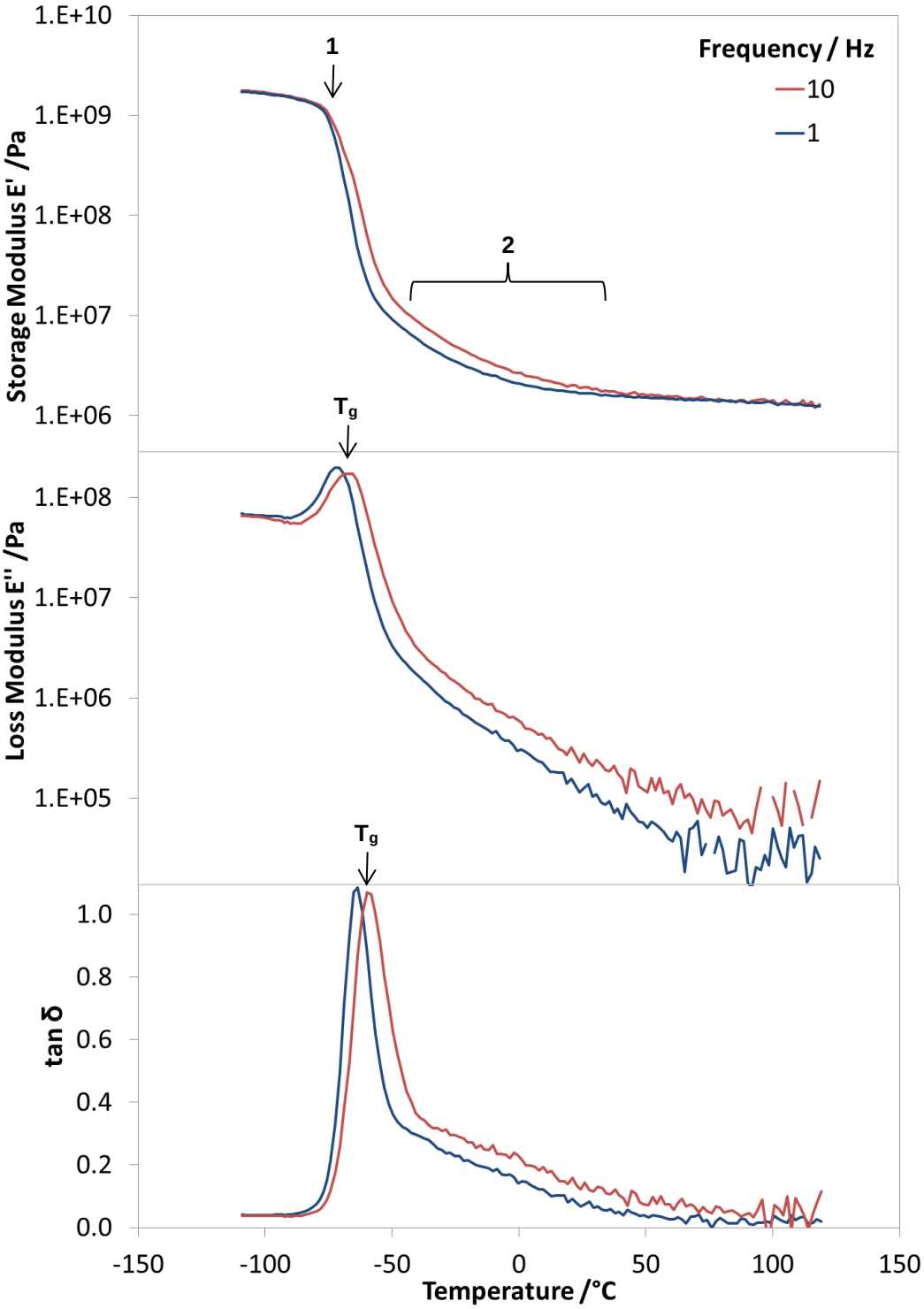

Figure 4-12 DMA thermogram of HTPB/N100. Single cantilever DMA at 10 & 1 Hz, 50 µm (1.25 %) displacement.

Table 4-18 Transitions on the DMA Scan of HTPB/N100

Frequency /Hz	First Transition (T_g)	
	tan δ Maximum /°C	Loss Modulus Maximum /°C
1	-64	-72
10	-59	-66

After the glass transition, instead of the storage modulus quickly reaching a plateau, it slowly decreases over time from ca. -50 to +70 ºC (2). This is believed to be a result of non-homogeneity in the HTPB network, caused by micro-separation of urethane and polybutadiene segments into hard and soft phases due to the difference in their polarity[245].

4.7 Dynamic Mechanical Analysis (DMA) – Frequency Scan

By utilising time temperature superpositioning (TTS) on DMA experiments over a range of frequencies at different temperature, master curves can be obtained over a very wide range of frequencies. This allows an estimation of how the polymer would respond to extreme frequencies.

4.7.1 PEBAX

The storage modulus curves have been shifted to create the master curve using the automated software to overlap the curves, extrapolation was used where the curves did not overlap. The reference temperature (T_0) was chosen as 0 °C. The shift factors (a_T) were then used to create master curve for the tan δ.

The frequency scans for the storage modulus of PEBAX have successfully created a master curve (Figure 4-13), while the loss modulus and tan δ have only created a reasonable master curve for temperatures below -40 °C. This is probably due to PEBAX not being rheologically simple. Around -20 °C there is a noticeable shoulder to the lower glass transition. It is believe that this could be due to the glass transition being combined with the melting transition[225]; if this

was the case it would explain the complex mechanical nature around this temperature.

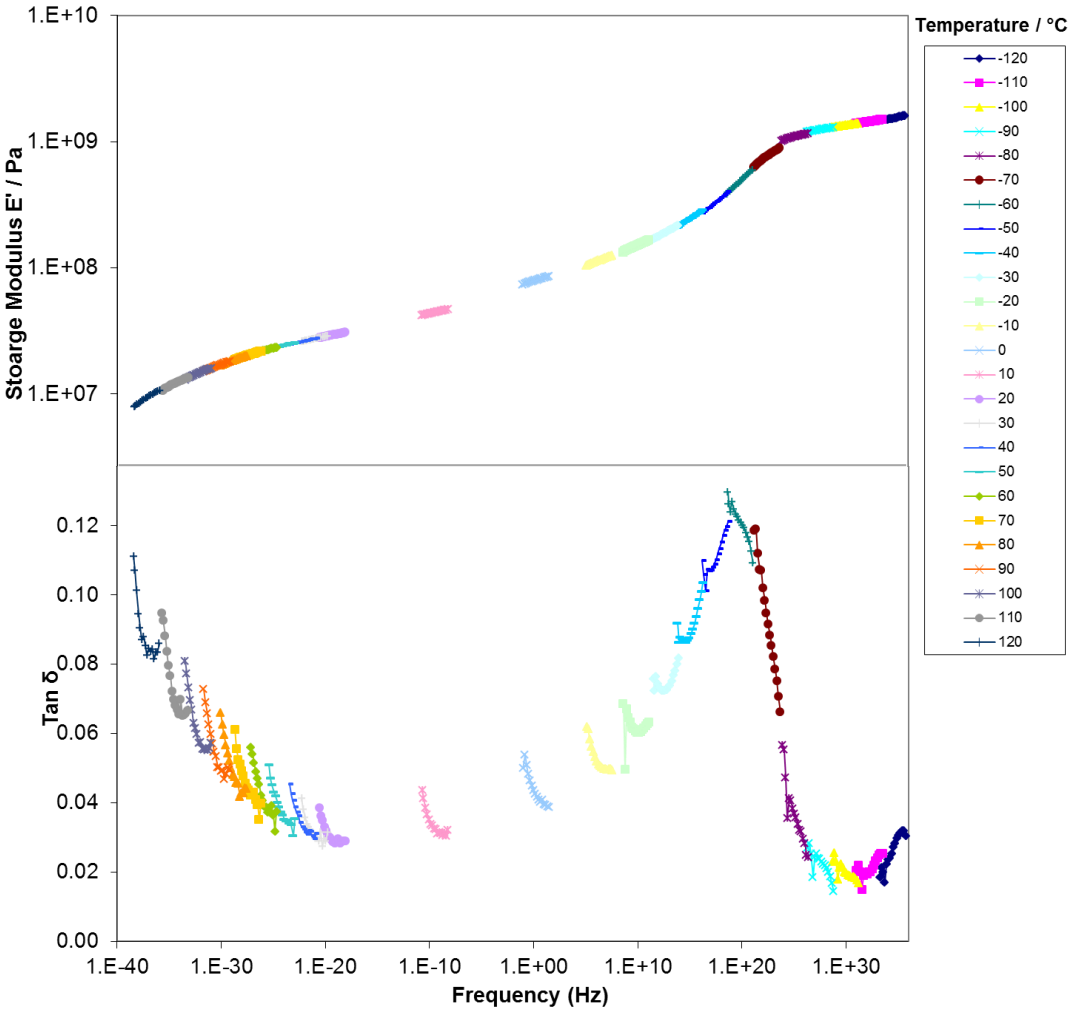

Figure 4-13 Master curve of the storage modulus (E') and tan δ for PEBAX. Curves were shifted to overlap the storage modulus values or by extrapolation. Reference temperature T_0=0 ºC. Data obtained for temperatures between 120 to 120 °C

The tan δ master curve (Figure 4-13) clearly show a glass transition at 10^{+20} Hz which has been assigned to the PTMO block. There is also some evidence for a secondary or β-transition at around 10^{+35} Hz, although this is not completely shown due to the start point of the experiment. At very low frequencies (10^{-40} Hz) there is an increasing drop in the storage modulus due the melting of the PA crystalline phase.

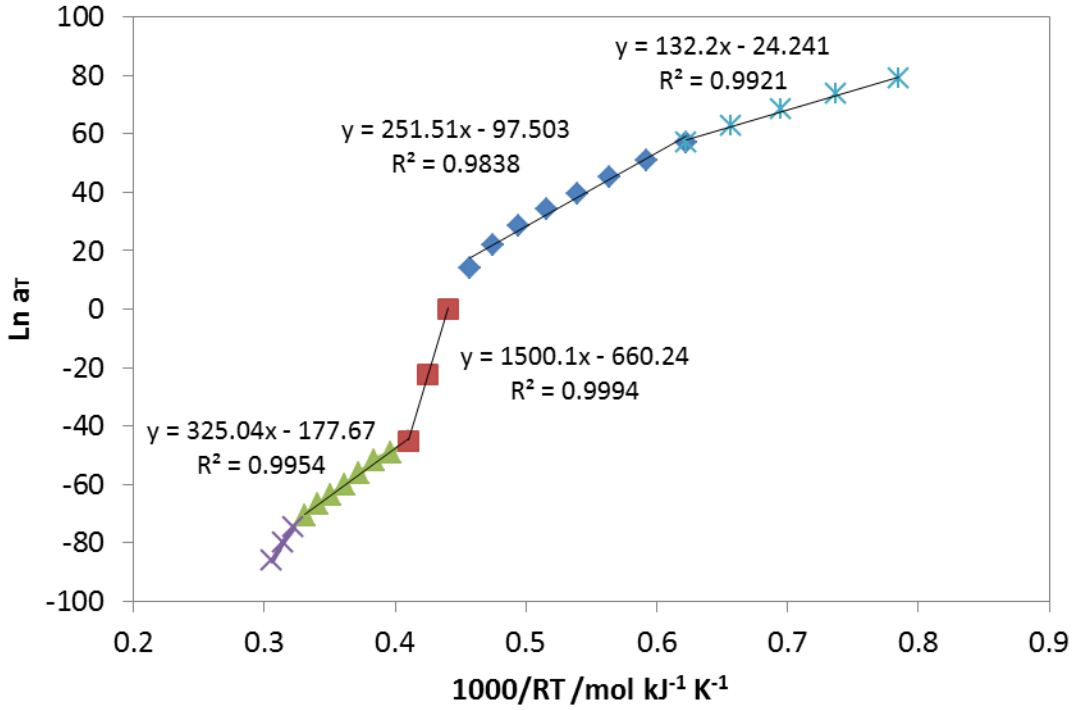

Figure 4-14 Arrhenius plot of the log of shift factors (a_T) against the inverse of absolute temperature (T(K)) for TTS of PEBAX.

Table 4-19 Determination of activation energies from shift factors of DMA TTS.

Phase (in temperature order)	1	2	3	4
Activation Energy (slope of line) / kJ mol^{-1}	132	252	1500	325

Looking at the plot of the log of the shift factors against the inverse of temperature, it is possible to see whether the shift factors follow the Arrhenius equation. From Figure 4-14 there appears to be in four sections. Phases 2 & 4 have apparent activation energies that are consistent with that expected for a glass transition (typically 300 to 400 kJ mol^{-1} [216]) and hence are likely to correspond to the glass transitions of the two blocks of the polymer (PMTO and PA). The middle phase (3) found between -20 and +20 °C could be attributed to the glass transition combining with the melting transition, this would explain the much higher apparent activation energy. Phase 1 however, has a much lower energy making it likely to be due to a beta-transition.[220]

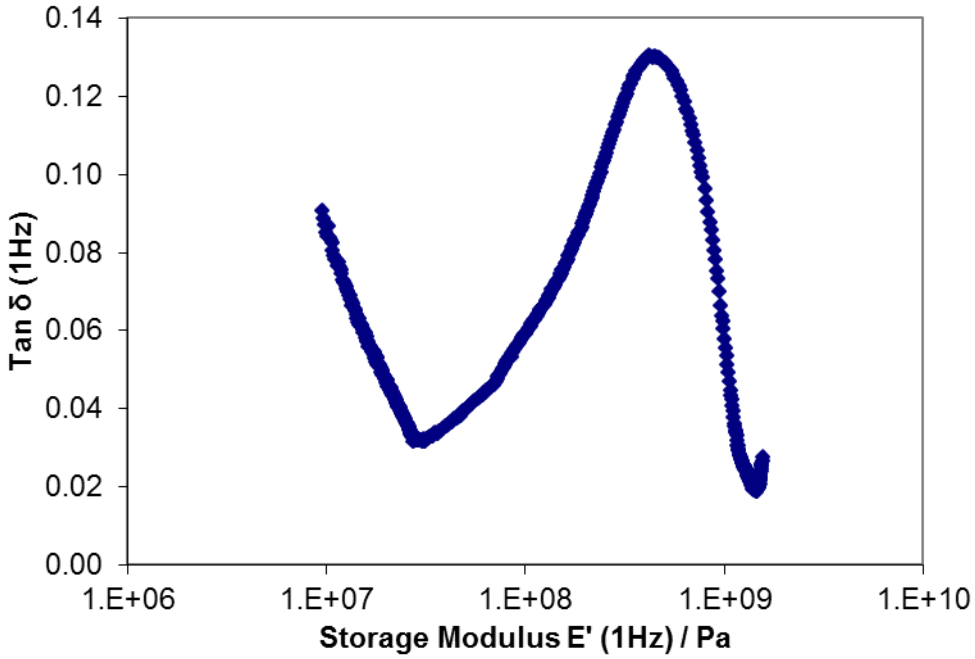

Figure 4-15 Cole-Cole plot for PEBAX using 1Hz data from section 4.6.1.

The Cole-Cole plot should be a smooth arc if the assumptions of the WLF (Williams–Landel–Ferry) equation are met[216]. As can be seen in Figure 4-15 there is a fair amount of non-uniformity in the central arc, indicating that the WLF equation is not applicable. Plotting a graph of $-(T-T_0)/\log a_T$ against $(T-T_0)$ was not successful either.

4.7.2 SEBS

Due to the greater variation in the curve, it was decided to manually shift the tanδ curves to overlap, taking 0°C as the reference temperature (T_0). Then these shift factors (a_T) were used to create the master curve for the storage modulus.

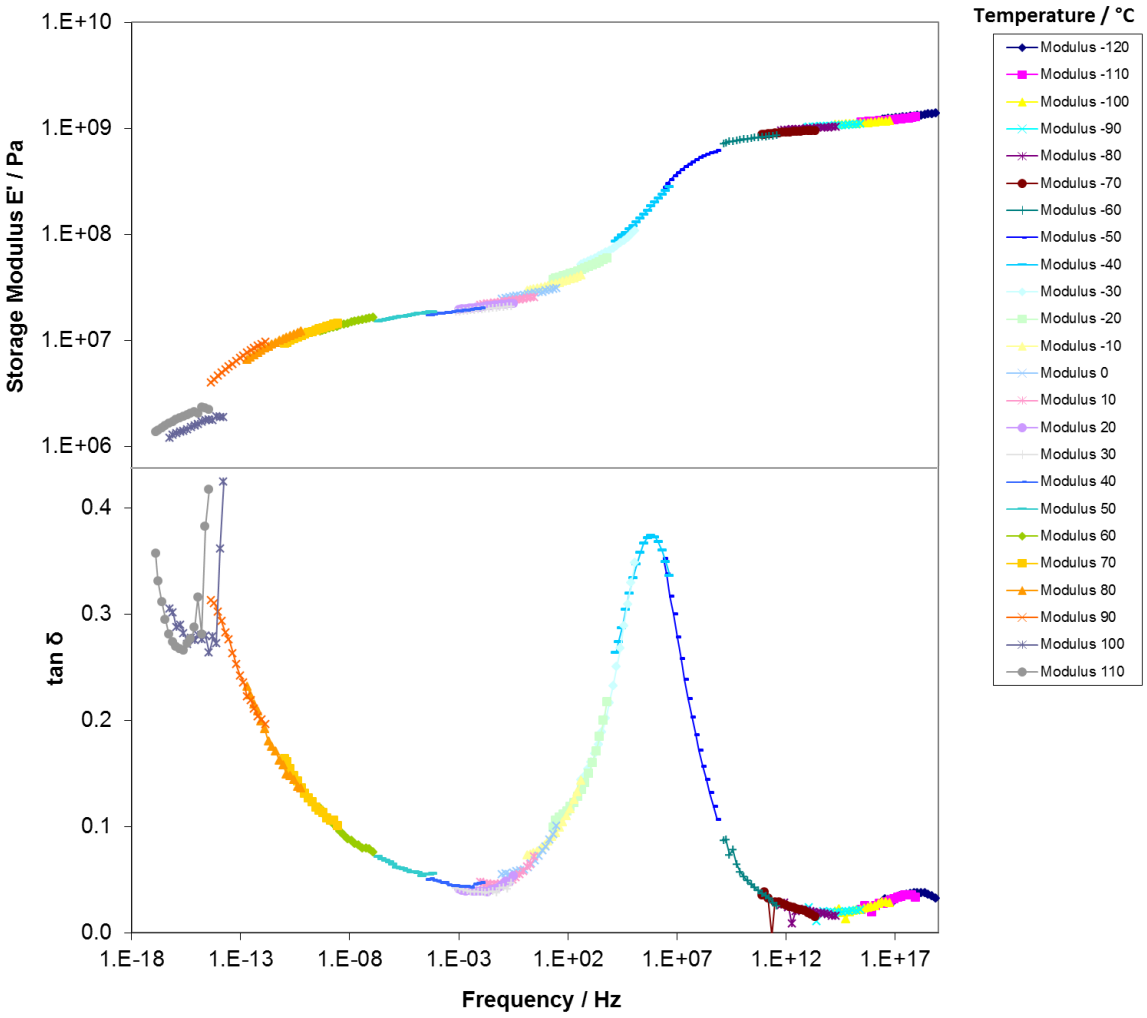

Figure 4-16 Master curve of the storage modulus (E') and tan δ for SEBS. Curves were shifted to overlap the tan δ values. Reference temperature T_0=0 ºC. Data obtained for temperatures between -120 to 110 °C

The tan δ master curve (Figure 4-16) show clearly three transitions. At 10^{-14} Hz there is the T_g of the polystyrene block, at 10^{+6} Hz is the transition due to the ethylene-butylene block, while at higher frequencies still 10^{+18} Hz is a secondary or β-transition. These values compare well with that obtained by Brass[247] of 10^{-11}Hz and 10^{+9}Hz for the polystyrene and ethylene-butylene block respectively using a reference temperature of 25 °C.

By plotting the log of the shift factor against the inverse of the temperature, the activation energy for the transition can be calculated. The graph (Figure 4-17) clearly shows three distinct phases, which fit well with the Arrhenius equation.

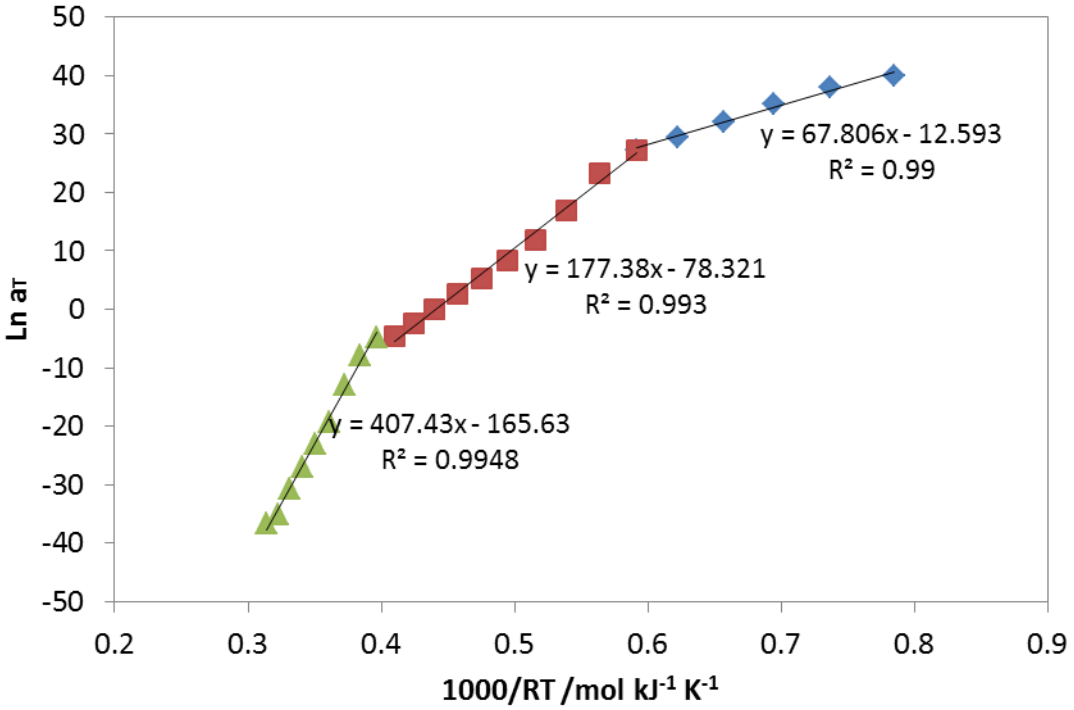

Figure 4-17 Arrhenius plot of the log of shift factors (a_T) against the inverse of absolute temperature (T(K)) for TTS of SEBS.

Table 4-20 Determination of activation energies from shift factors of DMA TTS.

Phase (in temperature order)	1	2	3
Activation Energy (slope of line) / kJ mol^{-1}	68	177	407

The lower activation energy of the third phase would indicate it being a beta transition, while the other two phase changes are more indicative of a glass transition.[216]

While the Cole-Cole plot (Figure 4-18) indicates that there is more than one transition present, the central arc that corresponds to the rubbery region appears relatively uniform and so may be applicable to the WLF equation.

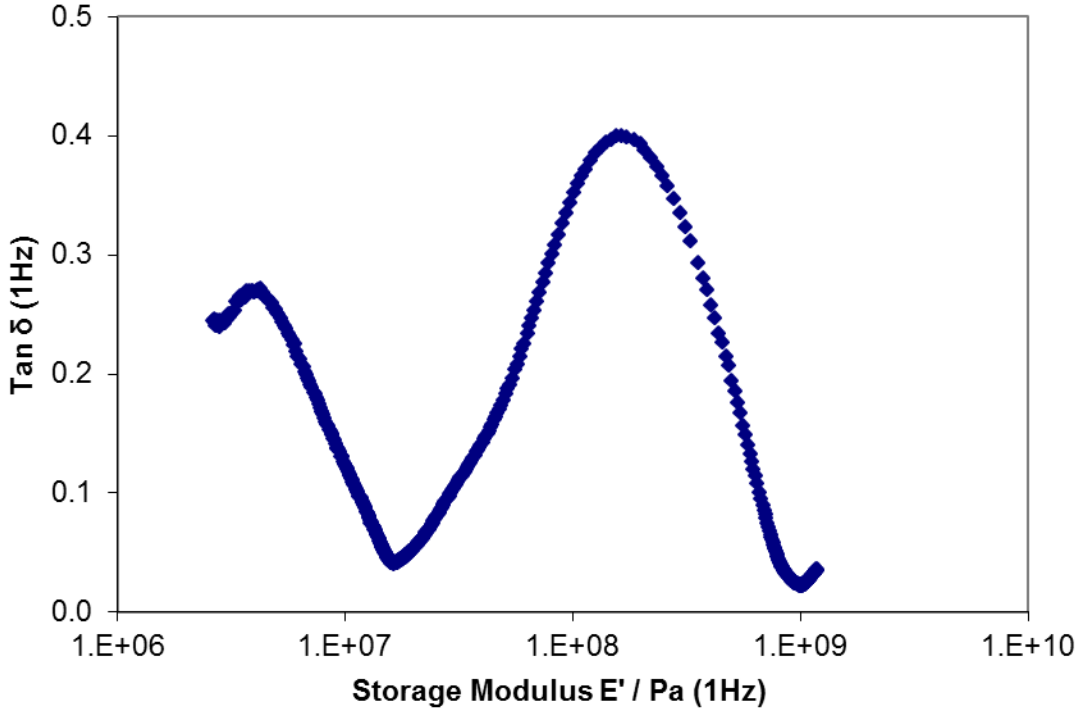

Figure 4-18 Cole-Cole plot for SEBS, using 1Hz data from section 4.6.2.

A plot of $-(T-T_0)/\log a_T$ against $(T-T_0)$ was plotted (Figure 4-19) to calculate the WLF constants C_1 & C_2. T_0 was chosen to be -40 °C as this was approximately the temperature of the lower glass transition; the trend was shown to continue to a temperature of +50 °C.

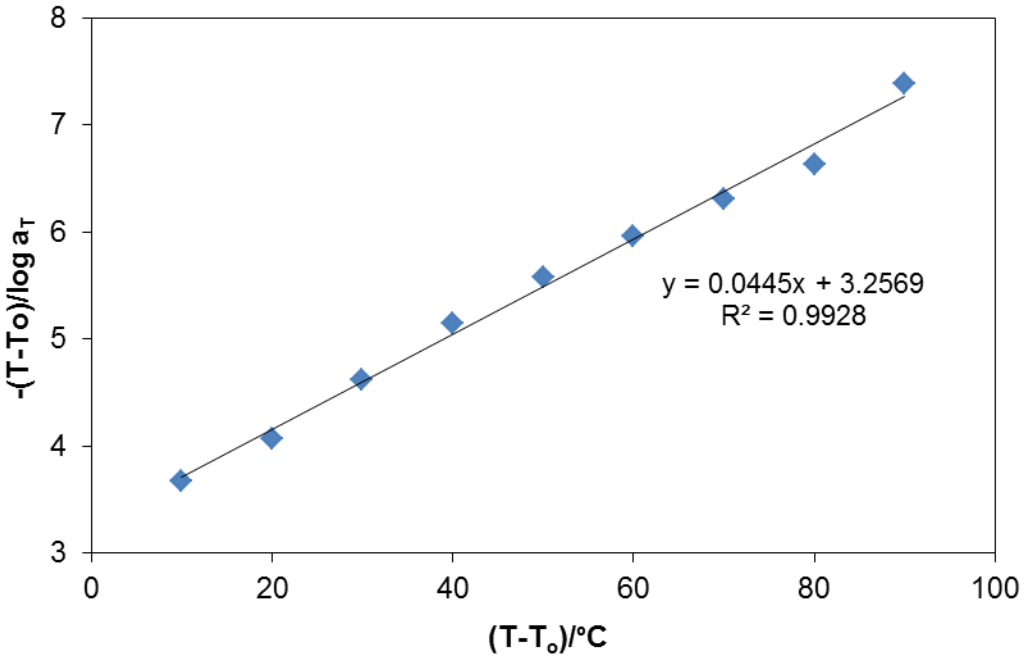

Figure 4-19 Plot of $-(T-T_0)/\log a_T$ against $(T-T_0)$ for temperatures from -50 to +30 °C (T_0=-60 °C).

By using the slope (m) and intercept (c) it is possible to obtain the WLF constants C_1 & C_2. In turn the fractional free volume at the glass transition temperature (f_g) and the thermal coefficient of expansion of the free volume (α_g) can be calculated from the WLF constants by assuming that the Doolittle constant (B) is 1 (Table 4-21). I have been unable to find any reported values for these constants in open literature. Figure 4-20 shows the fit of the WLF equation for the shift factors of SEBS.

Table 4-21 Calculating the WLF constants, f_g and α_f.

Slope(*m*)	***C*$_1$*=1/m***	***C*$_2$ = Intercept *C_1**	***f*$_g$*=B/(2.303*C*$_1$*) (assuming *B*=1)**	***α*$_f$ = *f*$_g$/*C*$_2$**
0.04452	22.5	73.2 °C	0.0193	2.64 x10^{-4}

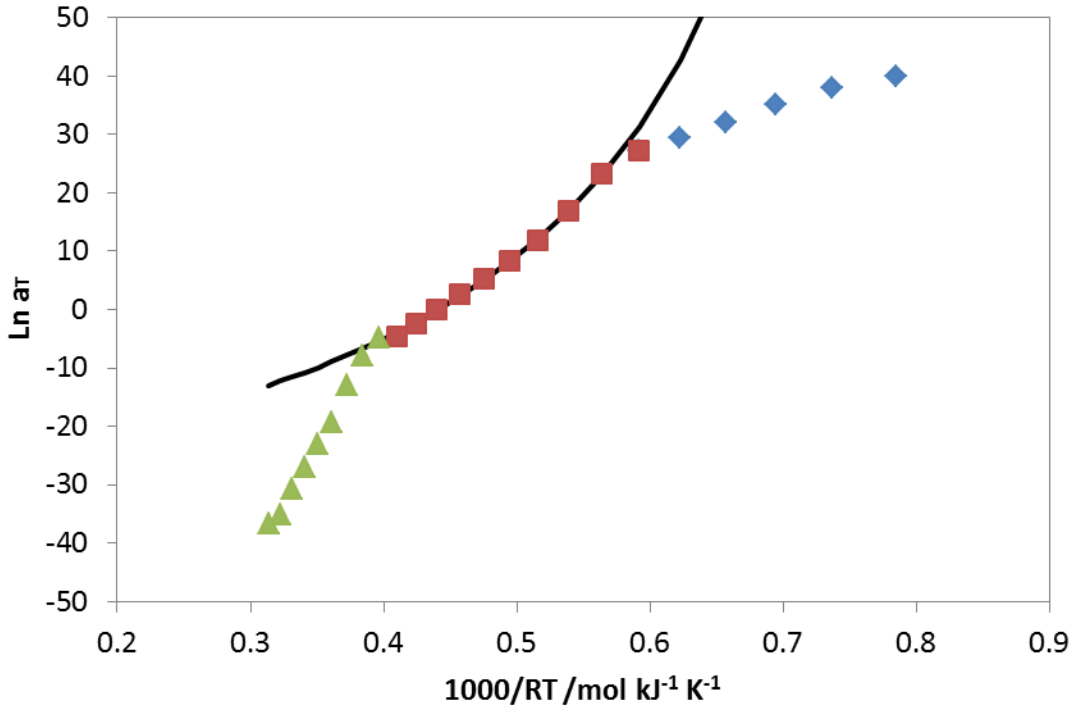

Figure 4-20 Plot showing the fit of the WLF equation for shift factors of SEBS.

4.7.3 HTPB/N100

Frequency scans in the single cantilever geometry were only achievable up to +30 °C due to the low modulus and slippage in the clamps. Time temperature superposition (TTS) was achieved by manual shifting of the tan δ curves to overlap (this had the greater variation and best fit), taking T_0=0 °C. These shift factors (a_T) were then used to create the storage modulus master curve.

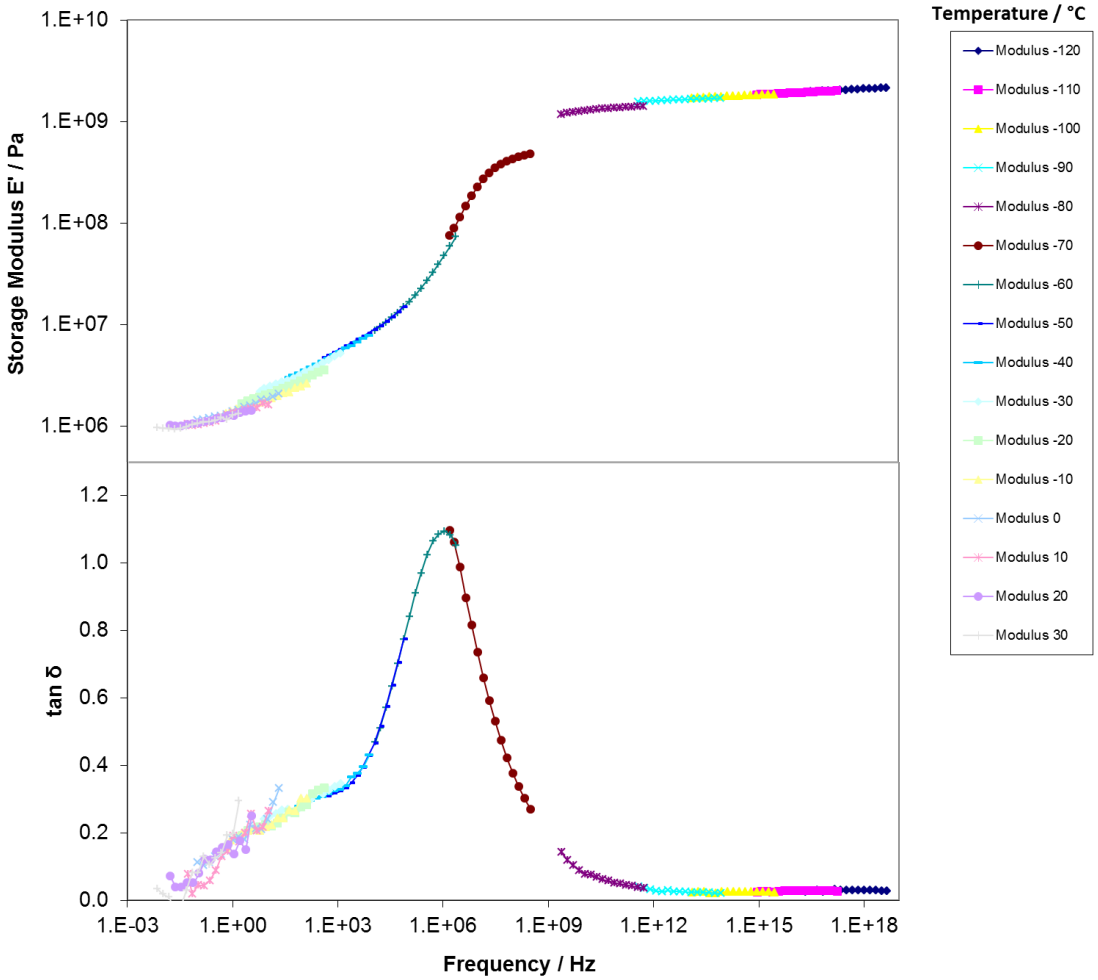

Figure 4-21 Master curve of the storage codulus (E') and tan δ for HTPB/N100. Curves were shifted to overlap the tan δ values or by extrapolation. Reference temperature T_0=0 ºC. Data obtained for temperatures between -120 to 30 °C.

The frequency scans superimposed well into the master curves (Figure 4-21) apart from a slight disconnect between the -80 and the -70 °C scans and some break down at higher temperatures (+10 to +30 °C), again probably due to slippage in the clamps. Both master curves clearly show a single transition, the peak of the tan δ curve being at 10^{+6} Hz.

The Arrhenius plot of the natural log of the shift factors against the inverse of temperature (Figure 4-22) appears to show three distinct phases. The first phase has a lower activation energy (Table 4-22) would be consistent with a beta-transition. The second phase has an activation energy of 184 kJ mol^{-1}, which is

in reasonable agreement with the values of 149 – 165 kJ mol^{-1} stated by Cerri *et al*[248] for HTPB propellants (found by using the frequency dependency of the maxima of the loss modulus). However, this activation energy is fairly low for a glass transition (typically 300 to 400 kJ mol^{-1} [216]). An apparent third phase is shown on the Arrhenius plot. However, by applying the WLF equation below, we see that this is in fact a continuation of the second phase (Figure 4-25).

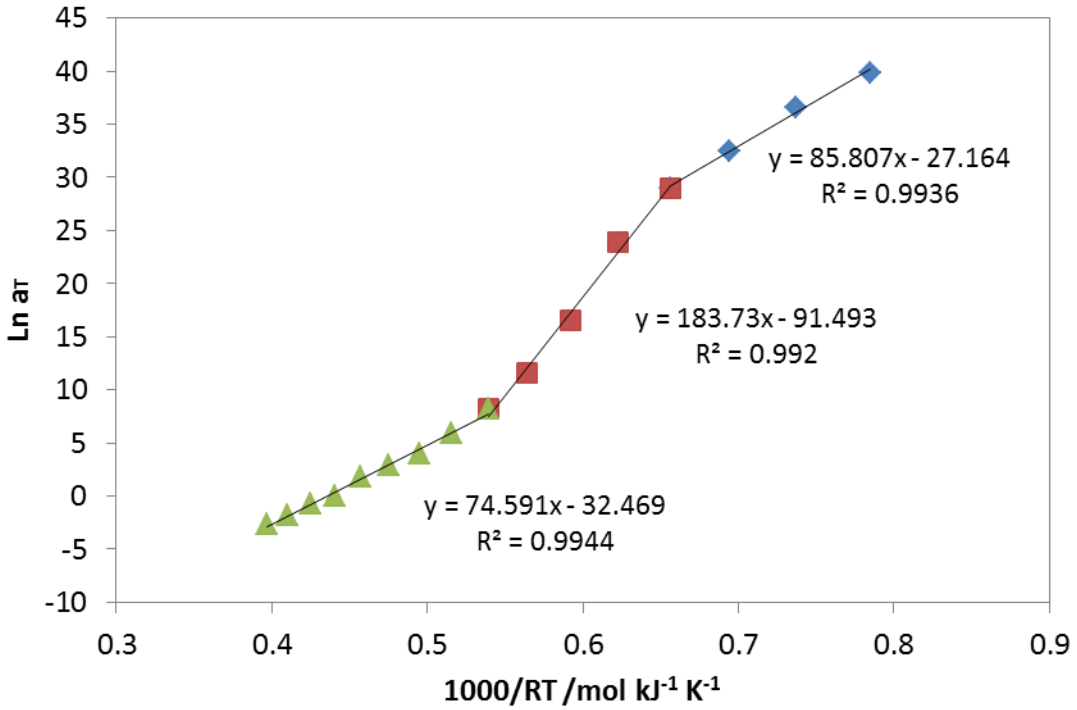

Figure 4-22 Arrhenius plot of the log of shift factors (a_T) against the inverse of absolute temperature (T(K)) for TTS of HTPB/N100.

Table 4-22 Determination of activation energies from shift factors of DMA TTS

Phase (in temperature order)	1	2	3
Activation Energy (slope of line) / kJ mol^{-1}	85	184	75

The Cole-Cole plot (Figure 4-23) shows a single arc, but there is a sizable shoulder to the curve at lower values of the storage modulus. This would indicate

that the WLF equation will not be applicable for the entire range of the data, this is not surprising as the equation is usually only valid for temperatures from the T_g to T_g+100 °C.

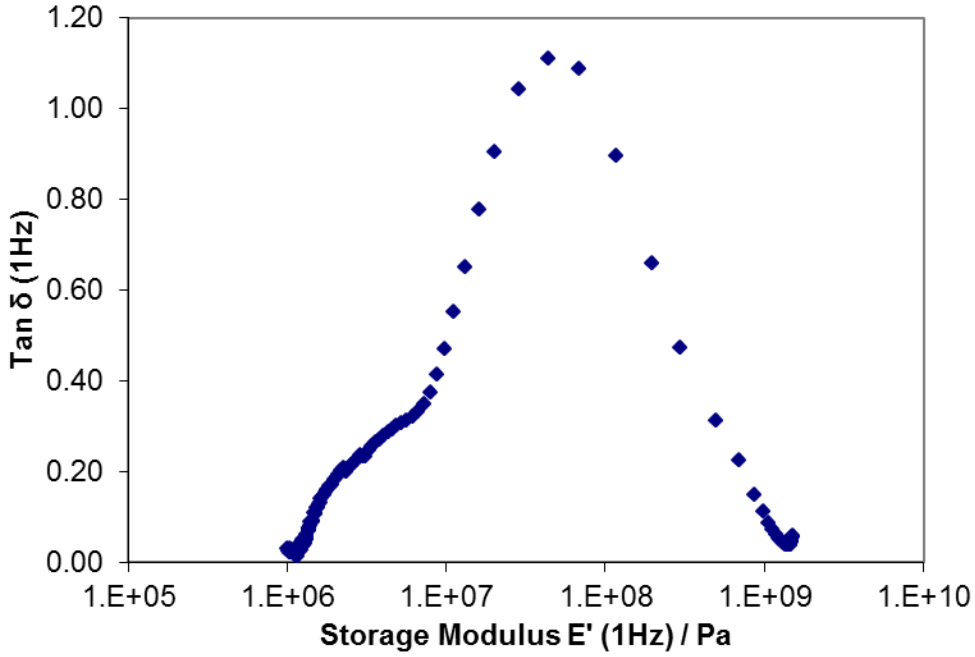

Figure 4-23 Cole-Cole plot for HTPB/N100 using 1Hz data from section 4.6.3

A plot of $-(T-T_0)/\log a_T$ aginst $(T-T_0)$ was plotted (Figure 4-24) to calculate the WLF constants, T_0 was chosen to be -80 °C and there was a good fit to the maxim temperature achieved in the test (+30 °C).

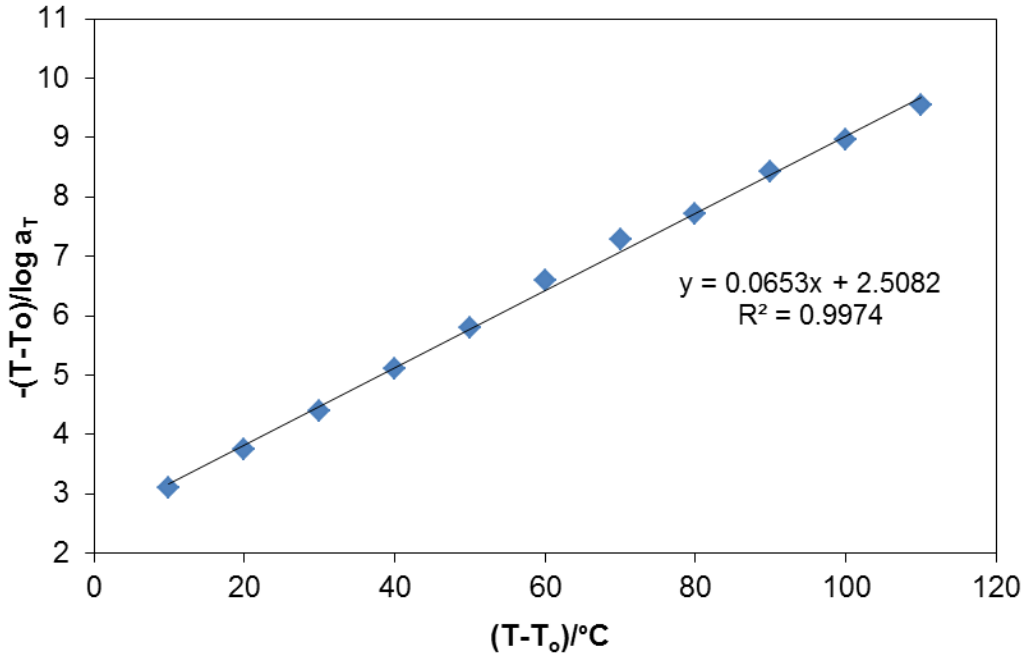

Figure 4-24 Plot of -(T-T_0)/log aT against (T-T_0) for temperatures from -70 to +30 °C (T_0=-80 °C).

Table 4-23 Calculating the WLF constants, f_g and α_f.

Slope(*m*)	$C_1=1/m$	C_2 = Intercept *C_1	$f_g=B/(2.303*C_1)$ (assuming *B*=1)	$\alpha_f = f_g/C_2$
0.0653	15.3	35.4	0.0283	8.00×10^{-4}

The WLF constants can then be converted into the fraction free volume at the glass transition (f_g) and the thermal coefficient of expansion of the free volume (α_f) (Table 4-23). These values compare well with that obtained by Stacer & Husband[9] (f_g = 0.025 to 0.028 and α_f = 4.5 to 5.7 x 10^{-4}) for various cured HTPB gunstocks.

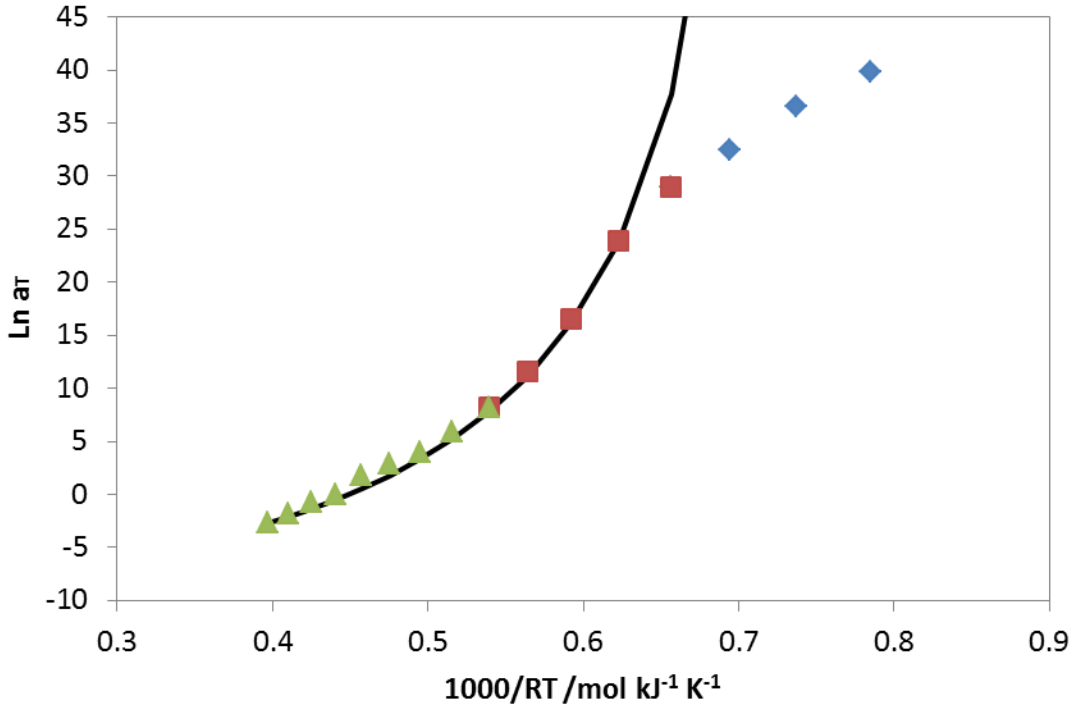

Figure 4-25 Plot showing the fit of the WLF equation for shift factors of HTPB/N100.

4.8 Comparison of Thermal and Mechanical Properties of TPEs with HTPB/N100

Overall, comparing the lower glass transitions and upper glass or melting transitions of the TPEs (Table 4-24), we see that PEBAX compares excellently with HTPB/N100. The service temperature range of PEBAX, as shown by its glass transition and melting transition, is greater than the desired operating temperature range (-54 to +74 ºC). SEBS also has reasonable characteristics, the lower glass transition found by DSC is below our desired operating temperature, however when found by DMA is above our minimum temperature and is noticeable higher than HTPB. This would indicate that the SEBS polymer might not be suitable for use in extreme cold temperatures (-54 °C), however further mechanical testing of the filled material would be necessary to corroborate this. Both PEBAX and SEBS have upper transitions above our upper working temperature. This is not surprising as being commercial polymers they are required to work in a wide range of conditions without failure, for instance, the inside of a car which can heat up to these temperature in extreme conditions.

HTPB/N100 being a thermoset polymer has no upper working temperature due to melts or transitions.

Table 4-24 Comparison of Thermal and Mechanical Properties of TPEs with HTPB/N100.

Polymer		PEBAX	SEBS	HTPB/N100
DSC	**Lower glass transition (midpoint / °C)**	-75.8	-55.2	-74.6
	Upper glass or melting transition / °C	122.3 (melt onset)	Not identifiable by DSC	None
DMA	**Lower glass transition (tan δ maximum at 1 Hz /°C)**	-58.9	-41.0	-64
	Upper glass or melting transition at 1 Hz /°C	115.7 (melt / tan δ above 0.5)	114.6 (glass transition)	None

By comparing the DMA scans (Figure 4-26) of the TPEs against HTPB/N100, we can see that the TPEs have a higher storage modulus in the working temperature range, due to these polymers being stiffer. An important property of a propellant is its ability to hold its shape and not break up in storage, in service or when ignited. In theory, a stiffer material should hold together better, providing it is able to absorb any impacts without fracturing. The tan δ, provides information on the dampening of the material, that is the amount of energy that is absorbed by the material when it is oscillated in the DMA. Both PEBAX & SEBS have a lower tan δ than HTPB/N100 below 40 °C (excluding the effects of the glass transition) indicating that it is less effective in absorbing the energy of impact. However, as PEBAX & SEBS have higher storage modulus, so they will deform less for the same force applied.

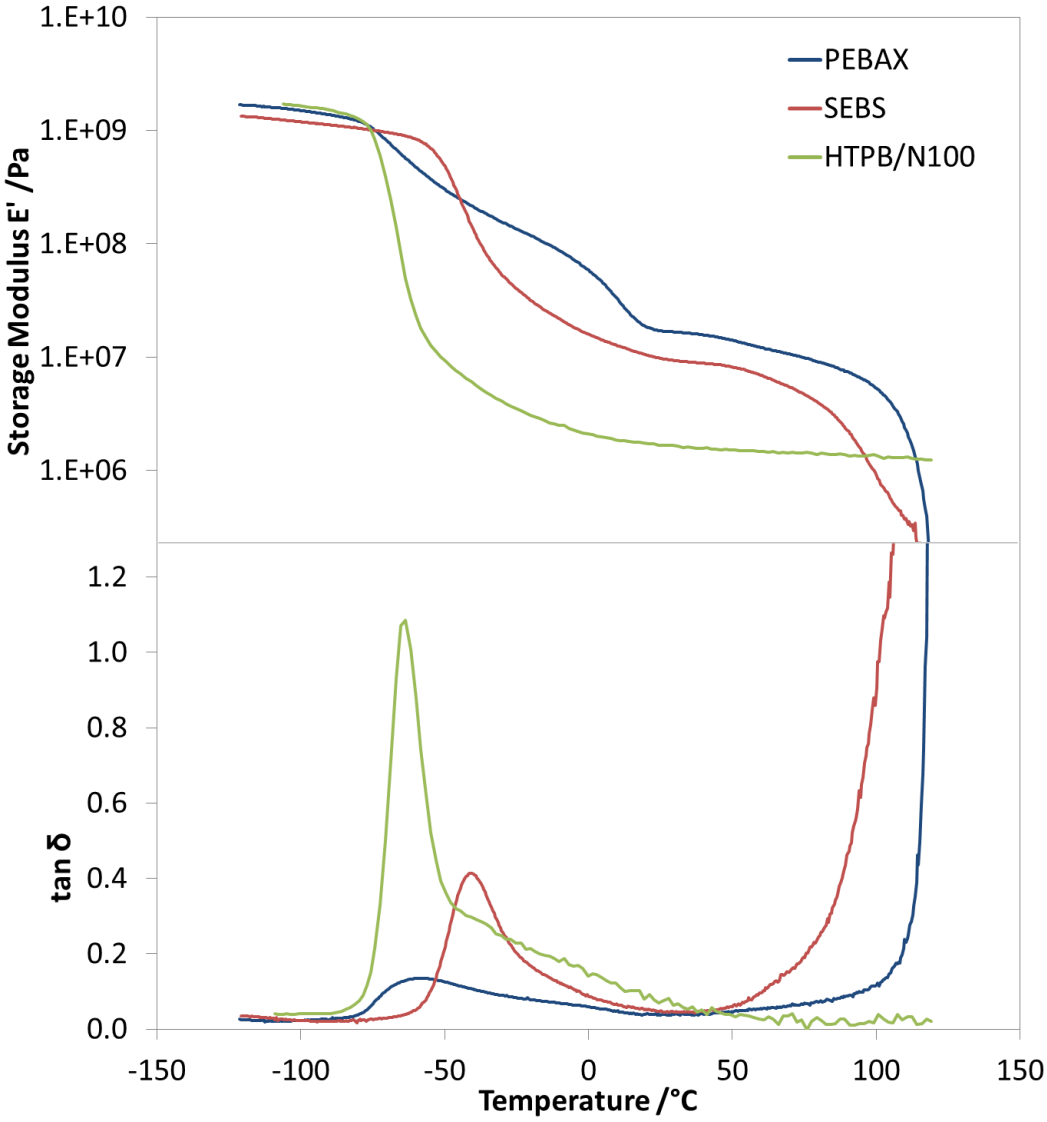

Figure 4-26 Comparisons of DMA Temperature Scans for PEBAX, SEBS & HTPB/N100.

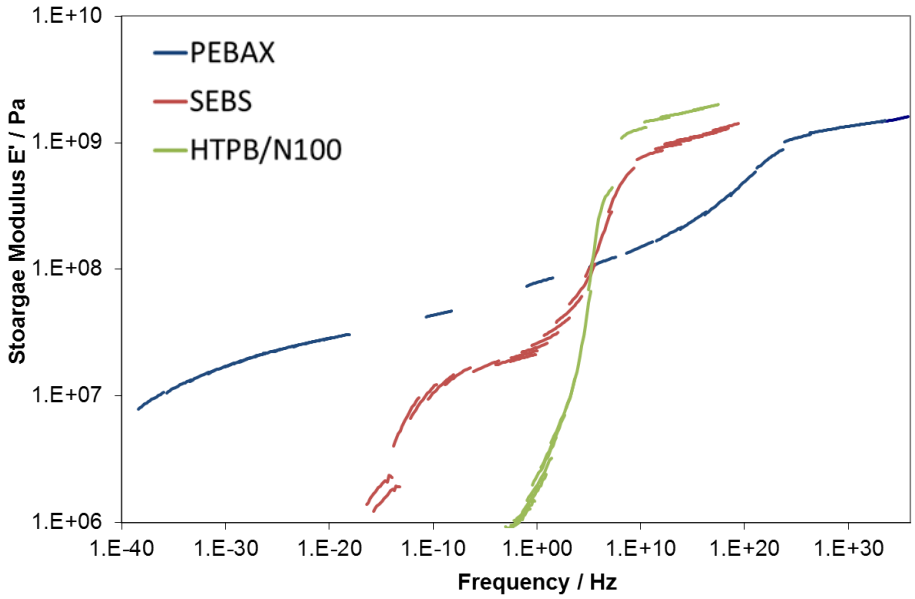

Figure 4-27 Comparison of Master Curves of the Storage Moduli for PEBAX, SEBS & HTPB/N100 calculated by TTS. Reference Temperature T_0=0 ºC.

There is clearly a difference in the master curves of the storage moduli of the TPEs compared to HTPB/N100 (see Figure 4-27). The storage modulus of SEBS and especially PEBAX are less affected by frequency, than HTPB/N100. The 'lower' (in terms of temperature) glass transition can be seen around 10^{+8} Hz for both SEBS and HTPB/N100, while for PEBAX it is around 10^{+20} Hz. This is certainly very promising as it suggests that the TPEs would at least be as good as HTPB/N100 at staying in a rubbery state even at high frequencies. This would reduce the likelihood of fracturing as a binder at high strain rates.

In summary, both TPEs appear suitable for a wide range of propellant uses and compare well with HTPB. PEBAX even has some characteristics which are better, most notable the higher frequency of the lower glass transition, shown by TTS. SEBS does have a higher, lower glass transition than HTPB, which may limit it uses.

5 Characterisation of TPEs Blended with Plasticisers

5.1 Introduction

Plasticisers are commonly incorporated into binders used in composite propellants for a variety of reasons. Firstly, they can improve the mechanical properties of the polymer by increasing flexibility and reducing stiffness, they can also lower the glass transition (T_g) point. A plasticiser can also be added as a processing aid, lowering the viscosity of the polymer making it easier for processing during manufacture. Dioctyl Sebacate (DOS) was chosen, it is non-hazardous and often used in the energetics industry. In this chapter both TPEs (PEBAX & SEBS) have been plasticised with DOS to various concentration. The thermal and mechanical characteristics of these samples have been ascertained to see what effect the plasticiser has and whether this is an improvement for use as a binder. A sample of cured plasticised HTPB (R45M) is compared against the TPE samples. Firstly, this will show if the TPEs can be plasticised by a typically plasticiser used in the energetics industry. Then the thermal properties were analysed by DSC and mechanical properties by DMA to see if a propellant made from these TPEs would have suitable properties.

Initial testing indicated that 20 % m/m of DOS plasticiser could be incorporated in to PEBAX, while SEBS could accept 25 % m/m. A range of samples with different concentration of plasticiser was prepared (Table 5-1). Due to limited available resources only one plasticised sample of cured HTPB could be produced, a typically value of 33.3 % m/m (33 % v/v) concentration of DOS plasticiser was chosen.

Table 5-1 Composition of plasticised thermoplastic elastomers samples.

Sample	Composition by volume			Composition by mass		
	PEBAX / % v/v	SEBS / % v/v	DOS plasticiser / % v/v	PEBAX / % m/m	SEBS / % m/m	DOS plasticiser / % m/m
P97.3D2.7	97.3		2.7	97.5		2.5
P95D5	94.5		5.5	95		5
P89D11	89.1		10.9	90		10
P84D16	83.7		16.3	85		15
P78D22	78.4		21.6	80		20
S97.5D2.5		97.5	2.5		97.5	2.5
S95D5		95.0	5.0		95	5
S90D10		90.0	10.0		90	10
S85D15		85.1	14.9		85	15
S80D20		80.1	19.9		80	20
S75D25		75.1	24.9		75	25

5.2 Density Measurements

Obtained densities of PEBAX plasticised with DOS are reported in Table 5-2. By looking at Figure 5-1 it can be seen that the densities of plasticised PEBAX follows the predicted values well. The densities are slightly lower than of the predicted values, this could be experimental error or possibly be due to the plasticiser disrupting the intermolecular forces between the polymer chains, hence increasing the average intermolecular distance. However, I cannot find any reference to this effect in open literature.

Table 5-2 Density of hot pressed samples of PEBAX unplasticised and plasticised with DOS found by helium pycnometery. Standard deviation (σ) x1 is reported throughout this thesis.

Sample	Plasticiser (DOS) / % m/m	Average Density/ g cm^{-3}	Predicted Density* / g cm^{-3}
PEBAX	0	1.0077 (σ = 0.0002)	-
P97.3D2.7	2.5	1.0044 (σ = 0.0006)	1.0051
P95D5	5	1.0019 (σ = 0.0006)	1.0026
P89D11	10	0.9962 (σ = 0.0011)	0.9975
P84D16	15	0.9919 (σ = 0.0007)	0.9924
P78D22	20	0.9853 (σ = 0.0011)	0.9875

* Predicted density is based on the volume fraction using the obtained density for unplasticised PEBAX and the literature value of 0.914 g mol^{-1} for DOS[249].

The densities of SEBS plasticised with DOS are in Table 5-3. As expected, due to the polymer and the plasticiser having similar densities (SEBS = 0.909 g cm^{-3} & DOS = 0.914 g cm^{-3}) there is little change in the density of plasticised SEBS. As can be seen in Figure 5-1, there is a reasonable trend of density increasing with plasticiser content. This effect appears to be slightly larger than that expected just from their volume fractions. This different would probably be an experimental error, but it could be explained by more efficient pressing of the plasticised sample in comparison to the unplasticised SEBS.

Table 5-3 Density of hot pressed samples of SEBS unplasticised and plasticised with DOS found by gas pycnometery.

Sample	Plasticiser (DOS) / % m/m	Average Density/ g cm^{-3}	Predicted Density* / g cm^{-3}
SEBS	0	0.9094 (σ = 0.0002)	-
S97.5D2.5	2.5	0.9094 (σ = 0.0008)	0.9095
S95D5	5	0.9109 (σ = 0.0012)	0.9096
S90D10	10	0.9133 (σ = 0.0006)	0.9099
S85D15	15	0.9119 (σ = 0.0009)	0.9101
S80D20	20	0.9119 (σ = 0.0007)	0.9103
S75D25	25	0.9137 (σ = 0.0008)	0.9105

* Based on the volume fraction using the obtained density for unplasticised SEBS and the literature value of 0.914 g mol^{-1} for DOS[249].

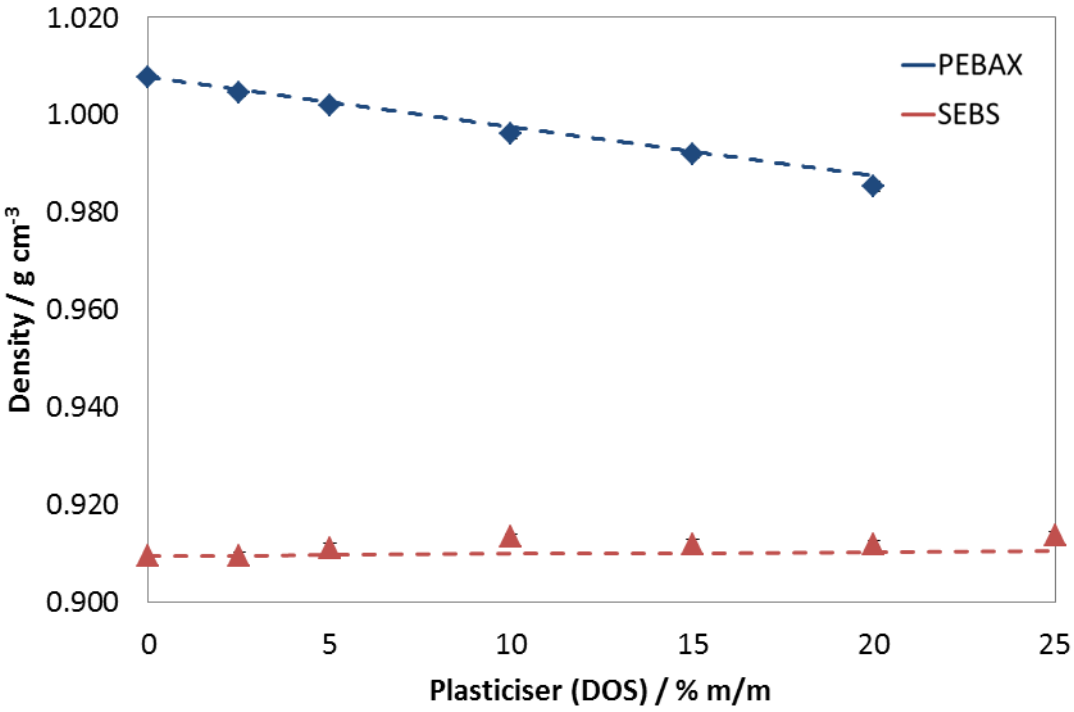

Figure 5-1 Graph of the density (helium pycnometery) against percentage of plasticiser (DOS) in PEBAX and SEBS. Dotted line represent the predicted densities based on volume fraction. Error bars represent the standard deviation (x1) throughout this thesis.

5.3 Differential Scanning Calorimetry (DSC) Analysis

DSC analysis of the plasticised TPEs was employed to determine the glass transition temperature and melting points. These were compared with a cured plasticised HTPB sample (HTPB/N100/DOS).

5.3.1 PEBAX Plasticised with DOS

Looking at the DSC heating scans in Figure 5-2 (lower), the glass transition (T_g) (shown by the characteristic step) found around -77 °C in pure PEBAX has been lowered by the addition of DOS plasticiser (Table 5-4). This transition has been confidently assigned to the soft PTMO block, hence some of the plasticiser must be incorporated into this block.

Table 5-4 Glass transition found by DSC (10 °C min^{-1} heating rate) for different blends of PEBAX with DOS plasticiser. Averages are of three heating cycles.

Sample	Plasticiser (DOS) / % m/m	Average Glass Transition [T_g] (Midpoint) /°C
PEBAX	0	-77.2 (σ = 0.7)
P97.5D2.5	2.5	-78.2 (σ = 0.7)
P95D5	5	-80.2 (σ = 0.1)
P90D10	10	-82.5 (σ = 0.6)
P85D15	15	-85.3 (σ = 1.0)
P80D20	20	-91.1 (σ = 1.0)

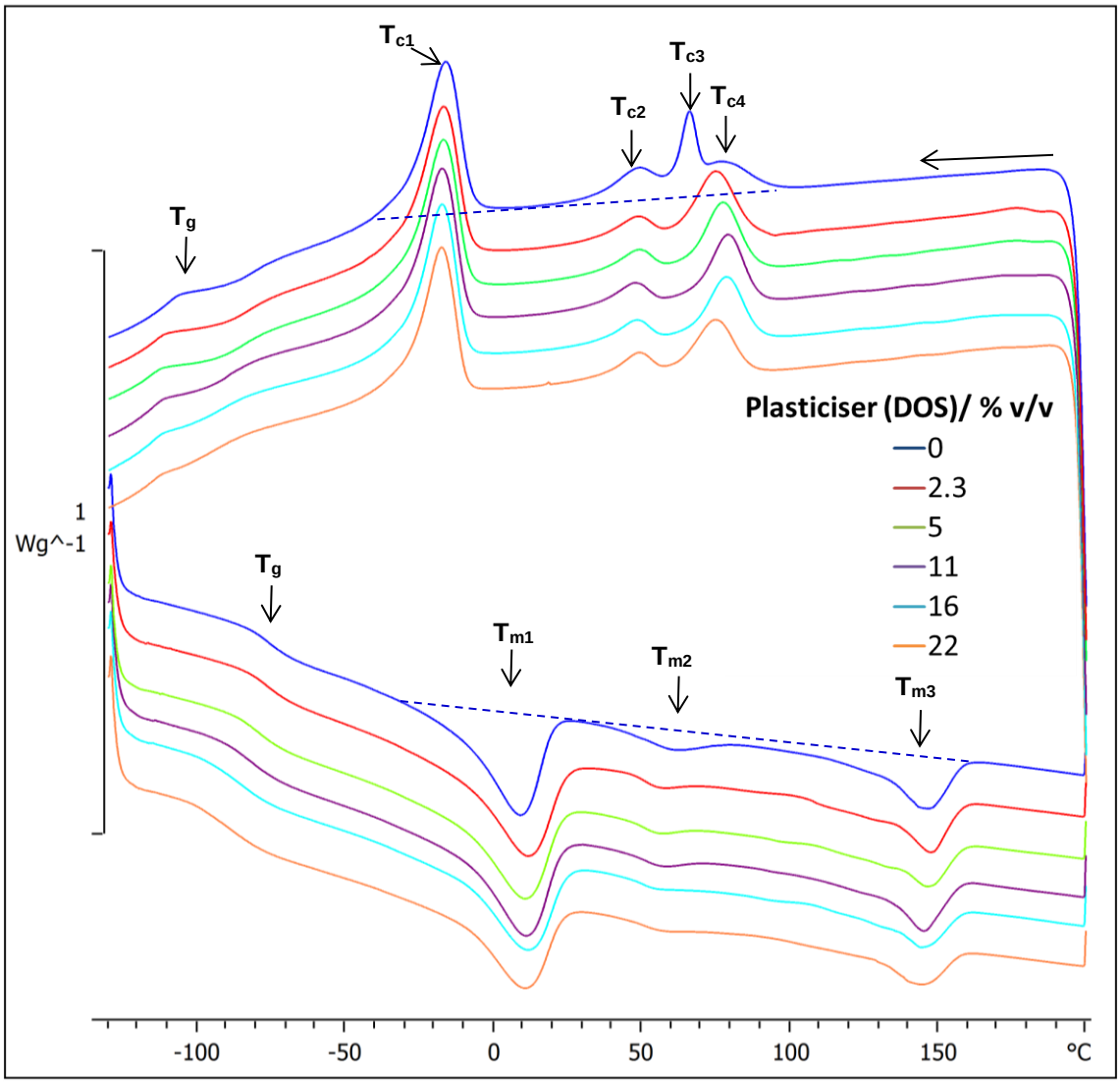

Figure 5-2 DSC thermogram of scans for different blends of PEBAX with DOS plasticiser. Only first heating (lower) and cooling curves (upper) are shown.

Figure 5-3 shows a linear decrease ($R^2 = 0.970$) in the glass transition (T_g) found by DSC as plasticiser concentration increases. This indicating that there is good solubility of the plasticiser up to this concentration. The value of the plasticiser coefficient (k) (see section 2.6.2) was found to be 66.1 °C (the slope multiplied by 100).

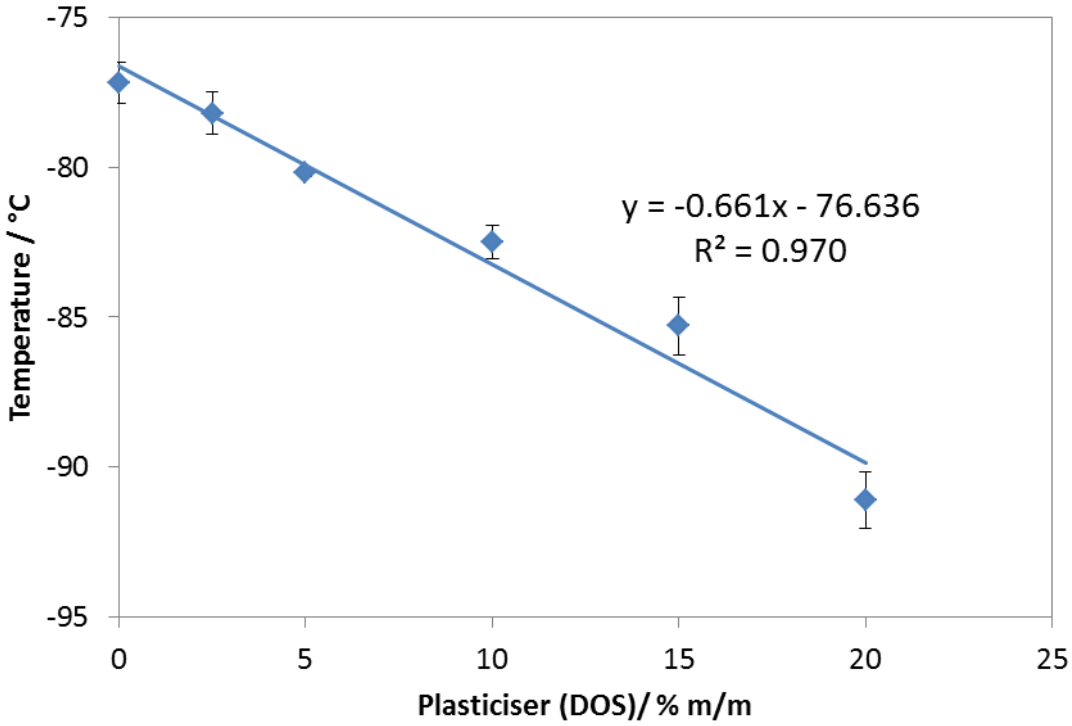

Figure 5-3 Graph of glass transition (T_g) against DOS plasticiser concentration found by DSC. Results are averages of three heating cycles.

The presence of plasticiser had no measurable effect on the first endotherm (T_{m1}). As this is attributed to the melting of the PTMO block, a reduction in the melting point would be expected. However this endotherm is at a much lower temperature than that of pure PTMO (peak at 36 °C, 10 °C min^{-1} [233]), which Sheth[225] suggested was due the inability to form thicker more perfect lamellae crystals as compared to the homopolymer. Hence it is reasonable to suggest that if the melting point has already been reduced, the presence of the plasticiser may have little or no further effect.

The second (T_{m2}) and third (T_{m3}) endotherms also show no effect due to the plasticiser, this however is not unexpected. With the second endotherm being due to the PA block or possibly a mixed region and the third endotherm being confidently assigned to the PA block, and the solubility of an ester plasticiser (such as DOS) in a polyamide polymer will be very low. Hence the very small presence of the plasticiser in the PA block would have very little effect on the melting points.

The same trend of decreasing glass transition (T_g) temperature with increasing plasticiser concentration can be seen on the cooling curve (Figure 5-2, upper). There is again very little effect of the plasticiser on the first exotherm (T_{c1}), assigned to the PTMO block. There does appear to be a slight decrease in the peak temperature with increasing plasticiser concentration. The second exotherm (T_{c2}), like the second endotherm (T_{m2}) is also unaffected by the plasticiser.

There is a change with the third and fourth exotherms (T_{c3} & T_{c4}) between the unplasticised pressed sample and all of the plasticised samples. T_{c3} completely disappears in the plasticised samples, while T_{c4} is much larger. These peaks are attributed to the crystallisation of the PA block, but the crystallisation point has been dramatically reduced due to delayed supercooling. In these samples the plasticiser appears to be aiding the crystallisation, possibly acting as a nucleating agent, hence increasing the crystallisation point.

5.3.2 SEBS Plasticised with DOS

The first transition (T_{g1}) can be seen in the heating curves for plasticised (DOS) samples of SEBS in the lower curves of Figure 5-4. This transition is due to ethylene-butylene midblock in SEBS. Table 5-5 and Figure 5-5 show the transition lowering with the increasing concentration of DOS plasticiser up to 15 % v/v. This provides evidence that the plasticiser has become incorporated into this segment. At higher concentration of DOS (20 & 25 % v/v) there appears to be no further decrease in the T_g found by DSC. Apparent on the 20 % v/v DOS scan and clearly evident on the 25 % v/v DOS scan is a new transition (T_{g-P}) with a midpoint of around -95 °C which corresponds closely to that of pure DOS plasticiser (midpoint -104.9 °C found by DSC). This would suggest that the DOS plasticiser is miscible in SEBS for concentrations up to 15 % v/v, above which there is evidence of separation.

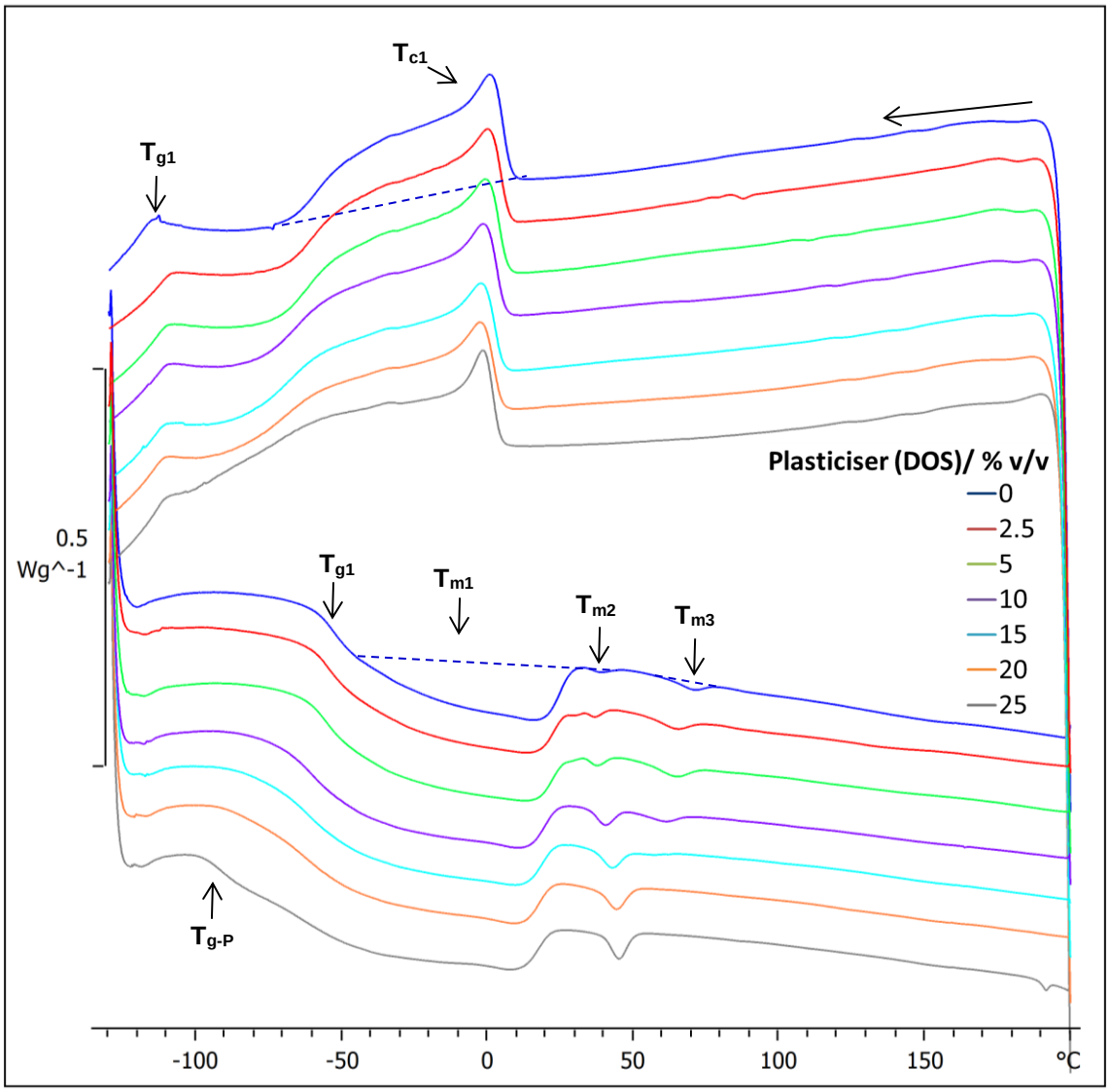

Figure 5-4 DSC thermogram of scans for different blends of SEBS with DOS plasticiser. Only first heating (lower) and cooling curves (upper) are shown.

Table 5-5 Glass transition found by DSC (10 °C min^{-1} heating rate) for different blends of SEBS with DOS plasticiser. Averages are of three heating cycles.

Sample	Plasticiser (DOS) / % m/m	Average Glass Transition [T_{g1}] (Midpoint) /°C
SEBS	0	-53.3 (δ = 0.6)
S97.5D2.5	2.5	-53.9 (δ = 0.2)
S95D5	5	-55.5 (δ = 0.0)
S90D10	10	-59.1 (δ = 0.9)
S85D15	15	-63.0 (δ = 0.4)
S80D20	20	-62.9 (δ = 0.2)
S75D25	25	-63.4 (δ = 0.9)

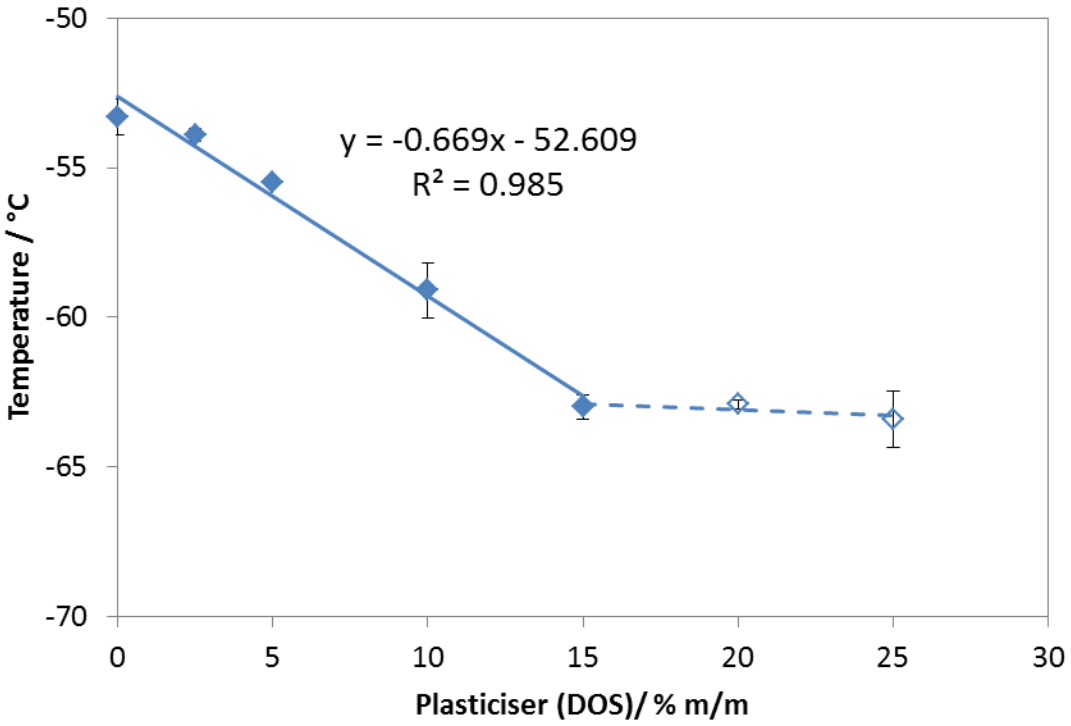

Figure 5-5 Graph of first transition (T_{g1}) against DOS plasticiser concentration found by DSC. Results are averages of three heating cycles.

Figure 5-5 shows for 0 to 15 % v/v concentrations of DOS there is a close fit (R^2 = 0.984) to the linear approximation of the effect of the plasticiser on the T_g. This gives a value the plasticiser coefficient (k) being 66.9 °C, a similar value to that found with PEBAX (66.1 °C). For concentrations of DOS greater than

15 % v/v it now longer appears to acting as a plasticiser, at least in terms of lowering the T_g.

Looking again at the heating curves (Figure 5-4, lower curves), the first endotherm (T_{m1}) is also clearly affected by the DOS plasticiser. As the concentration of plasticiser increases the onset occurs earlier while the endset remains at around the same point. This provides further evidence of the plasticiser presence in the ethylene-butylene midblock. The heat of melting of the first endotherms remains approximately the same when the proportion of SEBS polymer is taken into account.

The second (T_{m2}) and third endotherms (T_{m3}), which are only seen in the first heating cycle, also seem to be affected by the presence of the plasticiser. T_{m2} appears to increase in size and shift to a slightly higher temperature while T_{m3} shifts to a lower temperature. The two endotherms then appear to merge at around 20 % DOS concentrations. Zhou *et al*[232] showed by thermal correlation spectroscopy that these endotherms originate at the phase interfaces between the ethylene-butylene and styrene blocks. This shows that the plasticiser is also occupying this region, at least for the blend with higher concentrations of plasticiser.

Now looking at the cooling curves (Figure 5-4, upper curves) the first transition (T_{g1}) decreases in temperature as the proportion of plasticiser increases, as seen with the heating curves. There is also a widening of the crystallisation exotherm (T_{c1}). However, there is no clear evidence of a new transition ($T_{g\text{-}P}$) around -95 °C with the 20 and 25 % v/v DOS blends, as seen with the heating cycle, although there is a slight bend in the line. This is indicative of the plasticiser becoming immiscible with the polymer.

5.3.3 HTPB/N100 Plasticised with DOS

As expected the presence of DOS plasticiser lowers the glass transition (T_g) temperature from -75 °C to -88 °C (Figure 5-6 & Table 5-6). This corresponds reasonably well with the value found by Fuente[243] (-83.7 °C midpoint at

10 °C min^{-1}) for HTPB propellant made with IPDI and plasticised with 21 % (mass of total binder) dioctyl adipate (DOA). Similarly to the unplasticised HTPB, a small wide transition (T_2) is observed on the first heating cycle. The cooling curves only show the single glass transition (T_g), these showed the same trend as the heating scan.

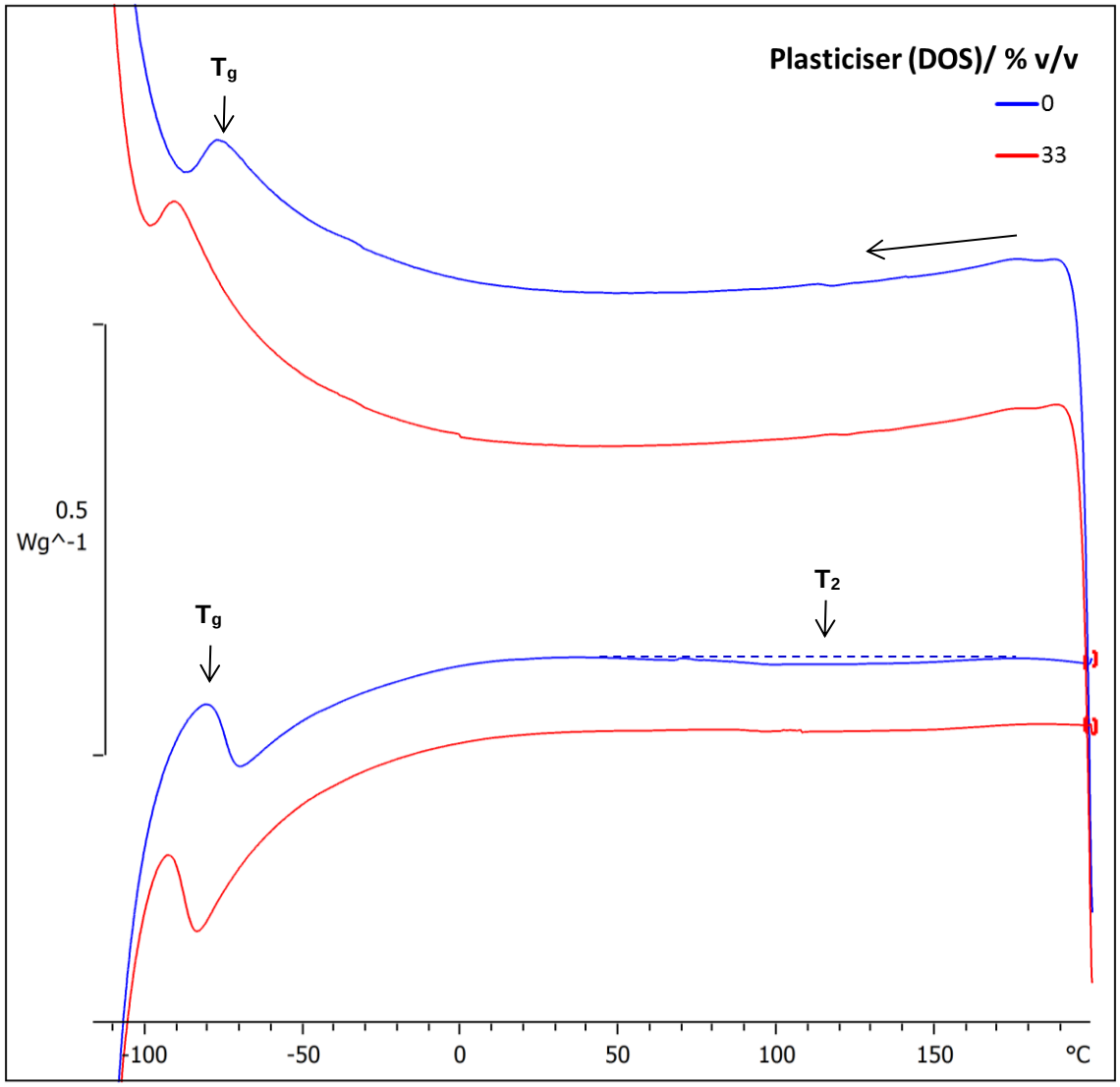

Figure 5-6 DSC thermogram of scans for unplasticised HTPB cured with desmodur N-100 (HTPB/N100) and plasticised with 33 % v/v DOS (HTPB/N100/DOS). Only first heating (lower) and cooling curves (upper) are shown.

Table 5-6 Glass transition found by DSC (10 °C min^{-1} heating rate) for plasticised and unplasticised HTPB/N100. Averages are of three heating cycles.

Sample	Plasticiser (DOS) / % v/v	Average Glass Transition [T_g] (Midpoint) /°C	Second Transition [T_2] (first heating scan only)		
			Onset / °C	Peak / °C	Normalized heat of fusion / J g^{-1}
HTPB/N100	0	-74.6 (δ = 0.4)	50.4	99.1	-3.0
HTPB/N100 /DOS	33	-87.9 (δ = 0.2)	106.7	107.9	-1.8

5.4 Dynamic Mechanical Analysis (DMA) – Temperature Scans

DMA was utilised to obtain the mechanical properties of the selected plasticised TPEs and compare them against a sample of cured plasticised HTPB (HTPB/N100/DOS). By conducting temperature scans, the storage modulus (E'), loss modulus (E'') and tan δ were obtained, this was then used to determine the glass transition (T_g) temperatures of the selected TPEs.

5.4.1 PEBAX Plasticised with DOS

In general there is a reduction in the storage modulus (E') with increasing concentration of the plasticiser. However before the polymer starts to soften (*ca.* -90 °C) the storage modulus of all sample is broadly similar. Despite DSC analysis showing no reduction in the melting point of the PA block, the plasticiser has softened the polymer at higher temperatures. At 20 °C the storage modulus was reduced by around 50 %, from 3.9 x 10^7 Pa for the unplasticised sample to 1.9 x 10^7 Pa for 22 % v/v plasticised (DOS) PEBAX.

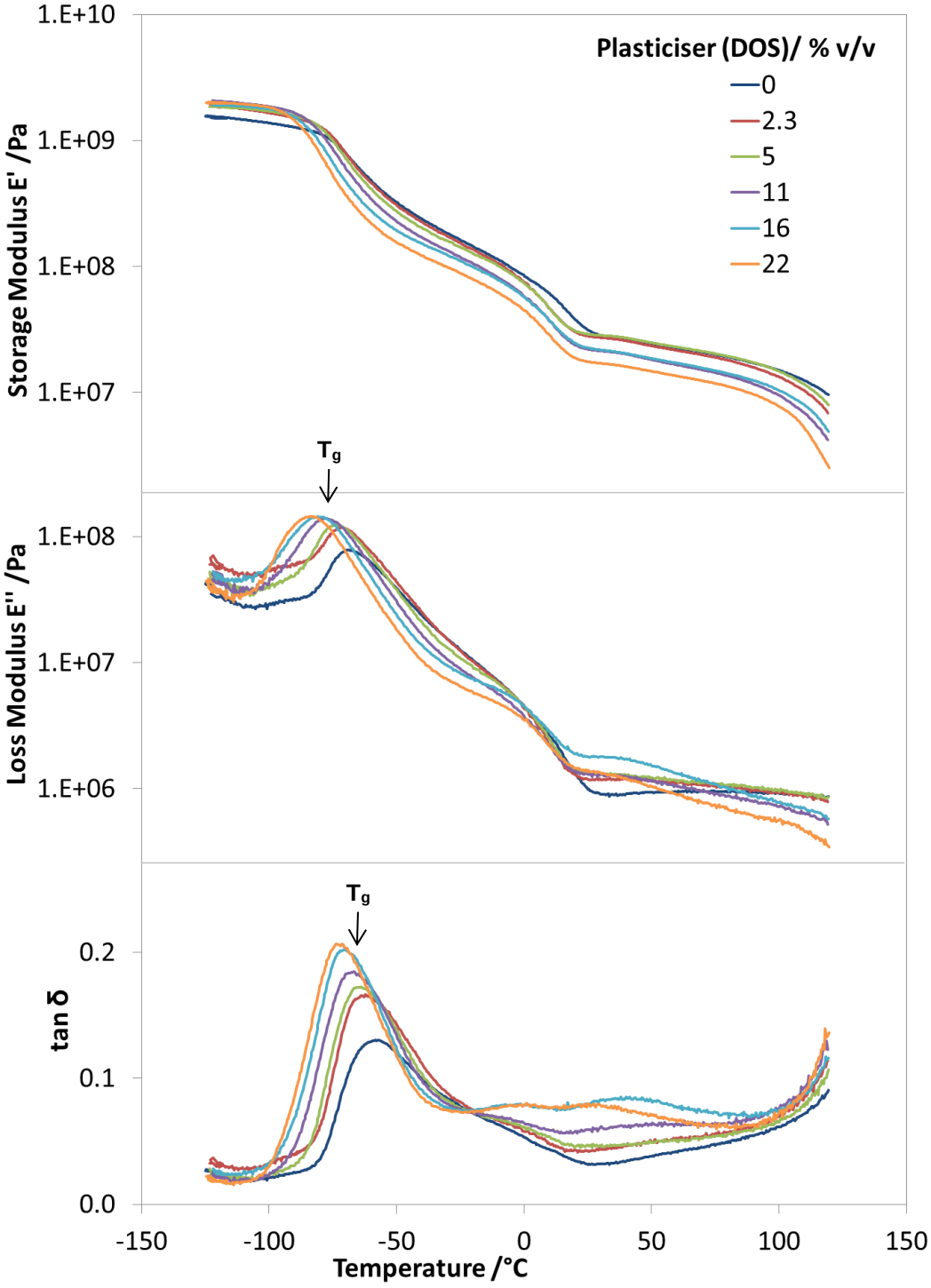

Figure 5-7 DMA thermogram of PEBAX with varying plasticiser (DOS) content. Single cantilever DMA at 1 Hz, 50 µm (1.25 %) displacement.

Table 5-7 Glass transition for different PEBAX/DOS blends found by DMA (1 Hz).

Sample	Plasticiser (DOS) / % m/m	Glass Transition (T_g)	
		tan δ Maximum / °C	Loss Modulus Maximum / °C
PEBAX	0	-56.9	-69.3
P97.3D2.7	2.5	-62.1	-71.4
P95D5	5	-64.0	-73.8
P89D11	10	-67.1	-77.8
P84D16	15	-69.9	-80.6
P78D22	20	-73.7	-84.1

Both the graphs of the loss modulus (E'') and tan δ show clearly a glass transition (T_g) with all of the polymer blends, indicated by a peak on the curve. The maxima of these peaks reduce in a fairly linear trend, as shown in Figure 5-8 The tan δ peak also increases in size as the plasticiser content increases; this is due to the increase free volume or mobility of the PMTO block.

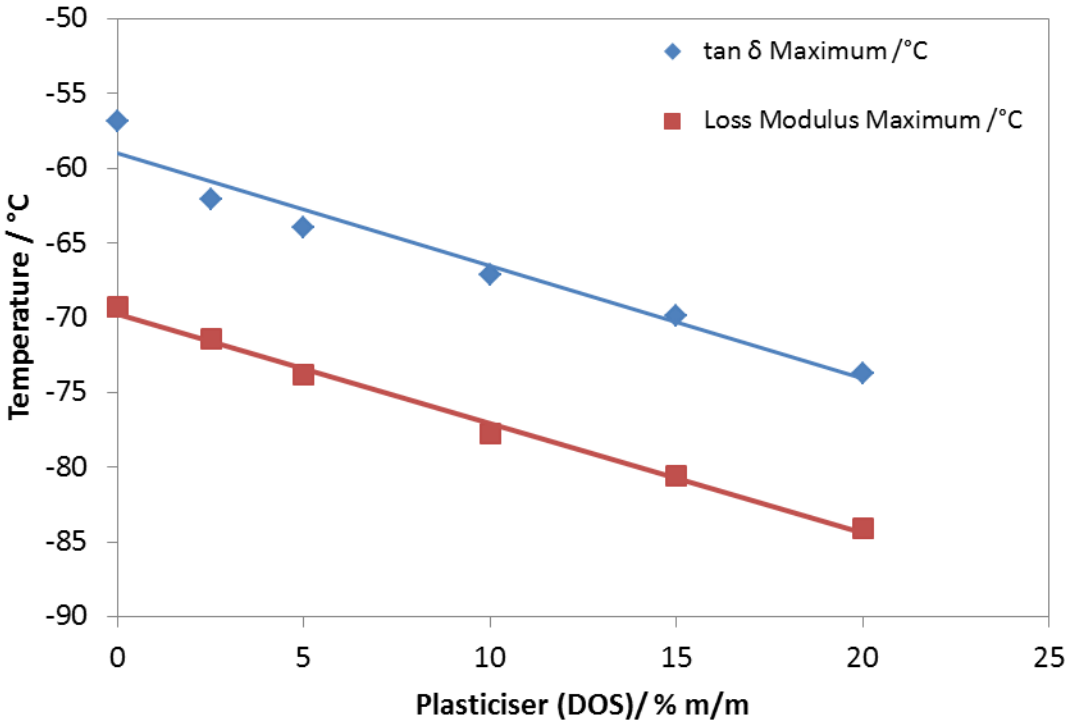

Figure 5-8 Glass transitions found by DMA for different PEBAX/DOS blends.

5.4.2 SEBS Plasticised with DOS

Again, as the proportion of plasticiser was increased the storage modulus has generally decreased (Figure 5-9). At 20 °C the storage modulus was reduced by around 75 %, from 1.2 x 10^7 Pa for the unplasticised sample to 2.9 x 10^6 Pa for 20 % v/v plasticised (DOS) SEBS. However, at very low temperature (*ca.* -100 °C) before the first transition (T_{g1}) there is only a small different blends.

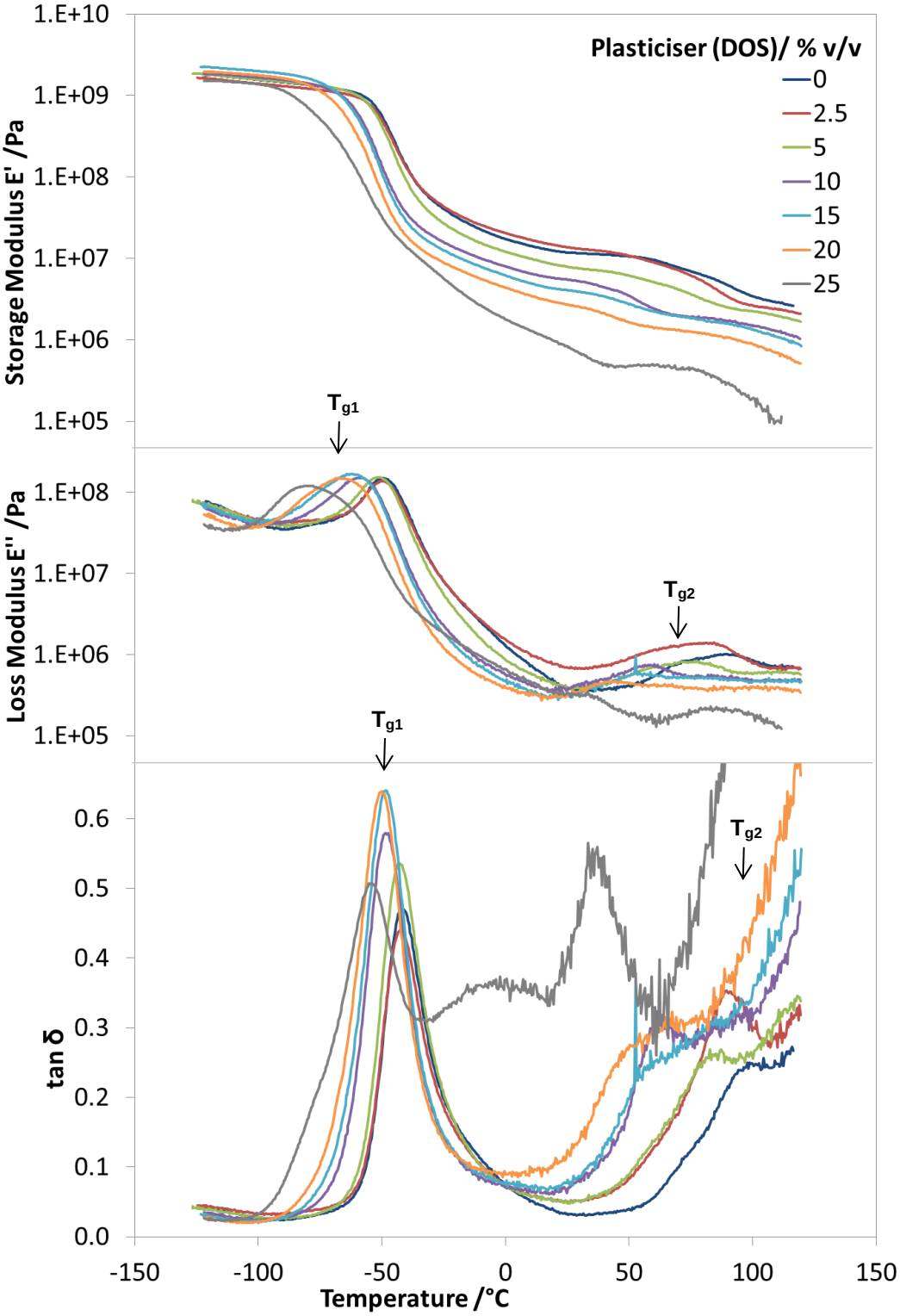

Figure 5-9 DMA thermogram of SEBS with varying plasticiser (DOS) content. Single cantilever DMA at 1 Hz, 50 µm (1.25 %) displacement.

Table 5-8 Transition for different SEBS/DOS blends found by DMA (1 Hz).

Sample	Plasticiser (DOS) / % m/m	First Transition (T_{g1})		Second Transition (T_{g2})	
		tan δ Maximum / °C	Loss Modulus Maximum / °C	tan δ Maximum / °C	Loss Modulus Maximum / °C
SEBS	0	-41.0	-48.3	114.6	86.8
S97.5D2.5	2.5	-42.5	-49.8	90.6	84.3
S95D5	5	-42.7	-51.3	82.6	76.5
S90D10	10	-48.5	-58.8	61.5	60.3
S85D15	15	-48.1	-64.4	ca. 54	54.0
S80D20	20	-49.9	-68.0	ca. 48	46.3
S75D25	25	-58.3	-80.7	8.0 & 37.1	32.7 & 83.0

For all the blends there are peaks in both the loss modulus and the tan δ due to the first transition (T_{g1}) (Table 5-8). They decrease in temperature as the proportion of DOS plasticiser increases. Figure 5-10 shows an almost linear relationship for the maxima of both the tan δ and loss modulus of T_{g1} with respect to the weight fraction of DOS. There is also a notable increase in the size of the tan δ peak with increasing plasticiser content, until it reaches 25 % v/v when it suddenly lowers (Figure 5-9). This can be attributed to the increase in mobility or free volume of the ethylene-butylene block. There is also a very noticeable shoulder (*c.a.* -75 °C) to the peak of the tan δ curve with the 25 % v/v DOS blend. This is likely to be due to separation of the plasticiser, creating a lower temperature transition.

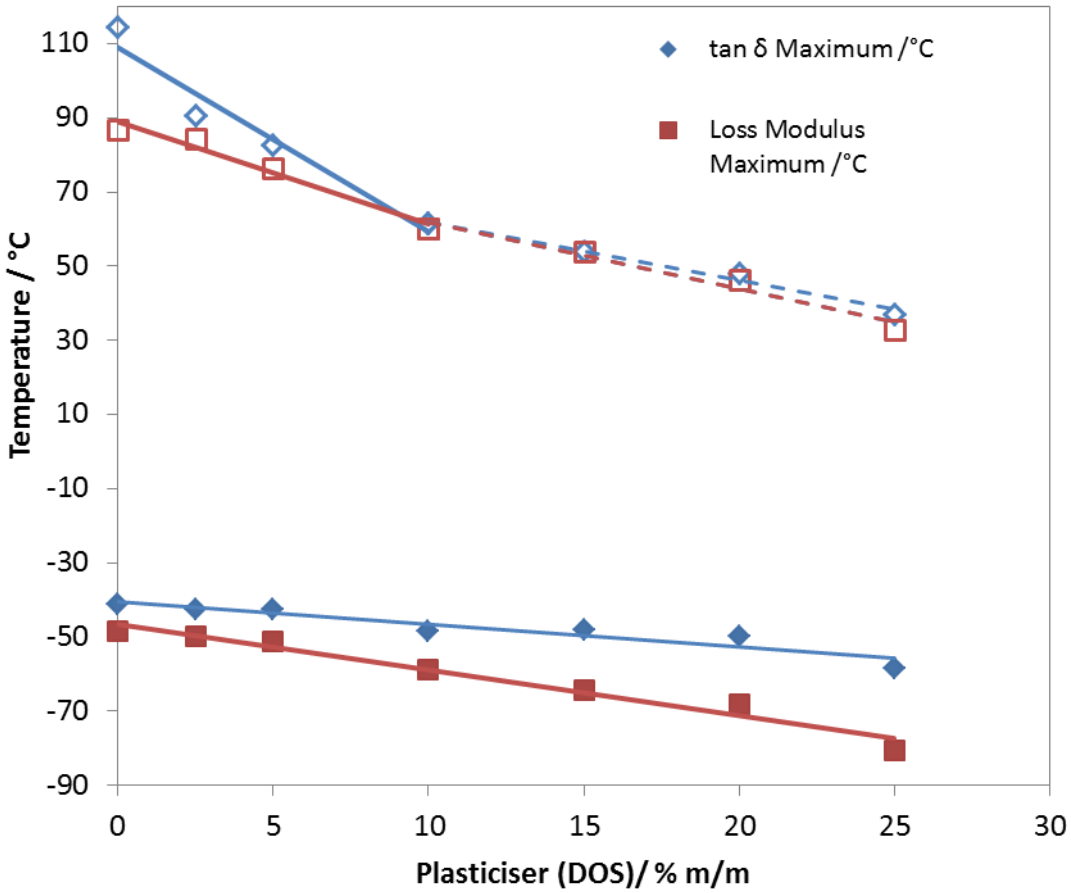

Figure 5-10 Graph comparing the first (T_{g1}) and second transition (T_{g2}) for SEBS/DOS blends as reported in Table 5-8. Solid marker represents the first transition, with hollow markers for the second.

For the second transition (T_{g2}) there is also a similar decreasing in temperature of the peak values of both the loss modulus and the tanδ as the proportion of plasticiser increases, although the relationship seems more complicated. Figure 5-10 shows a rapid reduction in the transition temperature of T_{g2} for up to 10 % m/m DOS, after this there is a much slower decrease. With the second transition there is no real increase in the height of the tanδ peaks as seen with the first transition, this can be attributed to the plasticiser not increasing the mobility or free volume of the styrene block. Again the 25 % v/v DOS blend does not fit neatly, a new transition has appeared around 10 °C, with a peak both in the loss modulus and the tan δ. This is again probably due to separation of the plasticiser from the polymer.

5.4.3 HTPB/N100 Plasticised with DOS

Due to the low modulus of the plasticised HTPB/N100 sample, it was not possible to record results above -50 °C using the single cantilever geometry. Instead the shear geometry was used, which could record results above -50 °C, but not below because of the stiffness of the sample. The single cantilever experiment was performed as with PEBAX and SEBS samples. The shear experiment was also conducted in a similar manner except that the sample under test comprised of two disc of *ca.* 7.5 mm and the displacement was set to 0.010 mm (0.25 %).

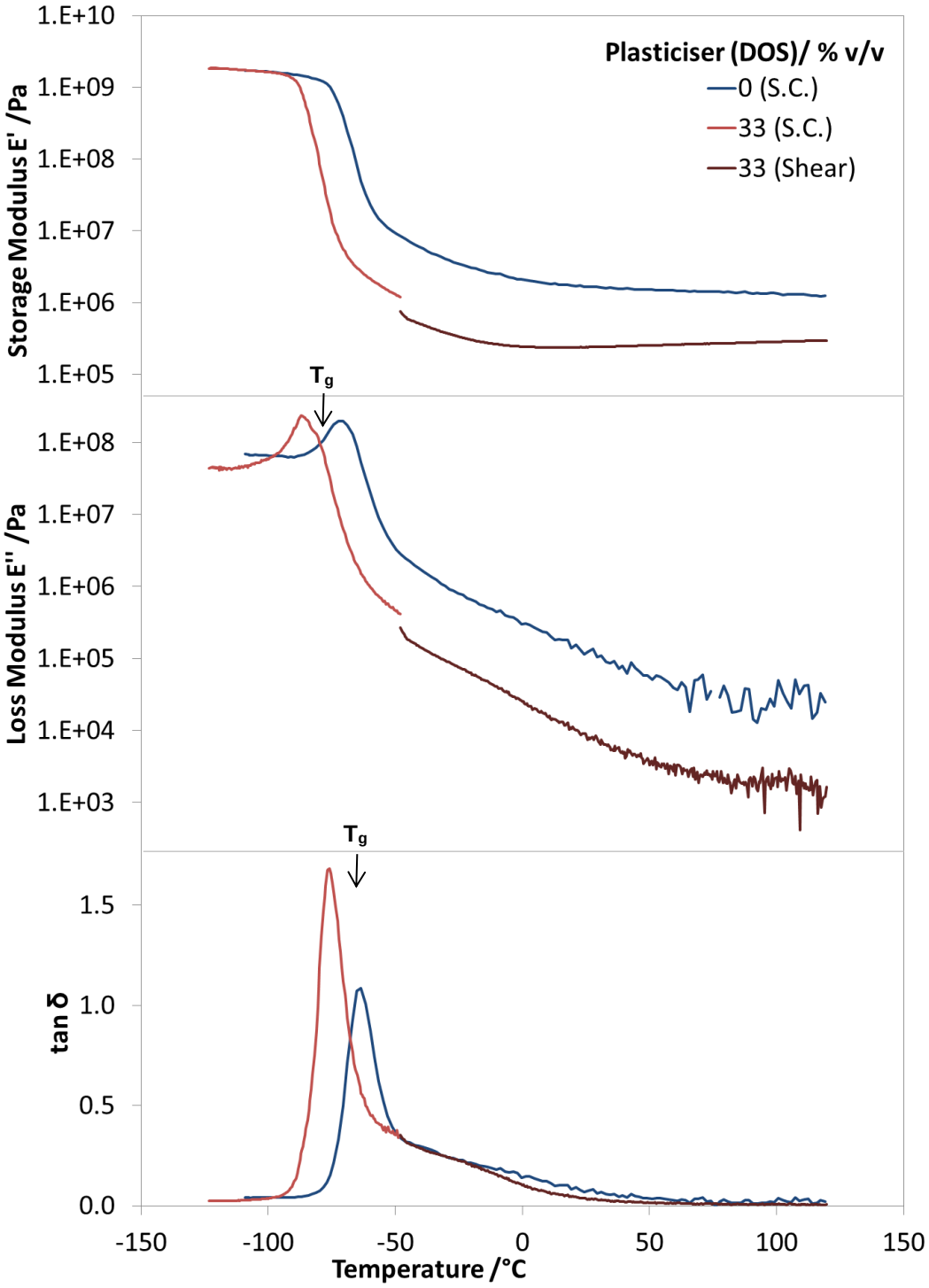

Figure 5-11 DMA thermogram of unplasticised and plasticised (30 % v/v DOS) HTPB/N1000. Single cantilever (S.C.) geometry was used for unplasticised and plasticised samples below -50 °C, plasticised samples above -50 °C was placed in shear geometry. 1 Hz frequency data reported.

Table 5-9 Transition for unplasticised and plasticised HTPB/N1000 found by DMA (1 Hz).

Sample	Plasticiser (DOS) / % v/v	Glass Transition (T_g)	
		tan δ Maximum / °C	Loss Modulus Maximum / °C
HTPB/N100	0	-63.6	-72.5
HTPB/N100/DOS	33	-76.0	-86.4

The overall the shape of the storage modulus, loss modulus and tan δ is very similar to that seen with the unplasticised HTPB/N100. Above the glass transition (T_g) the storage modulus has been clearly reduced, at 20 °C there is a ca. 85 % reduction between the unplasticised and plasticised samples (1.7×10^6 to 2.4×10^5 Pa, respectively). As anticipated the glass transition (T_g) has been reduced, the peak of the tan δ curve at 1 Hz has reduced from -64 °C to -76 °C. This is with close agreement with the reported value from Bohn & Cerri[242] (-78 °C at 0.1 Hz) for HTPB/IPDI plasticised with 25 % DOA. This value is also consistent with the reduction seen by DSC.

5.5 Comparison of the Thermal and Mechanical Properties of TPEs and HTPB/N100 Plasticised with DOS

Looking at Table 5-10, as expected DOS plasticiser lowers the lower glass transition (T_g) of both TPEs. Roughly 20 % v/v of plasticiser lowers the T_g by 10 °C, a similar reduction to that seen with HTPB/N100. The lower glass transition for plasticised SEBS is still not below minimum temperature for extreme conditions (-54 °C). The plasticiser also lowered the upper glass transition, although here the effect was much larger, seen by a reduction of over 50 °C by DMA. This indicates we might have an issue at higher temperatures (ideal maximum 74 °C) with plasticised SEBS. PEBAX upper working limit is determine by the melting of the polyamide (PA) block, this appears virtually unaffected by the addition of DOS plasticiser. Hence, it upper working limit should not be affected.

Table 5-10 Comparison of thermal and mechanical properties of TPEs and HTPB/N100 unplasticised and plasticised with DOS.

	PEBAX		SEBS		HTPB/N100		Proposed Acceptable Properties for Solid Rocket Motor (Tactical Air-to-Air) Stacer *et al.* [9]
	Unplasticised	**Plasticised with DOS (22 % v/v)**	**Unplasticised**	**Plasticised with DOS (20 % v/v)**	**Unplasticised**	**Plasticised with DOS (33 % v/v)**	
DSC							
Lower glass transition (midpoint / °C)	-77.2	-91.1	-53.3	-62.9	-74.6	-88.0	<-54
Upper glass or melting transition / °C	125.3 (melt onset)	123.5 (melt onset)	Not identifiable by DSC		None		>74
DMA							
Lower glass transition (tan δ maximum at 1 Hz /°C)	-56.9	-73.7	-41.0	-49.9	-63.6	-76.0	<-54
Upper glass or melting transition (tan δ maximum at 1 Hz /°C)	Not identifiable by DMA		114.6 (glass transition)	ca. 48 (glass transition)	None		>74

Looking at the comparison of the DMA scans of the plasticised polymers (Figure 5-12), the storage modulus (E') of SEBS has been reduced far more than PEBAX. However, both TPEs still have a noticeably higher storage modulus than the corresponding HTPB/N100 equivalent. As with the unplasticised samples, both PEBAX & SEBS have lower tan δ, below -40 °C (excluding the effect of glass transitions), this has been discussed in section 4.8.

In summary, both PEBAX & SEBS were plasticised with DOS, causing a reduction in the Storage Modulus (stiffness). The lower glass transitions of both TPEs were reduced, SEBS was still noticeably higher than HTPB/N100. In addition the upper glass transition for SEBS was dramatically reduced, which could considerable limit its applications. However, the upper limit of PEBAX appeared unaffected.

Based on this evidence PEBAX appears to have suitable properties, which are improved by use of DOS plasticiser. SEBS has acceptable properties, but these do not appear to be enhanced with DOS (plasticiser). A different plasticiser, which is more selective to the ethylene/butylene block of SEBS might improve its properties. An important aspect of using these TPEs as a binder is filling then to a high solid loading. The effect of the filler will be determined in the following chapters.

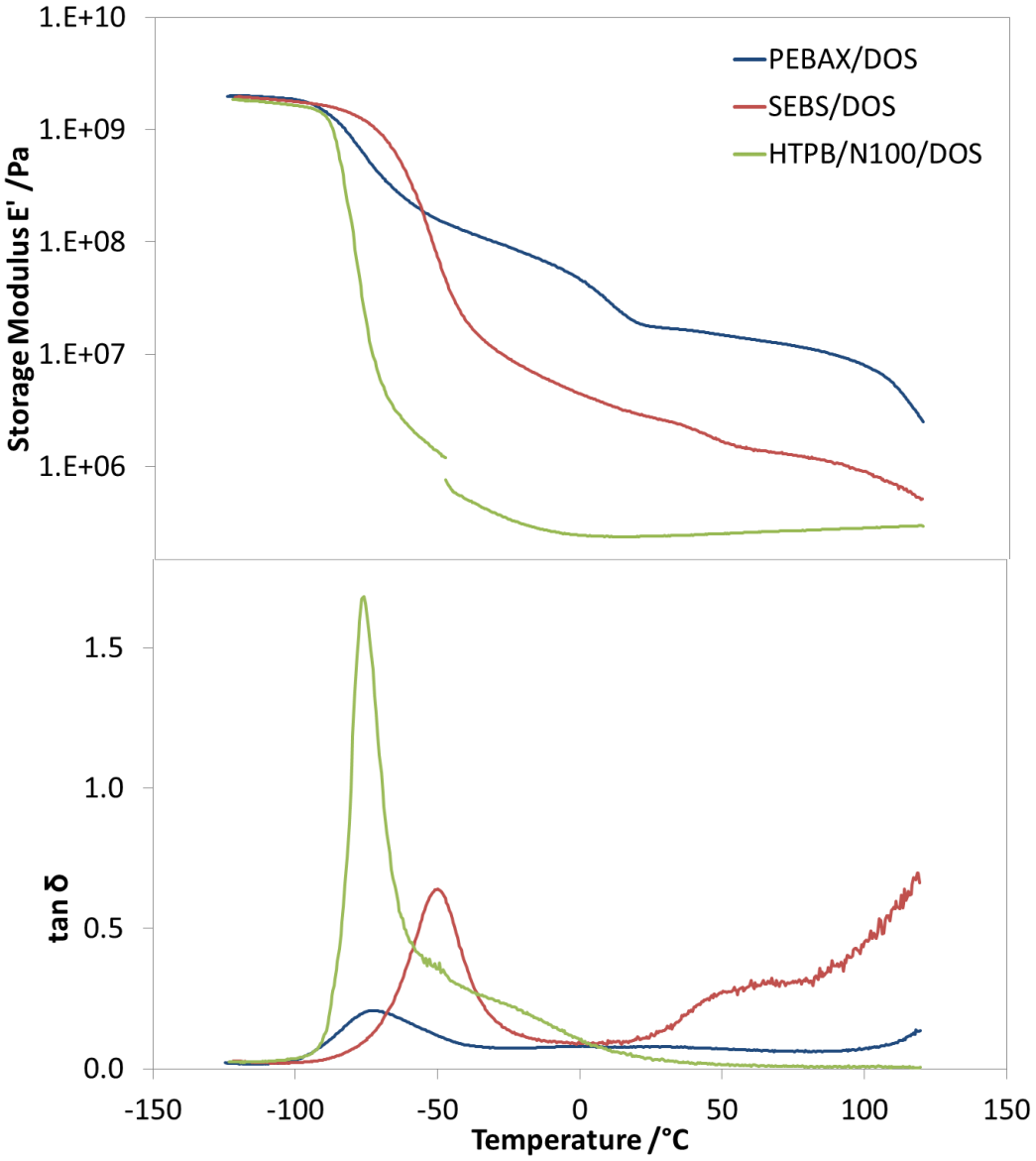

Figure 5-12 Comparison of DMA temperature scans (1 Hz) for PEBAX & SEBS plasticised with 22 & 20 % v/v DOS, respectively and HTPB/N100 plasticised with 33 % v/v DOS.

6 Characterisation of TPEs Filled with an Inert Filler (Hand Mixed)

6.1 Introduction

To better understand how the selected thermoplastic elastomers (PEBAX & SEBS) would act as a binder in a propellant, they were first filled with an inert filler. Sugar (sucrose) was chosen as inert filler, this has previously been used with cured HTPB binders[246,250]. To achieve high solid loading in composite propellants a bimodal or trimodal distribution of the fillers particle size is required[251]; for ease a bimodal mixture was chosen. A typical bimodal mixture for an ammonium perchlorate / aluminium based composite rocket propellant would contain 48 % m/m of the larger AP (ca. 200 µm) and 36 % m/m of the smaller AP and aluminium (ca. 20 µm)[242]. Household caster sugar (D_{50} = ca. 250 µm) was chosen as a substitute for the larger AP, while the smaller AP and aluminium were replace with icing sugar (D_{50} = ca. 15 µm). These had similar particles sizes as determined by laser diffraction (see Table 6-1, Figure 6-1 & Figure 6-2). The effect on the mechanical properties of plasticising these inert filled polymers was then investigated. A simple hand mixed method using solvent evaporation was used for these tests, before being hot pressed.

Table 6-1 Particle size distribution for inert fillers, as determined by laser diffraction using a Cilas 1190 in dry mode.

Inert Filler	Diameter at 10 % (D_{10}) / µm	Diameter at 50 % (D_{50}) / µm	Diameter at 90 % (D_{90}) / µm
Caster Sugar (Tate and Lyle)	191	254	374
Icing Sugar (Tate and Lyle)	3.3	15.6	27.0

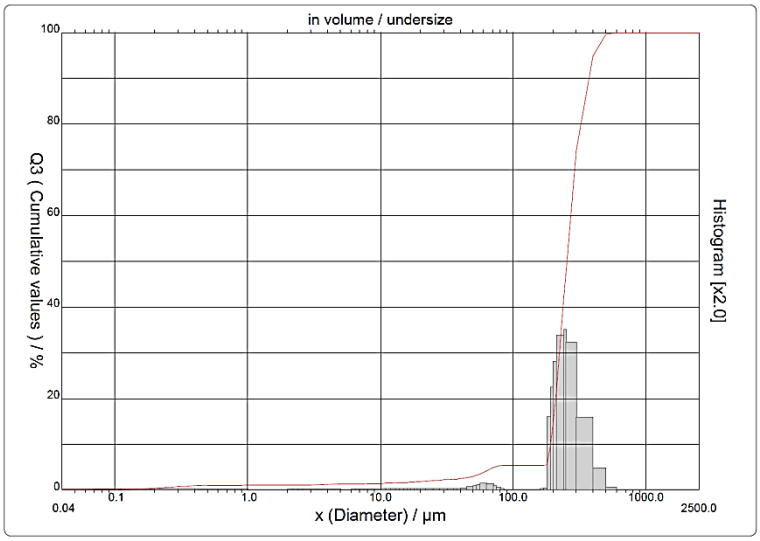

Figure 6-1 Particle size distribution for Tate and Lyle caster sugar, found by laser diffraction.

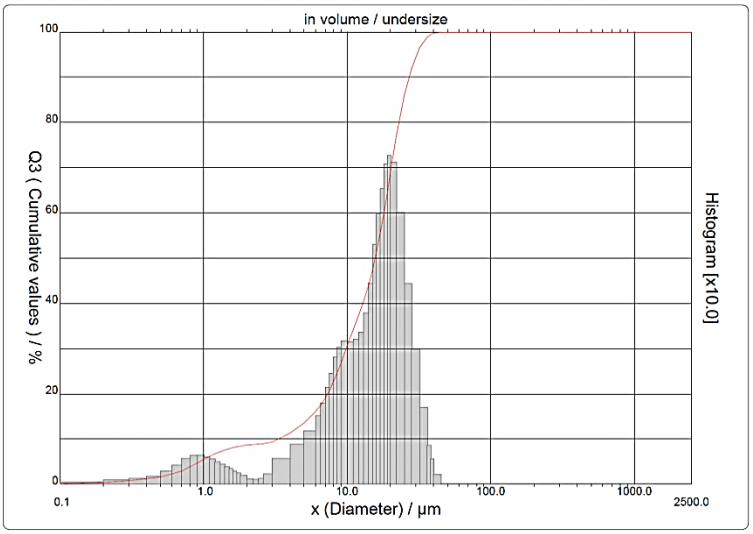

Figure 6-2 Particle size distribution for Tate and Lyle icing sugar, found by laser diffraction.

6.2 TPEs Filled with an Inert Filler

Compositions of both PEBAX and SEBS TPEs filled with sugar as an inert simulant were made by the hand mixed method, see Table 6-2. Mechanical analysis by dynamic mechanical analysis (DMA) was performed and the density was measured by helium pycnometry.

Table 6-2 Compositions of inert (sugar) filled TPEs (hand mixed).

Sample	Composition by volume			Composition by mass		
	Sugar* / % v/v	PEBAX / % v/v	SEBS / % v/v	Sugar* / % m/m	PEBAX / % m/m	SEBS) / % m/m
S49P51	49	51		60	40	
S60P40	60	40		70	30	
S72P28	72	28		80	20	
S77P23	77	23		84	16	
S46S54	46		54	60		40
S57S43	57		43	70		30
S70S30	70		30	80		20
S75S25	75		25	84		16

*Sugar was a 4:3 bimodal mixture of caster (D_{50} = ca. 250 µm) and icing (D_{50} = ca. 15 µm) sugar.

6.2.1 PEBAX Filled with Sugar

6.2.1.1 Dynamic Mechanical Analysis (DMA) – Temperature Scans

In general, there is an increase in the storage modulus (E') with increased solid loading of the filled PEBAX (see Figure 6-3). This is due to the reinforcement effect of the solid filler. The effect of the storage modulus reducing with temperature is less pronounced as the solid loading increased, resulting in a flatter curve. Increasing the solid loading appears to have no effect on the point where the polymer starts to soften (1) or plateau (3). For 49 and 60 % v/v loadings the shape of the curves are broadly similar to that of the pure PEBAX. The 72 and 77 % v/v curves show an additional feature at around -40 °C (**2**).

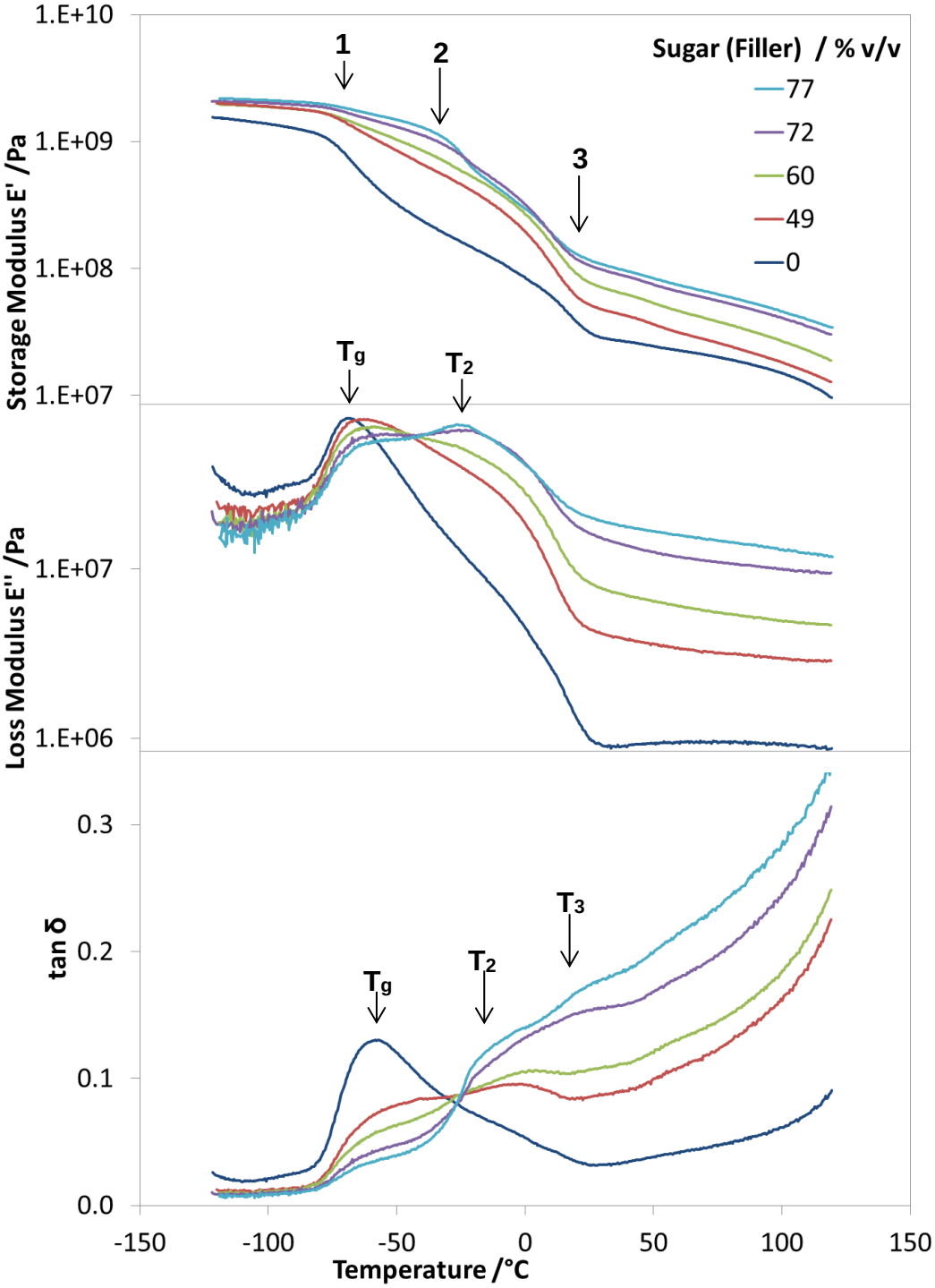

Figure 6-3 DMA Thermogram of PEBAX filled with sugar at different solid loadings. Single cantilever DMA at 1 Hz, 50 µm (1.25 %) displacement.

For the tan δ curves (Figure 6-3), the most noticeable effect is the increase in the drift of the baseline. This starts from the glass transition and increases at higher temperatures. This drift of the baseline increases with increasing loading. This effect can be explained by the deformation energy applied on the sample being partly absorbed by the sample, increasing the tan δ. This is notable at the glass transition, were energy is absorbed for molecular rearrangements, producing the peak in the tan δ curve. There is also a dissipative effect, where friction inside the sample converts this energy to thermal energy. For unfilled polymers in the rubbery state this effect is very small. However, for highly filled polymers this effect can become very substantial[252], as seen with the filled PEBAX.

In all the filled polymers a second transition (T_2) is evident around 0°C. For 72 and 77 % v/v solid loading a third transition (T_3) is present at around 20°C. This can be explained by filler interacting strongly with the polymer, forming a more rigid layer of polymer around particle. The mobility is reduced to such an extent that new transitions are created. This region has a much lower free volume and hence a higher temperature is necessary to undergo the molecular motions[242].

The size of tan δ peak at the T_g reduces with increased solid loading. This likely to partly due of the new transitions at T_2 and T_3, but the decrease is much greater than the size of the new peaks. Bohn[253] explains this as being due to the decrease in the mobility of the polymer chains due to the filler particles imposing geometrical conditions. The higher the loading, the more filler particles are restricting the mobility of the polymer chains, hence the decrease in the tan δ peak. This intermolecular interaction between the filler and polymer will result in larger reductions in the tan δ peak and a shift in the T_g to higher temperatures. Interestingly, with PEBAX the peak in the tan δ shifts to a slightly lower temperature, but the peak in the loss modulus is shifted higher. The peak remains evident as not all of the polymer is close enough to a filler to be affected.

Table 6-3 Thermal transitions of PEBAX filled with sugar at varying solid loading, found by DMA.

	Glass Transition (T_g)		Second Transition (T_2)	
Sugar (Filler) / % v/v	**tan δ Maximum /°C**	**Loss Modulus Maximum /°C**	**tan δ Maximum /°C**	**Loss Modulus Maximum /°C**
0	-56.9	-69.3		
49	ca. -60	-64.5	ca. -3	
60	ca. -62	-58.9	ca. 3	
72	ca. -65	c.a.-55		ca.-22
77		ca. -55	ca.-22	-26.3

6.2.1.2 Density Measurements

Table 6-4 Density measurements (helium pycnometry) of sugar filled PEBAX. Standard deviation (σ) x1 is reported throughout this thesis.

Sugar (Filler) / % v/v	Density / g cm^{-3}	Theoretical Maximum Density* (TMD) / g cm^{-3}	Percentage of TMD / %
0	1.0077 (σ = 0.0002)	-	-
49	1.2940 (σ = 0.0003)	1.2903	100.3
60	1.3621 (σ = 0.0005)	1.3537	100.6
72	1.4290 (σ = 0.0004)	1.4235	100.4
77	1.4556 (σ = 0.0005)	1.4535	100.1

*Predicted density is based on the volume fraction using the obtained density for unfilled PEBAX and Sugar (1.5872 g mol^{-1}) and the literature value of 0.914 g mol^{-1} for DOS[249].

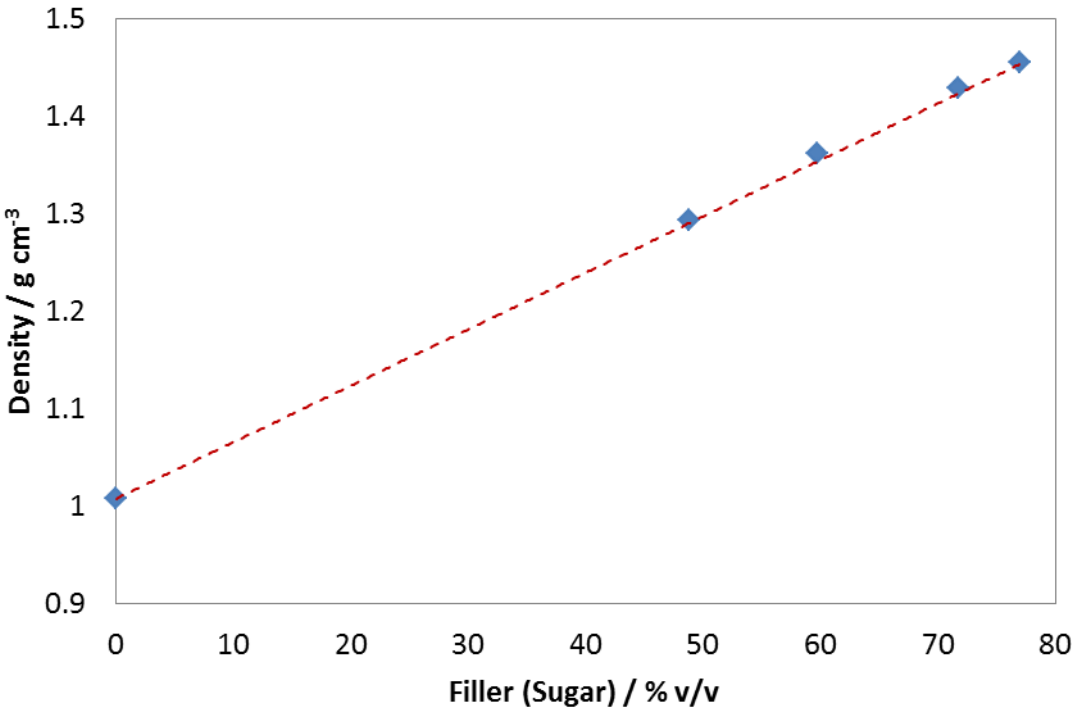

Figure 6-4 Graph of density found by helium pycnometry against solid loading for PEBAX filled with sugar. Red dotted line represents the theoretical maximum density (TMD). Error bars represent the standard deviation (x1) throughout this thesis.

High densities were achieved with all of the different loadings of the polymer, with densities close to the theoretical maximum density (Table 6-4 & Figure 6-4).

6.2.2 SEBS Filled with Sugar

6.2.2.1 Dynamic Mechanical Analysis (DMA) – Temperature Scans

As clearly seen in Figure 6-5, there is an increase in the storage modulus (E') with solid loading for the sugar filled SEBS, again this due to the reinforcement effect. This increase in the storage modulus is greater at higher temperatures, resulting in a flatter curve after point 1. Apart from this flattening of the shape, the curves are very similar between the different solid loading, with perhaps a small hump (2) on the 75% v/v loading at around 25°C.

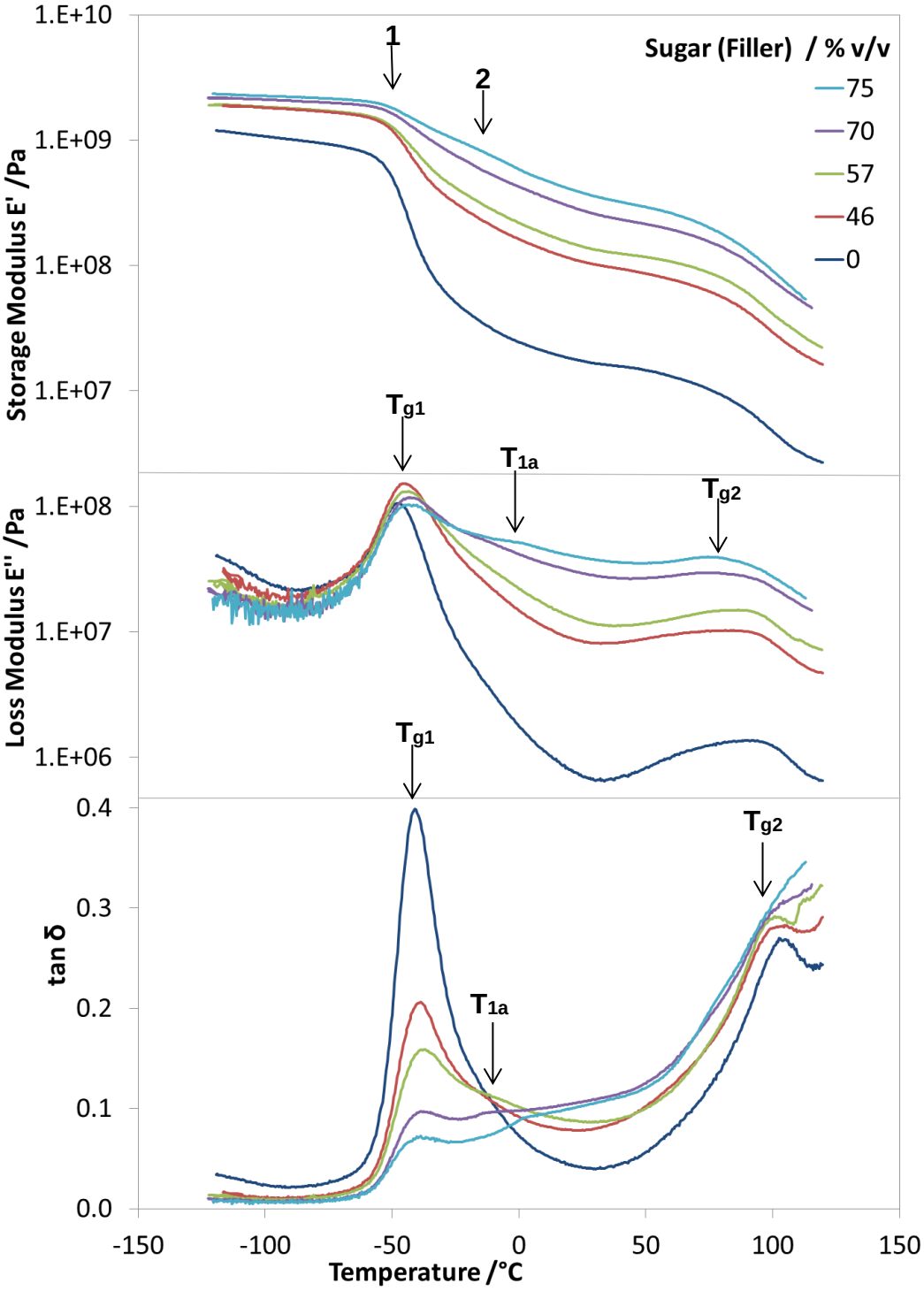

Figure 6-5 DMA Thermogram of sugar filled SEBS. Single cantilever DMA at 1 Hz, 50 µm (1.25 %) displacement.

As expected the first glass transition (T_{g1}) shifts to higher temperatures with increased loading, indicated by the peaks in the tan δ and loss modulus curves (see Table 6-5 and Figure 6-6). Both the tan δ peaks (T_{g1} & T_{g2}) clearly reduce in size with increased load, resulting in the T_{g2} peak not even being visible at 75 % v/v solid loading. There is again a noticeable shift in the baseline, becoming more offset with increased loading. These effects have been discussed in section 6.2.1. Conversely to the first glass transition (T_{g1}), the second glass transition (T_{g2}) appears to shift to lower temperatures. The effect is not easy to explain, but has been seen in some other case with fillers in elastomers[254]. A possible theory is that the effect of the filler on the glass transition depends on the nature of the specific interaction between the polymer and filler[255].

Similar to PEBAX a new peak (T_{1a}) tan δ curve for 70, 75 and possibly 57 % v/v is observed at around 0 °C. Likewise, there is a new peak (T_{1a}) in the loss modulus curve for 75 % v/v loading around 0 °C. Again this is likely to be explained by the rigid layer of polymer chains around the filler particles, see section 6.2.1 for further explanation.

Table 6-5 Thermal transitions of SEBS filled with sugar at varying loading solid loading, found by DMA.

	First Glass Transition (T_{g1})		Second Glass Transition (T_{g2})	
Sugar (Filler) / % v/v	**tan δ Maximum /°C**	**Loss Modulus Maximum /°C**	**tan δ Maximum /°C**	**Loss Modulus Maximum /°C**
0	-41.0	-47.5	105.3	93.8
46	-38.8	-45.1	105.6	c.a. 80
57	-37.4	-43.4	101.0	86.3
70	-37.5	-43.2	*	ca. 71
75	-38.7	-43.5	*	ca. 72

*Peak could not be assigned.

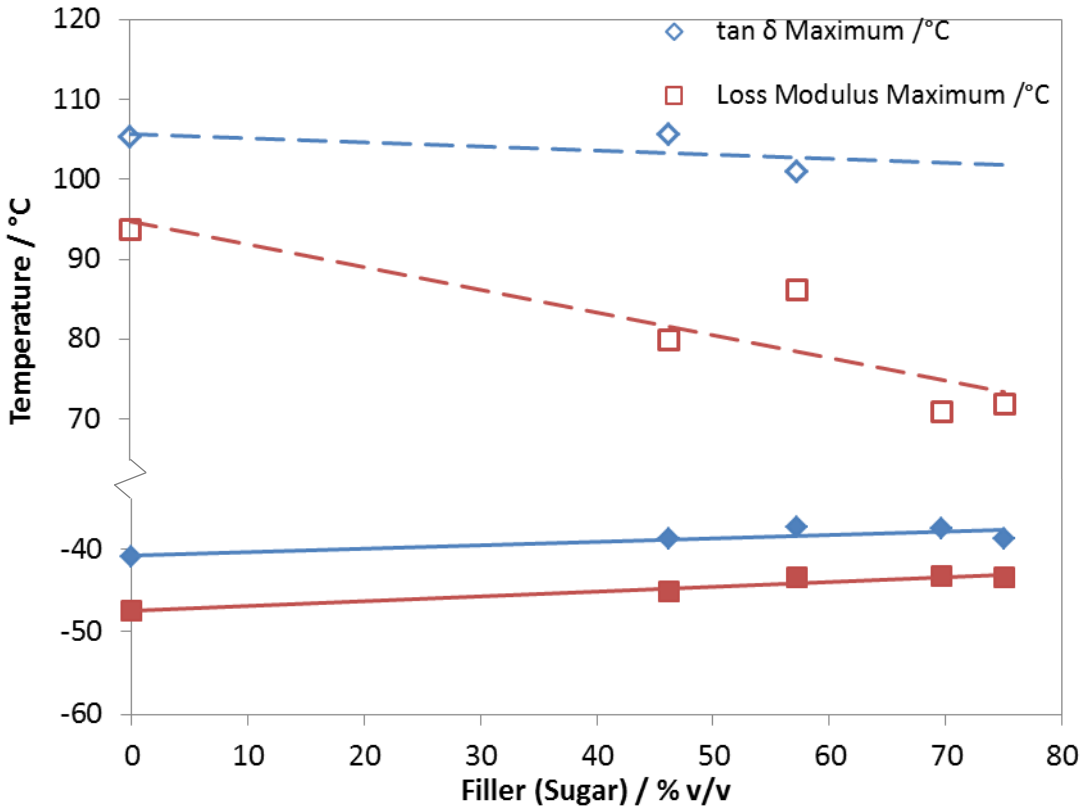

Figure 6-6 Graph comparing the thermal transitions for sugar filled SEBS as reported in Table 6-5. Solid marker represents the first transition (T_{g1}), with hollow markers for the second (T_{g2}).

6.2.2.2 Density Measurements

Table 6-6 Density measurements (helium pycnometry) of SEBS filled with sugar at varying solid loading.

Sugar (Filler) / % v/v	Density / g cm^{-3}	Theoretical Maximum Density (TMD) / g cm^{-3}	Percentage of TMD / %
0	0.9094 (σ = 0.0004)	-	-
46	1.2235 (σ = 0.0001)	1.2227	99.7
57	1.2908 (σ = 0.0004)	1.2972	99.5
70	1.3812 (σ = 0.0001)	1.3813	100.0
75	1.4212 (σ = 0.0002)	1.4181	100.2

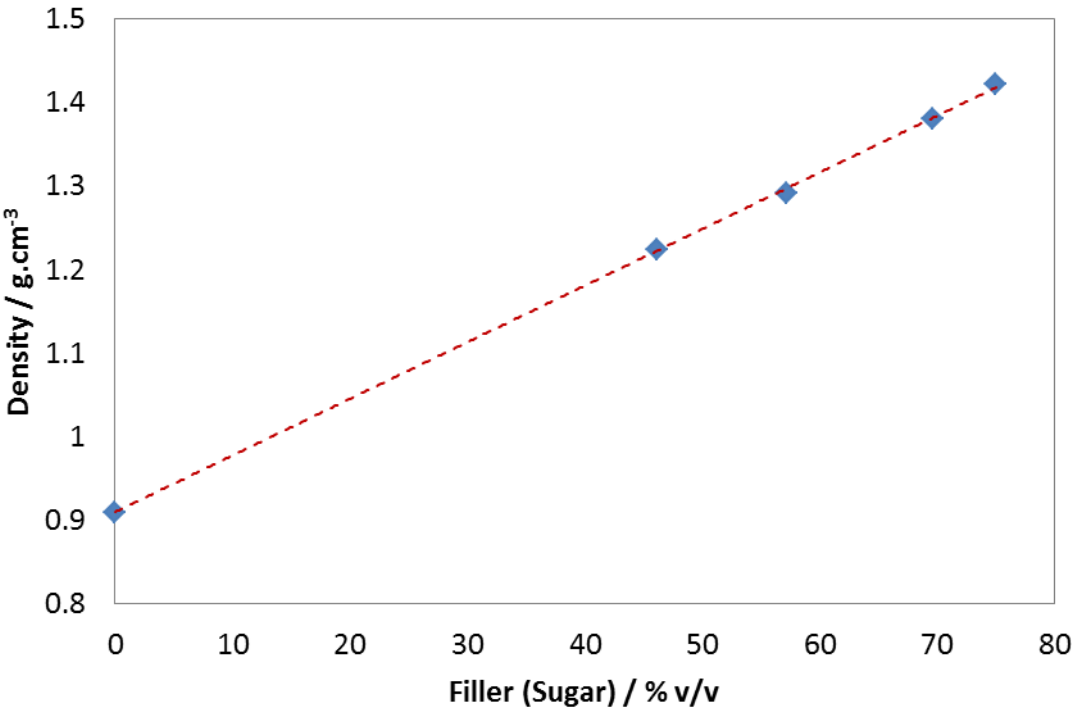

Figure 6-7 Graph of density found by helium pycnometry against solid loading for sugar filled SEBS. Red dotted line represents the theoretical maximum density (TMD).

Similarly to PEBAX, densities close to the theoretical maximum density (TMD) were achieved for all the different loadings (Table 6-6 & Figure 6-7).

6.3 Plasticised TPEs Filled Sugar (Hand Mixed)

Compositions of both PEBAX and SEBS filled with sugar were plasticised with varying concentration of Dioctyl Sebacate (DOS) plasticiser, see Table 6-7 and Table 6-8. Mechanical analysis by DMA was performed and the density was measured by helium pycnometry.

Table 6-7 Composition of plasticised, sugar filled PEBAX (hand mixed).

Sample	Composition by volume			Composition by mass		
	Sugar* / % v/v	PEBAX / % v/v	Plasticiser (DOS) / % v/v	Sugar* / % m/m	PEBAX / % m/m	Plasticiser (DOS) / % m/m
S70P30	60	40	0	70	30.0	0
S70P28.5D1.5	60	38	2	70	28.5	1.5
S70P27D3	59	36	4	70	27.0	3.0
S70P25.5D4.5	59	34	7	70	25.5	4.5
S70P245D6	59	32	9	70	24.0	6.0
S70P22.5D7.5	59	30	11	70	22.5	7.5

*Sugar was a bimodal mixture of caster (D_{50} = ca. 250 µm) and icing (D_{50} = ca. 15 µm) sugar.

Table 6-8 Composition of plasticised, sugar filled SEBS (hand mixed).

Sample	Composition by volume			Composition by mass		
	Sugar* / % v/v	SEBS / % v/v	Plasticiser (DOS) / % v/v	Sugar* / % m/m	SEBS / % m/m	Plasticiser (DOS) / % m/m
S70S30	57	43	0	70	30.0	0
S70S28.5D1.5	57	41	2	70	28.5	1.5
S70S27D3	57	39	4	70	27.0	3.0
S70S25.5D4.5	57	36	6	70	25.5	4.5
S70S245D6	57	34	9	70	24.0	6.0
S70S22.5D7.5	57	32	11	70	22.5	7.5

*Sugar was a bimodal mixture of caster (D_{50} = ca. 250 µm) and icing (D_{50} = ca. 15 µm) sugar.

6.3.1 Plasticised Sugar Filled PEBAX (Hand Mixed)

6.3.1.1 Dynamic Mechanical Analysis (DMA) – Temperature Scans

As expect, as the concentration of the DOS plasticiser is increase there is a reduction in the storage modulus (E'), except before the glass transition were the modulus is consistent (see Figure 6-8).

In the loss modulus (E'') curve, the peak (T_g) representing the glass transition can be seen shifting to lower temperatures as the concentration of the plasticiser

increases (see Table 6-9 & Figure 6-9). This is the same trend as seen with the unfilled sample (see section 5.4.1). However, the second transition (T_2) appears to reduce in size and possibly shift to higher temperatures.

Both peaks on the tan δ curve have increased, due to the plasticiser increasing the mobility of the polymer chains, hence increasing the free volume. However, both peaks appear to be shifted to slightly higher temperatures, indicating an increase in the T_g and the second transition (T_2) (see Table 6-9 & Figure 6-9). This indicates that the plasticiser interaction is complex and I have found no evidence of this effect before. This may be due to plasticised polymer interacting stronger with the filler than the unplasticised polymer. This would cause the polymer to be held tighter around the filler, causing an increase in the glass transition.

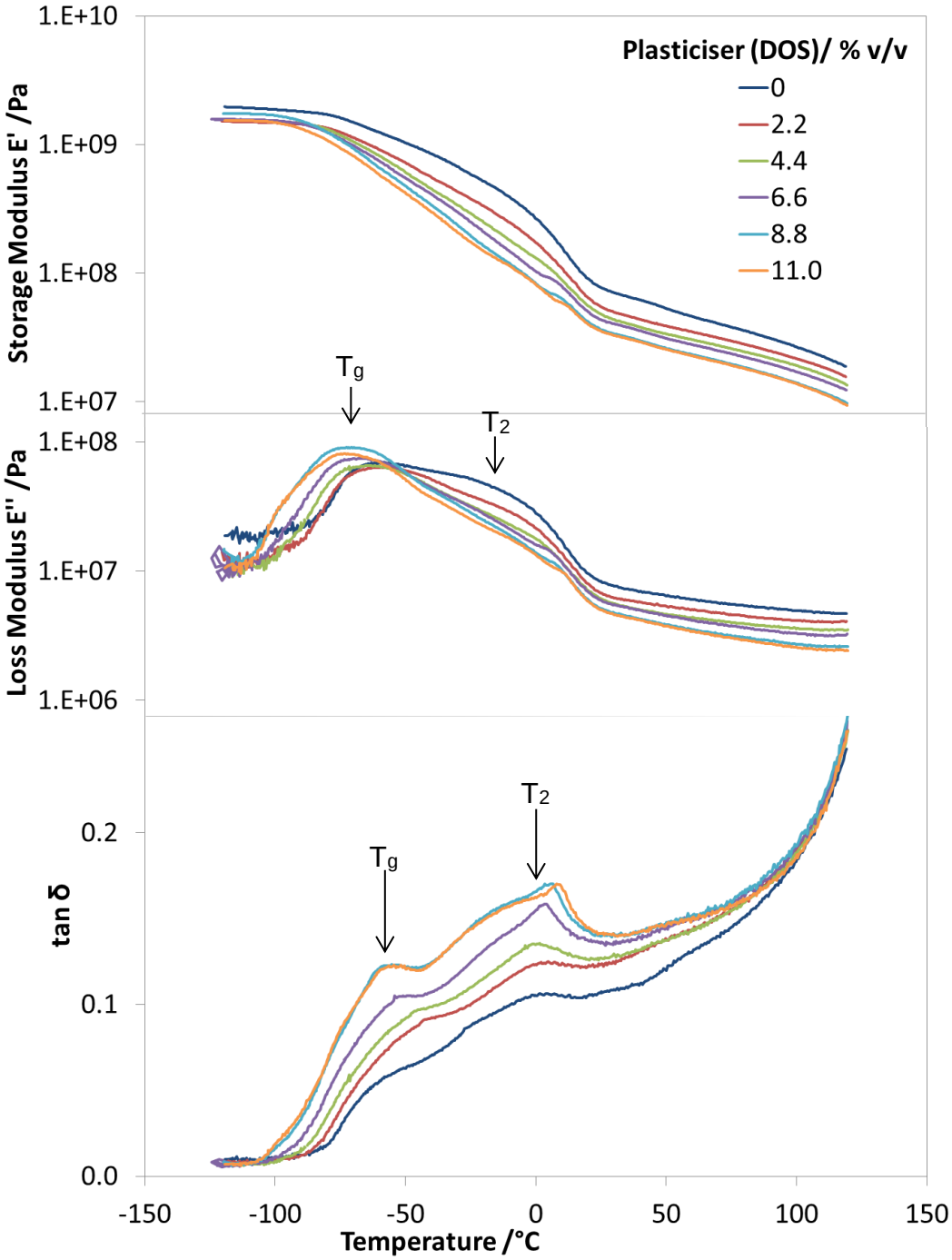

Figure 6-8 DMA thermogram of 60 % v/v sugar PEBAX with varying plasticiser (DOS) content. Single cantilever DMA at 1 Hz, 50 µm (1.25 %) displacement.

Table 6-9 Thermal transition of 60 % v/v sugar PEBAX with varying plasticiser (DOS) content, found by DMA.

	Glass Transition (T_g)		Second Transition (T_2)	
Plasticiser (DOS) / % v/v	**tan δ Maximum /°C**	**Loss Modulus Maximum /°C**	**tan δ Maximum /°C**	**Loss Modulus Maximum /°C**
0	ca. -62	-58.9	ca. 3	*
2.2	ca. -56	-59.3	ca. 3	*
4.4	ca. -53	-64.7	ca.-1	*
6.6	ca. -62	-58.9	ca. 3	*
8.8	ca. -56	-59.3	ca. 3	*
11.0	ca. -53	-64.7	ca.-1	*

*Peak could not be assigned.

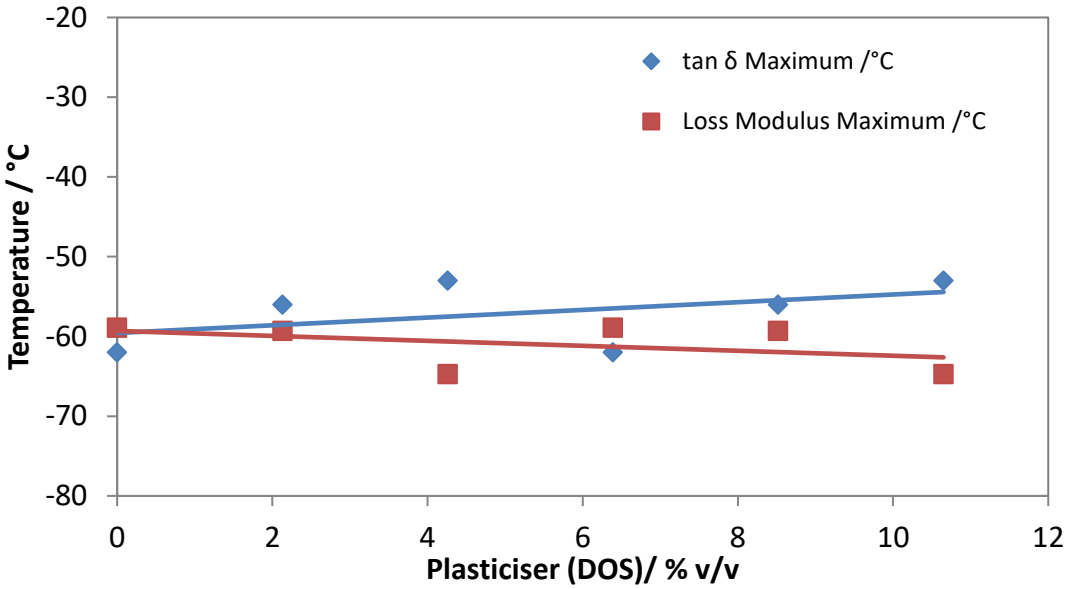

Figure 6-9 Graph of the glass transition (T_g) found DMA against plasticiser (DOS) content for 60 % v/v sugar PEBAX.

6.3.1.2 Density Measurements

Table 6-10 Density Measurements (helium pycnometry) of 60 % v/v sugar PEBAX at varying plasticiser (DOS) content.

Plasticiser (DOS) / % v/v	Density / g cm^{-3}	Theoretical Maximum Density (TMD) / g cm^{-3}	Percentage of TMD / %
0.0	1.3621 (σ = 0.0005)	1.3537	100.6
2.2	1.3573 (σ = 0.0005)	1.3509	100.5
4.4	1.3470 (σ = 0.0005)	1.3481	99.9
6.6	1.3463 (σ = 0.0009)	1.3453	100.1
8.8	1.3416 (σ = 0.0012)	1.3426	99.9
11.0	1.3450 (σ = 0.0004)	1.3398	100.4

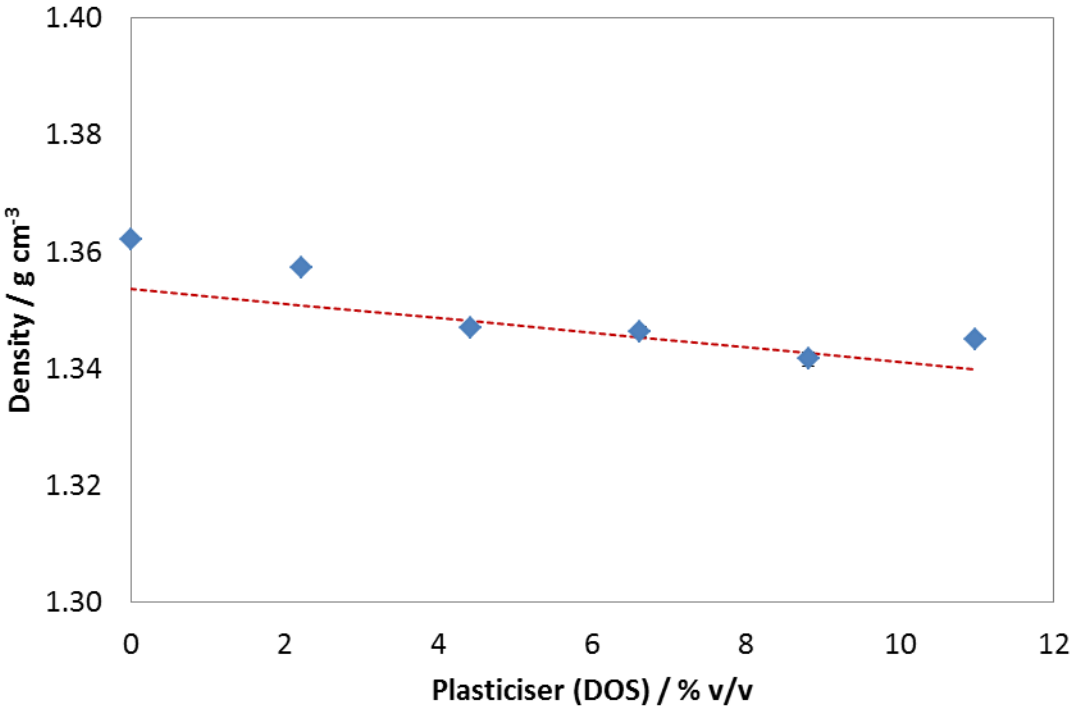

Figure 6-10 Graph of density found by helium pycnometry against plasticiser (DOS) content for 60 % v/v sugar PEBAX with varying plasticiser (DOS) content. Red dotted line represents the theoretical maximum density (TMD).

The different filled plasticised samples all had densities close to their theoretical maximum density (Table 6-10 & Figure 6-10).

6.3.2 Plasticised Sugar Filled SEBS

6.3.2.1 Dynamic Mechanical Analysis (DMA) – Temperature Scans

Predictably above the first transition (1), increasing the plasticiser content has the effect of reducing the storage modulus (E') (see Figure 6-11). However, at lower temperatures the reverse is true. This is possibly due to the plasticiser aiding the compaction of the composite in the hot press. The shape of the curve is broadly similar for different plasticiser contents, except for a greater decrease in the storage modulus at higher temperatures. Otherwise, the plasticiser has a similar effect on the sugar filled SEBS as it does on the pure SEBS polymer (see section 5.4.2). There is the same reduction in both glass transitions (T_{g1} & T_{g2}) as the plasticiser content is increased (see Table 6-11 and Figure 6-12). The size of both peaks in the tan δ curve increases with increasing plasticiser content.

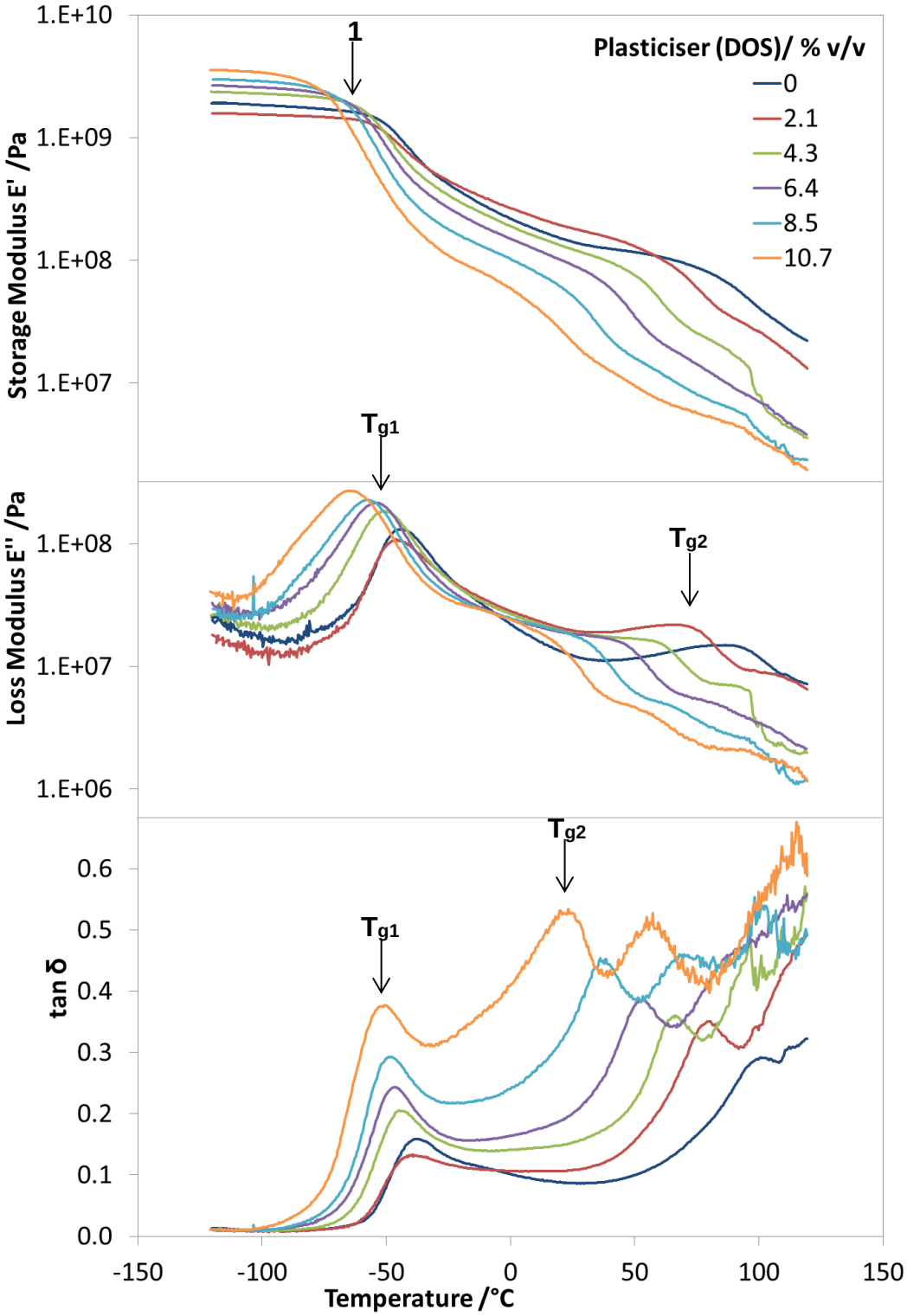

Figure 6-11 DMA thermogram of 57 % v/v sugar SEBS with varying plasticiser (DOS) content. Single cantilever DMA at 1 Hz, 50 µm (1.25 %) displacement.

Table 6-11 Thermal transitions of 57 % v/v sugar SEBS at varying plasticiser (DOS) content, found by DMA.

	First Glass Transition (T_{g1})		Second Glass Transition (T_{g2})	
Plasticiser (DOS) / % v/v	tan δ Maximum /°C	Loss Modulus Maximum /°C	tan δ Maximum /°C	Loss Modulus Maximum /°C
0	-37.4	-43.4	101.0	86.3
2.1	-39.5	-46.2	81.3	70.3
4.3	-44.7	-51.2	66.4	ca. 56
6.4	-47.1	-54.1	53.6	ca. 42
8.5	-49.0	-57.7	36.1	ca. 25
10.7	-50.4	-64.8	23.2	ca. 5

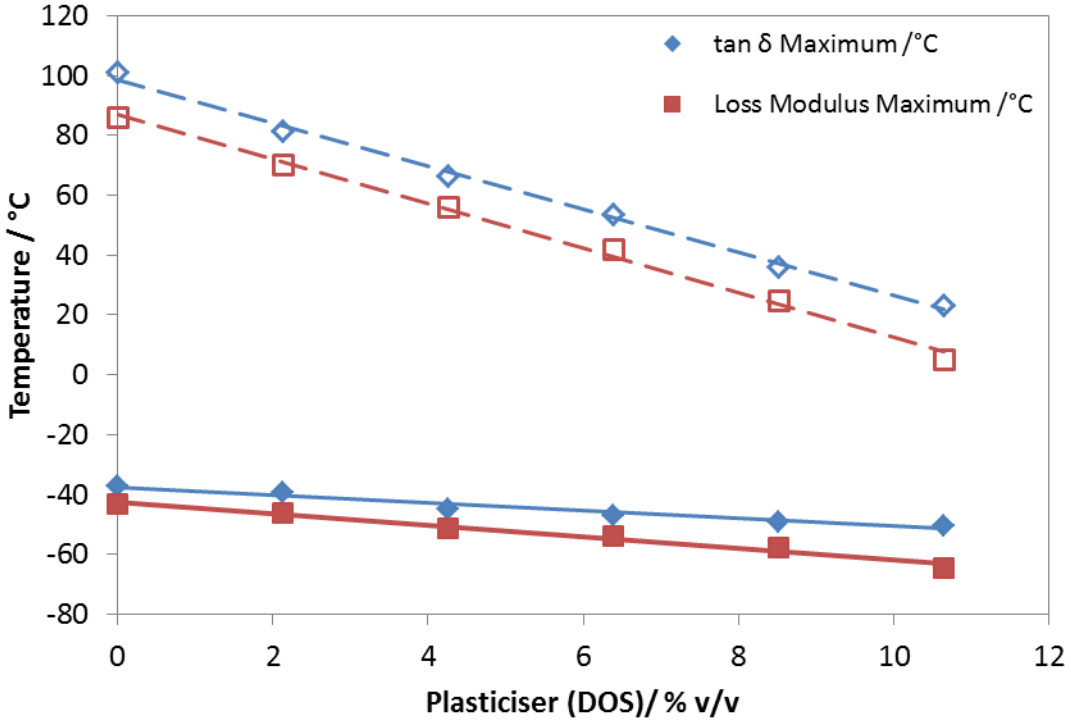

Figure 6-12 Graph comparing the thermal transitions for plasticised (DOS) formulations of 57 % v/v sugar SEBS as reported in Table 6-11. Solid marker represents the first transition (T_{g1}), with hollow markers for the second (T_{g2}).

6.3.2.2 Density Measurements

Table 6-12 Density measurements of 57 % v/v sugar SEBS at varying plasticiser (DOS) content.

Plasticiser (DOS) / % v/v	Density / g cm^{-3}	Theoretical Maximum Density (TMD) / g cm^{-3}
0.0	1.2908 (σ = 0.0004)	1.2972
2.1	1.2997 (σ = 0.0013)	1.2973
4.3	1.2908 (σ = 0.0025)	1.2974
6.4	1.2982 (σ = 0.0012)	1.2976
8.5	1.2945 (σ = 0.0003)	1.2977
10.6	1.3001 (σ = 0.0006)	1.2979

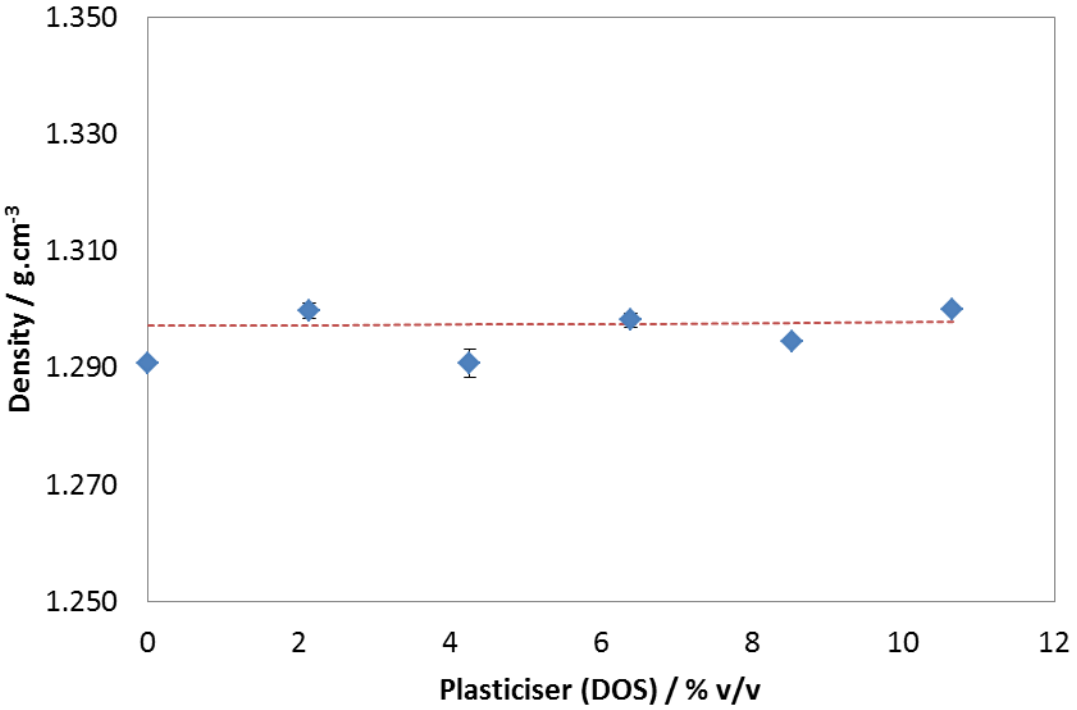

Figure 6-13 Graph of density found by helium pycnometry against plasticiser (DOS) content for 57 % v/v sugar SEBS. Red dotted line represents the Theoretical Maximum Density (TMD).

There is very little difference in the densities of the filled SEBS polymer as the plasticiser content has been altered, with densities between 1.29 and 1.30 g cm^{-3}(Table 6-12 & Figure 6-13).

6.4 Conclusion

Both PEBAX and SEBS TPEs were successfully filled with inert fillers and plasticised. DMA showed that above the first glass transition, the storage modulus increased with solid loading for both PEBAX and SEBS. This is due to the reinforcement effect making the filled TPEs stiffer. This effect was greater for SEBS than PEBAX, which saw an increase of 23 fold (75 % v/v solid loading) in the storage modulus at 20 °C, compared to 3.4 fold for PEBAX (77 % v/v solid loading). DMA also show that glass transitions were affected, high solid loading should impose geometrical conditions on the polymer, restricting it mobility, therefore increasing the glass transition point[253]. As expected, the glass transition reported by the loss modulus maxima increased for PEBAX, conversely according to the tan δ maxima it had decreased. With SEBS, the first glass transition increased slightly, however the second glass transition decreased. This decreasing of the glass transition with introduction of a filler has been seen with some other fillers and is believed to be linked to the nature of the interaction between the filler and polymer[254,255]. Reduction in the size of the tan δ peaks at the glass transition was seen with both PEBAX and SEBS, this is due to the decrease in the mobility of the polymer and new transitions. The tan δ showed a general increase at temperature above the glass transition, due to additional dampening cause by a friction effect within the sample[252].

The storage modulus of plasticised PEBAX was less affected by temperature than the plasticised SEBS (Figure 6-14). However, addition of plasticiser to the sugar filled PEBAX saw an increasing in the glass transition point by DMA, opposite to that seen with the unfilled polymer (section 5.4.1). The author can find no other examples of this reported in the literature. This may be due to an increased interaction between the filler and the plasticised polymer over the unplasticised polymer. With filled SEBS, plasticisation saw the expected decrease in both glass transitions, as seen with the unfilled samples (section 5.4.2).

The glass transitions of PEBAX and SEBS provides an estimate of the lower and upper working limits, this can be compared to the ideal limits of -54 to 74 °C. Looking at Table 6-13, it can be seen that for the sugar filled PEBAX (60 % v/v), the first glass transition increased from -62 to -53 °C with increasing plasticiser content, slightly above the lower limit. For sugar filled SEBS (57 % v/v) the glass transition increased from -37.4 to -50.4 °C with increasing plasticiser content, consistently above the lower limit of -54 °C. Unfortunately, the second glass transition, indicating the upper working limit is reduced from 101 to 23.2 °C, now falling well below the upper limit (74 °C). Based on these results PEBAX appears to have the superior mechanical properties

Table 6-13 Comparison of mechanical properties of filled TPEs, unplasticised and plasticised with DOS.

	PEBAX (filed with sugar, 60 % v/v)		**SEBS (filled with sugar, 57 % v/v)**		**Proposed Acceptable Properties for Solid Rocket Motor (Tactical Air-to-Air) Stacer *et al.*** [9]
	Unplasticised	**Plasticised with DOS (11 % v/v)**	**Unplasticised**	**Plasticised with DOS (11 % v/v)**	
First glass transition (tan δ maximum at 1 Hz /°C)	ca. -62	ca. -53	-37.4	-50.4	-54
Second glass or melting transition (tan δ maximum at 1 Hz /°C)	Not identifiable by DMA		101	23.2	74

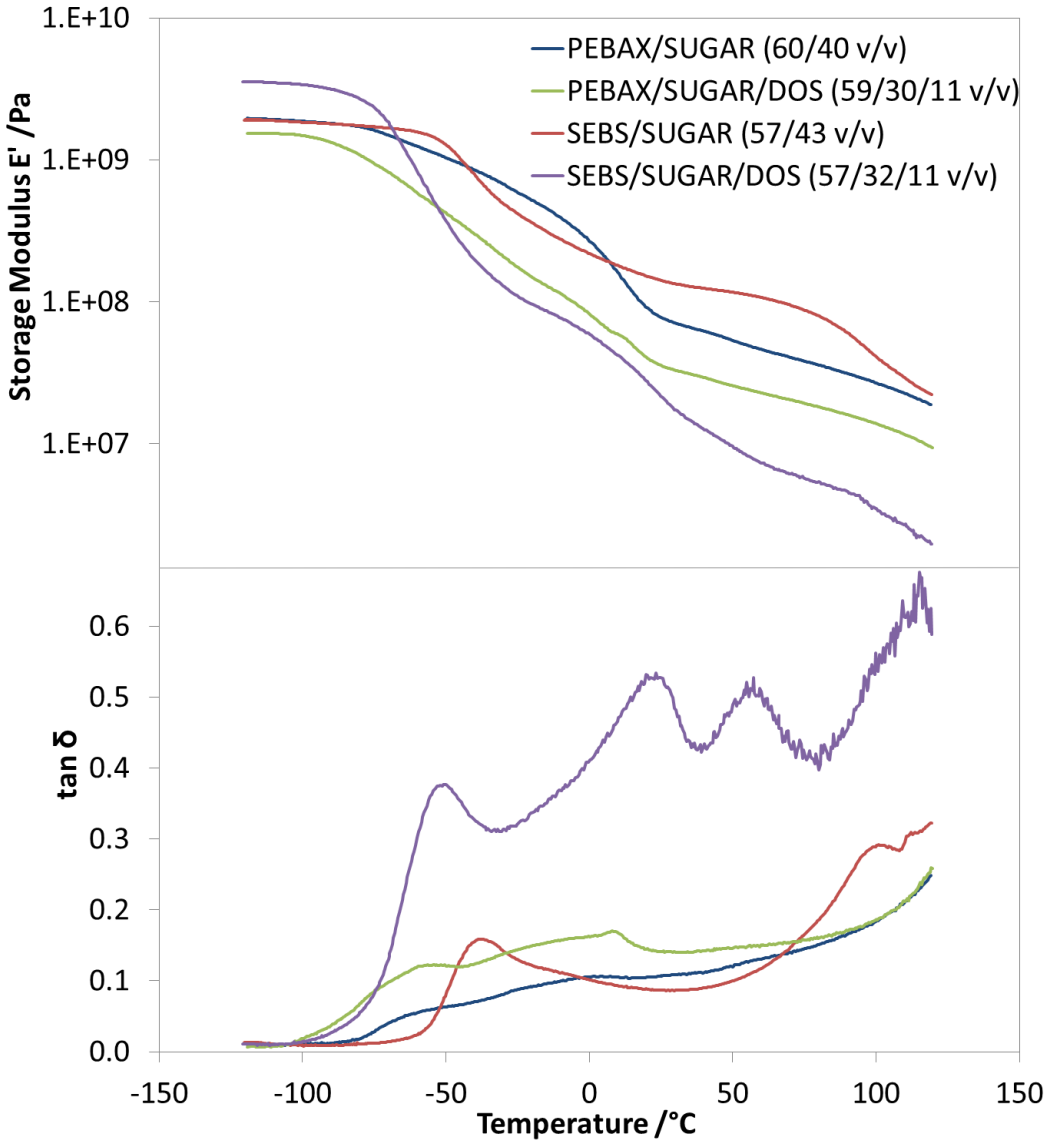

Figure 6-14 Comparison of the storage modulus (E') and tan δ of plasticised (11 % v/v DOS) and unplasticised PEBAX and SEBS filled ca. 60 % v/v sugar. Single cantilever DMA at 1 Hz, 50 µm displacement.

7 SEBS Filled with an Inert Fillers (RAM Slurry Mix)

To safely manufacture energetic propellants based on TPEs, a remote coating and pressing method needed to be developed. TPEs are thermoplastics, as such are generally heated above their softening point and extruded or injection moulded. Heating to the typically processing temperatures of TPEs (205 °C for PEBAX 3533[226], 140 to 200 °C for SEBS MT940[230]) would not be suitable for the manufacturing of propellant on safety grounds, lower temperatures would be too viscous for processing, especially given the high solid loadings. Instead a solvent process was chosen, this was based on the slurry process more commonly used for manufacture of polymer bonded explosives (PBX). A novel process was developed using a resonant acoustic mixer (RAM) in place of a traditional slurry mixer (see section 3.1). This coated the filler with the binder creating a moulding powder which was then remotely hot pressed into sheets and then cut up using a guillotine for analysis.

Due to supply issues and purity of PEBAX, it was decided to continue the research only with SEBS as the binder despite its inferior mechanical properties. Additionally, SEBS has the advantage of being soluble in toluene, allowing for safer manufacturing of the moulding powder without chlorinated solvents.

In addition to the bimodal mixtures of sugars to represent a rocket propellant, talc (see Table 7-1 & Figure 7-1) was used to represent the finer RDX used in LOVA gun propellants (D_{50} = ca. 5 µm)[150]. Samples inert 1 to 4 were filled with a bimodal mixture of sugar (Table 7-2). The percentages of filler were chosen so that the percentage fill by volume of samples *inert 1 to 4* are the same as the AP/SEBS propellants manufactured (*mix 1 to 4*) in chapter 8. Samples *inert 5 to 8* were filled with talc, to be representative of a gun LOVA propellant. These would have the same percentage fill by volume as RDX/SEBS propellant of 60, 70, 80 and 84% m/m solid loading. The RDX/SEBS propellant mix 7, manufactured in chapter 8 is analogous with sample inert 7.

Mechanical analysis by DMA and uniaxial tensile testing was performed. Bulk density was obtained by hand measurements of the samples, while true density was determined by helium pycnometry.

Table 7-1 Particle size distribution for inert fillers, as determined by laser diffraction using a Cilas 1190 in dry mode. Graphs of caster and icing sugar can be seen in Figure 6-1 and Figure 6-2.

Inert Filler	Diameter at 10 % (D_{10}) / µm	Diameter at 50 % (D_{50}) / µm	Diameter at 90 % (D_{90}) / µm
Caster Sugar (Tate and Lyle)	191	254	374
Icing Sugar (Tate and Lyle)	3.3	15.6	27.0
Talc (Sigma-Aldrich)	1.0	5.0	11.2

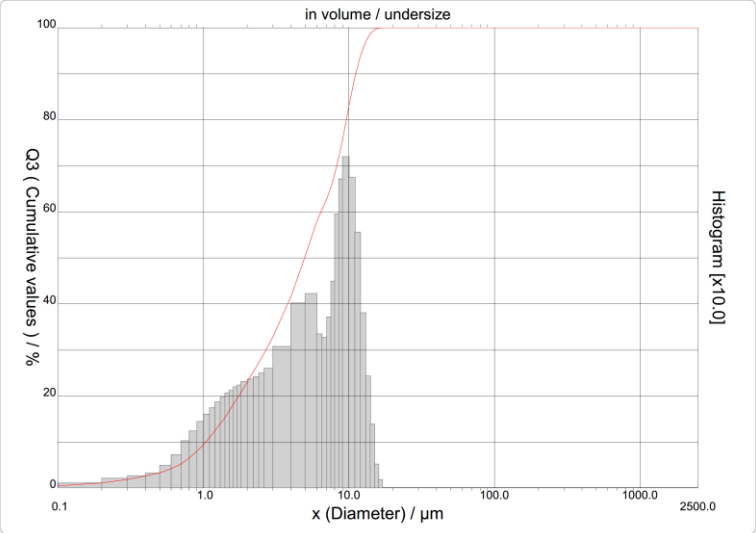

Figure 7-1 Particle Size Distribution for talc (Sigma-Aldrich), found by laser diffraction.

Table 7-2 Composition of inert (sugar) filled TPEs (RAM slurry mixed).

Sample	Composition by volume			Composition by mass		
	Sugar* / % v/v	Talc† / % v/v	SEBS / % v/v	Sugar* / % m/m	Talc† / % m/m	SEBS / % m/m
Inert1	41		59	55.0		45.0
Inert2	52		48	65.6		34.4
Inert3	65		35	76.5		23.5
Inert4	71		29	81.1		18.9
Inert5		43	57		69.4	30.6
Inert6		54	46		77.9	22.1
Inert7		67	33		85.8	14.2
Inert8		72	18		88.8	11.2

*Sugar was a bimodal mixture of caster (D_{50} = ca. 250 µm) and icing (D_{50} = ca. 15 µm) sugar.

†D50 = ca. 5 µm

7.1 Density Measurements

7.1.1 Density of SEBS Filled with Sugar (RAM Slurry Mix)

Densities found by helium pycnometry were in good correlation with the calculated theoretical maximum density (TMD) (Table 7-3 & Figure 7-2). Hand measurements of the density reports the bulk density of the composite. These densities were fairly close (96.7 %) to the TMD for the 46 and 57 % v/v filled samples. For the higher solid loadings (70 & 75 % v/v), the hand density was lower compared to the TMD. This indicates that there are voids in the composite, probably due to insufficient binder to completely fill the gaps between the filler particles.

Table 7-3 Density Measurements (helium pycnometry & hand measurements) of SEBS filled with sugar at varying solid loading. Samples were in duplicate. Standard deviation (σ) x1 is reported throughout this thesis.

Sugar (Filler) / % v/v	TMD / g cm^{-3}	Pycnometry		Hand Measurements	
		Average Density / g cm^{-3}	Percentage of TMD / %	Average Density / g cm^{-3}	Percentage of TMD / %
41	1.189	1.168 (σ = 0.051)	98.3	1.149 (σ = 0.008)	96.7
52	1.263	1.277 (σ = 0.018)	101.2	1.221 (σ = 0.013)	96.7
65	1.351	1.347 (σ = 0.004)	99.7	1.236 (σ = 0.025)	91.5
71	1.391	1.404 (σ = 0.016)	100.9	1.308 (σ = 0.035)	94.0

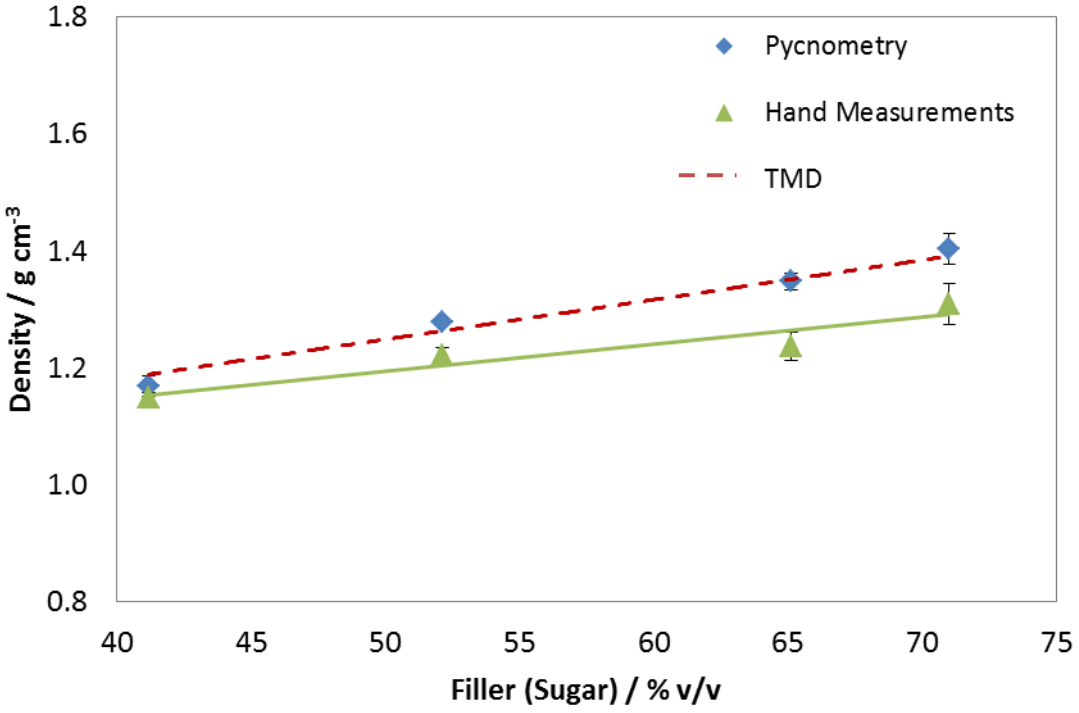

Figure 7-2 Graph of density (helium pycnometry & hand measurements) against solid loading for SEBS filled with sugar. Red dotted line represents the theoretical maximum density (TMD). Samples were in duplicate. Error bars represent the standard deviation (x1) throughout this thesis.

7.1.2 Density of SEBS Filled with Talc (RAM Slurry Mix)

Again the densities by helium pycnometry are close to the theoretical maximum densities (TMD) (Table 7-4 & Figure 7-3). The hand density measurements show

a generally trend of achieving a lower percentage of the TMD as the percentage of filler increases. Only the lowest filled composites (43 % v/v) achieved a high percentage of the TMD. This is expected as the talc filler was a mono-modal distribution, which will pack more inefficient than the bimodal distribution of the sugar. This poor packing give rises to a large volume of void between the particles, requiring more polymer to fill them.

Table 7-4 Density measurements (helium pycnometry & hand measurements) of SEBS filled talc at varying solid loadings. Samples were in duplicate.

Talc (Filler) / % v/v	TMD / g cm^{-3}	Pycnometry		Hand Measurements	
		Average Density / g cm^{-3}	Percentage of TMD / %	Average Density / g cm^{-3}	Percentage of TMD / %
43	1.698	1.691 (σ = 0.001)	99.6	1.615 (σ = 0.052)	95.1
54	1.900	1.895 (σ = 0.004)	99.7	1.774 (σ = .0550)	93.3
67	2.136	2.142 (σ = 0.007)	100.3	1.666 (σ = 0.120)	78.0
72	2.242	2.200 (σ = 0.000)	98.1	1.754 (σ = 0.166)	78.2

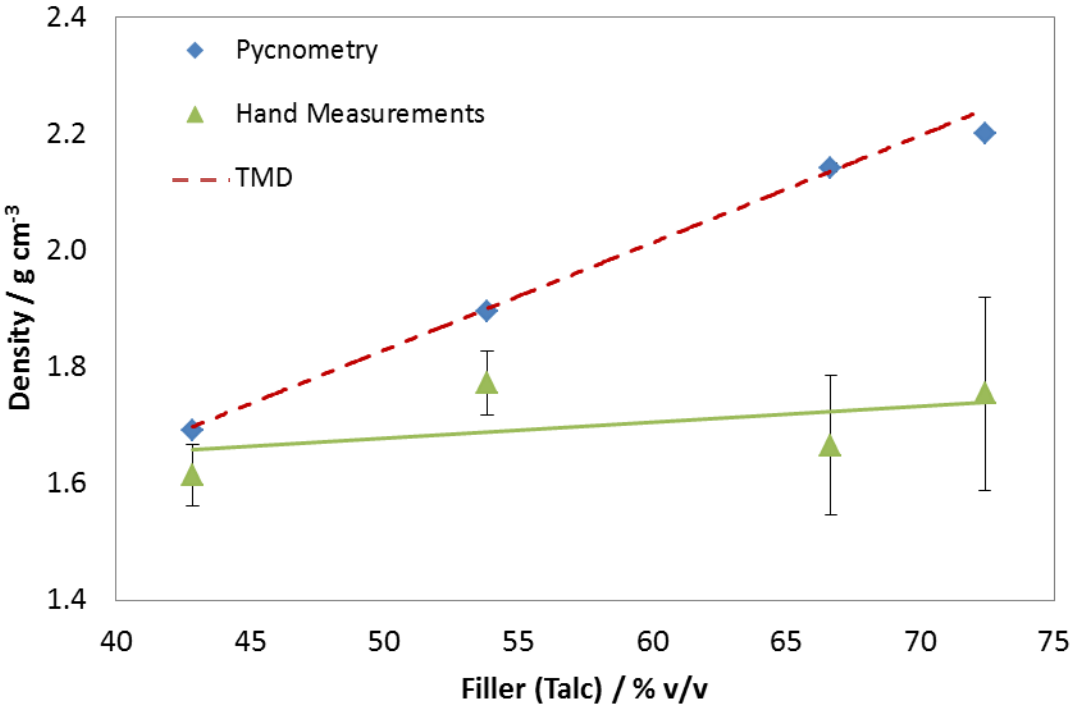

Figure 7-3 Graph of density measurements (helium pycnometry & hand measurements) against solid loading for talc filled SEBS filled with talc. Red dotted line represents the theoretical maximum density (TMD). Samples were in duplicate.

7.2 Dynamic Mechanical Analysis (DMA)

7.2.1 DMA of SEBS Filled with Sugar (RAM Slurry Mix)

As expected the results of the DMA tests (see Figure 7-4) on sugar filled SEBS using the RAM slurry method, was very similar to the samples from the hand mixed method (see Figure 6-5). The general shape of all of the curves are in good agreement with each other. Comparing the first glass transitions (T_{g1}) between the two sets of samples (see Table 7-5 & Figure 7-5 for RAM slurry, Table 6-5 & Figure 6-6 for hand mixed) both show shifts to higher temperature, this shift is larger for the tan δ peak with the RAM slurry, conversely there is a larger shift in the loss modulus peak for the hand mixed. As for the second glass transitions (T_{g2}), the RAM slurry samples all appear to have a similar shift to lower temperatures, regardless of the solid loadings. A similar reduction in the second

transition is present for the hand mix samples, although this appears to more of a steady reduction.

Overall, it appears that hand and RAM mixed methods are largely consistent with each other. This would indicate that the RAM slurry method is coating as well as the hand mixed method.

Table 7-5 Thermal transitions of sugar filled SEBS, found by DMA.

	First Glass Transition (T_1)		Second Glass Transition (T_2)	
Sugar (Filler) / % v/v	**tan δ Maximum /°C**	**Loss Modulus Maximum /°C**	**tan δ Maximum /°C**	**Loss Modulus Maximum /°C**
0	-41.0	-47.5	105.3	93.8
41	-42.3	-47.6	94.3	86.4
52	-39.3	-45.2	94.7	84.8
65	-38.7	-45.5	96.5	83.1
71	-36.0	-45.1	96.3	84.2

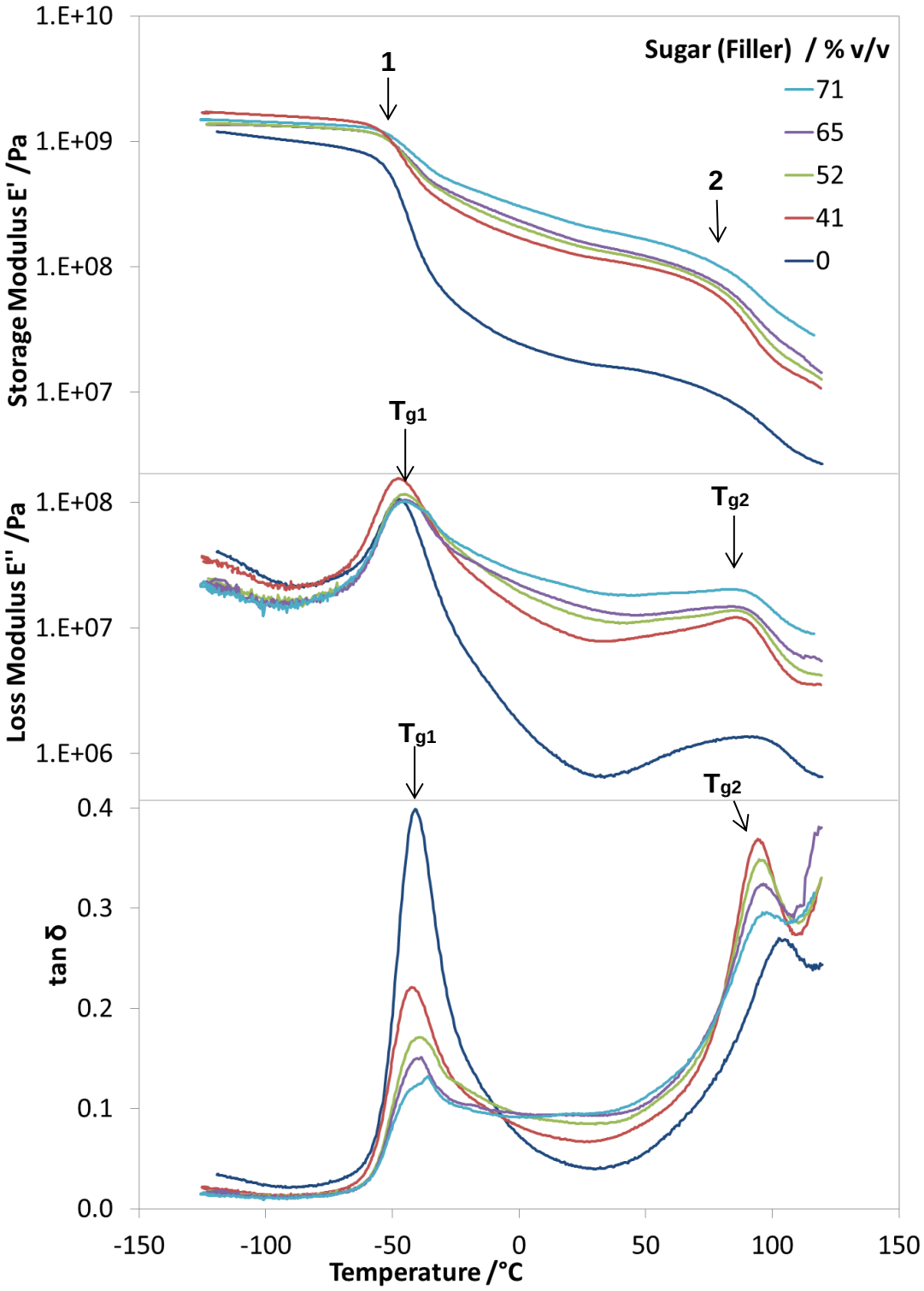

Figure 7-4 DMA thermogram of sugar filled SEBS. Single cantilever DMA at 1 Hz, 50 µm (1.25 %) displacement.

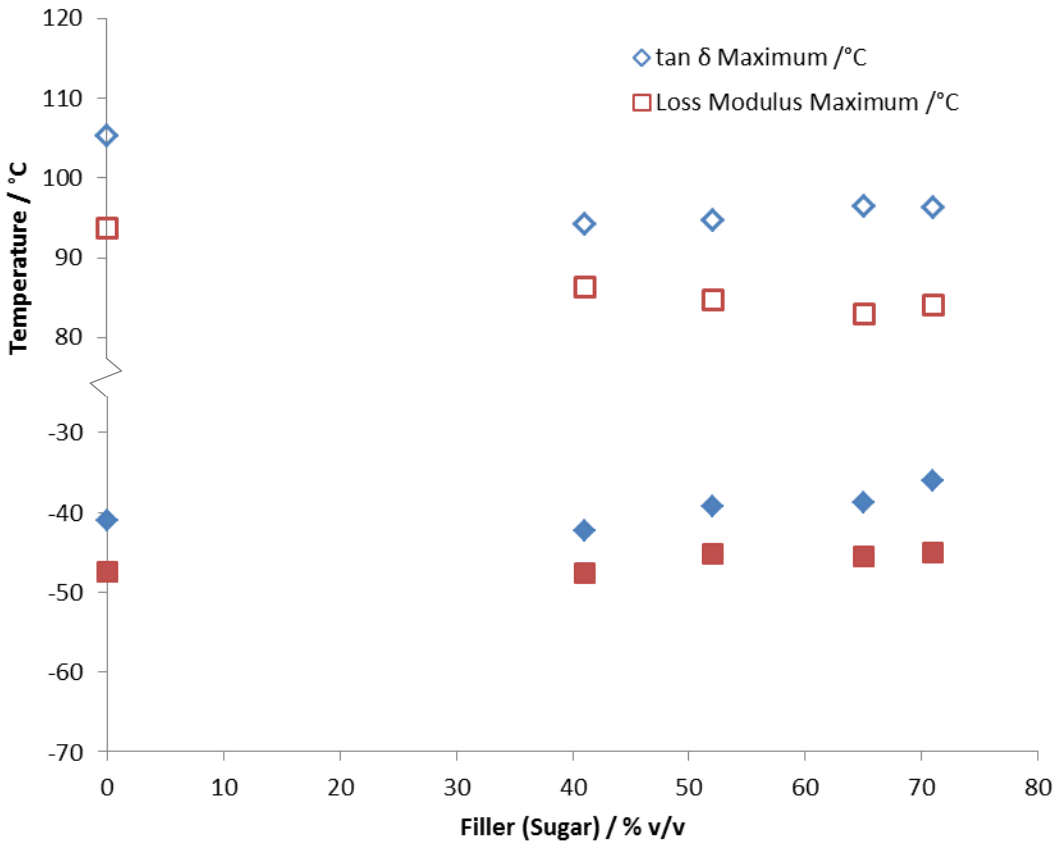

Figure 7-5 Graph comparing the thermal transitions for sugar filled SEBS as reported in Table 7-5. Solid marker represents the first transition (T_{g1}), with hollow markers for the second (T_{g2}).

7.2.2 DMA of SEBS Filled with Talc (RAM Slurry Mix)

Comparing the DMA results for SEBS filled with talc (Figure 7-6) with SEBS filled with sugar (Figure 7-4), we see that all the curves are of a similar shapes and trends. However, the talc filler has a greater effect on increasing the storage modulus and loss modulus above -40 °C. The increase in the storage modulus with increasing filler percentage is explained by the reinforcement effect, this effect appeared to be greater for the same volume of talc compared to sugar. This is most likely due to the reduction in the particle size of the two fillers. Talc is finer (D_{50} = 5 µm) than the coarser bimodal sugar mix (D_{50} = 254 & 16 µm, in a 4:3 ratio). Hence the filler has a greater overall surface area, resulting in a greater surface area in contact with the polymer, leading to greater reinforcement[256]. This increased surface area in contact with the filler will lead to greater internal

friction, resulting in a greater loss modulus. As seen with the SEBS filled with sugar, as the reinforcement effect increases, the storage modulus becomes larger relative to the loss modulus. This results in the tan δ becoming smaller, reducing the dampening effect of the composite.

Looking at the first (T_{g1}) and second (T_{g2}) glass transitions indicated by the peaks in the loss modulus and tan δ curves for SEBS filled with talc (Table 7-6 & Figure 7-7). Both the first and second show a reduction in transition point as the percentage of talc is increased. This effect on the first glass transition (T_{g1}) is the opposite to what was seen with SEBS filled with sugar (Table 7-5 & Figure 7-5). This further collaborates that these shifts in the glass transition depend on the specific intermolecular interaction between the filler and polymer. Changing between sugar and talc filler results in a shift of the glass transition in a different direction[254].

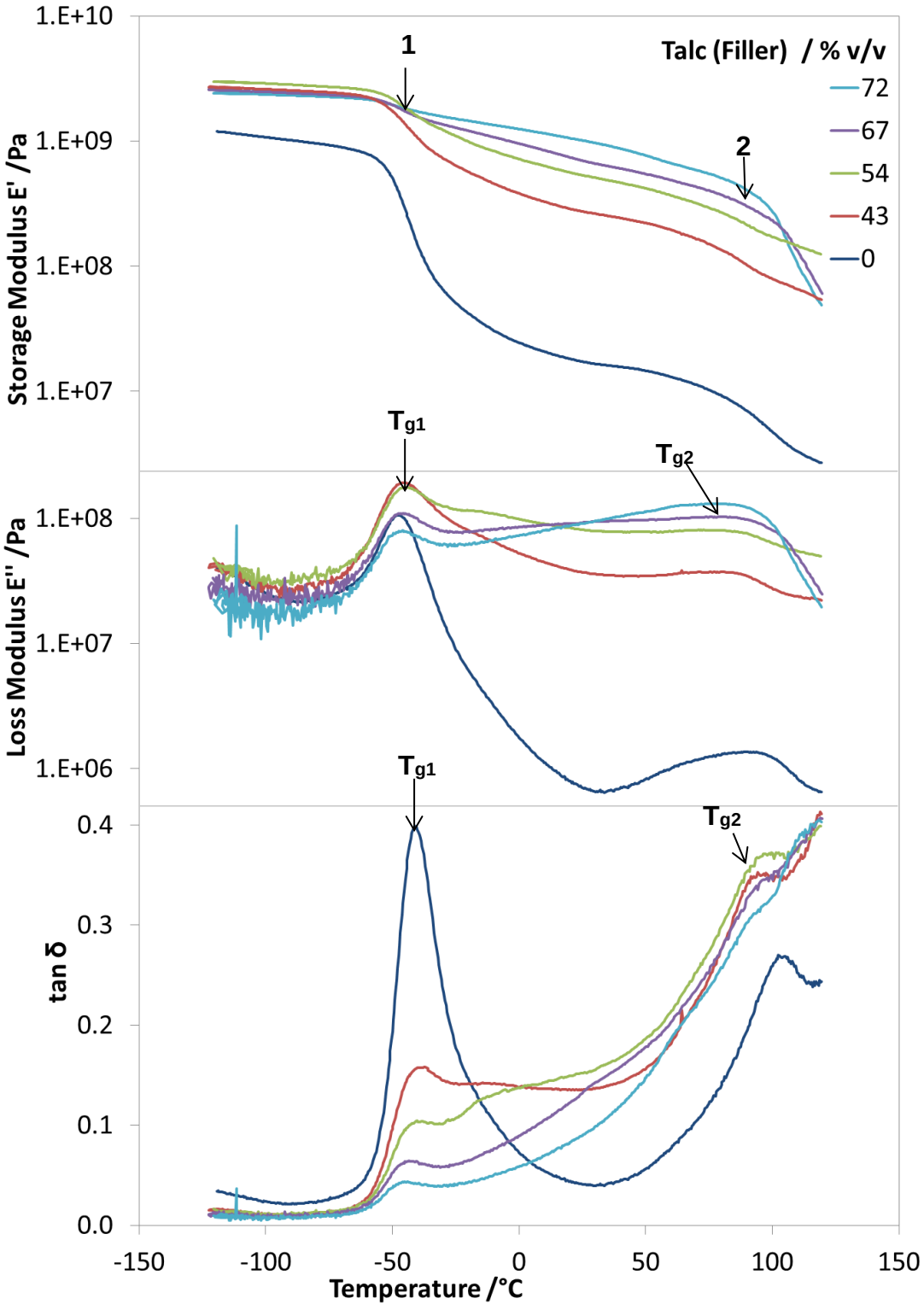

Figure 7-6 DMA thermogram of talc filled SEBS. Single cantilever DMA at 1 Hz, 50 µm (1.25 %) displacement.

Table 7-6 Thermal transitions of talc filed SEBS, found by DMA.

	First Transition (T_1)		Second Transition (T_2)	
Talc (Filler) / % v/v	tan δ Maximum /°C	Loss Modulus Maximum /°C	tan δ Maximum /°C	Loss Modulus Maximum /°C
0	-41.0	-48.3	114.6	86.8
43	-37.5	-45.7	94.2	77.0
54	-40.2	-45.3	102.6	69.4
67	-43.5	-47.5	*	80.8
72	-45.9	-45.9	*	79.9

*could not be determined

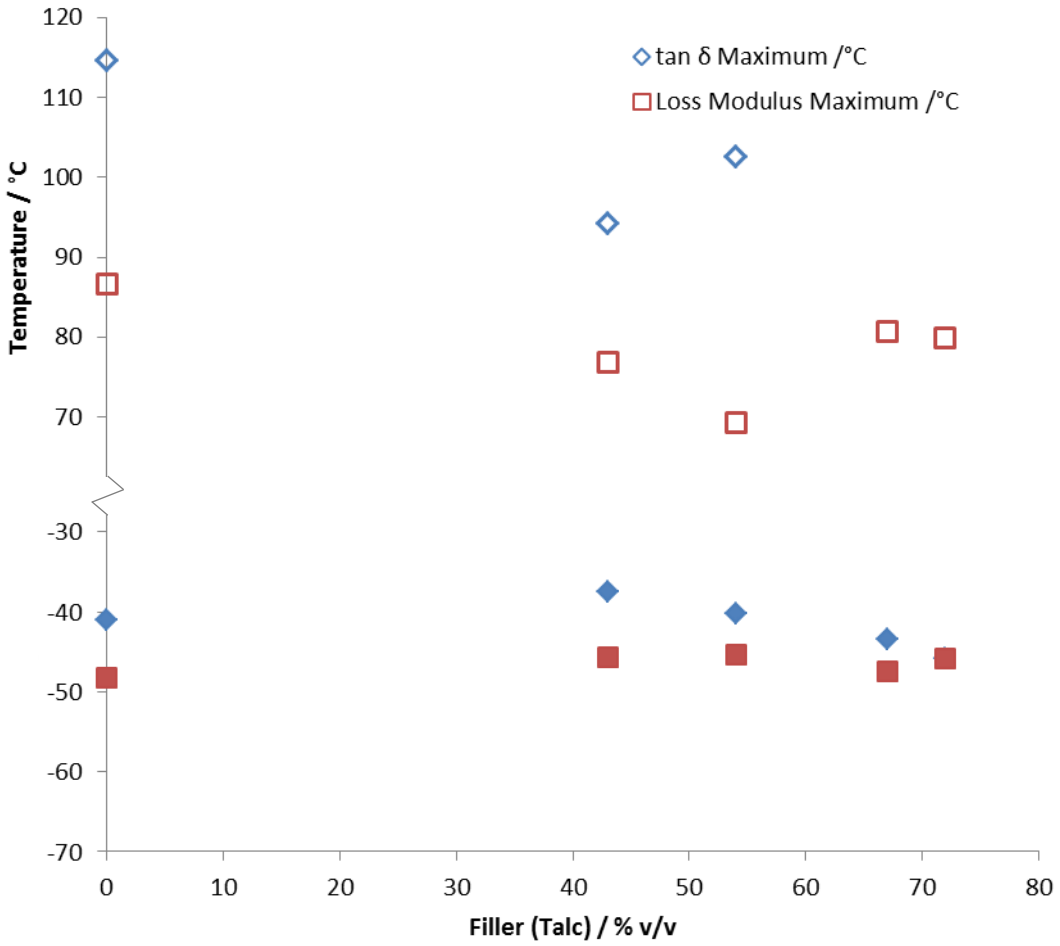

Figure 7-7 Graph comparing the thermal transitions for talc filled SEBS as reported in Table 7-6. Solid marker represents the first transition (T_{g1}), with hollow markers for the second (T_{g2}).

7.3 Tensile Testing

Results by DMA (see section 7.2) indicated that SEBS would be unlikely to have good elasticity at the target minimum operating temperature of -54 °C. Hence a higher minimum temperature of -40 °C was used for tensile testing.

7.3.1 Tensile Testing of SEBS Filled with Sugar (RAM Slurry Mix)

The results from uniaxial tensile testing of SEBS filled with sugar can be seen in Figure 7-8 and Table 7-7. The Young's modulus (E_0), maximum stress (σ_m) & maximum extension (ε_b) have then been graphed against the solid loading of the composite at the different temperatures (-40 °C, room temperature 20 °C & 74 °C), see Figure 7-9. From the first graph it can be seen that, in general, the Young's Modulus decreases with increasing temperature. The graph of maximum stress also shows the same trend of decreasing with temperature. These trends can be explained by the increase in molecular mobility as temperature increases, resulting in less stiffness (modulus) and reduced maximum stress[257]. This effect should increase the ductility (maximum extension) of the polymer with temperature. Looking at the graph of maximum extension against percentage of filler, there is an increase in the maximum extension from -40 to 20 °C, however, it then decreases again at 74 °C. This decrease at 74 °C is as we are approaching the upper transition for SEBS. Here the fugitive cross-links that hold the elastomer together break apart. This results in the polymer becoming less elastic and more viscous in behaviour, reducing the maximum extension.

At 20 and 74 °C the Young's modulus shows a clear trend of increasing with solid loading, which can be explained by the reinforcing effect of the filler[258]. At -40 °C the same trend is seen at higher solid loadings, but for lower loadings the Young's modulus decreases with solid loading. This is probably due to the reduction in the percentage of the binder, being a more dominant effect than the reinforcement effect, due to the increase in the Young's modulus of the binder itself. The maximum stress does not change by much as the solid loading is varied. At -40 °C there is a reduction in maximum stress as solid loading is increased, there is very little change at 20 °C. At 74 °C the maximum stress

increases with solid loading. Again the reinforcing effect and percentage of the binder present are competing. At -40 °C the binder has greater maximum stress, so the effect of the reduction in the percentage of binder is the dominant effect. While at 74 °C, the binder has a much lower maximum stress and so the reinforcement effect is dominant. The maximum extension decreases rapidly with increasing percentage of filler. This is due to the rigid solid filler hindering the ductile behaviour of the polymer binder and the reduction of the percentage binder present.

Table 7-7 Tensile testing results of sugar filled SEBS. Results are an average of 5 replicates.

74 °C			
Sugar (Filler) / % v/v	**Young's Modulus (E_0) / MPa**	**Maximum Stress (σ_m) / MPa**	**Maximum Extension (ε_b) / %**
41	27.2 (σ = 5.3)	1.37 (σ = 0.16)	21.1 (σ = 4.3)
52	33.9 (σ = 8.5)	1.61 (σ = 0.25)	13.2 (σ = 2.2)
65	62.0 (σ = 17.2)	1.62 (σ = 0.30)	5.9 (σ = 0.8)
71	55.2 (σ = 20.3)	1.66 (σ = 0.70)	6.2 (σ = 0.9)

20 °C			
Sugar (Filler) / % v/v	**Young's Modulus (E_0) / MPa**	**Maximum Stress (σ_m) / MPa**	**Maximum Extension (ε_b) / %**
41	38.2 (σ = 7.0)	2.02 (σ = 0.60)	309.3 (σ = 211.3)
52	36.9 (σ = 8.7)	1.82 (σ = 0.44)	39.5 (σ = 10.2)
65	57.0 (σ = 33.0)	1.54 (σ = 0.57)	10.6 (σ = 2.8)
71	65.3 (σ = 14.8)	1.95 (σ = 0.56)	9.9 (σ = 1.7)

-40 °C			
Sugar (Filler) / % v/v	**Young's Modulus (E_0) / MPa**	**Maximum Stress (σ_m) / MPa**	**Maximum Extension (ε_b) / %**
41	141.4 (σ = 21.9)	5.47 (σ = 0.69)	29.1 (σ = 12.1)
52	118.2 (σ = 42.3)	4.56 (σ = 0.66)	15.9 (σ = 6.6)
65	109.8 (σ = 33.3)	3.65 (σ = 1.00)	7.0 (σ = 1.6)
71	140.7 (σ = 24.7)	3.76 (σ = 0.62)	4.7 (σ = 1)

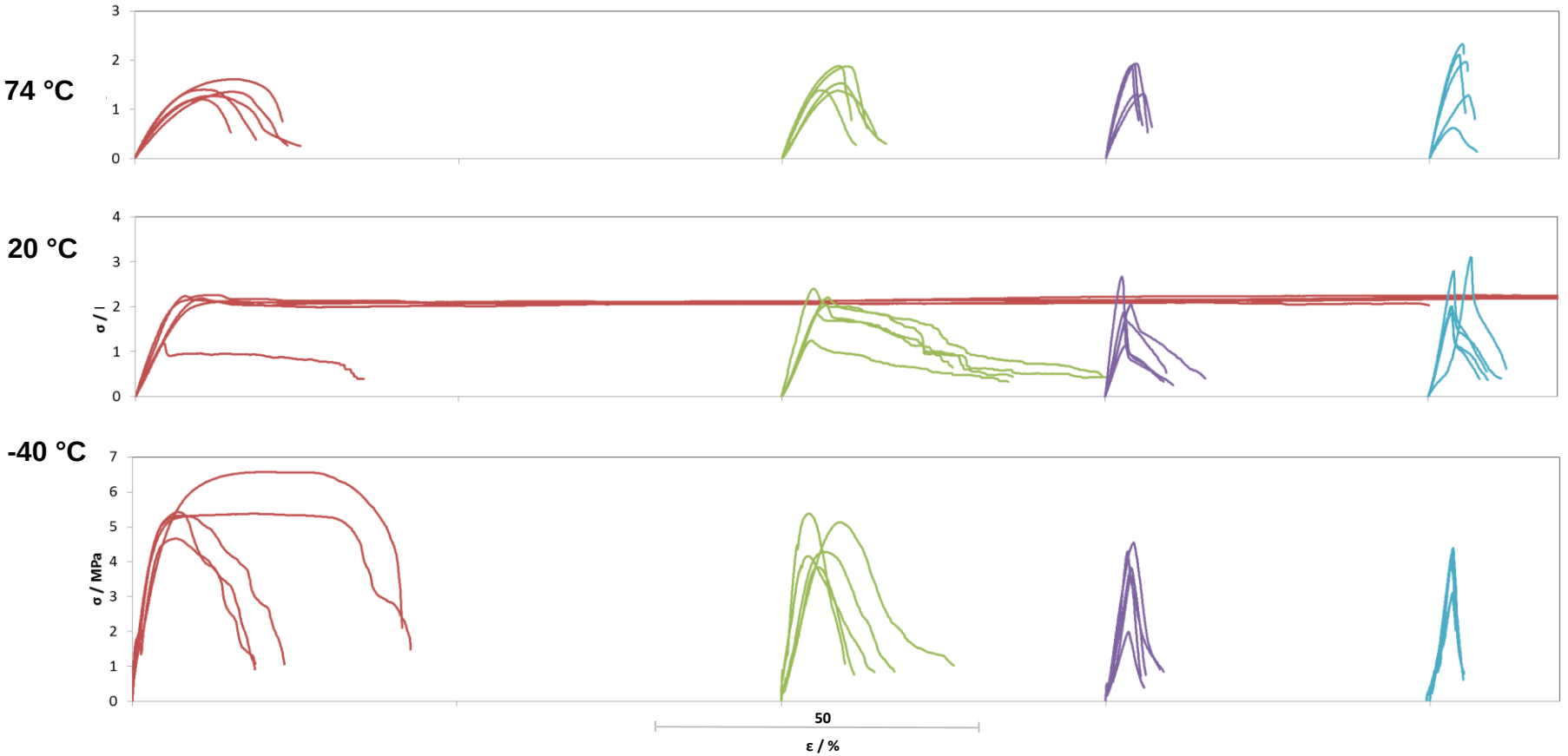

Figure 7-8 Graph of stress (σ) against extension (ε) for sugar filled SEBS from tensile tests. Each graph shows a different temperature, 5 replicates were tested. Different solid loadings have been shifted horizontally for clarity. Key: – 41 – 52 – 65 – 71 % v/v sugar (filler).

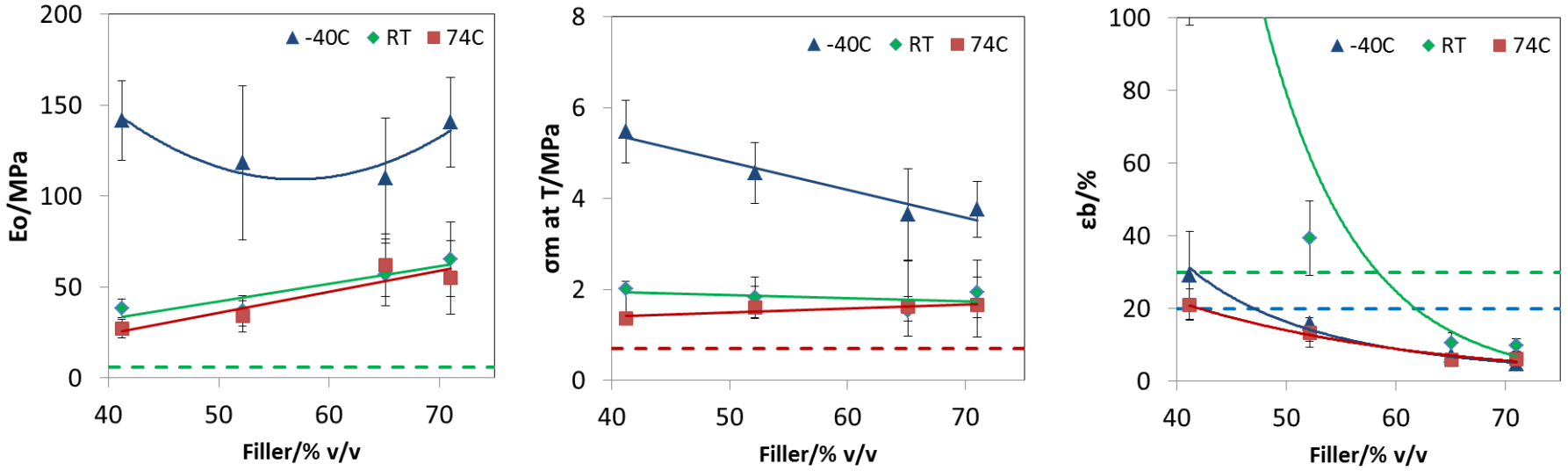

Figure 7-9 Graphs showing the Young's modulus (E_0), maximum stress (σ_m) & maximum extension (ε_b) for sugar fiiled SEBS (-40 °C, RT = 20 °C & 74 °C). Results are an average of 5 replicates. Dotted lines represents the acceptable properties for solid rocket motor (tactical air-to-air) proposed by Stacer et al.[9]**. Green dotted line represents for E_0 and minimum ε_b at 20 °C, red dotted line is the minimum σ_m at 74 °C & blue dotted line is the minimum ε_b at -54 °C.**

7.3.2 Tensile Testing of SEBS Filled with Talc (RAM Slurry Mix)

The results of tensile testing of SEBS filled with talc (see Figure 7-10, Table 7-8 & Figure 7-11) show the same general trend seen with SEBS filled with sugar (see section 7.3.1). Figure 7-12 shows a comparison of typical results for SEBS filled with talc (67 % v/v), with sugar (65 % v/v). The greatest difference is the Young's modulus is much greater for the talc samples of similar loading, e.g. 138 MPa, compared to 57 MPa at 20 °C. This effect is due to the smaller particle size of the talc compared to the sugar, resulting in a larger specific surface area. This increased area of contact with the polymer gives rise to a greater reinforcement[256]. Unlike the results for sugar filled SEBS, the Young's modulus at -40 °C increases with solid loading for all the solid loadings, due to the larger reinforcement effect. There is also an increase in the maximum stress 3.5 MPa compared 1.6 MPa at 20 °C. This again can be linked to the increase reinforcement effect of the talc filler. The maximum extensions are less for talc samples in comparison to sugar. This again is likely to be due to the increase surface area of the talc. Hence the binder is spread thinner over the filler particles.

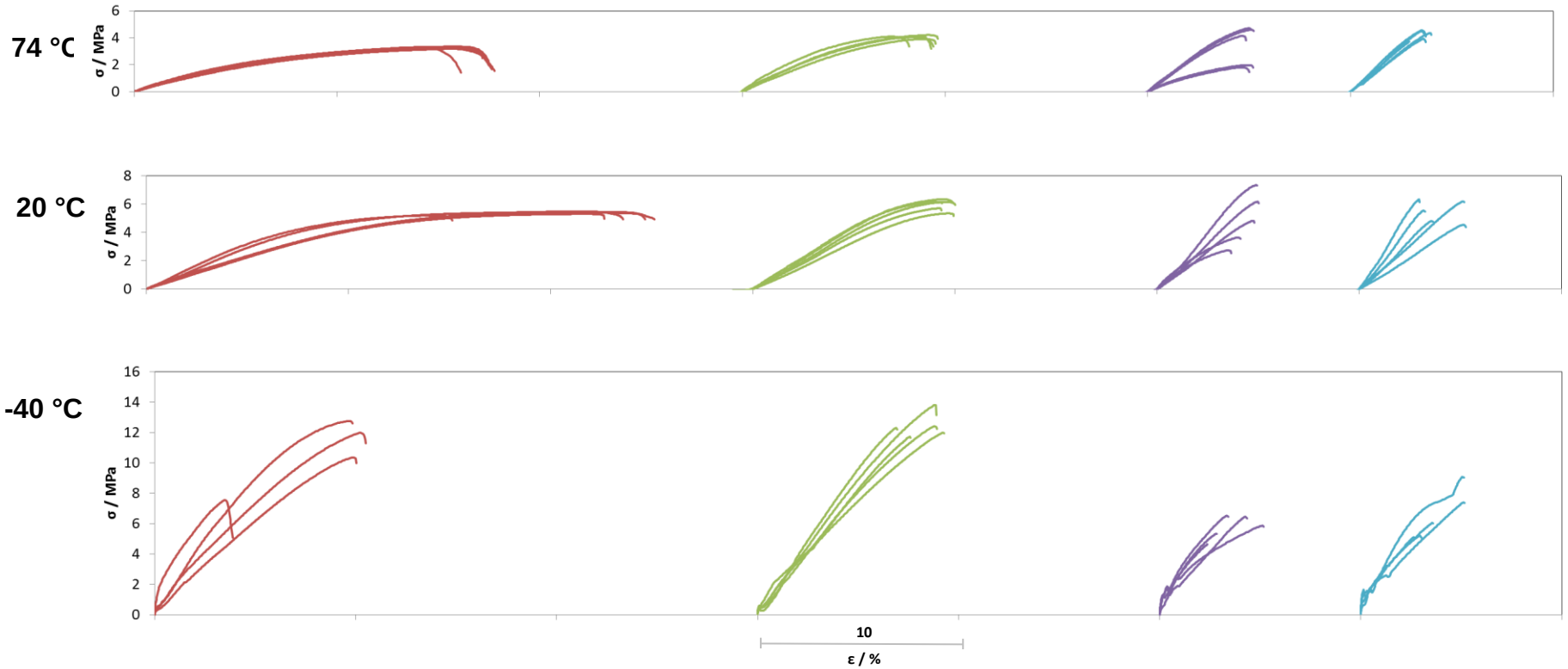

Figure 7-10 Graph of stress (σ) against extension (ε) for talc filled SEBS from tensile tests. Each graph shows a different temperature the tests were conducted at. 5 replicates were tested, except for 43 & 72 % v/v at -40 °C where only 4 replicates were performed due to lack of sample. Different solid loadings have been shifted horizontally for clarity. Key: – 43 – 54 – 67 – 72 % v/v talc (filler)

Table 7-8 Tensile testing results of talc filled SEBS. 5 replicates were tested, except for 43 & 72 % v/v at -40 °C where only 4 replicates were performed due to lack of sample.

74 °C			
Talc (Filler) / % v/v	**Young's Modulus (E_0) / MPa**	**Maximum Stress (σ_m) / MPa**	**Maximum Extension (ε_b) / %**
43	47.2 (σ = 3.8)	3.28 (σ = 0.08)	17.2 (σ = 0.7)
54	83.9 (σ = 8.6)	4.09 (σ = 0.11)	9.2 (σ = 0.5)
67	103.0 (σ = 33.5)	3.45 (σ = 1.44)	5.1 (σ = 0.2)
72	136.3 (σ = 9.9)	4.34 (σ = 0.25)	3.7 (σ = 0.1)

20 °C			
Talc (Filler) / % v/v	**Young's Modulus (E_0) / MPa**	**Maximum Stress (σ_m) / MPa**	**Maximum Extension (ε_b) / %**
43	54.1 (σ = 11.3)	5.35 (σ = 0.12)	22.3 (σ = 4.1)
54	84.9 (σ = 10.1)	6.05 (σ = 0.56)	9.7 (σ = 0.3)
67	137.9 (σ = 27.0)	4.93 (σ = 1.86)	4.5 (σ = 0.6)
72	168.2 (σ = 60.6)	5.47 (σ = 0.80)	4.1 (σ = 1.1)

-40 °C			
Talc (Filler) / % v/v	**Young's Modulus (E_0) / MPa**	**Maximum Stress (σ_m) / MPa**	**Maximum Extension (ε_b) / %**
43	191.0 (σ = 56.0)	10.66 (σ = 2.30)	8.6 (σ = 3.1)
54	212.2 (σ = 33.6)	12.44 (σ = 0.81)	8.4 (σ = 1.0)
67	450.1 (σ = 96.7)	5.76 (σ = 0.79)	3.6 (σ = 1.1)
72	369.9 (σ = 47.0)	6.93 (σ = 1.69)	4.2 (σ = 1.1)

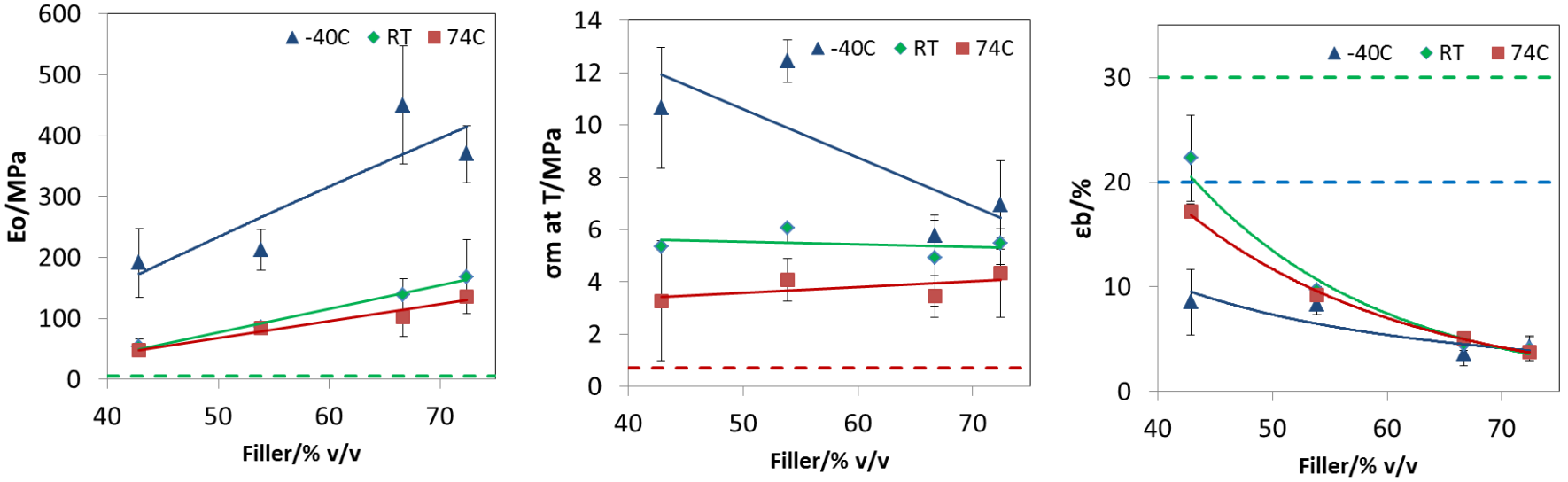

Figure 7-11 Graphs showing the Young's modulus (E_0), maximum stress (σ_m) & maximum extension (ε_b) for talc filled SEBS (-40 °C, RT = 20 °C & 74 °C). 5 replicates were tested, except for 43 & 72 % v/v at -40 °C where only 4 replicates were performed due to lack of sample. Dotted lines represents the acceptable properties for solid rocket motor (tactical air-to-air) proposed by Stacer *et al.*[7]. Green dotted line represents for E_0 and minimum ε_b at 20 °C, red dotted line is the minimum σ_m at 74 °C & blue dotted line is the minimum ε_b at -54 °C.

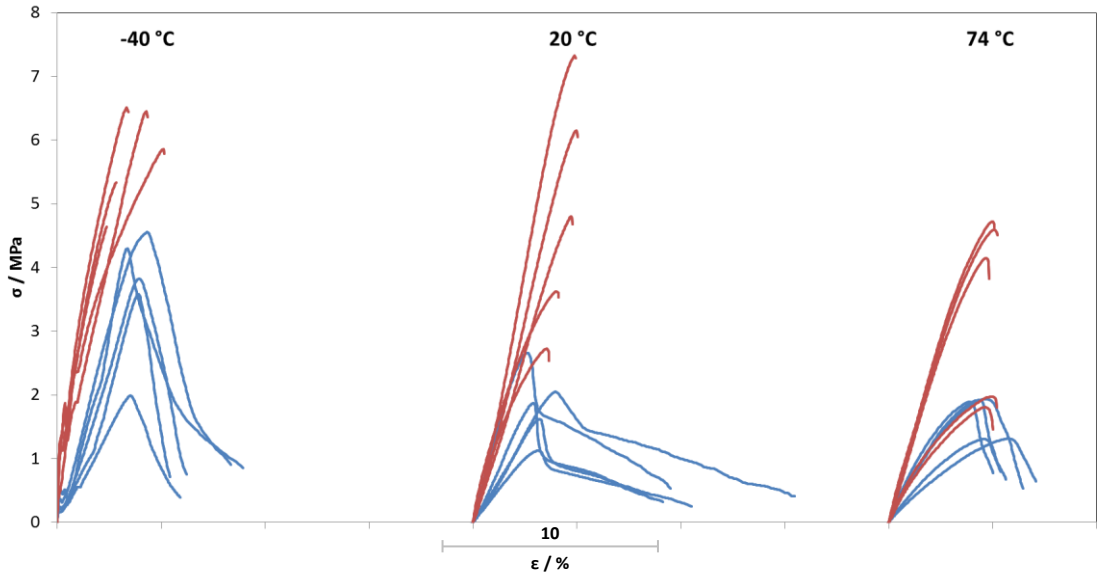

Figure 7-12 Graph of stress (σ) against extension (ε) for SEBS filled with sugar (–) and talc (–) from tensile tests. 5 replicates. Different temperatures have been shifted horizontally for clarity.

7.4 Conclusion

The RAM slurry method effectively produced a moulding powder, which on being pressed produced a composite very similar to the hand mixed method. Tensile testing of SEBS filled with both sugar and talc, produced composites with relatively high Young's moduli and maximum stress, but fairly poor maximum extensions for higher solid loadings, see examples in Table 7-9. From this data it is clear that the reinforcement effect of filler in SEBS is not solely dependent on the solid loading. Switching between the larger bimodal sugar and the finer mono-modal talc has produced a sizable difference in the properties found by mechanical analysis. For instance filling SEBS with sugar resulted in an increase in the first glass transition (T_{g1}) point, while with talc there was a decrease. SEBS filled with talc had a higher Young's modulus and maximum stress, but with lower maximum extensions than sugar filled. The tensile testing can be linked to the increase in surface area as the particle size decreases. The reduction of the first glass transition (T_{g1}) with talc as opposed to the increase with sugar is harder to explain. This has been linked again to the surface area, but it may be due to the nature of the interfacial interaction between the polymer and filler[254]. This

significant difference between the fillers highlight that using inert fillers will not necessarily provide you with similar results to an actual filler. Hence it is important to test this binder with energetic fillers such as ammonium perchlorate or RDX.

Table 7-9 Comparison of sugar filled SEBS with AP/AL/HTPB (lit.) and proposed acceptable properties for solid rocket motor, talc filled SEBS with JA2 (DB) propellant (lit.) and suggested widest requirements.

	Rocket Propellant			Gun Propellant	
	SEBS filled with sugar (65 % v/v)	**AP/Al/HTPB (lit.)** ***Cerri *et al.*[248]** **†Adel *et al.*[259]*Uniaxial tensile testing.***	**Proposed Acceptable Properties for Solid Rocket Motor (Tactical Air-to-Air) Stacer *et al.* [9]**	**SEBS filled with talc (67 % v/v)**	**Suggested widest requirements by Nguyen et al.[13]**
DMA					
First glass transition, T_{g1} (tan δ maximum at 1 Hz /°C)	-38.7	-75*	<-54	-43.5	<-51
Second glass transition, T_{g2} (tan δ maximum at 1 Hz /°C)	96.5	N/A	>74	could not be determined	>63
Tensile Testing					
Young's Modulus (E_0) at room temperature / MPa	57.0	3.3†	2-6	137.9	
Maximum Stress (σ_m) at T_{max} / MPa	1.62 (@ 74 °C)	0.4 (@ 76 °C)†	>0.7 (@ 74 °C)	3.45 (@ 74 °C)	
Maximum Extension (ε_b) at room temperature / %	10.6	36†	>30	4.5	
Maximum Extension (ε_b) at T_{min} / %	7.0 (@ -40 °C)	56 (@ -40 °C)†	>20 (@ -54 °C)	3.6 (@ -40 °C)	

8 Characterisation of SEBS Propellants

8.1 Introduction

Two different types of novel propellants were made in small quantities (ca. 60 g using the commercially available polymer SEBS (Styrene-ethylene/butylene-styrene) from Sigma-Aldrich (see section 4.2.2). One of these being a possible propellant for a rocket motor, contained AP (Ammonium Perchlorate) as the filler. While the other contained fine RDX (1,3,5-Trinitro-1,3,5-triazinane), being more suited for gun propellant. Four different compositions of the AP/SEBS propellants were made with varying percentage loadings (41 to 71 % v/v). Due to limited supply of suitable RDX, only one composition of RDX/SEBS propellant was manufactured (67 % v/v). AP/SEBS were made with a typically bimodal mixture[242] of coarse AP (AP200) and fine (AP90) in a 4:3 ratio. While RDX/SEBS used a mono-modal finer class 5 RDX (D_{50} = ca. 25 µm), which is closer to the ultra-fine RDX (ca. D_{50} = 5 µm) used in LOVA propellant than standard RDX (class 1)[26]. Particle size distribution of the fillers was obtained by laser diffraction, see Table 7-1. Two propellant 'sheets' of each composition were hot pressed, ca. 30 g each, measuring 100 x 55 x 4 mm. To make comparisons between fillers (particularly inert fillers of very different densities) the percentage filler is shown is *by volume*. The table below compares the filler loadings *by mass* for reference.

Table 8-1 Composition of AP/SEBS and RDX/SEBS propellants

Sample number	Composition by volume			Composition by mass		
	AP / % v/v	RDX / % v/v	SEBS / % v/v	AP / % m/m	RDX / % m/m	SEBS / % m/m
Mix 1	41		59	60		40
Mix 2	52		48	70		30
Mix 3	65		35	80		20
Mix 4	71		29	84		16
Mix 7		67	33		80	20

Table 8-2 Particle size distribution for fillers, as determined by laser diffraction using a Cilas 1190 in dry mode (AP samples) and wet mode (RDX).

Filler	Diameter at 10 % (D_{10}) / µm	Diameter at 50 % (D_{50}) / µm	Diameter at 90 % (D_{90}) / µm
AP (200)	185	225	301
AP (90)	54	119	240
RDX class 5	10	24	45

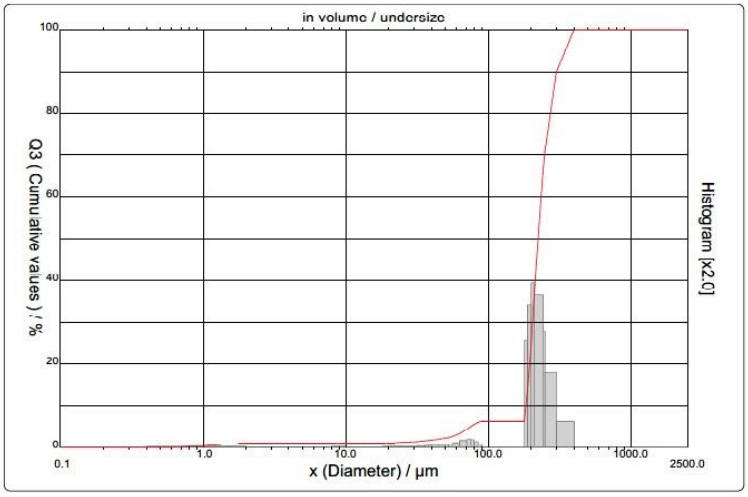

Figure 8-1 Particle Size Distribution for AP200 found by laser diffraction.

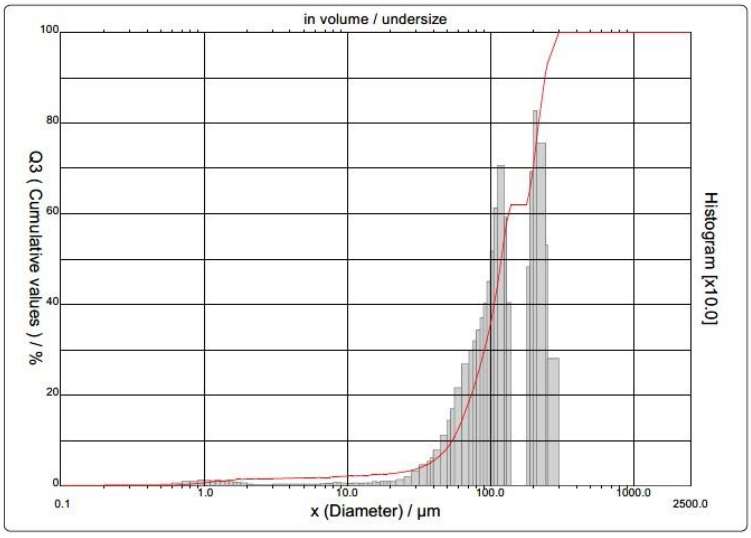

Figure 8-2 Particle Size Distribution for AP90 found by laser diffraction.

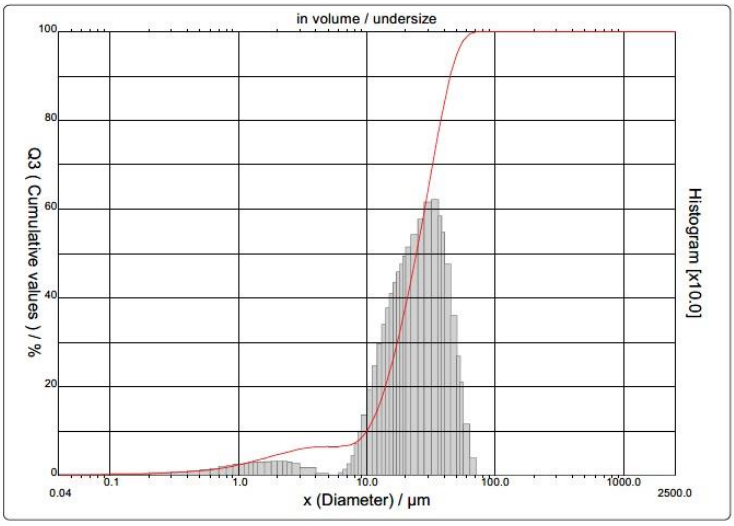

Figure 8-3 Particle Size Distribution for RDX class 5 found by laser diffraction.

Thermal and mechanical analysis was performed on the samples, as well as, visual inspection and density measurements.

8.2 Compatibility Testing of Raw Ingredients

Compatibility testing of the raw ingredients was conducted to evaluate the stability of the composite propellants being formulated. This was assessed by vacuum stability, conducted in-house in accordance to STANAG 4147 part 1B[260]. Results (shown in Table 8-3) show that SEBS is compatible with both ammonium perchlorate and RDX.

Table 8-3 Vacuum stability compatibly testing of SEBS with AP and RDX, in accordance with STANAG 4147 part 1B[260]**.**

Test Materials	Volume of gas from 5 g of mixture subtract volume of gas from 2.5 g of each component* (V_R) / ml	Compatible (V_R < 5 ml)
SEBS & AP	0.14	Yes
SEBS & RDX	0.49	Yes

*Test conditions: 100 °C, 40 hrs.

8.3 Propellant Hazard Testing

Propellant hazard testing was conducted on the moulding powder produced by the RAM slurry mixing technique. Rotter impact, electrical spark, mallet friction

and temperature of ignition was conducted in-house in accordance with the EMTAP manual of test 2016[261] (Table 8-4). The results from samples of AP/SEBS propellants were as expected with a FoI slightly below that of RDX (reference FoI 80). Results for RDX/SEBS (67/33 % v/v) yield a lower FoI (39), this was expected to be closer to that of pure RDX. Also smaller scale preliminary work on the sample composition found the FoI to be 69 (Langlie 10 test). Possibly small amount of solvent within the moulding powder was causing sensitisation of the composite.

Table 8-4 Propellant hazard testing of AP/SEBS and RDX/SEBS propellants. Standard deviation (σ) x1 is reported throughout this thesis

Sample	Percentage Filler (AP or RDX) / % v/v	Rotter impact test*; full 50 shot Bruceton (EMTAP 1A),	Electric spark test; 4.5J (EMTAP test 6)	Mallet friction; steel on steel (EMTAP test 2)	Temperature of ignition (EMTAP test 3)
AP/SEBS (41/59)	41	FoI 60.7 (σ = 0.0965)	Does not ignite at 4.5J	Steel / Steel 50%	274.7 to 274.9 °C
AP/SEBS (52/48)	52	FoI 60.0 (σ = 0.1032)	Does not ignite at 4.5J	Steel / Steel 50%	272.5 to 274.9 °C
AP/SEBS (65/35)	65	FoI 72.7 (σ = 0.1215)	Does not ignite at 4.5J	Steel / Steel 50%	273.4 to 273.5 °C
AP/SEBS (71/29)	71	FoI 60.2 (σ = 0.1095)	Does not ignite at 4.5J	Steel / Steel 50%	273.2 to 274.3 °C
RDX/SEBS (67/33)	67	FoI 39 (σ = 0.3499)	Does not ignite at 4.5J	Steel / Steel 50%	214.4 to 214.5 °C

*Referenced to RDX (FoI 80).

8.4 Theoretical Performance (ICT Code)

Theoretical performances of AP/SEBS and RDX/SEBS propellants were calculated using the ICT thermodynamic code, version 1.00, supplied by the Fraunhofer Institute for Chemical Technology. The specific impulse (I_{sp}) was calculated for AP/SEBS with a range of solid loadings. A pressure ratio of 70:1 was used. For comparison, results for AP/HTPB/DOA was also conducted, a typical 2:1 ratio by mass [246] of HTPB:DOA was maintained while the solid loading was altered. Similarly calculations for different solid loadings of RDX/SEBS were obtained, these were at constant volume yielding force constants, more typical of gun propellants. This was compared against a typical LOVA type gun propellant of RDX/CAB/NC [28,29]. The ratio of CAB:ATEC was maintained at a ratio of 12:7.6 by mass while NC and EC were fixed at 4 and 0.4 % m/m. Details of composition are in Table 8-5. Results were obtained for solid loadings between 60 and 98 % m/m solid loading (RDX/CAB/NC, 60 to 96 % m/m) at every percentage point. Standard values supplied with the software were used, except for SEBS were the reduced formula of $C_{10}H_{16.84}$ and heat of formation of -161.10 $kJ.mol^{-1}$(reduced formula) were inputted (see Appendix A for details of calculation).

Table 8-5 Composition of propellants for performance calculations by ICT thermodynamic code.

	Composition	
Rocket Propellants		
AP/SEBS	Ammonium Perchlorate (AP) SEBS	
AP/HTPB/DOA	Ammonium Perchlorate (AP) Hydroxyl-terminated polybutadiene (HTPB) Dioctyl adipate (DOA)	HTPB:DOA ratio maintained at 2:1 by mass
Gun Propellants		
RDX/SEBS	RDX SEBS	
RDX/CAB/NC	RDX Cellulose Acetate Butyrate (CAB) Acetyl Triethyl Citrate (ATEC) Nitrocellulose (NC) Ethyl Centralite (EC)	CAB:ATEC ratio maintained at 12:7.6 by mass NC and EC were fixed at 4 and 0.4 % m/m

Results for AP/SEBS show that a good specific impulse (I_{sp}) is obtainable, with a maximum of 2473 m s^{-1} at 90 % m/m AP fill. This maximum value is similar to that obtained for AP/HTPB/DOA (2477 m s^{-1}, 89 % m/m AP), however, looking at Figure 8-4 comparing the two propellants, AP/SEBS has lower specific impulses for the same solid loadings (for AP < 90 % m/m). The difference in the specific impulse at a particular solid loading is relatively small. For example, at a solid loading of 84 % m/m AP, AP/SEBS has an I_{sp} of 2326 m s^{-1} compared to 2377 m s^{-1} for AP/HTPB/DOA. This is expected as both binders are inert and most contain only hydrogen and carbon.

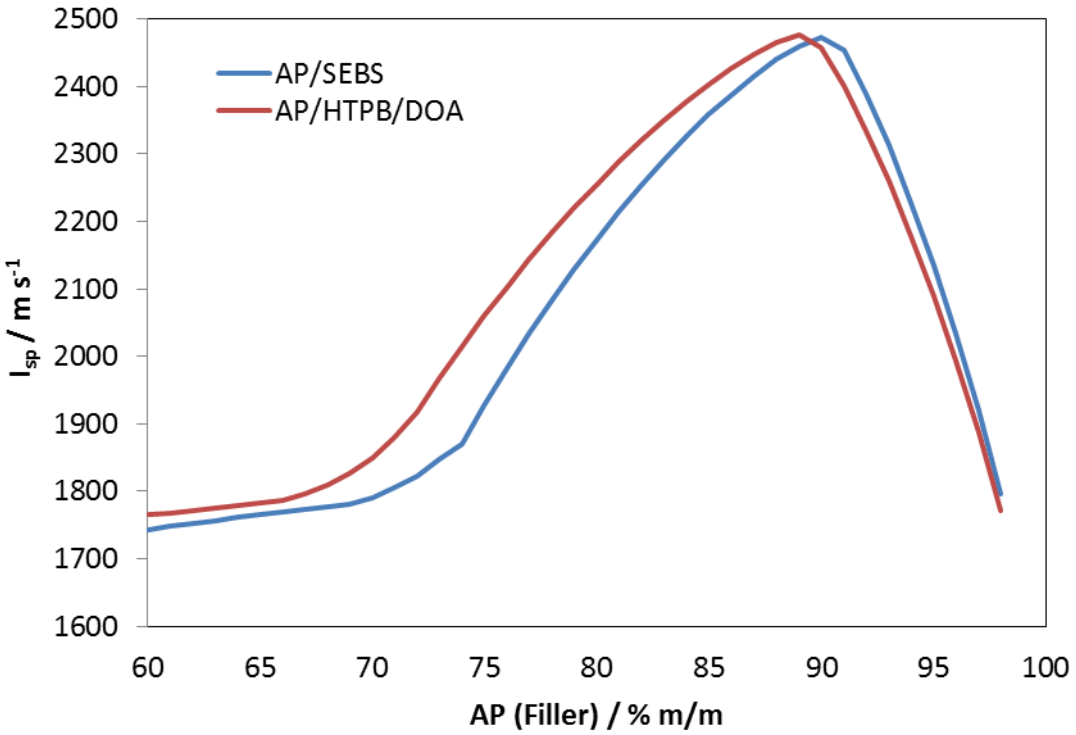

Figure 8-4 Graph of specific impulse (I_{sp}) against percentage of ammonium perchlorate (AP) filler for AP/SEBS and AP/HTPB/DOA propellants, calculated using the ICT thermodynamic code (pressure ratio of 70:1).

Similarly RDX/SEBS compositions are theoretically capable of obtaining high force constants, this would require high solid loadings. For instance a 84 % m/m solid loading of RDX theoretically would result in an I_{sp} of 1043 m s^{-1}, the same value as the theoretical value obtain for a typical composition of a RDX/CAB/NC type LOVA propellant (containing 76 % m/m RDX). Comparing RDX/SEBS with RDX/CAB/NC in Figure 8-5 we see an expected lower force constant for RDX/SEBS with the same solid loading. This is due to RDX/CAB/NC composition containing 4 % m/m nitrocellulose, an energetic binder increasing the force constant.

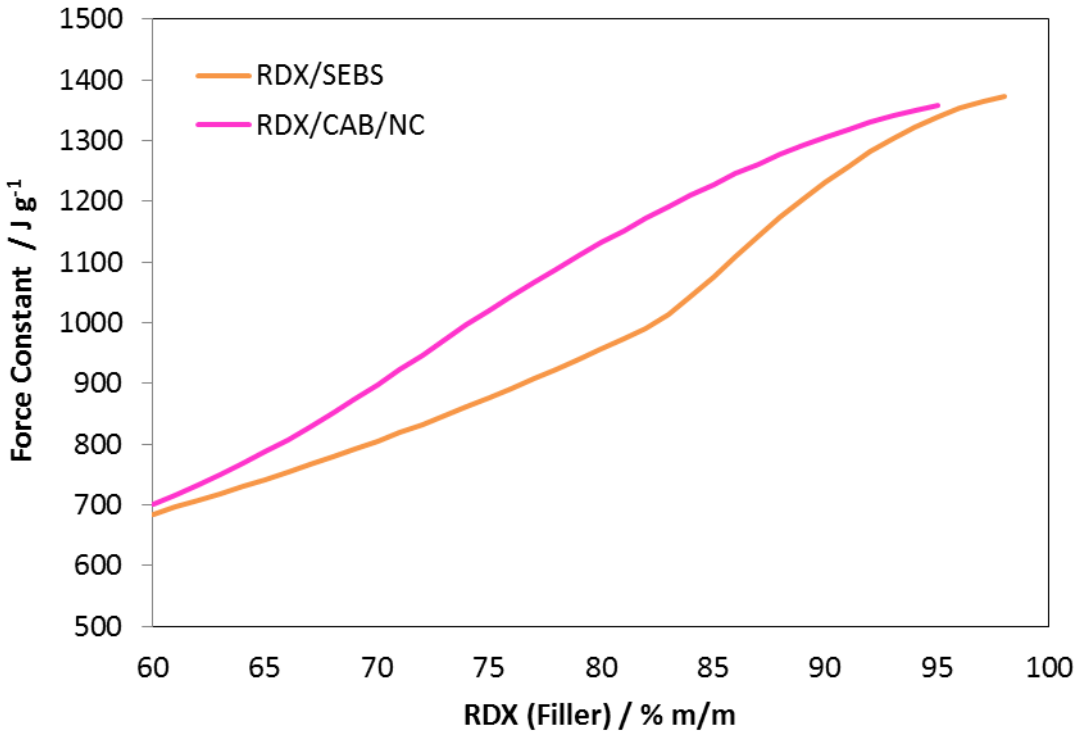

Figure 8-5 Graph of force constant against percentage of RDX filler for RDX/SEBS and RDX/CAB/NC propellants, calculated using the ICT thermodynamic code.

8.5 Microscopy

8.5.1 Introduction

In order to assess the effectiveness of the manufacturing process, optical microscopy was performed. The samples were cut with a razor blade to expose the internal structure. In particular interest is the coating of the filler and the consolidation of the propellant. Poor coating should be seen by gaps around the filler particles; bubbles and gaps elsewhere would indicate poor consolidation.

8.5.2 AP/SEBS Microscopy

Optical microscopy was difficult due to both AP and SEBS being transparent and of similar diffractive indexes. A blue background was used to improve the imagines. Both particle sizes in the bimodal mixture of AP (AP200 & AP90) were visible at 200x magnification, see Figure 8-6. In the image of AP/SEBS (41/59 % v/v), AP particles are clearly separated by the SEBS polymer between them. As

International Journal of Chemical Engineering and Applications. 2012; 3(2): 114–124.

11. Davenas A. The Main Families and Use of Solid Propellants. In: Davenas A (ed.) Solid Rocket Propulsion Technology. Peramon Press; 1993. pp. 329–367. Available at: DOI:10.1016/b978-0-08-040999-3.50013-8

12. Agrawal JPP. High Energy Materials: Propellants, Explosives and Pyrotechnics. John Wiley & Sons; 2010. Chapter 4 p.

13. Nguyen TT., Sear RJ. Approaches to Reducing the Temperature Sensitivity of Propulsion Sustems for Artillery Ammunition (DSTO-TR-0102). DSTO Aeronautical and Maritime Research Laboratory, Melbourne, Australia. 1994;

14. NAMMO. Nammo Ammunition Hanbook. 2nd edn. NAMMO; 2014.

15. G. Leadore M. Mechanical Properties of Aerojet, Thiokol, and JA2 High-Energy Gun Propellants at 1.5 m/s Deformation Rate (ARL-TR-2654). U.S. Army Research Laboratory, Aberdeen Proving Ground, MD, USA. 2002; (January): 34.

16. Mortimer JR., Hart AH., Huf J. Development of a Low Strain-Rate Gun Propellant Bed Compression Test and its Use in Evaluating Propellant Mechanical Response (DST-Group-TR-3291). Weapons and Combat Systems Division, Defence Science and Technology Group, Edinburgh, Australia. 2016;

17. Howard SL., Leadore MG., Newberry JE. High-Rate Mechanical Properties of JA2 Propellant at Temperatures from – 50 to 80 ° C (ARL-MR-0894). US Army Research Laboratory, Aberdeen Proving Ground, MD, USA. 2015;

18. Lieb RJ. The Mechanical Response of M30, JA2 AND XM39 Gun Propellants to High-Rate Deformation (BRL-TR-3023). US Army Ballistic Research Lab, Aberdeen Proving Ground, MD, USA. 1989;

19. Rozumov E. Recent Advances in Gun Propellant Development: From

Molecules to Materials. In: Shukla MK, Boddu VM, Steevens JA, Damavarapu R, Leszczynsk J (eds.) Energetic Materials From Cradle to Grave. Springer; 2017. Available at: DOI:10.1002/adma.19900020404

20. Miller MS., Vanderhoff JA. Burning Phenomena of Solid Propellants (ARL-TR-2551). U.S. Army Reserach Laboratory. 2001;

21. Baer PG. Prediction of High Velocity Solid Propellant Performance by Gas Dynamic Computer Program. National Technical Information Service, Ballistic Research Laboratories Report, Aberdeen Proving Ground, Maryland. 1970;

22. FORDHAM S. Design and Application of Propellants. In: Fordham S (ed.) High Explosives and Propellants. Elsevier; 1980. pp. 184–196. Available at: DOI:10.1016/b978-0-08-023833-3.50028-1

23. Freedman E. Thermodynamic Properties of Military Gun Propellants. In: L. Stiefel (ed.) Gun Propulsion Technology. AIAA; 1987.

24. Anderson RD., Rice BM. Minimizing Life-Cycle Costs of Gun Propellant Selection Through Model-Based Decision Making: A Case Study in Environmental Screening and Performance Testing (ARL-TR-2326). Army Research Laboratory, USA. 2000;

25. Archambault P. Reduced Vulnerability Gun Propellants. Insensitive Munition and Energetic Materials Technology Symposium, Miami, USA. 2007. pp. 1–21.

26. Environmental Security Technology Certification Program (ESTCP). Closed Loop Energetics with VOC Emission Reduction (CLEVER). US Department of Defence. 2003;

27. http://www.navweaps.com/Weapons/WNUS_5-62_mk45.php. 2019. Available at: http://www.navweaps.com/Weapons/WNUS_5-62_mk45.php (Accessed: 8 February 2019)

28. Schroeder MA., Fifer RA., Miller MS., Pesce-Rodriguez RA., Selawski CJ.

Condensed-Phase Processes During Solid Propellant Combustion. 3. Preliminary Depth-Profiling Studies on XM39, JA2, M9, M30, and HMX2 (ARL-TR-346). Army Research Laboratory, USA. 1994; (January).

29. Hsieh WH., Li WY. Combustion Behavior and Thermochemical Properties of RDX-Based Solid Propellants. Propellants, Explosives, Pyrotechnics. 1998; 23(3): 128–136.

30. MSIAC. MSIAC Newsletter, 3rd Quarter. Munitions Safety Information Analysis Center (MSIAC). 2011;

31. Vogelsanger B., Andres H., Schädeli U., Huber A., Skriver A., Ryf K. Tomorrow's LOVA-Propellant - Polymer-Bonded or Nitrocellulose-Based? 35th International Annual Conference of ICT, Germany. 2004; : 1–15.

32. Penny MJ. Development of Insensitive Munitions (IM) Thermoplastic elastomer (TPE) propellants for Large Calibre Gun Systems. NC Symposium 31st May to 1st June. 2016; (June).

33. BAE Systems plc. European Patent EP 2 784 054 A1. 2014.

34. Penny MJ. Development of Insensitive Munitions (IM) Thermoplastic elastomer (TPE) propellants for Large Calibre Gun Systems. OME Symposium, 31st October – 1st November. 2017; (18034585).

35. Pillai AGS., Joshi MM., Barve AM., Velapure SP., Karir JS. Cellulose Acetate Binder-Based LOVA Gun Propellant for Tank Guns. Defence Science Journal. 1999; 49(2): 141–149. Available at: DOI:10.14429/dsj.49.3799

36. Sanghavi RR., Kamale PJ., Shaikh MAR., Shelar SD., Kumar KS., Singh A. HMX Based Enhanced Energy LOVA Gun Propellant. Journal of Hazardous Materials. 2007; 143(1–2): 532–534. Available at: DOI:10.1016/j.jhazmat.2006.09.087

37. Leach C., Debenham D., Kermarree J-Y., Tormo C. Co-Operation Between the United Kingdom and France on the Assessment of Gun Propellants.

Energetic Material, Analysis, Diagnostics and Testing 31st International Annual Conference of ICT. 2000. pp. 1–1 to 1–5.

38. Wildegger-Gaissmaier AE. Influence of Ignition Related Parameters and Charge Configuration on XKTC Model Predictions (MRL-TR-92-31). DSTO Material Reserch Laboratory, Austrailia. 1993;

39. Kirshienbaum MS., Avrami L., Strauss B. Sensitivity Characterization of Low Vulnerability (LOVA) Propellants. US Army Armament and Development Command. 1983; Available at: http://www.dtic.mil/dtic/tr/fulltext/u2/a126130.pdf

40. Driel, C.A., Zebregs, M., Ramlal D., Driel C Van., Ramlal D., Zebregs M. Improved IM Properties of an RDX/TPE Based LOVA Propellant for Artillery Applications. 2012 Insensitive Munition and Energetic Materials Technology Symposium, Las Vegas, NV, USA. 2012.

41. Pillai AGS., Sanghavi RR., Dayanandan CR., Joshi MM., Karir JS. Ballistic Evaluation of LOVA Propellant in High Calibre Gun. Defence Science Journal. 2001; 51(2): 147–153. Available at: DOI:10.14429/dsj.51.2224

42. Hasenbein RG. Wear and Erosion in Large Caliber Gun Barrels. Benet Laboratories, Watevliet Arsenal, US Army Arament Research, Development & Engineering Center. 2003; (June 2003).

43. Wildegger-Grissmaier AE. Firing Trial of 5" / 54 LOVA Technology Demonstrator Charge (DSTO-TR-0011). Aeronatical and Maritime Research Laboratory, Australia. 1997;

44. Taylor MJ., Fuller SR., Woodley CR., Gransden JI., Chapman P. Studies of Ignition Delay at 40 mm Calibre. 23RD International Symposium on Ballistics, Tarragona, Spain. 2007. pp. 489–497.

45. Chemring Energetics UK. EDB Propellant - Mechanite. 2016. Available at: http://www.chemringenergetics.co.uk/~/media/Files/C/Chemring-Energetics-V2/documents/Datasheets 0216/EDB propellant Aug 2016.pdf (Accessed: 13 March 2019)

46. Sutton GP., Bibarz O. Solid Propellants. Rocket Propulsion Elements. Wiley; 2016. Available at: DOI:10.1016/B978-1-85617-912-6.10001-5.

47. Sun S., Ma S., Zhao B., Zhang G., Luo Y. A Facile Way to Prolong Service Life of Double Base Propellant. Materials. 2018; 11: 2236. Available at: DOI:10.3390/ma11112236

48. Sućeska M., Mušanić SM. Study of Mechanical Properties of Naturally Aged Double Base Rocket Propellants. Central European Journal of Energetic Materials, 2010, 7(1), 47-60 ISSN 1733-7178. 2010; 7(1): 47–60.

49. Davenas A. Development of Modern Solid Propellants. Journal of Propulsion and Power. 2003; 19(6): 1108–1128.

50. Austruy H. Double-base Propellants. In: Davenas A (ed.) Solid Rocket Propulsion Technology. Peramon Press; 1993. p. Chapter 9.

51. Bailey A., Murray S. Rocket Propellants. In: Explosives, Propellant & Pyrotechnics. Brassey's; 1989.

52. Kubota N. Propellant Chemistry. Pyrotechnic Chemistry. Journal of Pyrotechnics Inc; 2004. p. Chapter 11.

53. Sutton GP., Biblarz. O. Solid Propellant Rocket Motor Fundamentals. In: Sutton GP, Biblarz. O (eds.) Rocket Propulsion Elements. John Wiley & Sons; 2016. pp. 434–490.

54. Lengellé G., Duterque J., Trubert JF. Combustion of Solid Propellants (RTO-EN-023). Internal Aerodynamics in Solid Rocket Propulsion, Belgium. 2002.

55. Davenas A. Composite Propellants. In: Davenas A (ed.) Solid Rocket Propulsion Technology. Peramon Press; 1993.

56. Daniel MA. Polyurethane Binder Systems for Polymer Bonded Explosives (DSTO-GD-0492). Weapons System Divison, DSTO Defence Science and Technology Organisation, Australia. 2006; Available at: http://nla.gov.au/nla.arc-52839

57. Provatas A. Energetic Polymers and Plasticisers for Explosive Formulations - A Review of Recent Advances (DSTO-TR-0966). DSTO, Aeronautical and Maritime Research Laboratory, Australia. 2000; : 1–37.

58. Brydson JA. Thermoplastic Elastomers - Properties and Applications. Rapra Review Reports, Rapra Technology Ltd. 1995;

59. Cowie JM. Polymers: Chemistry & Physics of modern materials. International Textbook Company Ltd; 1973. Chapter 14 p.

60. Atkins P. Physical Chemistry. Sixth Edit. Oxford Univeristy Press; 1998. 179 p.

61. Schneider HA. Conformational entropy contributions to the glass temperature of blends of miscible polymers. Journal of Research of the National Institute of Standards and Technology. 1997; 102(2): 229. Available at: DOI:10.6028/jres.102.018

62. Khanna YP., Turi EA., Taylor TJ., Vickroy V V., Abbott RF. Dynamic Mechanical Relaxations in Polyethylene. Macromolecules. 1985; 18(6): 1302–1309. Available at: DOI:10.1080/00222346908217102

63. Popli R., Glotin M., Mandelkern L., Benson RS. Dynamic Mechanical Studies of α and β Relaxations of Polyethylenes. Journal of Polymer Science: Polymer Physics Edition. March 1984; 22(3): 407–448. Available at: DOI:10.1002/pol.1984.180220306

64. Boyd RH. Strengths of the Mechanical a-,b-and y- Relaxation Precess in linear Polyethylene. Macromolecules. 1984; 17: 903–911.

65. Grand View Research. Thermoplastic Elastomers Market | Global TPE Market Report , 2022. 2019. Available at: https://www.grandviewresearch.com/industry-analysis/thermoplastic-elastomers-market (Accessed: 11 April 2019)

66. Grand View Research. Elastomers Market Size , Industry Trands Report, 2019 - 2025. 2019. Available at:

https://www.grandviewresearch.com/industry-analysis/elastomers-market (Accessed: 11 April 2019)

67. British Plastisic Federation. Thermoplastic Elastomers TPE, TPR. Available at: https://www.bpf.co.uk/plastipedia/polymers/thermoplastic_elastomers.aspx (Accessed: 13 March 2019)

68. Kraton Coporation. Kraton G (SBS) Polymer Grades. Available at: http://boundarybayenterprises.com/files/Kraton_D_SBS_.pdf (Accessed: 13 March 2019)

69. Kraton Coporation. Kraton G (SEBS, SEP, SEPS) Polymer Grades. Available at: http://boundarybayenterprises.com/files/Kraton_G.pdf (Accessed: 13 March 2019)

70. Kraton Coporation. Kraton D (SIS) Polymer Grades. Available at: http://kraton.com/products/KRATON_D_SIS.php (Accessed: 13 March 2019)

71. Drobny JG. Styrenic Block Copolymers. Handbook of Thermoplastic Elastomers. Elsevier; 2014. pp. 175–194. Available at: DOI:10.1016/B978-0-323-22136-8.00005-3

72. Whelan T. Polymer Technology Dictionary. Chapman & Hall; 1994. 440–441 p.

73. Aldrich: Polyethylenecovinylacetate. Available at: https://www.sigmaaldrich.com/catalog/substance/polyethylenecovinylacetate123452493778811 (Accessed: 13 March 2019)

74. DuPont. DuPont Hytrel Thermoplastic Polester Eleastomers: Design Guide. 2013. Available at: http://www.dupont.com/content/dam/dupont/products-and-services/plastics-polymers-and-resins/thermoplastics/documents/Hytrel/Design Guide for Hytrel.pdf

75. Drobny JG. Thermoplastic Polyether Ester Elastomers. Handbook of Thermoplastic Elastomers. Elsevier; 2014. pp. 271–286. Available at: DOI:10.1016/B978-0-323-22136-8.00011-9

76. McKeen LW. Thermoplastic Elastomers. Fatigue and Tribological Properties of Plastics and Elastomers. Elsevier; 2016. pp. 279–289. Available at: DOI:10.1016/B978-0-323-44201-5.00010-1

77. Despotopoulou M., Brien GO. The Superior Dynamic Properties of Pebax ® Resins. 2000. Available at: https://www.extrememateriais-arkema.com/

78. Drobny JG. Thermoplastic Elastomers Based on Polyamides. Handbook of Thermoplastic Elastomers. Elsevier; 2014. pp. 255–269. Available at: DOI:10.1016/B978-0-323-22136-8.00010-7

79. Lubrizol. Lubrizol ESTANE ® 5703 Ester Based Thermoplastic Polyurethane Datsheet. Available at: www.matweb.com/search/datasheet.aspx?matguid=0c4c562426e64d768e3ee5d294da5fbc&ckck=1 1/2 (Accessed: 19 April 2019)

80. Kress JD. Aging of the Binder in Plastic-Bonded Explosive PBX 9501 and Free-Radical Oxidation. Nuclear Weapons Highlights, Los Alamos. 2007;

81. Drobny JG. Thermoplastic Polyurethane Elastomers. Handbook of Thermoplastic Elastomers. Elsevier; 2014. pp. 233–253. Available at: DOI:10.1016/B978-0-323-22136-8.00009-0

82. Lyondellbasel. Dexflex - Product Information. Available at: https://www.lyondellbasell.com/en/products-technology/polymers/trade-name/dexflex/ (Accessed: 12 April 2019)

83. Drobny JG. Thermoplastic Elastomers Prepared by Dynamic Vulcanization. Handbook of Thermoplastic Elastomers. Elsevier; 2014. pp. 195–207. Available at: DOI:10.1016/B978-0-323-22136-8.00006-5

84. Shanks R., Kong I. Thermoplastic Elastomers. In: El-Sonbati A (ed.) Thermoplastic Elastomers Edited. InTech; 2012. Available at:

DOI:10.1016/B978-0-12-394584-6.00013-3

85. British Plastisic Federation. Ethylene Vinyl Acetate (EVA). 2019. p. 2019. Available at: https://www.bpf.co.uk/plastipedia/polymers/eva.aspxEVA (Accessed: 12 April 2019)

86. Kirchner DB., Gaydos JC., Battigelli MC. Chapter 10 Combustion Products of Propellants and Ammunition History of Propellants. In: Deeter DP, Gaydos JC (eds.) Occupational Health: The Soldier and the Industrial Base. Office of the Surgeon General, U.S. Dept. of the Army; 1993. pp. 359–396.

87. Nair CPR., Devi CH., Prasad V., Ninan KN. Effect of Process Parameters on the Viscosity of AP / Al / HTPB Based Solid Propellant Slurry. Journal of Energy and Chemical Engineering. 2013; 1(1): 1–9.

88. Cray Valley. Technical Data Sheet Poly bd® R-45M. Oaklands Corporate Center, Exton, PA, USA. Available at: www.CrayValley.com (Accessed: 11 April 2019)

89. Florczak B. Viscosity Testing of HTPB Rubber Based Pre-Binders. Central European Journal of Energetic Materials. 2014; 11(4): 625–637.

90. Steinberger R., Drechsel PD. Manufacture of Cast Double-Base Propellant. In: Klager, Boyar (eds.) Propellants Manuifacture, Hazards, and Testing. Washington, DC: American Chemical Society; 1969. pp. 1–28. Available at: DOI:10.1021/ba-1969-0088.ch001

91. Strategic Environmental Research and Development Program (SERDP). Additive Manufacture of Gun Propellants with Reduced Environmental Impact. FY 2019 Statement of Need, Weapons Systems and Platforms (WP) Program Area, Department of Defense, USA. 2017;

92. Tan, H., Duo, Y. Chen F. Molecular Structure Tailoring of Binders in Solid Propellants. In: Yang, V., Brill, T. B., Ren W-Z (ed.) Solid Propellant Chemistry, Combustion, and Motor Interior Ballistics. AIAA; 2000.

93. Gevgilili H., Kalyon DM., Shah A. Processing of Gun Propellants in Continuous Shear Roll Mills. Journal of Energetic Materials. 2008; 26(1): 29–51. Available at: DOI:10.1080/07370650701719196

94. Venugopalan S. Demystifying Explosives: Concepts in High Energy Materials. Elsevier; 2015. Chapter 5 p.

95. Manning TG., Zebregs M., van Driel CA., Leone J., Ramlal DR. Definition of a JA-2 Equivalent Propellant to be Produced by Continuous Solventless Extrusion. Journal of Applied Mechanics. 2013; 80(3): 031405. Available at: DOI:10.1115/1.4023315

96. Reed RC. US4379903: US Patent - Propellant Binder Cure Catalyst. US; 1983.

97. Varghese TL., Muthiah R., David J., Kurian AJ., Athithan SK., Krishnamurthy VN., et al. Studies on Composite Extrudable Propellant with Varied Burning Rate Pressure Index ‘n’. Defence Science Journal. 1989; 39(1): 1–12. Available at: DOI:10.14429/dsj.39.4743

98. HEXPOL TPE - TPE Processing. Available at: https://www.hexpoltpe.com/getfile.php?type=downloads&id=tpe-processing-guide.pdf

99. Barnes HA. A Review of the Rheology of Filled Viscoelastic Systems. Rheology Reviews 2003,. 2003; 38(1): 1–36. Available at: DOI:10.1081/ASR-120017479

100. Karl M., Nalawade S., Maschke A., Djuric D., Kolter K. The 37th Annual Meeting and Exposition of the Controlled Release Society. Suitability of Pure and Plasticized Polymers for Hot Melt Extrusion The 37th Annual Meeting and Exposition of the Controlled Release Society. 2010. p. 67056.

101. Huang S., Miller A., Zhang F., William BO. The Effect of Solvent Injection on the Hot-Melt Extrusion Process. AAPS Annual Meeting and Exposition Oct. 25–29. 2015.

102. Gul RM., Mcgarry FJ. Processing of Ultra-High Molecular Weight Polyethylene by Hot Isostatic Pressing, and the Effect of Processing Parameters on its Microstructure. Polymer Engineering and Science. 2004; 44(10): 1848–1857. Available at: DOI:10.1002/pen.20186

103. Schwarzl FR. On Mechanical Properties of Unfilled and Filled Elastomers. In: Erigen, A. C., Liebowitz, H., Koh, S. L., Crowley JM (ed.) Mechanic and Chemistry of Solid Propellants, Proceddings of the forth Synposium on Naval Structural Mechanics. Pergamon Press; 1967.

104. Steinberger R. Preparation and Properties of Double-Base Propellant. In: Penner, S. S., Ducarme J (ed.) The Chemistry of Propellants. Pergamon Press; 1959.

105. Dündar D., Güllü M., Ak MA., Püskülcü G., Yildirim C. Synthesis and Application of Bonding Agents Used in Rocket Propellants. RAST 2005 - Proceedings of 2nd International Conference on Recent Advances in Space Technologies. 2005; 2005: 335–338. Available at: DOI:10.1109/RAST.2005.1512587

106. Allan WD., Baumgartner W., Myers GE. HTPB Polymer Improvement (AFRPL-TR-72-89). Air Force Rocket Propulsion Laboratory, Air Force Systems Command, US Air Force. 1972; (January).

107. Markarian J. Impact Modifiers: How to Make Your Compound Tougher. Plastics Additives & Compounding. 2004; (May/June): 46–49.

108. Data for RTP 2700 Series (SBC). Available at: https://www.rtpcompany.com/products/elastomer/tpe-property-comparison/ (Accessed: 16 November 2016)

109. Woodley C., Critchley R., Wallington D., Tn K. QinetiQ Studies on Wear and Erosion in Gun Barrels. The Control and Reduction of Wear in Military Platforms, Williamsburg, USA, 7-9 June. 2003. pp. 15–1 to 15–12.

110. Lengellé, G., Duterque, J., Trubert JF. Combustion Instabilities In Solid Propellant Rocket Motors (RTO-EN-023). Internal Aerodynamics in Solid

Rocket Propulsion held in Rhode-Saint-Genèse, Belgium, 27-31 May. 2002.

111. MacKichan, A.S., Barnes, P., Sharp M. Insensitive Munitions Understanding the Risks, Reaping the Benefits. IMEMTS BRISTOL, 24-28 APRIL. 2006.

112. Schultz E. Reducing Munitions Response to Shaped Charge Jets , Fragments and Explosively Formed Projectiles. MSIAC IM Technology Gap Workshop, Gun Propulsion Technology. 2012.

113. Thermoplastic Elastomers. Available at: https://www.plasteurope.com/news/THERMOPLASTIC_ELASTOMERS_t209586/ (Accessed: 16 November 2017)

114. Yang, X., Sun, C., Zhang, J., Xu, J., Tan B. Mechanical Properties Experimental Investigation of HTPB Propellant After Thermal Accelerated Aging. AIP Conference Proceedings 1834, Busan, South Korea. 2017.

115. Zepnik S. Ageing of TPE. elasoMer 2017, Merseburg 27.9.17. 2017.

116. Dey A., Sikder AK., Talawar MB., Chottopadhyay S. Towards New Directions in Oxidizers/Energetic Fillers for Composite Propellants: An Overview. Central European Journal of Energetic Materials. 2015; 12(2): 377–399.

117. Wilkinson, J., Watt D. Review of Demilitisation and Disposal Techniques for Munitions and Related material. Munitions Safety Information Analysis Centre (MSIAC), NATO Headquarters, Brussels, Belgium. 2010;

118. Bennett RR. Low Acid Producing Solid Propellants. Aerospace Environmental Technology Conference NASA, Marshall Space Flight Center,. 1995.

119. Bennett RR., Hinshaw JC., Barnes MW. The Effects of Chemical Propulsion on the Environment. Acta Astronautica. 1992; 26(7): 531–541. Available at: DOI:10.1016/0094-5765(92)90124-2

120. EPA Fact Sheet: Final Regulatory Determination for Perchlorate. Available at: http://water.epa.gov/drink/contaiminants/unregulated/upload/FactSheet_PerchlorateDetermination.pdf, accessed 21-5-11 (Accessed: 21 May 2011)

121. Environmental Protection Agency (EPA). Drinking Water: Regulatory Determination on Perchlorate. Federal Register, USA. 2011; 76(29): 7762–7767. Available at: https://www.govinfo.gov/content/pkg/FR-2011-02-11/pdf/2011-2603.pdf, accessed 21-2-19

122. Eickhoff P. Effects of Ordnance, Munitions and Explosives on the Environment. In: North Atlantic Treaty Organisation NATO (ed.) Environmental Impact of Munition and Propellant Disposal, RTO-TR-AVT-115. 2010.

123. Jos J., Mathew S. Ammonium Nitrate as an Eco–Friendly Oxidizer for Composite Solid Propellants: Promises and Challenges. Critical Reviews in Solid State and Materials Sciences. Taylor & Francis; 2017; 42(6): 470–498. Available at: DOI:10.1080/10408436.2016.1244642

124. Oommen C., Jain SR. Ammonium Nitrate: A Promising Rocket Propellant Oxidizer. Journal of Hazardous Materials. 1999; 67(3): 253–281. Available at: DOI:10.1016/S0304-3894(99)00039-4

125. Brinck T. Green Energetic Materials. John Wiley & Sons, Ltd; 2014. 1–290 p. Available at: DOI:10.1002/9781118676448

126. Carvalheira P., Gadiot GMHJL., de Klerk WPC. Thermal Decomposition of Phase-Stabilised Ammonium Nitrate (PSAN), Hydroxyl-terminated Polybutadiene (HTPB) Based Propellants. The Effect of Iron(III) Oxide Burning-Rate Catalyst. Thermochimica Acta. 1995; 269–270(C): 273–293. Available at: DOI:10.1016/0040-6031(95)02366-6

127. Fisher M., Sharp M. Solid Rocket Propellants for Improved IM Response – Recent Activities in the NIMIC Nations. Advances in Rocket Performance Life and Disposal. Denmark; 2002.

128. Shiguo D., Jianfei C., Yinghong X., Faxiang J., Xiaoying J. Effect of Coupling Agents on Mechanical Property of AN/PU Energy Composite. Journal of Applied Polymer Science. 1997; 63(10): 1259–1263.

129. Manelis GB., Lempert DB. Ammonium Nitrate as an Oxidizer in Solid Composite Propellants. Progress in Propulsion Physics. 2009; 1: 81–96. Available at: DOI:10.1051/eucass/200901081

130. Babuk VA., Gleboc A., Arkhipov VA., Vorozhtsov A., Klyakin GF., Severini F., et al. Dual-Oxidizer Solid Rocket Propellants for Low-Cost Access to Space. 10-IWCP - The Tenth International Workshop on Combustion and Propulsion. 2005; (November).

131. Negri M. Technology Development for ADN-Based Green Monopropellant Thrusters – an Overview of the Rheform Project. 7th European Conference for Aeronautics and Space Sciences (EUCASS). 2017; (2): 1–13. Available at: DOI:10.13009/EUCASS2017-319

132. Larsson A., Winbord N. Green Propellants Based on ADN. In: Hall J (ed.) Advances in Spacecraft Technologies. IntechOpen; 2011.

133. Sjoberg P., Skifs H., Thormahlen P., Anflo K. A Stable Liquid Mono-Propellant based on ADN. Insensitive Munitions and Energetic Materials Technology Symposium, Tucson, USA. 2009. pp. 1–28.

134. Eureno Website - ADN. Available at: http://www.eurenco.com/content/explosives/defence-security/oxidizers-energetic-polymers/adn/ (Accessed: 25 February 2018)

135. Rahman A., Chin J., Cheah K. Prilling and Coating of Ammonium Dinitramide (ADN) Solid Green Propellant in Toluene Mixture Using Ultrasound Sonication. Aerospace. 2018; 5(1): 29. Available at: DOI:10.3390/aerospace5010029

136. Yang R., Thakre P., Yang V. Thermal Decomposition and Combustion of Ammonium Dinitramide (review). Combustion, Explosion and Shock Waves. 2005; 41(6): 657–679. Available at: DOI:10.1007/s10573-005-

0079-y

137. de Flon J., Andreasson S., Liljedahl M., Oscarson C., Wanhatalo M., Wingborg N. Solid Propellants based on ADN and HTPB. AIAA/ASME/SAE/ASEE Joint Propulsion Conference & Exhibit. 2011; (August): 1–12.

138. Fujisato K., Habu H., Shibamoto H., Yu X., Miyake A., Hori K. Combustion Characteristics of ADN-based solid propellants. Transactions of the Japan Society for Aeronautical and Space Sciences, Aerospace Technology Japan. 2012; 10: 89–92.

139. Krause HH. New Energetic Materials. In: Teipel U (ed.) Energetic Materials. 2005. p. Chapter 1.

140. Tagliabue C., Weiser V., Imiolek A., Bohn MA., Heintz T. Burning Behavior of AN / ADN Propellants. 47th International Annual Conference of ICT on 'Energetic Materials – Synthesis, Characterization, Processing', Jun28 to Jul 1, Germany. 2016. pp. 36–1 to 36–15.

141. Gettwert V., Tagliabue C., Weiser V. Burning Behavior of Aluminized ADN / PSAN Propellants. Eucass2017-72. 2017; Available at: DOI:10.13009/EUCASS2017-72

142. Van Der Heijden AEDM., Keizers HLJ., Welland-Veltsmans WH. HNF : Oxidiser for High Performance , Low-Signature Propellants. Advances in Rocket Performance Life and Disposal, 23-26 September. 2002.

143. Dendage PS., Sarwade DB., Asthana SN., Singh H. Hydrazinium Nitroformate (HNF) and HNF Based Propellants: A Review. Journal of Energetic Materials. 2001; 19(1): 41–78. Available at: DOI:10.1080/07370650108219392

144. Talawar MB., Sivabalan R., Mukundan T., Muthurajan H., Sikder AK., Gandhe BR., et al. Environmentally Compatible Next Generation Green Energetic Materials (GEMs). Journal of Hazardous Materials. 2009; 161(2–3): 589–607. Available at: DOI:10.1016/j.jhazmat.2008.04.011

145. Trache D., Klapötke TM., Maiz L., Abd-Elghany M., DeLuca LT. Recent Advances in New Oxidizers for Solid Rocket Propulsion. Green Chemistry. 2017; 19(20): 4711–4736. Available at: DOI:10.1039/c7gc01928a

146. Athar J., Ghosh M., Dendage PS., Damse RS., Sikder AK. Nanocomposites: An Ideal Coating Material to Reduce the Sensitivity of Hydrazinium Nitroformate (HNF). Propellants, Explosives, Pyrotechnics. 2010; 35(2): 153–158. Available at: DOI:10.1002/prep.200900024

147. Ding P., Wang H., Wen L., Cheng G., Lu C., Yang H. Studies on Synthetic Technology and Reduced Sensitivity Technology of Hydrazinium Nitroformate. Industrial and Engineering Chemistry Research. 2014; 53(36): 13851–13855. Available at: DOI:10.1021/ie5023139

148. van der Heijden AEDM., Leeuwenburgh AB. HNF/HTPB propellants: Influence of HNF particle size on ballistic properties. Combustion and Flame. The Combustion Institute. Published by Elsevier Inc. All rights reserved.; 2009; 156(7): 1359–1364. Available at: DOI:10.1016/j.combustflame.2009.03.007

149. Unneberg E., Karsrud TKE., Johannessen TC., Sollien I. Development of Smokeless GAP Propellants with Various Oxidizers. Advances in Rocket Performance Life and Disposal, Aalborg, Denmark,. 2002. pp. 23–26.

150. Indian Head Division Surface Naval Warfare Center. Closed Loop Energetics with VOC Emission Reduction. ESTCP Project Number PP-9704, US Department of Defence. 2002;

151. Song X., Li F. Dependence of Particle Size and Size Distribution on Mechanical Sensitivity and Thermal Stability of Hexahydro-1, 3, 5-trinitro-1, 3, 5-triazine. Defence Science Journal. 2009; 59(1): 37–42. Available at: DOI:10.14429/dsj.59.1482

152. Spear RJ., Nanut V. Mechanism of and Particle Size Effects on Shock Sensitivity of Hetrogenous Pressed Explosive: Preliminary Assessment of Binderless RDX in Fuse Trains (MRL-R-1077). DSTO Material Reserch

Laboratory, Austrailia. 1987;

153. Horst A., Baker P., Rice B., Kaste P., Colburn J., Hare J., et al. Insensitive High Energy Propellants for Advanced Gun Concepts. 19th International Symposium on Ballistics. 2001; 1(October): 17–24.

154. Khasainov BA., Ermolaev BS., Presles HN., Vidal P. On the Effect of Grain Size on Shock Sensitivity of Heterogeneous High Explosives. Shock Waves. 1997; 7(2): 89–105. Available at: DOI:10.1007/s001930050066

155. Pillai AG., Dayanandan CR., Joshi MM., Patgaonkar SS., Karir JS. Studies on the Effects of RDX Particle Size on the Burning Rate of Gun Propellants. Defence Science Journal. 1996; 46(2): 83–86.

156. Pillai AGS., Sanghavi RR., Dayanandan CR., Joshi MM., Velapure SP., Singh A. Studies on RDX Particle Size in LOVA Gun Propellant Formulations. Propellants, Explosives, Pyrotechnics. 2001; 26(5): 226–228. Available at: DOI:10.1002/1521-4087(200112)26:5<226::aid-prep226>3.0.co;2-9

157. Taylor JW. A Melting Stage in the Burning of Solid Secondary Explosives. Combustion and Flame. 1961; 6(November): 103–107. Available at: DOI:10.1016/0010-2180(62)90076-7

158. Kubota N. Combustion of Composite Propellants. Propellant and Explosives: Thermochemical Aspects of Combustion. Wiley VCH; 2015.

159. Johnson OH. HMX as a Miltary Explosive (NAVORD Report 4371). US Naval Ordance Laboratory, Maryland, USA. 1974;

160. Kubota N. Combustion Mechanisms of Nitramine Composite Propellants. Eighteenth Symposium (International) on Combustion, The Combsution Institue, Pittsburgh, USA. 1981. pp. 187–194.

161. Cohen NS., D SL. Nitramine Smokeless Propellant Research (JPL 78-6). Annual Research Progress Report, Jet Propulsion Laboratory, California, USA. 1977;

162. Beckstead MW. Overview of Combustion Mechanisms and Flame Structures for Advanced Solid Propellants. In: Brill TB, Ren W-Z, Yang V (eds.) Solid Propellant Chemistry, Combustion, and Motor Interior Ballistics, Progress in Astronautics and Aeronautics. 2000. pp. 267–285.

163. Latypov N V., Bergman J., Langtet A., Wellmar U., Bemm U. Synthesis and Reactions of 1,1-Diamino-2,2-dinitroethylene. Tetrahedron. 1998; 54(38): 11525–11536. Available at: DOI:10.1016/S0040-4020(98)00673-5

164. Zhang Y., Sun Q., Xu K., Song J., Zhao F. Review on the Reactivity of 1 , 1-Diamino-2 , 2-dinitroethylene (FOX-7). Propellants, Explosives, Pyrotechnics. 2016; 41: 35–52. Available at: DOI:10.1002/prep.201500065

165. Chen Z-E., Li Z -y., Yao N., Lei Q., Wang D. Safety Property of FOX-7 and HTPB Propellants with FOX-7. Chinese Journal of Energetic Materials, cited in: Trache, D., Klapötke, T. M., Maiz, L., Abd-Elghany, M. and DeLuca, L. T. (2017) 'Recent advances in new oxidizers for solid rocket propulsion', Green Chemistry, 19(20), pp. 4711–4736. 2010; (3): 316–319.

166. Florczak B. A Comparison of Properties of Aluminized Composite Propellants Containing HMX and FOX-7. Central European Journal of Energetic Materials. 2008; 5: 3–4.

167. Lempert DB., Dorofeenko EM., Shu Y. Energy Potential of Solid Composite Propellants Based on 1,1-Diamino-2,2-dinitroethylene. Russian Journal of Physical Chemistry B. 2016; 10(3): 483–489. Available at: DOI:10.1134/s1990793116030258

168. Lips H., Helou S., Kentgens H., Menke K., Barilla A., Eisele S. Less Sensitive Smoke Reduced Rocket Propellants Based on FOX 7. Int. Annu. Conf. ICT. 2012; 43rd(Energ. Mater.): 22/1-22/11.

169. Jensen TL., Unneberg E., Kristensen TE. Smokeless GAP-RDX Composite Rocket Propellants Containing Diaminodinitroethylene (FOX-7). Propellants, Explosives, Pyrotechnics. 2017; 42(4): 381–385. Available at: DOI:10.1002/prep.201600278

170. Dorofeeva O V., Suntsova MA. Enthalpy of Formation of CL-20. Computational and Theoretical Chemistry. Elsevier B.V.; 2015; 1057: 54–59. Available at: DOI:10.1016/j.comptc.2015.01.015

171. Golfier M., Graindorge H., Longevialle Y., Mace H. New Energetic Molecules and Their Applications in Energetic Materials. Energetic Materials, International Annual Conference of ICT. Karlsruhe; 1998. pp. 3–1 to 3–17.

172. Weiser V., Fisenreich N., Eckl W., Eisele S., Menke K. Burning Behaviour of CL-20/GAP and HMX/GAP-Propellants. Eneretic Materials, Analysis, Diagnostics and Testing, International Annual Conference of ICT. Karlsruhe; 2000. p. 144.

173. Volk F., Bohn MA., Wunsch G. Determination of Chemical and Mechanical Properties of Double Base Propellants during Aging. Propellants, Explosives, Pyrotechnics. 1987; 12(3): 81–87. Available at: DOI:10.1002/prep.19870120305

174. Urbanski T. Chemistry and Technology of Explosives, Volume 3. Peramon Press; 1964. Chapter 8 p.

175. Jain S., Mehilal., Nandagopal S., Singh P., Radhakrishnan K., Bhattacharya B. Size and Shape of Ammonium Perchlorate and their Influence on Properties of Composite Propellant. Defence Science Journal. 2009; 59(3): 294–299. Available at: DOI:10.14429/dsj.59.1523

176. Hetayothin B. Effect of Structure and Plasticizer on the Glass Transition of Adsorbed Polymer (PhD thesis). Missouri University of Science and Technology; 2010.

177. Patrick SG. Practical Guide to Polyvinyl Chloride. Rapra Technology Limited; 2005. Section 3.2 p.

178. Dubault A., Bokobza L., Gandin E., Halary JL. Effects of Molecular Interactions on the Viscoelastic and Plastic Behaviour of Plasticized Poly(vinyl chloride). Polymer International. 2003; 52(7): 1108–1118.

Available at: DOI:10.1002/pi.1189

179. Corti HR., Angell CA., Auffret T., Levine H., Buera MP., Reid, David S.Roos YH., et al. Empirical and Theoretical Models of Equilibrium and Non-Equilibrium Transition Temperatures of Supplemented Phase Diagrams in Aqueous Systems (IUPAC Technical Report). Pure and Applied Chemistry. 2010; 82(5): 1065–1097. Available at: DOI:10.1351/pac-rep-09-10-24

180. Muthiah R., Somasundaran UI., Verghese TL., Thomas VA. Energetics and Compatibility of Plasticizers in Composite Solid Propellants. Defence Science Journal. 1989; 39(2): 147–155. Available at: DOI:10.14429/dsj.39.4759

181. Wypych G. Handbook of Plasticizer. 3rd edn. Wypych G (ed.) ChemTec Publishing; 2017.

182. Akhavan J. Chemistry of Explosives. Cambridge: Royal Society of Chemistry; 2004. Available at: DOI:10.1039/9781847552020

183. Reese DA., Groven LJ., Son SF. Formulation and Characterization of a New Nitroglycerin-Free Double Base Propellant. Propellants, Explosives, Pyrotechnics. 2014; 39(2): 205–210. Available at: DOI:10.1002/prep.201300105

184. Kumari D., Balakshe R., Banerjee S., Singh H. Energetic Plasticizers for Gun & Rocket Propellants. Review Journal of Chemistry. 2012; 2(3): 240–262. Available at: DOI:10.1134/s207997801203003x

185. NIMIC. Lettre du Newsletter. 2003; (1st Quater): 1–14.

186. Comfort T., Grow S. Updates on HTPE Propellant Service Life. Insensitive Munition and Energetic Materials Technology Symposium, Lucson, Arizona, USA. 2009.

187. Rindone R., Geiss DA., Miyoshi H. BDNPA / BDNPF Shows Long-Term Aging Stability. Insensitive Munitions and Energetic Materials Technology Symposium, IM / EM Technology Implementation in the 21 st Century,

Texas, USA. 2000.

188. Hobbs ML., Kaneshige MJ., Erikson WW. Modeling the Measured Effect of a Nitroplasticizer (BDNPA/F) on Cookoff of a Plastic Bonded Explosive (PBX 9501). Combustion and Flame. 2016; 173: 132–150. Available at: DOI:10.1016/j.combustflame.2016.08.014

189. Allen HC. 4361526: US Patent - Thermoplastic composite rocket. 1982.

190. Allen HC., Clarke FW. 4,597,924: US Patent - Tetra-Alkyl Titanates as Bonding Agents for Thermoplastic Propellants. 1986.

191. B.D.Nahlovsky., G.A.Zimmerman. 4,985,094: United States Patent - Thermoplastic Castable Rocket Propellant. 1991.

192. Klohn W., Rassinfosse A. Base Bleed Solid Propellants Containing Thermoplastic Elastomers as Binders. AD-P004 448, Defence Technical Information Center. 1982;

193. Hordijk AC. Processing of Highly Filled Prepolymers or TPE's by Casting or Extrusion – the Role of Rheological Equipement. Polymer Rheology '99, Shawbury, Shopshire, UK. 1999.

194. Hordijk, A.C., Schoolderman, C., van der Heijden AEDM. Highly filled TPEs – Processing and Rheology. Polymer Rheology Conference 2001, Shawbury, Shopshire, UK. 2001.

195. van Driel CA., Hordijk C., Schoolderman C., Bakker MJG., Zevenbergen JF. TNO Defence, Security and Safety, Lange Kleiweg 137, P.O.Box 45, 2280 AA Rijswijk, Netherlands. 23RD International Symposium on Ballistics, Tarragona, Spain. 2007. pp. 531–539.

196. Bozic, V., Krakovsky I. Analysis of Thermoplastic Propellants Based on Novel Binder System. Eighth International Symposium on Special Topics in Chemical Propulsion, Cape Town, South Africa. 2009.

197. Stephens T. Solventless Manufacture of Artillery Propellant Using Thermoplastic Elastomer Binder. Annual Technical Report for FY98, Naval

Air Warfare Center Weapons Division, China Lake, CA. 1999;

198. Sanghavi RR., Asthana SN., Karir JS., Singh H. Studies on Thermoplastic Elastomers Based RDX-Propellant Compositions. Journal of Energetic Materials. 2001; 19(1): 79–95. Available at: DOI:10.1080/07370650108219393

199. Mulage KS., Patkar RN., Deuskar VD., Pundlik SM., Kakade, S. D.Gupta M. Studies on a Novel Thermoplastic Polyurethane as a Binder for Extruded Composite Propellants. Journal of Energetic Materials. 2007; 25(4): 233–245. Available at: DOI:10.1080/07370650701205964

200. Bailey A., Murray S. Gun Propellants. In: Explosives, Propellant & Pyrotechnics. Brassey's; 1989.

201. Bailey A., S. Murray. The Manufacture and Filling of Explosive Charges. In: Explosives, Propellant & Pyrotechnics. Brassey's; 1989.

202. US Army. United States Boosters and Secondary Explosives. Miltary Explosives (TM 9-1300-214). Headquaters, Department of Army, USA; 1984.

203. Olinger B. Compacting Plastic-Bonded Explosive Molding Powder to Dense Solids. 2005;

204. Kasprzyk DJ., Bell DA., Flesner RL., Larson SA. Characterization of a Slurry Process Used to Make a Plastic-Bonded Explosive. Propellants, Explosives, Pyrotechnics. 1999; 24(6): 333–338. Available at: DOI:10.1002/(SICI)1521-4087(199912)24:6<333::AID-PREP333>3.0.CO;2-T

205. Akhavan J., Burke TC. Polymer Binder for High Performance Explosives. Propellants, Explosives, Pyrotechnics. 1992; 17(6): 271–274. Available at: DOI:10.1002/prep.19920170602

206. Thompson DG., Brown GW., DeLuca R., Giambra AM., Sandstorm MM. Thermal Expansion of PBX 9501 and PBX 9502 Plastic-Bonded

Explosives. Proceedings of the 37th Annual Conference of the North American Thermal Analysis Society, 21-23 September 2009. Lubbock, TX; 2009.

207. Coguill SL. Synthisis of Highly Loaded Gelled Propellants Scott L. Coguill. AIChE Annual Meeting, At San Fransico CA, USA. 2003.

208. Resodyn. Energetic Mixing - Technical Paper. Available at: https://resodynmixers.com/technical-library/

209. Resodyn. Mixing Highly Loaded Polymers - Techical Paper. Available at: https://resodynmixers.com/technical-library/

210. ResodynAcoustic Mixing I. RAM Technical White Paper. Resodyn Acoustic Mixers, Inc. 2009; : 1–8.

211. Resodyn. How RAM Mixes - Resodyn Website. 2020. Available at: https://resodynmixers.com/how-ram-mixes/ (Accessed: 22 May 2020)

212. Briard A., Gostiaux L., Gréa BJ. The turbulent Faraday instability in miscible fluids. Journal of Fluid Mechanics. 2020; 883: A57. Available at: DOI:10.1017/jfm.2019.920

213. Briard A., Gréa BJ., Gostiaux L. The transition and mixing efficiency of the turbulent Faraday instability. 11th International Symposium on Turbulence and Shear Flow Phenomena, TSFP 2019. 2019; : 1–5.

214. Nelson AP., Cross TA. Processing Benefits of Resonance Acoustic Mixing on High Performance Propellants and Explosives. Proc. Int. Pyrotech. Semin. 2012. pp. 190–206.

215. Siviour CR., Jordan JL. High Strain Rate Mechanics of Polymers: A Review. Journal of Dynamic Behavior of Materials. Springer International Publishing; 2016; 2(1): 15–32. Available at: DOI:10.1007/s40870-016-0052-8

216. Menard K. Frequency Scans. Dynamic Mechanical Analysis. CRC; 2008. Available at: DOI:10.1201/9781420049183.ch7

217. Nielsen LE. Mechanical properties of polymers. Van Nostrand Reinhold; 1962.

218. Williams ML., Landel RF., Ferry JD. The Temperature Dependence of Relaxation Mechanisms in Amorphous Polymers and Other Glass-forming Liquids. Journal of the American Chemical Society. 1955; 77(14): 3701–3707. Available at: DOI:10.1021/ja01619a008

219. McCrum NGG., Read BEE., Williams G. Anelastic and Dielectric Effects in Polymeric Solids. 1st edn. John Wiley & Sons, Inc.; 1969. Chapter 4.2c p.

220. N.Okubo. Preparation of Master Curves by Dynamic Viscoelastic Measurements. Application Brief. 1990; Available at: www.siint.com

221. Doolittle AK., Doolittle DB. Studies in Newtonian Flow. V. Further Verification of the Free-Space Viscosity Equation. Journal of Applied Physics. 1957; 28(8): 901–905. Available at: DOI:10.1063/1.1722884

222. North Atlantic Treaty Organization (NATO). STANAG 4115 (ed2) Ballistics of Gun Propellants.pdf. 1997.

223. Stennet C. Modified Friability Test Development - Phase 1 (XS160309). 2016.

224. Sheth JP. Personal Communications From Atofina via B. B. Sauer: Cited In 'Investigation of the Influence of Selected Variables on the Solid State Structure-Property Behaviour of Segmented Copolymers'. Virginia Polytechnic Institute, USA; 2004.

225. Sheth J.P. Investigation of the Influence of Selected Variables on the Solid State Structure-Property Behaviour of Segmented Copolymers. DPhil Thesis. Virginia Polytechnic Institute, Blacksburg, Virginia, USA; 2004.

226. Arkema. PEBAX 3533 SA 01 Datasheet. Arkema, Colomes, France; 2008. Available at: www.pebax.com

227. Personal Communication with Cranfiled University From a Represenstive of Arkema. 2009.

228. Sigma-Aldrich. 200565 Sigma-Aldrich Polystyrene-block-poly(ethylene-ran-butylene)-block-polystyrene average Mw ~89,000 by GPC, powder (Coarse). 2019. Available at: https://www.sigmaaldrich.com/catalog/product/aldrich/200565 (Accessed: 3 May 2019)

229. Sierra CA., Galán C., Fatou JG., Parellada MD., Barrio JA. Thermal and Mechanical Properties of Poly-(styrene-b-ethylene-co-butylene-b-styrene) Triblock Copolymers. Polymer. 1997; 38(17): 4325–4335. Available at: DOI:10.1016/S0032-3861(96)01045-2

230. Wittenburg B.V. Crawiton MT Series Datasheet. Wittenburg B.V., Koohaaspark, The Neverlands; 2010.

231. Personal Communication From a Representive of Wittenburg B.V. with Cranfield Univeristy. 2009.

232. Zhou T., Zhang A., Zhao C., Liang H., Wu Z., Xia J. Molecular Chain Movements and Transitions of SEBS above Room Temperature Studied by Moving-Window Two-Dimensional Correlation Infrared Spectroscopy. Macromolecules. 2007; 40(25): 9009–9017. Available at: DOI:10.1021/MA071630P

233. Konyukhova E., Buzin A., Godovsky Y. Melting of Polyether Block Amide (Pebax): The Effect of Stretching. Thermochimica Acta. August 2002; 391(1–2): 271–277. Available at: DOI:10.1016/S0040-6031(02)00189-2

234. Boulares A., Tessier M., Maréchal E. Synthesis and Characterization of Poly(copolyethers-block-polyamides). II. Characterization and Properties of the Multiblock Copolymers. Polymer. 2000; 41(10): 3561–3580. Available at: DOI:10.1016/S0032-3861(99)00526-1

235. Holden G., Kricheldorf HR., Quirk RP. Thermoplastic Elastomers. 3rd edn. Carl Hanser Verlag GmbH & Co; 2004. Chapter 9 p.

236. Van Bogart JWC., Bluemke DA., Cooper SL. Annealing-Induced Morphological Changes in Segmented Elastomers. Polymer. 1981; 22(10):

1428–1438. Available at: DOI:10.1016/0032-3861(81)90250-0

237. Huitric J., Pillin I., Moan M., Pimbert S. Rheological and Thermal Study of Delayed Crystallization in Poly (butylene terephthalate)/ Ethylene- co - Ethyl. Journal of Polymer Science: Part B: Polymer Physics. 2004; 42: 714–721.

238. De Keyzer N., Vermunicht G. New Hydrogenated Styrenic Block Copolymers for Pressures Sensitive Adhesives. Belgium Plastic and Rubber Institute Annual Meeting. Belgium. 2005.

239. Norman D., Ye P. Detect Weak Tg Polymer. Available at: http://las.perkinelmer.com/content/ApplicationNotes/APP_DetectWeakTgPolymer.pdf (Accessed: 21 March 2011)

240. Dainton FS., Evans DM., Hoare FE., Melia TP. Thermodynamic Functions of Linear High Polymers. Part I-Polyoxymethylene. Polymer. 1962; 3: 263–321. Available at: DOI:10.1016/0032-3861(62)90087-3

241. Hitachi High-Tech Science Corporation. DSC Measurements of Polystyrene. Application Brief. 1995; : 5–8. Available at: https://www.hitachi-hightech.com/file/global/pdf/products/science/appli/ana/thermal/application_TA_068e.pdf

242. Bohn MA., Cerri S. Ageing Behaviour of Composite Rocket Propellant Formulations Investigated by DMA , SGA and GPC. International Progress in Insensitive Munitions and Energetic Materials. 2010; Session 9(October): 1–32.

243. de la Fuente JL. An Analysis of the Thermal Aging Behaviour in High-Performance Energetic Composites Through the Glass Transition Temperature. Polymer Degradation and Stability. Elsevier Ltd; 2009; 94(4): 664–669. Available at: DOI:10.1016/j.polymdegradstab.2008.12.021

244. Zawadzki SF., Akcelrud L. HTPB-based polyurethanes: A correlation study between morphology and mechanical behaviour. Polymer International.

1997; 42(4): 422–428. Available at: DOI:10.1002/(SICI)1097-0126(199704)42:4<422::AID-PI737>3.0.CO;2-T

245. Plesse C., Vidal F., Gauthier C., Pelletier JM., Chevrot C., Teyssié D. Poly(ethylene oxide)/Polybutadiene Based IPNs Synthesis and Characterization. Polymer. 2007; 48(3): 696–703. Available at: DOI:10.1016/j.polymer.2006.11.053

246. Siviour C., Laity P., Proud W., Field J., Porter D., Church P., et al. High Strain Rate Properties of a Polymer-Bonded Sugar: Their Dependence on Applied and Internal Constraints. Proceedings of the Royal Society A: Mathematical, Physical and Engineering Sciences. 2008; 464(2093): 1229–1255. Available at: DOI:10.1098/rspa.2007.0214

247. Brass D. Contact Studies of Weak Adhesive Interactions in Water with Membrane Enhanced Surface Acoustic Wave Analysis, Doctor of Philosophy Thesis. Northwestern University, Evanston, Illinois, USA,; 2008.

248. Cerri S., Bohn MA., Menke K., Galfetti L. Ageing Behaviour of HTPB Based Rocket Propellant Formulations. Central European Journal of Energetic Materials. 2009; 6(2): 149–165.

249. Sigma-Aldrich. Bis(2-ethylhexyl) Sebacate Safety Data Sheet. 2019.

250. Cornish R., Porter D., Church P., Gould P., Andrews T., Proud B., et al. Comparison of Porter-Gould constitutive model with compression test data for HTPB/SUGAR. AIP Conference Proceedings. 2007; 955: 777–780. Available at: DOI:10.1063/1.2833239

251. Qi F., Tanner RI. Relative Viscosity of Bimodal Suspensions. Korea Australia Rheology Journal. 2011; 23(2): 105–111. Available at: DOI:10.1007/s13367-011-0013-7

252. Cerri S., Bohn MA., Menke K., Galfetti L. Aging of HTPB/Al/AP rocket propellant formulations investigated by DMA measurements. Propellants, Explosives, Pyrotechnics. 2013; 38(2): 190–198. Available at:

DOI:10.1002/prep.201200186

253. Bohn MA. Impacts on the Loss Factor Curve and Quantification of Molecular Rearrangement Regions from it in Elastomer Bonded Energetic Formulations. In: Ronald W. Armstrong, James M. Short, Robert A. Kavetsky DKA (ed.) Energetics Science and Technology in Central Europe. CALCE EPSC Press; 2012. p. Chapter 10.

254. Robertson CG., Lin CJ., Rackaitis M., Roland CM. Influence of Particle Size and Polymer filler coupling on viscoelastic glass transition.pdf. 2008; : 2727–2731.

255. LEE KJ., LEE DK., KIM YW., CHOE W-S., KIM JH. Theoretical Consideration on the Glass Transition Behavior of Polymer Nanocomposites. Journal of Polymer Science: Part B: Polymer Physics. 2007; 45: 2232–2238. Available at: DOI:10.1002/polb

256. Skelhorn D. Particulate Fillers in Elastomers. In: Rothon R (ed.) Encyclopedia of Polymers and Composites. Rapra Technology Limited; 2003. Available at: DOI:10.1007/978-3-642-37179-0_9-1

257. Plaseied A., Fatemi A. Strain Rate and Temperature Effects on Tensile Properties and their Representation in Deformation Modeling of Vinyl Ester Polymer. International Journal of Polymeric Materials and Polymeric Biomaterials. 2008; 57(5): 463–479. Available at: DOI:10.1080/00914030701729677

258. Ornaghi HL., Bolner A., Fiorio R., Zattera AJ., Amico SC. Mechanical and Dynamic Mechanical Analysis of Hybrid Composites Molded by Resin Transfer Molding. Journal of Applied Polymer Science. 2010; 118(2): 887–896. Available at: DOI:10.1002/app32388

259. Adel WM., Guo-zhu L. Analysis of Mechanical Properties for AP / HTPB Solid Propellant under Different Loading Conditions. International Journal of Aerospace and Mechanical Engineering. 2017; 11(12): 1915–1919.

260. North Atlantic Treaty Organization (NATO). STANAG 4147 (Edition 2) -

Chemical Compatibility of Ammunition Components with Explosives (Non-Nuclear Applications). 2001; 4147(Edition 2): 1–93.

261. Defence Ordnance Safety Group. EMTAP Manual of Tests Volume 1. 2016; 1(5).

262. Kerstein AR. Percolation Model of Polydisperse Composite Solid Propellant Combustion. Combustion and Flame. 1987; 69(1): 95–112. Available at: DOI:10.1016/0010-2180(87)90023-X

263. Brouwers HJH. Particle-Size Distribution and Packing Fraction of Geometric Random Packings. Physical Review E - Statistical, Nonlinear, and Soft Matter Physics. 2006; 74(3): 1–15. Available at: DOI:10.1103/PhysRevE.74.031309

264. Weinheimer R. Properties of Selected High Explosives. International Pyrotechnics Seminar, 16-21 July. 2002; (July): 37.

265. Vyazovkin S., Wight CA. Kinetics of Thermal Decomposition of Cubic Ammonium Perchlorate. Chemistry of Materials. 1999; 11(11): 3386–3393. Available at: DOI:10.1021/cm9904382

266. Sadek MA., Moeen MH., Radwan MA., Ameen HH. Effect of Aging on Thermal Decomposition of Ammonium Perchlorate. 32nd International Conferrence of ICT. Karlsruhe, Germany; 2001. pp. 129–1 to 192–12.

267. Abd-Elghany M., Elbeih A., Hassanein S. Thermal Behavior and Decomposition Kinetics of RDX and RDX/HTPB Composition using Various Techniques and Methods. Central European Journal of Energetic Materials. 2016; 13(3): 714–735. Available at: DOI:10.22211/cejem/64954

268. Qu X., Yang Q., Han J., Wei Q., Xie G., Chen S., et al. High Performance 5-Aminotetrazole-Based Energetic MOF and its Catalytic Effect on Decomposition of RDX. RSC Advances. Royal Society of Chemistry; 2016; 6(52): 46212–46217. Available at: DOI:10.1039/c6ra07301h

269. Ozawa T. Kinetic Analysis of Derivative Curves in Thermal Analysis.

Journal of Thermal Analysis. 1970; 2(3): 301–324. Available at: DOI:10.1007/BF01911411

270. Mušanić SM., Houra IF., Sućeska M., Mušanić SM., Houra IF., Sućeska M. Applicability of Non-isothermal DSC and Ozawa Method for Studying Kinetics of Double Base Propellant Decomposition. Central European Journal of Energetic Materials. 2010; 7(3): 233–251.

271. Kissinger H. Reaction Kinetics by DTA. Analytical Chemistry. 1957; : 1702.

272. GORE GM., NAZARE AN., DIVEKAR CN., HAIT SK., ASTHANA SN. Studies on Nonaluminized High Burning Rate AP-Composite Propellants. Journal of Energetic Materials. 2004; 22(3): 151–169. Available at: DOI:10.1080/07370650490522785

273. Goncalves RFB., Rocco J a FF., Iha K. Thermal Decomposition Kinetics of Aged Solid Propellant Based on Ammonium Perchlorate - AP/HTPB Binder. 44th AIAA/ASME/SAE/ASEE Joint Propulsion Conference & Exhibit. 2008; (July): 325–342. Available at: DOI:10.5772/52109

274. Lemos MF., Mussbach G., Bohn MA. Evaluation of Filler Effects on the Dynamic Mechanical Behavior of HTPB-Elastomer Used as Binder in Exemplary Composite Formulations. Journal of Aerospace Technology and Management. 2017; 9(3): 379–388. Available at: DOI:10.5028/jatm.v9i3.795

275. Behera S. Effect of RDX on Elongation Properties of AP / HTPB Based Case. DRDO SCIENCE SPECTRUM. 2009; (March): 31–36.

276. Enew AM., El-Marsafy S., Abadeer E., Rutkevicius M. Effects of Bonding Agents, Curative Ratio and Burning Rate Modifiers on the Composite Polyurethane Studied by an Aging Program. International Journal of Engineering Research and Technology (IJERT). 2017; 6(03): 16–20.

277. Mehta P., Shetty CP., Pundkar RN., Shekhar H. Effect of Loading Densities in Closed Vessel Tests on the Burning Rate of a Propelling Charge. Defence Science Journal. 2015; 65(2): 126–130. Available at:

DOI:10.14429/dsj.65.8158

278. VihtaVuori. VihtaVuori N100 & N300 Series - Safety Data Sheet. 2015; (March 2015).

279. Gavrilov AA., Chertovich A V., Khalatur PG., Khokhlov AR. Study of the Mechanisms of Filler Reinforcement in Elastomer Nanocomposites. Macromolecules. 2014; 47(15): 5400–5408. Available at: DOI:10.1021/ma500947g

280. IMMERGUT EH., MARK HF. Principles of Plasticization. 1965. 1–26 p. Available at: DOI:10.1021/ba-1965-0048.ch001

281. Ali. MA elall., Lin G. Effect of Bonding Agent Production Materials on the Mechanical Properties of Composite Solid Rocket Propellant. Asnafi N (ed.) MATEC Web of Conferences. 10 August 2018; 189: 08001. Available at: DOI:10.1051/matecconf/201818908001

282. North Atlantic Treaty Organization (NATO). STANAG 5606, Explosive Materials, Physical/Mechanical Properies Uniaxial Tensile Test. NATO, Brussels; 2003.

283. Babrauskas V., Grayson SJ. Heat Release in Fires. London: Elsevier; 1992. Chapter 8 p.